Novel Mechanisms of Resistance to Enzalutamide in Prostate Cancer

A thesis submitted to the University of Dublin, Trinity College for

the degree of **Doctor of Philosophy (Ph.D.)** *by* **Dr. Marvin Lim Chang Jui**

Supervisors:

Prof Stephen Finn, Trinity College Dublin

Prof Ray McDermott, Tallaght University Hospital

April 2023

Declaration

I declare that this thesis has not been submitted as an exercise for a degree at this or any other university and it is entirely my own work.

I agree to deposit this thesis in the University's open access institutional repository or allow the Library to do so on my behalf, subject to Irish Copyright Legislation and Trinity College Library conditions of use and acknowledgement.

I consent to the examiner retaining a copy of the thesis beyond the examining period, should they so wish (EU GDPR May 2018).

_____

Marvin Lim Chang Jui

2023

Summary

Prostate cancer (PCa) is the second most common invasive cancer in men worldwide. In Ireland, PCa is the third leading cause of male cancer related mortality. Every year, over 3000 Irish males are diagnosed with the condition, with over 500 dying as a result. AR directed therapies have remained the primary therapeutic strategy for individuals with PCa as this disease is principally driven by androgens acting through the AR. Recent advances in anti-androgen therapy have resulted in the introduction of novel powerful AR inhibitors like enzalutamide, which have shown superior efficacy than first generation anti-androgen therapies. Despite its initial effectiveness, primary or acquired resistance remains a significant clinical issue. It is essential to develop useful biomarkers that can enhance the provision of precision medicine for people with PCa. The mechanisms by which resistance occurs remains a dynamic area of investigation. Ongoing translational methods are being employed to further understand the molecular mechanisms of enzalutamide resistance PCa.

circRNA dysregulation in human cancer has raised the question of whether circRNA may be used to build a molecular signature of aggressive PCa or as a biomarker to inform treatment resistance. In this study, circRNAs were initially investigated across a panel of prostate cell lines to identify potential circRNA signatures reflective of the continuum of prostate pathology. The circRNA microarray profiles revealed that the normal group had the most up-regulated circRNAs, followed by the malignant cell groupings. RT-qPCR was used to verify five of the circRNAs that were consistently expressed in both groups of prostate cell lines. Of particular interest, hsa_circ_0066631 expression decreased during early malignant events, where PCa cells were still AR dependent, but increased as the disease progressed to the AR independent stage based on the cell line models of disease. Additionally, hsa_circ_00066631 expression differed considerably across the normal and malignant groupings, suggesting that it might be a potential therapeutic target in PCa progression.

circRNA microarray data was also investigated in an enzalutamide resistant cell model, and the results were validated using RT-qPCR. hsa_circ_0001275 was overexpressed in Clone 1 (drug resistant) *vs.* Control (drug sensitive). The stable overexpression of hsa_circ_0001275 in the Control cell line, resulted in increased

resistance to enzalutamide, based on cellular proliferative capacity ($p < 0.05$). Based on the *in vitro* results, hsa_circ_0001275 was explored as a possible biomarker to inform enzalutamide resistance in plasma samples from 44 participants with PCa undergoing enzalutamide treatment in a clinical study (CTRIAL-IE 13-21, NCT02225704). The plasma hsa_circ_0001275 RT-ddPCR findings revealed a trend that corresponded to the activity of the disease as defined by PSA level, however, this did not reach statistical significance. hsa_circ_0001275 was not abundantly expressed in plasma, which restricts its potential application as a liquid-based predictive biomarker of enzalutamide response.

The transcriptomic landscape of enzalutamide resistant PCa *in vitro* was investigated through RNA-Seq to elucidate other potential mechanisms associated with the development of enzalutamide resistance. The RNA-Seq data revealed a substantial number of differentially expressed genes (DEGs) between Clone 1 *vs.* Control, but a smaller number of DEGs between Clone 9 (weakly drug resistant) *vs.* Control, indicating that the highly resistant clone was phenotypically distinct from the other two cell lines. The RNA-Seq analysis discovered a number of pathways that provide greater insight into the possible molecular mechanisms of enzalutamide resistance in PCa. The EMT pathway is of importance as it has been demonstrated to be a hallmark of metastatic cancer spread and recent *in vitro* studies have linked EMT to the development of PCa resistance to ADT and chemotherapy. In this study, the EMT pathway was significantly enriched in the Hallmark pathway of Clone 1 *vs.* Control. RT-qPCR validation of the common EMT markers confirmed that the highly and weakly enzalutamide resistant cell lines displayed EMT expression patterns. Western blot was also used to confirm the expression of EMT markers.

Besides EMT, NEPCa differentiation is also an emerging mechanism of resistance to AR targeted therapy that involves epithelial plasticity. In Clone 1 *vs.* Control, 10 DEGs were consistent within the two NEPCa data sets, thus creating a signature gene set, which may inform development of NEPCa. RT-qPCR validation of common NEPCa markers confirmed that the strongly enzalutamide resistant cells displayed NEPCa characteristics.

Although molecular profiling is not, yet the clinical standard of care in PCa, increasing evidence is emerging to support its utility in guiding therapeutic decisions. This project included a retrospective study to evaluate the landscape of actionable gene mutations. This was undertaken using targeted NGS in 164 Irish patients with mCRPC, who progressed on a second generation hormonotherapy. There was a high rate of potentially

actionable gene mutations within the tumour samples tested (between 47% and 60%), which could have therapeutic implications in the future. Notably, between 13% and 25% of participants in this research had somatic mutations in the DNA damage response and repair (DDR) gene, which can be targeted with a PARP Inhibitor (PARPi). While tissue-based NGS remains the gold standard, this study demonstrated that blood-based targeted NGS might be as beneficial for PCa molecular characterisation. Furthermore, the frequency of the DDR gene mutation in Irish patients with mCRPC was similar with earlier NGS investigations in the literature.

The data produced in this project characterised circRNA profiles in PCa and demonstrated for the first time that overexpression of certain circRNA enhanced resistance to enzalutamide *in vitro*. This study examined a variety of methodologies to assess circRNA expression in PCa, and has laid the groundwork for future research in this novel area. This study also used RNA-Seq to identify a number of pathways that may provide more insight into the molecular mechanisms of enzalutamide resistance in PCa.

Thus, this body of work lays the groundwork for the identification of unique mechanisms of enzalutamide resistance in PCa, as well as novel targets for therapy.

Acknowledgements

I wish to express my most sincere gratitude to my wonderful supervisors, Professor Ray McDermott and Professor Stephen Finn, for their assistance and guidance throughout the course of this project. Their unwavering support and inspiration, both professionally and personally has been crucial over the last five years.

I would also like to thank Dr. Steven Gray for his help and advice during the study process, which has been instrumental to the development of this work. I would especially like to thank Dr. Anne-Marie Baird for her unending assistance, without which this project would not have been feasible. You have gone above and beyond time and again to help me out; for that, I am forever grateful – thank you "lab mommy"!

My grateful appreciations also to the following people for their help throughout the project; Dr. John Greene, Barry Digby, Dr. Pilib O' Broin, Dr. Martin Barr, Dr. Kathy Gately, Dr. Ezgi Oner, Dr. Lauren Brady, Dr. Stephen Smith, Dr. Elaine Kenny, Dr. Paul Smith and the staff in the clinical trials unit at Tallaght University Hospital.

Finally, I would like to express my gratitude for my family, without whom I would not have endured down this long and strenuous path. My sisters, brothers and nephew; Jessica, Grace, Joanne, Eldwin, Bryan and Aaron, who have been unfailingly loving and supportive throughout my PhD and it is very much appreciated. My nephew Aaron, thank you for bringing the sunshine into the family. I must also thank my grandparents, Loo Siew Chin, Lim Tang Too, Wung Ngt Kim and Chia Yam Kung, who have always been my most zealous supporters. It is with my heavy hearts and profound sadness that both Lim Tang Too and Wung Ngt Kim are not here to witness this accomplishment.

I would also like to express my genuine gratitude to my girlfriend, Joanne. Thank you for being there for me. Your constant love that you have provided helps to enhance my perseverance in particular during the arduous times. Your reassuring words, have guided me and I cannot express how grateful I am to you. I also would like to thank my very best friend, Wong Lian Chin for being a "bro" throughout these years. Without your support and assistance with everything, my life journey all these years abroad would not have been smooth sailing.

I owe my earnest gratitude to both my parents, Lim Boon Seng and Chia Siew Huay. Their unreserved love and kindest support has provided a constant source of comfort and

motivation. Their perseverance and fortitude in the face of hardship have been an immense source of inspiration to me. To you both, I dedicate this work.

This work was supported by the Irish Cancer Society and the Prostate Cancer Foundation.

Dedication

This thesis is dedicated to my parents, Lim Boon Seng and Chia Siew Huay.

Publications and presentations

Peer-reviewed publications

Lim MCJ, Baird AM, Greene J, McNevin C, Ronan K, Podlesniy P, Sheils O, Gray SG, McDermott RS, Finn SP. hsa_circ_0001275 Is One of a Number of circRNAs Dysregulated in Enzalutamide Resistant Prostate Cancer and Confers Enzalutamide Resistance In Vitro. Cancers (Basel). 2021 Dec 20;13(24):6383. PMID: 34945002

McDermott RS, Greene J, McCaffrey J, Parker I, Helanova S, Baird AM, Teiserskiene A, **Lim M**, Matthews H, Deignan O, Feeney J, Thirion PG, Finn SP, Kelly PJ. Radium-223 in combination with enzalutamide in metastatic castration-resistant prostate cancer: a multi-centre, phase II open-label study. Ther Adv Med Oncol. 2021 Sep 6;13:17588359211042691. PMID: 34512801

Greene J, Baird AM, **Lim M**, Flynn J, McNevin C, Brady L, Sheils O, Gray SG, McDermott R, Finn SP. Differential CircRNA Expression Signatures May Serve as Potential Novel Biomarkers in Prostate Cancer. Front Cell Dev Biol. 2021 Feb 25;9:605686. PMID: 33718350

Lim MCJ, Baird AM, Aird J, Greene J, Kapoor D, Gray SG, McDermott R, Finn SP. RNAs as Candidate Diagnostic and Prognostic Markers of Prostate Cancer-From Cell Line Models to Liquid Biopsies. Diagnostics (Basel). 2018 Aug 30;8(3). PMID: 30200254

Greene J, Baird AM, Casey O, Brady L, Blackshields G, **Lim M**, O'Brien O, Gray SG, McDermott R, Finn SP. Circular RNAs are differentially expressed in prostate cancer and are potentially associated with resistance to enzalutamide. Sci Rep. 2019 Jul 24;9(1):10739. PMID: 31341219

Aird J, Baird AM, **Lim MCJ**, McDermott R, Finn SP, Gray SG. Carcinogenesis in prostate cancer: The role of long non-coding RNAs. Noncoding RNA Res. 2018 Feb 1;3(1):29-38. PMID: 30159437

Greene J, Baird AM, Brady L, **Lim M**, Gray SG, McDermott R, Finn SP. Circular RNAs: Biogenesis, Function and Role in Human Diseases. Front Mol Biosci. 2017 Jun 6;4:38. PMID: 28634583

Article publications

Marvin Lim Chang Jui. Prostate cancer highlights at ESMO 2021. Irish Medical Times. October 6, 2021

Lim, M., Baird, A. M., Finn, S. The New Kid on the Block- Next Generation Sequencing (NGS) for Anaplastic Lymphoma Kinase (ALK) Translocation Detection in Non-small Cell Lung Carcinoma (NSCLC). Pathology and Diagnostics Hospital Healthcare Europe. October 2, 2018

Poster presentations

Marvin Lim, Stephen P. Finn, Umair Aleem, Anne-Marie Baird, Diya Sabu, Bryan Lim, Lisa Prior, Ruth McGinn, Ray McDermott. Targeted Next Generation Sequencing (NGS) in Metastatic Castration Resistant Prostate Cancer (mCRPC): Experience from Two Tertiary Centres. 27th Annual PCF Scientific Retreat Virtual Poster Session. October 20-23, 2020

M.C.J. Lim, J.P. Greene, A. Baird, S. Gray, C. McNevin, R. McDermott, S.P. Finn. Circular RNA is associated with enzalutamide resistant prostate cancer. Annals of Oncology (2020) 31 (suppl_4): S1034-S1051. 10.1016/annonc/annonc294

John Patrick Greene, **Marvin Chang Jui Lim**, Anne-Marie Baird, Olwyn Deignan, John McCaffrey, Lisa Mary Prior, Imelda Parker, Alison Bowes, Ausra Teiserskiene, John Feeney, Pierre Guillame Thirion, Stephen P. Finn, Paul J. Kelly, and Ray McDermott. An updated analysis evaluating skeletal related events (SREs) in CTRIAL-IE 13-21: Phase II trial of radium-223 (R223) in combination with enzalutamide (ENZA) for patients (pts) with metastatic castration-resistant prostate cancer (mCRPC). Journal of Clinical Oncology 2019 37:7_suppl, 215-215

Lim, M., Greene, J., Aird, J., Baird, A. M., Gray S., McDermott, R., Finn, S. Dysregulated epithelial–mesenchymal transition (EMT) marker expression is evident in enzalutamide resistant prostate cancer cell lines. TCD 11th International Cancer Conference, 2019

Abbreviations

ADT	Androgen deprivation therapy
AGO	Argonaute Protein
ALL	Acute lymphoblastic leukaemia
ANOVA	Analysis of variance
AR	Androgen receptor
AR-FL	Androgen receptor full length
ARV7	Androgen receptor variant 7
ATCC	American Type Culture Collection
BCL	B-cell lymphoma
BPH	Benign prostatic hyperplasia
ceRNA	Competitive endogenous RNA
circRNA	Circular RNA
CRPC	Castrate resistant prostate cancer
Ct	Cycle threshold
cfDNA	Circulating cell-free DNA
DEGs	Differentially express genes
DDR	DNA damage response and repair
DHT	Dihydrotestosterone
DMEM	Dulbecco's modified eagle's medium
DNA	Deoxyribonucleic acid
EDTA	Ethylenediaminetetraacetic acid
EGF	Epidermal growth factor

EMT	Epithelial mesenchymal transition
EpCAM	Epithelial cell adhesion molecule
ERG	ETS-related gene
ERK	Extracellular receptor kinase
ETS	E26 transformation specific
ETV1	ETS variant 1
FBS	Foetal bovine serum
FC	Fold change
FDR	False discovery rate
FFPE	Formalin fixed paraffin embedded
FGF	Fibroblast growth factor
GFP	Green fluorescent protein
GO	Gene ontology
GSEA	Gene set enrichment analysis
GSP	Gene specific priming
IMS	Industrial methylated spirits
KEGG	Kyoto encyclopaedia of genes and genomes
LBD	Ligand binding domain
LHRH	Luteinizing hormone-releasing hormone
LncRNAs	Long non-coding RNAs
mCRPC	Metastatic castrate resistant prostate cancer
MEM	Minimum essential medium eagle
miRNA	microRNA

MMR	Mismatch repair
mPCa	Metastatic prostate cancer
mTOR	Mammalian target of rapamycin complex
MYC	Myeloctomatosis oncogene cellular homolog
MRE	miRNA response elements
mRNA	Messenger RNA
NCBI	National Centre for Biotechnology
ncRNA	Noncoding RNAs
NEPCa	Neuroendocrine prostate cancer
NGS	Next-generation sequencing
OS	Overall survival
PARPi	Poly(ADP-ribose) polymerase inhibitor
PBS	Phosphate buffered saline
PBST	PBS tween
PCa	Prostate cancer
PCR	Polymerase chain reaction
PCWG3	Prostate Cancer Working Group 3
PSA	Prostate specific antigen
PTEN	Phosphatase and tensin homologue
QC	Quality control
QoL	Quality of life
RBP	RNA-binding proteins
RIN	RNA integrity number

RNA	Ribonucleic acid
RNA-Seq	RNA sequencing
RNase	R Ribonuclease
RP	Random priming
RT	Room temperature
RT-ddPCR	Reverse transcription digital droplet polymerase chain reaction
RT-qPCR	Reverse transcription quantitative polymerase chain reaction
SEM	Standard error of the mean
SFM	Serum free media
TBS	Tris-buffered saline
TE	Tris-EDTA
TMPRSS2-ERG	Transmembrane protease serine ETS-related gene fusion
US	United States
VEGF	Vascular endothelial growth factor

Units

bp	Base pairs
°C	Degrees Celsius
g	Grams
h	Hour(s)
IU	International Units
µg	Microgram
µL	Microliter
µM	Micrometre
µM	Micromolar
kB	Kilobases
kDa	Kilodaltons
kg	Kilograms
L	Litre(s)
M	Molar
mA	Milliamp
mg	Milligram
min	Minutes
mL	Millilitre
mM	Millimolar
mm	Millimetre
n	Number (sample size)
nM	Nanometres

ng	Nanogram
rpm	Revolutions per minute
s	Second(s)
U	Unit(s)
V	Volt
v/v	Volume per volume
w/v	Weight per volume
χ g	Relative centrifugal force

List of Figures

List of Tables

Table 7.0. Participant characteristics.

Table of Contents

Chapter 1 - Introduction

1.0 Introduction

1.1 Prostate anatomy and function

The prostate gland is located at the base of the bladder encasing the upper section of urethra. The organ begins to develop in the male foetus at the end of the first trimester (1). It contains both glandular and fibromuscular tissue, which plays important roles in the normal function of the prostate. The prostate contains three glandular zones, known as the central, peripheral, and transition zones with one non-glandular region of the anterior prostate that provides structural support consisting of fibromuscular stroma (2, 3). The fibromuscular tissue helps in the segregation of bodily fluids during micturition and ejaculation. The fibromuscular tissue contracts during micturition or ejaculation to prevent urine from entering prostatic ducts or back-flow of semen into the bladder, respectively. The glandular tissue plays a key role in reproductive function by secreting seminal fluid, containing ions such as zinc and citrate and proteins such as prostate-specific antigen (PSA), prostatic acid phosphatase, and β-microseminoprotein (4, 5). PSA is a glycoprotein produced by both normal and malignant prostate epithelial tissue. An increase in PSA levels in people with prostate cancer (PCa) is due to increased production by neoplastic cells and disruption of the tissue between the prostate and capillaries, hence allowing extravasation of PSA into the serum (6). Although not without controversy, pre-neoplastic disorders such as proliferative inflammatory atrophy (PIA) and prostatic intraepithelial neoplasia (PIN) are relatively common in the prostate, which may undergo a step-wise carcinogenesis process, which eventually leads to tumour development (7) (Figure 1.1).

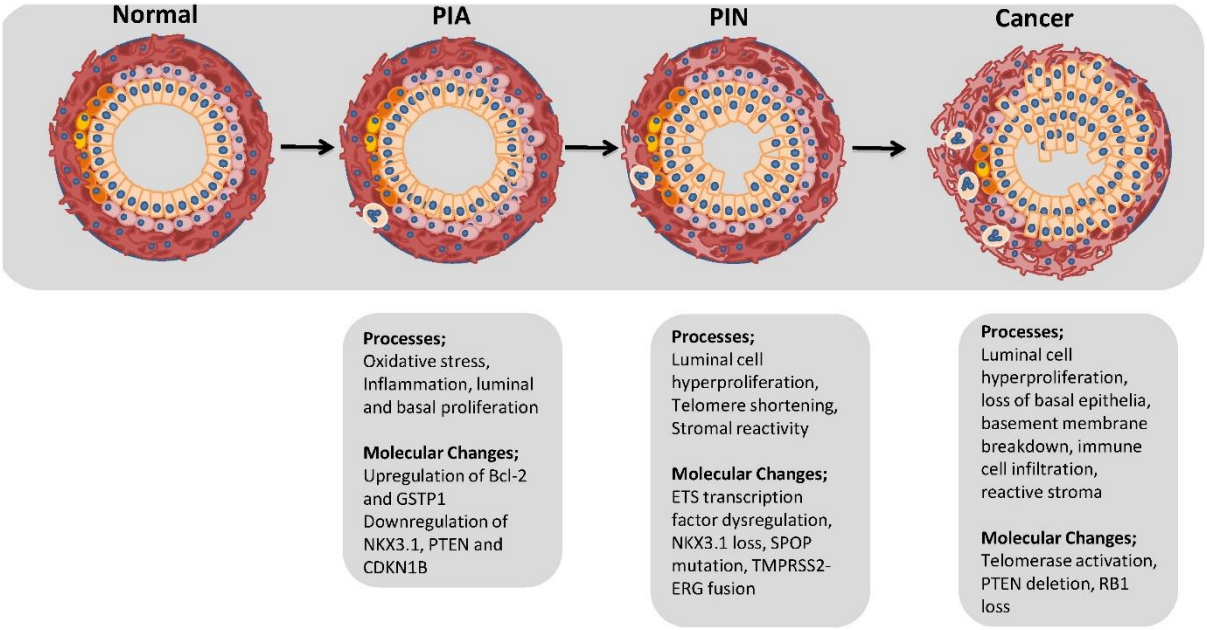

Figure 1.1. Phenotypic, micro-environmental and molecular changes incurred through the pre-malignant states of PCa.

Image taken from Packer *et al.* (8)

1.1.1 Androgen action in prostatic development

Androgens are mainly formed in the testes, which is controlled by the hypothalamic pituitary feedback system and accounts for more than 95% of total circulating testosterone. The adrenal glands produce the rest of the circulating androgens (Figure 1.2) (9). The prostate is entirely reliant on testicular androgens for both its growth and the preservation of its functional and structural integrity (10). The prostate is small weighing approximately 2 g during childhood but undergoes a period of rapid growth to approximately 20 g during puberty due to a rise in serum testosterone. This growth subsequently halts regardless of the sustained levels of androgen. This switch from rapid prostatic growth to a stable stage is maintained by an equilibrium of cell proliferation and death, which is controlled by androgen receptor (AR) signalling (10). Testosterone or its more potent metabolite, Dihydrotestosterone (DHT) is the main intracellular mediator of AR signalling, where on binding to the receptor, the AR dimerises, translocates to the nucleus, and AR-dependent gene transcription takes place (Figure 1.3) (11). Androgens are crucial for the development of the prostate gland and other reproductive organs in males *in utero* and there is early expression of AR in prostatic development (12).

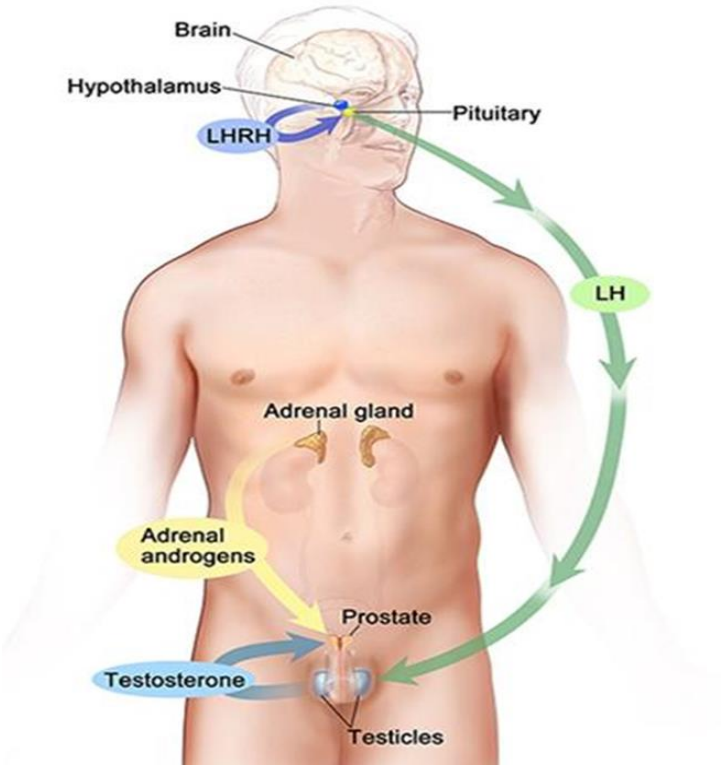

Figure 1.2. Androgen production in males.

Androgen production in males is regulated through the hypothalamic pituitary feedback system. Testosterone production is regulated by luteinizing hormone (LH) and luteinising hormone releasing hormone (LHRH). The hypothalamus releases LHRH, which stimulates the release of LH from the pituitary gland. LH acts on specific cells in the testes to produce the majority of testosterone in the body. Most of the remaining androgens are produced by the adrenal glands. Androgens are taken up by prostate cells, where they either bind to the AR directly or are converted to DHT, which has a greater binding affinity for the AR than testosterone.

Image taken from NCI (13).

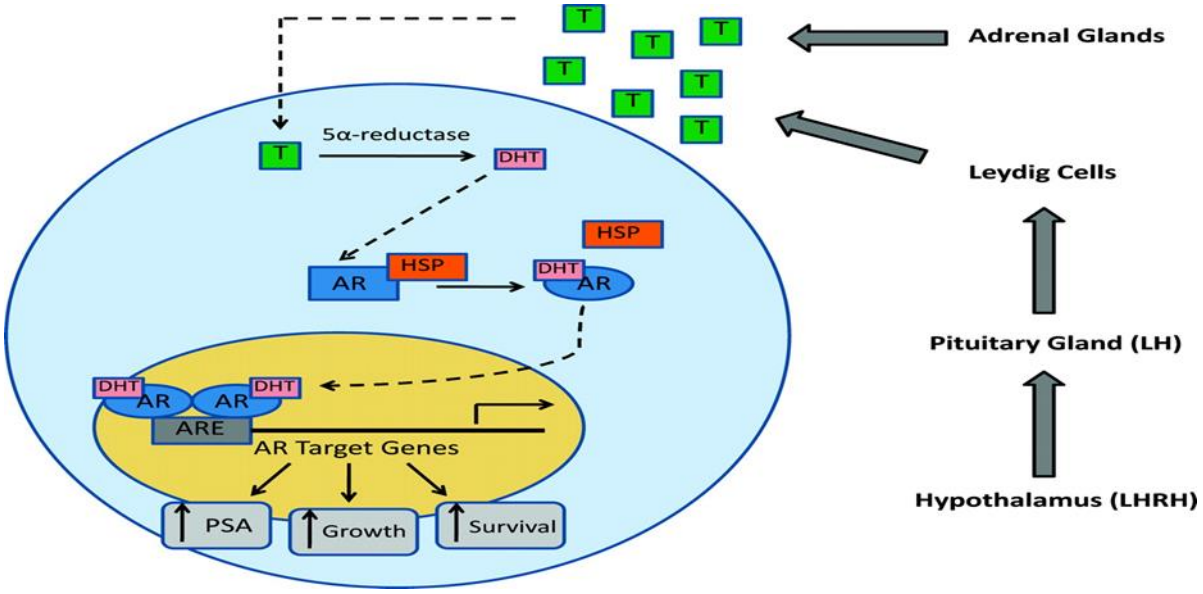

Figure 1.3. Mechanisms of androgen action and AR signalling in prostate cells.

Testosterone secreted from adrenal glands and leydig cells are converted to DHT intracellularly and binds to the AR resulting in AR dimerization, nuclear translocation, and AR-dependent gene transcription.

T, testosterone; HSP, heat-shock protein; ARE, androgen-responsive element; LH, luteinizing hormone; PSA, prostate-specific antigen.

Image taken from Saraon *et al.* (14)

1.1.2 AR structure and function in prostate cells

The AR is part of the steroid-thyroid-retinoid nuclear receptor superfamily found on the X chromosome (Xq11-12) spanning 180 kb of DNA with 8 exons (15). The AR consists of an amino-terminal activating domain (NTD), DNA binding domain (DBD) in the mid-region, hinge region and a carboxy-terminal ligand domain (LBD) (Figure 1.4). The NTD has an activation function (AF)-1 region that promotes transcriptional activity of the AR. The DBD comprises two zinc-finger domains, which recognise androgen-response elements (AREs), thus allowing for DNA-binding and transcriptional activation (16). The hinge region contains a nuclear localization signal that is exposed upon ligand binding to AR (17). The LBD contains an AF-2 region, which facilitates the binding of the AR ligand (testosterone or DHT) to the AR receptor and triggers down-stream androgen-signalling (18). Inactive AR is located in the cytoplasm, where it is complexed with chaperone proteins such as the heat shock protein (HSP) 70 and HSP40 to form a mature aporeceptor complex (19, 20). The LBD

of inactive AR undergoes a conformational change upon DHT ligand binding, resulting in the release of the chaperone complex, with phosphorylation, and dimerization of AR (20). The binding of HSP27 with the AR homodimer, prompts translocation to the nucleus and enables transcriptional activity of the AR (21). In the nucleus, AR can bind and promote transcription of specific genes by identifying sequence-specific regions of DNA, AREs. AR has also been shown to associate with other transcription factors via nuclear factor IB (NFIB) (22-24). AR transcriptional activity has been shown to substantially influence gene regulation within PCa cells. One study demonstrated that AR regulates the transcription of 1.5%–4.3% of all gene transcripts within LNCaP cells, which is a cell line that is representative of androgen-responsive PCa (25). The discovery of alternative splicing of the full-length AR mRNA transcript, which results in the production of AR variants (ARVs) more than two decades ago, has further increased the complexity of androgenic signalling (26). Many ARVs maintain the NTD and DBD, but are missing or contain variable LBD portions (Figure 1.4) (27, 28). It has been shown that ARVs can dimerize even without the presence of ligand by either homodimerising with one another or heterodimerising with full-length AR, thus resulting in the activation of AR target genes (29).

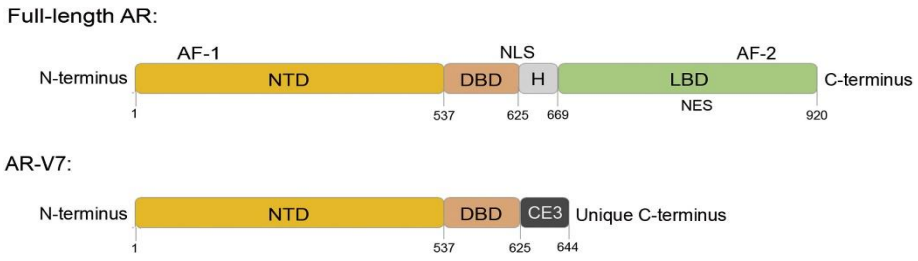

Figure 1.4. General protein structures of full length AR and AR-V7.

Full-length AR contains functional domains: NTD, N terminal domain; DBD, DNA-binding domain; H, hinge region; LBD, ligand-binding domain. General locations of the nuclear localisation signal (NLS) and nuclear export signal (NES) are indicated, along with regions of transcriptional activation function (AF)-1 and AF-2 binding sites. AR-V7 contains the NTD and DBD, but alternative splicing of the gene truncates the protein leaving only cryptic exon 3 (CE3) at the C-terminus. Numbers flanking domains indicate the approximate amino acid at that location.

Image taken from Vickman *et al.* (30).

1.2 Prostate Cancer

1.2.1 Epidemiology

PCa is the second most common invasive cancer in men worldwide (31). However, there is a high discrepancy in the incidence of PCa between countries (32). Oceania has the highest incidence of the disease, with an age-standardised rate (ASR) of 79.1 per 100,000 people followed by North America at 73.7 per 100,000 and finally Europe with 62.1 per 100,000 (32). This is in contrast to other nations such as Africa and Asia, where the incidence rate is lower (26.6 per 100,000 and 11.5 per 100,000, respectively) (32).The reasons behind this are complex and not fully understood, however, this may in part be attributed to variations in PSA testing (33). PCa is the fifth leading cause of male cancer-associated mortality globally (31). Central America has the highest mortality rates with 10.7 per 100,000, followed by Australia and New Zealand with 10.2 per 100,000 and Western Europe with 10.1 per 100,000, whereas countries in Asia have the lowest reported mortality (South-Central: 3.3 per 100,000; Eastern: 4.7 per 100,000 and South-Eastern: 5.4 per 100,000) (31). The PCa death rate increases with age and nearly 55% of all deaths occur after 65 years of age (31). In the USA, PCa is the second leading cause of cancer mortality among males (34) while in Ireland, PCa is the third leading cause of male cancer mortality with over 500 dying from it each year, which accounts for 11% of all cancer related deaths (35). Approximately 3,000 Irish men are diagnosed with the disease annually, however, most PCa cases are detected at an early stage in Ireland. Approximately 1 in 3 men (32%) are diagnosed at late stage (stage III/IV), and about 1 in 7 men (14%) are diagnosed at stage IV. The overall 5-year survival rate for Irish men diagnosed with PCa is around 97% (35). PCa survival in Europe has improved over time with the highest improvement witnessed in Eastern European countries (36).

1.2.2 Aetiology

Ageing is the most significant risk factor for the development of PCa, as autopsy studies performed in multiple countries has revealed widespread occult PCa in older men and a substantial increase in occult disease with age (37). For instance in an autopsy study of 249 cases, occult PCa was encountered in 2%, 29%, 32%, 55%, and 64% of men in the 3rd, 4th, 5th, 6th and 7th decades, respectively (38). PCa epidemiologic studies have revealed that

African Americans have a higher risk of PCa compared with other ethnic groups, and the disease also occurs at a younger age in this population (39, 40). The reasons for this are unknown and likely attributed to a combination of both genetic and environmental factors (37). Additionally, lower socioeconomic status or issues with healthcare access have been suggested as factors that contribute to the lower survival rate in African Americans with PCa (41). Genetic determinants are another important risk factor for PCa predisposition, particularly germline mutations in DNA repair genes such as BRCA2, which are also associated with more aggressive disease (42). Other factors, such as obesity, lifestyle and dietary factors appear to have limited roles in PCa predisposition (43-45). Hereditary PCa encompasses approximately 5% to 6% of all PCa cases and typically occurs 10 years earlier than sporadic cases (46). It is termed hereditary PCa when PCa is diagnosed in a family, which satisfies one or more of the following three criteria: (i) two relatives affected with PCa at 55 years of age or younger, (ii) three or more relatives affected with PCa or (iii) presence of PCa in each of three successive generations (46). Molecular studies have shown that PCa is genetically heterogeneous, with numerous genes having different penetrance and frequencies (47, 48). The first susceptibility locus for PCa on chromosome 1q23–25, known as Human Prostate Cancer 1 (HPC1) was discovered in 1996, this was followed by the detection of other candidate genes in this region, for instance mutations in RNASEL, appears to play a role in hereditary PCa carcinogenesis (47, 48). Other potential risk factors include vasectomy, sexual behaviour such as early intercourse or venereal disease and smoking history, however, the evidence remains inconclusive for these lifestyle factors (49-51).

1.2.3 Clinical manifestation and staging

Individuals may present with urinary retention, urinary frequency, urinary hesitancy, impotence, nocturia, and haematuria. However, most PCa cases are diagnosed at an early stage when people are asymptomatic (52), with abnormal prostate findings on digital rectal examination which is suggestive of PCa (52). The National Comprehensive Cancer Network (NCCN) guidelines recommended abdomen/pelvic computed tomography (CT) or magnetic resonance imaging (MRI) and conventional bone scan as part of initial staging workup and detection of metastases for those with newly diagnosed PCa (53). The American Joint Committee on Cancer (AJCC) TNM staging system is used to determine the stage of PCa

(54). The AJCC TNM system incorporates five pieces of vital information to stage the disease, where the T category evaluates the extent of primary tumour; the N category evaluates the lymph node status; the M category evaluates the extent of cancer metastasis to secondary sites; PSA level at diagnosis and grade group based on Gleason score. The disease is divided into four stages (I-IV) where stage I-II are considered as localised, stage III as locally advanced and stage IV as metastatic. Approximately 78% of people with PCa are diagnosed at a localized stage, 12% with regional lymph node involvement and 6% with distant metastasis based on the Surveillance, Epidemiology and End Results Program (SEER) data (55). Men with newly diagnosed PCa are classified into prognostic stage groups according to their risk of recurrence derived from the combined information of AJCC stage, serum PSA level and the histologic grade group based on the Gleason score (54). There is great variability in the clinical course of PCa whereby it can be an indolent, latent disease that will not result in clinical symptoms during a man's life time, however, it can also take an aggressive course, spreading into the bladder, seminal vesicles and metastasizing to lymph nodes, bones, lungs and other organs (56).

1.2.4 Current Diagnostic Strategies

PSA testing has transformed PCa diagnostics since its introduction as a serum tumour marker in 1987 (57). This is still the only universally utilized biomarker to identify men in whom a prostate biopsy would be appropriate. It also aids in monitoring the response to therapy in addition to its most contentious role, screening for the disease itself (58-60). Regarding its use in screening, it may lead to overtreatment of clinically indolent disease resulting in poor quality of life (61, 62). This is due to the scarcity of a useful screening tool to distinguish between indolent and aggressive disease (63). PSA is not an ideal biomarker due to poor tumor specificity and its level can be affected by many factors, such as prostatitis, trauma, age, and concomitant medication (64-66). Furthermore, there is no absolute PSA value below which there is a zero risk of disease (67). Thompson *et al.* demonstrated that approximately 15% of men with a PSA below the traditional cut-off of 4 ng/mL were still at risk for PCa and 15% of these men were diagnosed with high-grade disease (68). In one study, only 25%-30% of participants with PSA levels above 4 ng/mL were positive for the presence of cancer on tissue biopsy (69). When the cut-off value of 4 ng/mL is used, the specificity of PSA alone is only 12.8%, leading to a high false positive rate

and thus subjecting people to a high number of unwarranted successive biopsies (70). An ideal PSA cut-off point with both high sensitivity and specificity for a PCa diagnosis does not exist; however, many endeavours have been made to increase its diagnostic value. The Prostate Health Index (PHI), which combines PSA sub-forms [total PSA (tPSA), ratio between tPSA and free PSA (fPSA), isoform of proenzyme PSA (p2PSA)] into a diagnostic score has been appraised in a multicenter setting (71). Stephan *et al.* reported that PHI showed superior performance in detecting PCa compared to conventional PSA test alone (71). The group also found a significant association between high PHI score and higher Gleason score (71). PHI is one potential diagnostic marker test that has been endorsed by European Association of Urology (EAU); however, the level of evidence is still weak and this is not used in a clinical setting (72).

1.2.5 Current Prognostic Strategies

Risk stratification is crucial in providing the optimal treatment of PCa. Prognostic biomarkers are useful as part of risk stratification, where an individual's overall outcome can be evaluated such as the likelihood of cancer recurrence after standard curative treatment, which may dictate the need for adjuvant therapy (73). On the other hand, predictive markers seek to evaluate the probability of benefit from a specific therapy (73). Risk group stratification, which incorporates stage, grade and PSA has been extensively validated and provides better information for treatment recommendation compared to staging alone (74). The AJCC TNM system is used to determine the clinical stage at diagnosis, which is associated with survival (75). The Gleason grade delineates the histological features of the prostate carcinoma, which correlates with clinical behaviour (76). The International Society of Urological Pathology (ISUP) introduced a new PCa grading system in 2014 that assigns Gleason grade group from 1 to 5 (very low, low, intermediate, high and very high), which predicts the risk of recurrence after primary treatment, and has been validated in a several studies (77-79). This Gleason grade group system is superior to the Gleason score in terms of informing actual risk level and may prevent unnecessary treatment (77). Apart from using an individual's prognostic variables, a nomogram, which is a tool that combines the relevant prognostic parameters to generate more accurate results, can be used. A widely used nomogram, the Partin Tables, were the first used by urologists to counsel men with clinically localized PCa for the past few decades (80-82).

Other nomograms have also been developed according to the needs of a specific clinical settings such as assessing the risk of biochemical progression post curative therapy or suitability for active surveillance, however none has perfect prognostic precision (83, 84).

1.2.6 Current Predictive Strategies

The role of predictive markers in providing information on the likelihood of a positive or negative response to therapy is crucial for stratification, as the field of oncology enters the epoch of personalized medicine (85, 86). Tumour volume has significant value in selecting men with metastatic castrate sensitive disease for either upfront second generation anti-androgen therapy or chemotherapy in conjunction with traditional androgen deprivation therapy (ADT) (87, 88). ADT remains as the standard of care for the first-line treatment of metastatic PCa; however, eventually the disease will progress to castrate resistant PCa (CRPC), which is defined as progression of disease despite maximal ADT (89). Thus, it may be beneficial to identify markers to stratify people with CRPC to the plethora of second-line agents available. Recently, Antonorakis *et al.* have shown that those which are AR-V7 (which is an AR splice variant) positive had shorter progression-free survival (PFS), inferior PSA response rates and overall survival (OS) when treated with second generation antiandrogen therapy compared those who were AR-V7 negative (90). Individuals who were AR-V7 positive had a higher volume of disease, which may suggest that they have the overall poorer outcome (90). Another study has also indicated that AR-V7 positive PCa may benefit more from chemotherapy than hormonal therapy (91). However, in contrast, Bernemann *et al.* found that a subgroup of AR-V7 could still benefit from second generation antiandrogen treatment (92). Thus, AR-V7 might represent a marker of advanced disease and further prospective evaluation is required to determine its true predictive value. Additionally, the improvement in genetic analysis has led to increased recognition of mutations in genes that regulate DNA repair pathways especially homologous recombination (HR) and mismatch repair (MMR) in PCa (93). Approximately 15-25% of people with CRPC harbour somatic DNA repair gene mutations involving *BRCA1* or *BRCA2* and *ATM* (94). These cohorts have been shown to benefit from Olaparib, which is a type of PARP inhibitor (PARPi) (95) and platinum-containing chemotherapy (96). The flaws in the current diagnostic, prognostic and predictive strategies reflect the importance of molecular biomarkers in tailoring treatment in PCa.

1.2.7 Current treatments

Treatment choices such as radical prostatectomy, external beam radiotherapy (EBRT) or brachytherapy are principally recommended for localized curative PCa (97). Approximately 35% of men will experience a PSA relapse (98), and a higher relapse rate of 40–60% has been witnessed after EBRT or brachytherapy despite initial curative effort by radical prostatectomy for localized disease (99, 100). It is clinically challenging to deliver effective therapy to individuals with metastatic disease, however newer generations of antiandrogens are providing hope. The paramount rationale for treatment of metastatic PCa (mPCa) is to block the effect of androgens by either decreasing their circulating levels in the body or by impeding AR signalling, which can be accomplished through the exploitation of ADT such as LHRH agonists (e.g. leuprorelin acetate) or antiandrogens (e.g. bicalutamide), respectively (101). Treatment with ADT is the standard management for metastatic disease (89), providing an initial response of 18 months. However, resistance inexorably develops resulting in CRPC, which is currently incurable (101). CRPC is clinically defined as progression of disease despite androgen depletion with a serum testosterone level of ≤ 50 ng/dL (PCa Working Group 3) (102). Progression of disease can be defined by either one or both of the following criteria (Table 1.1) (103, 104).

Table 1.1. Types of disease progression in PCa.

Types of progression	**Definitions**
Biochemical progression	Three consecutive rises in PSA 1 week apart, resulting in two 50% increases over the nadir, and PSA >2 ng/mL.
Radiologic progression	The appearance of new lesions: either two or more new bone lesions on bone scan or a soft tissue lesion using the Response Evaluation Criteria in Solid Tumours (RECIST).

The treatment landscape of PCa has evolved rapidly in the last decade due to the greater availability and accessibility of therapeutic agents. In 2004, Docetaxel chemotherapy was first approved for the treatment of CRPC after being the earliest agent that successfully showed OS benefits (105). However, there was a scarcity of therapies that prolonged survival for those with CRPC until 2010. Since then, nine new treatments for CRPC that improve OS have been added to the inventory, comprising of chemotherapy (Cabazitaxel), novel second generation antiandrogens (Abiraterone, Enzalutamide, Apalutamide and

Darolutamide), immunotherapy (Sipuleucel-T), radionuclide therapy (alpha-radium 223 and Lutetium-177) and PARPi (Olaparib) (Table 1.2).

Table 1.2. CRPC treatments with an OS benefit.

Treatment	Trial	OS Benefit (Months)	Year (Reference)
Docetaxel + Prednisolone	TAX 327	2.4	2004 (105)
Sipuleucel-T	IMPACT	4.1	2010 (106)
Cabazitaxel + Prednisolone	TROPIC	2.4	2010 (107)
Enzalutamide	AFFIRM	4.8	2012 (108)
Abiraterone Acetate + Prednisolone	COU-AA-301	4.6	2012 (109)
Alpha-Radium 223	ALSYMPCA	3.6	2013 (110)
Apalutamide	SPARTAN	14	2018 (111)
Darolutamide	ARAMIS	6	2019 (112)
Olaparib	PROFOUND	3.4	2020 (113)
Lutetium-177	LuPSMA	4	2021 (114)

1.3 Enzalutamide

Enzalutamide competitively binds to the LBD of AR (108), thus hindering AR translocation, AR cofactor recruitment, and AR binding to DNA. Enzalutamide has been shown in previous phase 3 studies to prolong OS and PFS in participants who were chemotherapy naive (115) and in the cohort who had chemotherapy (108). However, between 20 to 40% of people present with intrinsic resistance, as measured by increasing PSA levels, and all will ultimately acquire secondary resistance resulting in disease progression (90). Although the precise mechanisms of enzalutamide resistance are yet to be completely understood, AR gene amplification arises during ADT and enables tumour growth in low androgen concentrations (116). Additionally, ARVs have also been implicated as a mechanism of resistance; AR-V7, may play a role in the development of resistance, as it is devoid of the LBD which is the target for enzalutamide (91, 117-119). Increasingly, there is a necessity to find clinically useful biomarkers to select people for enzalutamide therapy. An RNA biomarker would be of particular interest given they are easy to detect and quantify even

at very low abundance (120). Furthermore, RNA biomarkers possess the advantage in providing dynamic insights into cellular states and regulatory processes compared to DNA biomarkers and can be superior in terms of sensitivity and specificity compared to protein biomarkers (121, 122). Equally, refining our understanding of enzalutamide resistance will help to identify new biomarkers for therapy.

1.3.1 Enzalutamide Function at the Molecular Level

In 2006, 4-(3-(4-Cyano-3-(trifluoromethyl)phenyl)-5,5-dimethyl-4-oxo-2-thioxoimidazolidin-1-yl)-2-fluoro-N-methylbenzamide or MDV3100 or enzalutamide was synthesized, using RU-59063, which is a nonsteroidal agonist chemical scaffold (123). Enzalutamide has an eight-fold higher affinity to bind to AR compared to first-generation antiandrogens such as bicalutamide (123). Additionally, when enzalutamide binds to LBD, it also prevents N–C interaction, thus stopping nuclear translocation of the AR. On the other hand, first-generation antiandrogens do not prevent the N–C interactions when they bind to LBD, therefore allowing AR translocation to the nucleus, thus remaining as partial agonist (124). Partial agonism has been attributed to aberrant recruitment of coactivators to transcription complexes and consequent gene activation. Lastly, enzalutamide also prevents DNA binding and coactivator recruitment and consequently blocks AR signalling (125). Enzalutamide has a half-life of 5.8 days, which allows once-daily oral administration, and the molecule attains a steady state by day 28 (126). Enzalutamide is removed primarily by hepatic metabolism and some insignificant renal excretion (126).

1.3.2 Mechanism of Enzalutamide Resistance

1.3.2.1 AR amplification

The relative concentration of receptor to agonists and antagonists in a cell plays an important role in dictating the efficacy of antagonists in inhibiting their target during receptor-ligand interaction. AR protein overexpression was shown to be present in up to 80% of CRPC cases and approximately 30% of these had AR gene amplification (127). AR gene amplification, leading to AR overexpression, allows progression to CRPC even with the presence of very low circulating androgens levels (128). *In vitro* studies demonstrated higher levels of AR and AR splice variants in enzalutamide-resistant LNCaP compared to

enzalutamide-naive LNCaP cells (129). A recent study discovered that up to 50% of enzalutamide or orteronal (CYP17A1 inhibitor) pre-treated individuals were positive for AR amplification and had poorer response to treatment (130). Another study, the PREMIERE trial (n = 100), showed that participants with AR amplification had shorter PSA PFS (HR = 4.33; 95% CI, 1.94–9.68; $p < 0.001$), and inferior OS (HR = 11.08; 95% CI, 2.16–56.95; $p < 0.004$) (131). Numerous studies using liquid biopsies have similarly shown that AR amplification in circulating tumour DNA is associated with resistance to enzalutamide (132, 133).

1.3.2.2 AR Mutations

AR gene mutations are rare in primary PCa, however, it is estimated that up to 30% of CRPC cases could harbour the mutation in the re-biopsied tumour (134). In the setting of hydroxyflutamide and bicalutamide treatment, specific mutations at positions T877A and W741C in the LBD respectively, resulting in antagonist-to-agonist switch have been found in metastatic CRPC samples from people on these first generation antiandrogens (135, 136). Korpal *et al.* reported that F876L (substitution of phenylalanine for leucine at the 876 position) point mutation in the LBD alters the response to enzalutamide leading to enzalutamide resistance *in vitro* (137). The F876L mutation has also been shown in xenograft models treated with enzalutamide (138). Importantly, the F876L mutation was reported in the circulating tumour DNA of people on ARN-509 treatment, which is a drug compound with high chemical similarity to enzalutamide (139). The treatment withdrawal effects in terms of PSA improvement is witnessed in approximately 30% of those on hydroxyflutamide or bicalutamide upon stopping treatment. This reflects the paradox of antagonist-to-agonist switch, whereby the tumour regresses after drug discontinuation as AR mutations convert AR antagonists to agonists, thus facilitating tumour proliferation in the first place (140). At present, the frequency and clinical relevance of F876L mutation is uncertain in enzalutamide resistant disease. Enzalutamide withdrawal effects have been reported in an xenograft model, however, it is unclear if these events are also observed in the clinical setting (138, 141). There are pre-clinical data suggesting that enzalutamide and ARN-509 are at best weak agonists in the presence of the F876L mutation in contrast to hydroxyflutamide and bicalutamide, which has high agonist potency in the presence of T877A and W741C, respectively (138, 142).

1.3.2.3 AR Truncations

ARVs resulting in the absence of the LBD caused by somatic mutations in the AR gene were first described in advanced PCa in 2009 (29, 143, 144). Truncated ARs can arise through somatic mutations that introduce stop codons, which lead to intragenic deletions or alternative splicing of the primary transcript that result in a highly active, ligand-independent receptor variant (144). Since these truncated ARVs lack the LBD, they are unaffected by AR agonists or antagonists which target the LBD, thus they have an important roles in enzalutamide resistance (143, 145). ARVs can bind to canonical AREs on the chromatin, and drive transcription from AREs or heterodimerize with AR-FL and hence, are able to independently drive DNA repair and cell proliferation in CRPC (145-148). However, ARVs are very often observed in the presence of up-regulated AR-FL thus, its activity may be reliant on AR-FL (145, 148). There are numerous ARVs and they mainly appear in castration resistant settings especially after enzalutamide or abiraterone treatment (29, 143, 145, 148, 149). AR-V7 (AR3) is the most common ARV, which arises from aberrant mRNA splicing of *AR* exons 1-3, loss of exons 4-8 and inclusion of cryptic exon 3b (143, 150, 151). AR-V7 protein expression increases as people develop CRPC and resistance to enzalutamide (152-154). ARVs particularly AR-V7 in CRPC correlate with progression, poor survival, and treatment resistance (90, 150-154).

1.3.2.4 AR By-pass

The glucocorticoid receptor (GR) is a steroid hormone nuclear receptor, which has a very similar structure to the AR and can activate anti-inflammatory genes and suppress pro-inflammatory genes in cells (155-159). Overexpression of GR was reported in enzalutamide CRPC and is thought to mediate drug resistance through the bypass of AR signalling (160), as AR signalling normally inhibits GR expression. Enzalutamide causes enhanced GR expression through a de-repression mechanism by blocking AR signalling (160). From chromatin immunoprecipitation-sequencing (ChIP-seq) studies in enzalutamide-resistant cells, GR has been identified to bind over 50% of AR binding sites on the chromatin, and also regulate AR-regulated genes thus, it may serve as a functional substitute to AR (160). In addition, GR can promote PCa cell growth, for example by activating mutated ARVs, up-regulating the expression of HSPs or through effects on IL-6 signalling (160-162).

1.3.3 Novel Treatments

Novel small-molecule inhibitors targeting *AR* mutants are in development for example, darolutamide (ODM-201), which is an AR antagonist with the potential to inhibit three *AR* mutants (F877L, F877L/T878A, and H875Y/T878A). It has been shown to inhibit the growth of enzalutamide-resistant PCa *in vitro* and *in vivo* (163). Besides AR inhibitors, AR degradation enhancers are also under development such as ASC-J9 [5-hydroxy-1,7-bis(3,4-dimethoxyphenyl)-1,4,6-heptatrien-3-one], which has the potential to supress enzalutamide resistant PCa by degrading wild-type AR, AR-mutant and ARVs (164-172). In addition, BET [bromodomain (BRD) and extraterminal] inhibitors target the amino-terminus of BRD proteins, BRD4, and inhibit proliferation in CRPC. BET inhibitors such as JQ1 have been shown to inhibit the expression of AR-FL and AR-V, thus overcoming enzalutamide resistance; however, recent studies have shown acquired resistance to BET inhibitors in CRPC cells (173-175).

1.3.4 EMT in Enzalutamide Resistance

1.3.4.1 EMT

Epithelial mesenchymal transition (EMT) is a phenomenon when epithelial cells go through morphological alterations giving rise to a mesenchymal phenotype, which contributes to metastatic progression and treatment resistance (176, 177). Recently, numerous studies have established the presence of EMT-like states in PCa, suggesting its involvement in PCa development and metastasis (178, 179). Metastasis formation requires sequential steps such as dissemination, invasion and colonisation under a dynamic tumour microenvironment, which results in increased invasiveness and migratory ability of primary tumour cells (180-182). The loss of cellular properties of epithelial cells such as cell polarity and cell-cell adhesion accounts for its metastatic potential as well as contribution to therapeutic resistance (180-182). Additionally, several studies have shown that the EMT phenomenon can be induced by enzalutamide treatment through a number of mechanisms, such as Snail induction, up-regulation of *TGF-β1* and activation of *STAT3* (183-185). EMT also functionally protects tumour cells from immune surveillance, apoptosis and is capable of inducing tumour heterogeneity by conferring tumour cells with stem cell-like properties (186, 187). Further knowledge of the mechanisms contributing to EMT initiation

in PCa resistance could provide new therapeutic strategies to combat enzalutamide resistance.

1.3.4.2 Markers of EMT

Synchronized loss of epithelial (E-cadherin, β-catenin) and gain of mesenchymal (N-cadherin, SNAI1, vimentin, fibronectin, and α-smooth muscle actin) markers, signify the hallmarks of EMT where the tumour garners enhanced production of extracellular matrix elements, apoptosis resistance and metastatic invasive abilities (188, 189).

SNAI1 is capable of repressing the expression of the adhesion protein E-cadherin hence promoting EMT in epithelial tumours (190, 191).

E-cadherin is encoded by CDH1, which resides on chromosome 16q, is crucial in the preservation of epithelial phenotype however; 16q is a site of frequent allelic loss in PCa (192). E-cadherin plays an important role in facilitating intercellular adhesion by acting as a calcium dependent adhesion protein, forming networks between actin microfilaments (via α- and β-catenin) and immunoglobulin domains (189). Suppression of E-cadherin alone is enough to induce EMT (193), and trigger numerous transcriptional pathways that contribute to metastasis (194). Aberrant promoter methylation resulting in epigenetic changes is commonly attributed to the loss of E-cadherin expression (195). Metalloprotease-mediated cleavage of the E-cadherin protein resulting in the severance of E-cadherin from the cadherin/catenin complex leads to cell invasion in PCa (196). In high-grade prostate adenocarcinomas, the loss of E-cadherin is a common feature and is prognostic for survival (197, 198). A functional change from E-cadherin to cadherin-11, which is an osteoblast calcium dependent adhesion molecule during EMT, has been implicated in prostate metastases to bone (199).

TWIST1 and ZEB1 are two families of transcription factors that can directly regulate EMT. TWIST1 is able to induce metastasis (200) as well as EMT. TWIST1 plays an important role in Epithelial Growth Factor (EGF) induced EMT, whereby EGF causes tumour progression through coordinated Reactive Oxygen Species (ROS) production, the phosphorylation of *STAT3* and subsequently triggers of ROS/STAT3/HIF-1α/TWIST1/N-cadherin signalling pathway (201). ZEB1 may be an important mediator of EMT in PCa as the expression increases following castration and is associated with chemotherapy

resistance (202, 203). ZEB1 has been shown to mediate androgen deprivation–induced EMT via a bidirectional, negative feedback loop with AR (202).

N-cadherin is part of the type I Cadherin family that mediates cell-to-cell adhesion however, it confers increased motility and aggressiveness as shown by studies where it is capable of promoting tumour invasion regardless of presence of E-cadherin, reflecting that its effects predominate the suppressive roles of E-cadherin (204). Studies evaluating N-cadherin silencing, showed that it suppresses PCa growth and metastases, suggesting its potential therapeutic value (205). N-cadherin is also a prognostic marker of clinical recurrence after radical prostatectomy and emergence of CRPC (206).

Other phenotypic EMT markers play physiologic roles in cell-to-cell dynamics such as the catenins, which form complexes that stabilizes cell-to-cell adhesion through the actin cytoskeleton connections. Expression levels of α- and β-catenins are down-regulated in PCa with high clinical tumour grade and stage (207). Vimentin is a type III filament protein expressed in mesenchymal cells, which can act as a dynamic tether that maintains cell integrity. Vimentin overexpression is observed in aggressive, castrate resistant PCa cells (208) It is known to amplify the invasive phenotype, however does not confer migratory potential *in vitro* on its own (209).

1.3.4.3 Androgen signalling in EMT

Androgens can influence the process of EMT directly, by suppressing E-cadherin expression in prostate epithelial cells and trigger the expression of mesenchymal markers (210). Treatment with DHT has been shown to increase SNAI1 expression, independent of TGF-β signalling (211). TWIST1 can regulate AR expression in PCa cells during oxidative stress, reflecting its possible contribution to drug resistance in CRPC through an AR-dependent mechanism (212). However, the role of androgens in the control of EMT are controversial as some *in vivo* and *in vitro* PCa studies have demonstrated that EMT induction is due to androgen deprivation (202, 213) or low AR environment (214). These studies have shown a link between increased N-cadherin, androgen deprivation and metastasis formation (203, 205, 213, 214). For instance, androgen deprivation increases the expression of both N-cadherin and ZEB1 and is associated with chemotherapy resistance (202, 203). ZEB1 is a transcription factor with AR transcriptional suppressor potential where the expression of ZEB1 is greatly increased after chemical or physical castration in LuCaP35 normal prostate

xenograft model and LNCaP cell line (202). In contrast, ZEB2 expression is positively regulated by androgens in LNCaP cells (215). Excitingly, studies have shown that miRNAs are involved in the post-transcriptional modulation of ZEB2 expression mediated by AR (216). For instance, miR200 targets ZEB proteins responsible for the control of EMT (217).

1.4 Potential RNA biomarkers in PCa

A large proportion of the human genome (70-90%) is transcribed into RNA, however most RNA transcripts are non-coding and only 2% of the genome encodes for protein (218). Non-coding RNAs are starting to gain recognition as one of the key mediators in gene regulation (219-221). These vital players can generally be categorised into either small ncRNAs (<200 nucleotides long) which include micro RNA (miRNA), small nucleolar (snoRNA), piwi-interacting RNA (piRNA) or long non coding RNA (lncRNA) (>200 nucleotides long) and circular RNA (circRNA) (219-221) (Figure 1.5). The advent of Next Generation Sequencing (NGS) has furthered the understanding of the genomic and transcriptomic architecture of prostate and other cancers (94, 222), which has resulted in molecular biomarkers and new therapeutic strategies. Recently there has been a resurgence of interest in the role of non-coding RNA (ncRNA) in PCa biology where both miRNA and lncRNA, have been studied widely (223). Another recently discovered type of ncRNA, circRNA, appears to have important roles in cancer initiation, progression and treatment resistance and thus may potentially be an ideal biomarker (224-227).

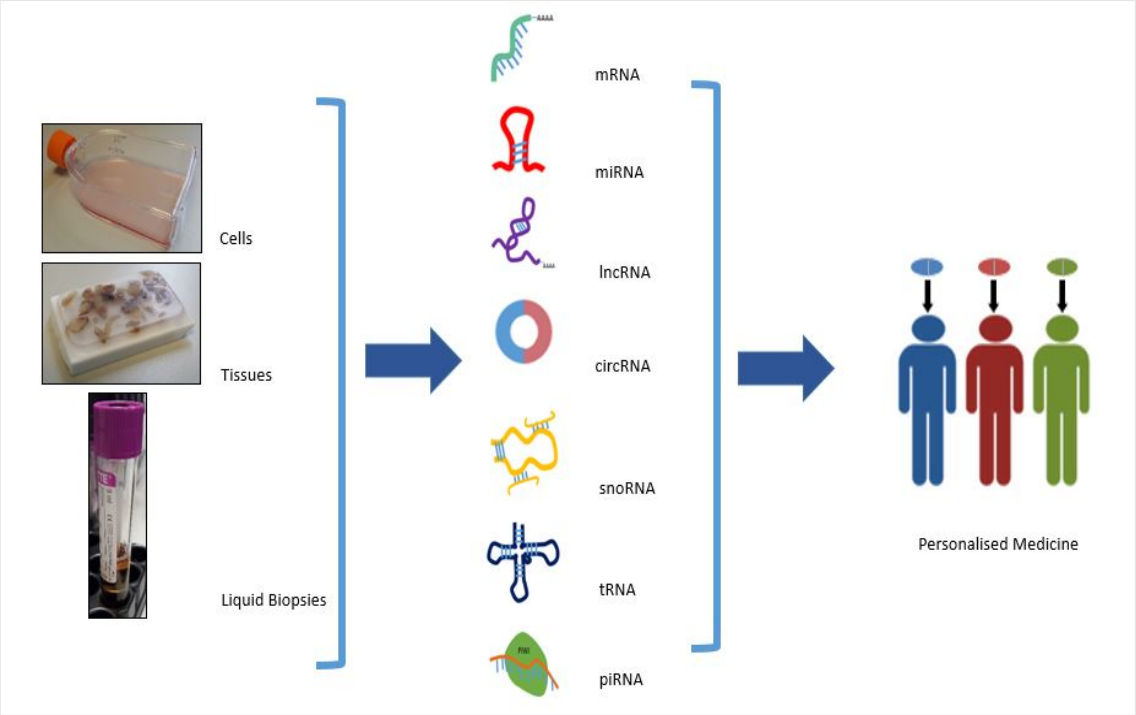

Figure 1.5. Schematic representation of candidate RNAs as potential biomarkers for PCa. Image taken from Lim *et al.* (228)

1.4.1 miRNA as a biomarker in PCa

miRNAs are approximately 22 nucleotides in length with the ability to regulate genes post-transcriptionally (229). miRNA originates from the primary transcript (pri-miRNA), which is initially processed into approximately 70 nucleotides long hair pin precursor miRNA (pre-miRNA) by cellular RNase III (Drosha) and double stranded RNA-binding domain protein (DGCR8) (230). Another RNase III (Dicer), then cleaves the pre-mRNA to form duplex strands termed miRNA-5p and miRNA-3p, whereby the '5p' and '3p' are named according to the 5'- or 3' arm of original transcript (230). miRNAs can exhibit affinity to bind to 3' untranslated region (UTR) of mRNA or to 5' UTR of mRNA leading to direct mRNA cleavage and translational repression (231). Besides gene repression, miRNA can directly or indirectly activate gene expression (232). Through these regulatory functions, miRNA is involved in cellular differentiation, proliferation, migration and apoptosis (233). miRNA can be considered as either an Onco-miR, if it inhibits tumour suppressor genes; or a tumour suppressor-miR if it inhibits proto-oncogenes (234). These critical functions have led to extensive investigations into the capacity of miRNAs to act as clinically relevant biomarkers in PCa for the past decade (Table 1.3) (235).

In 2006, Volina *et al.* (236) first observed a general trend of up-regulated miRNA expression in PCa, which was later supported by Ambs *et al.* in 2008 (237). Song *et al.* further validated this general up-regulated trend using NGS in 2015 (238). In contrast, several studies observed a general down-regulation of miRNA expression in PCa compared to the normal prostate (239, 240). This discrepancy in expression between studies may be linked to small sample size or variation in technical protocols. In 2012, Martens-Uzunova *et al.* utilized NGS and miRNA microarray, with results of both platforms cross validated by RT-qPCR, to analyse miRNA expression in 102 fresh frozen samples from those whose PCa had progressed (241). The group constructed a miR predictor consisting of 25 miRNAs, which could identify good prognosis and poor prognosis subgroups, comprising 13 miRNA that were down-regulated and 12 that were up-regulated (241). The same group examined an additional set of 49 PCa tissues and 25 normal controls for the presence of these 13 preselected miRNAs. Four miRNAs (miR-96-5p, miR-183-5p, miR-145- 5p, miR-221-5p) were selected to construct a miR index quote (miQ) based on the best diagnostic discrimination whereby two were up-regulated (miR-96-5p and miR-183-5p) and two were down-regulated (miR-145-5p and miR-221-5p). The group reported that the miQ score had good capability for diagnosing PCa with high accuracy (AUC: 0.931) and predicting tumour aggressiveness (AUC: 0.895), metastatic status (AUC: 0.827) and OS ($p = 0.0013$, Wilcoxon test HR = 6.5, median survival 2 *vs*. 5 years) (242). miR-96 can mediate cell proliferation and cell growth through *FOXO1* inhibition in PCa (243). miR-183 can regulate *PTEN*, which is a known tumour suppressor in PCa (244). Overexpression of miR-145 in PC3 PCa cells has been reported to cause cycle arrest and apoptosis as a result of up-regulating the pro-apoptotic gene, *TNFSF10* (245). miR-145 was also found to inhibit EMT, suggesting that a reduction of miR-145 may trigger some form of the metastatic cascade (246). Spahn *et al.* reported that down-regulation of miR-221 is correlated with up-regulation of c-Kit (247) and two other studies have shown the potential of c-Kit involvement in PCa bone metastasis progression (248, 249). Zheng *et al.* in 2014 further showed that low miR-221 (part of the miQ score) levels are associated with a higher biochemical recurrence rate after radical prostatectomy (250), in addition to its association with a PCa diagnosis (241, 242). However, the data is conflicting. Yaman *et al.* reported significantly higher expression of miR-221 in blood plasma of people with metastatic PCa compared to those with localized disease (251). miR-221 is associated with metastasis formation, thus in conjunction with

miR-141 could potentially be used to detect men with bone metastasis from those with localized disease (AUC: 0.755) (251). Furthermore, Sun *et al.* found significant expression of miR-221 in CRPC cell lines and tissue (252, 253). The study showed that up-regulation of miR-221 decreases HECTD2 or RAB1A, which promotes androgen independent PCa cell growth (254).

Table 1.3. miRNA expression in PCa and associated clinical outcomes.

miRNA Expression	**Samples**	**Associated Clinical Outcomes**	**Reference**
miR-96 ↑	Tissue	Increase biochemical recurrence Decreased recurrence-free survival.	(255)
miR-96 ↑	Tissue	Poor overall survival Increase tumor aggressiveness.	(243)
(miR-96-5p, miR-183-5p) ↑*, (miR-145-5p, miR-221-5p) ↓*	Tissue	Distinguish PCa from normal control. Increase tumor aggressiveness. Increase metastatic risk. Poor overall survival.	(242)
miR-221 ↓	Tissue	Increase biochemical recurrence.	(250)
(miR-21, miR-22, miR-141) ↑	Plasma	Distinguish PCa from normal control. Distinguished between metastatic and localized disease.	(251)
(miR-141, miR-375) ↑	Serum, Tissue	Associated with high risk PCa (Gleason score and lymph node involvement).	(256)
(miR-20a, miR-21, miR-145, miR-221) ↑	Plasma	Associated with high risk PCa (CAPRA and D'Amico score).	(257)
(miR-107, miR-574-3p) ↑	Urine	Distinguish PCa from normal control.	(258)
(miR-200b, miR-200c) ↑	plasma	Associated with high risk PCa (Gleason score, PSA, metastasis).	(259)

↓= decrease, ↑= increase, * part of miQ score

1.4.2 lncRNA as a biomarker in PCa

lncRNA is a group of non-coding RNA > 200 nucleotides in length. So far, 105,255 lncRNAs have been identified in the human genome (260). lncRNAs play a role in the regulation of gene expression affecting transcription and translation through chromatin complex

modulations (261, 262). In cancer, lncRNA may promote cell proliferation, invasion and progression, angiogenesis and facilitate resistance to apoptosis (263). Many lncRNA exhibit specific cell type expression patterns and have both nuclear and cytoplasmic localisation (262, 264). Given that lncRNA are present in bodily fluids such as urine, blood and serum and express specifically at different stages of PCa (265, 266), they may be a good candidate biomarker. For example *PCA3* (PCa Antigen 3) was discovered in 1999 and has been the primary focus as a prostate biomarker (267, 268). The PCA3 level was increased approximately 100-fold in PCa tissue compared to paired normal prostate tissues (267). Furthermore, *PCA3* knockdown led to an up-regulation of E-cadherin, claudin-3 and CK18 and down-regulation of vimentin, which suggests its involvement in EMT (269). Besides, it may also inhibit AR signalling, cell growth and viability (269). Additionally, *PCA3* regulates the expression of genes associated with angiogenesis, signal transduction and apoptosis (269). PCA3 can also regulate miR-1261 by acting as a miRNA sponge when the transcription factor SNA1L binds to its promoter region. This in turn, reduces miR-1261, resulting in increased expression of *PRKD3* (270). The high *PRKD3* expression can promote invasion and metastatic progression of PCa (270). Another study showed that knockdown of *PCA3* sensitized PCa cells to Enzalutamide (271), thus PCA3 may act as both a potential diagnostic and therapeutic biomarker. Urinary PCA3 diagnostic performance has been validated in a multicentre study of 534 men showing a sensitivity of 65% and specificity of 66% compared to serum PSA, which has the same sensitivity (65%) but lower specificity (47%) (272). Urinary PCA3 assay (Progensa) was approved by the FDA in 2012 for men above 50 years of age for whom a subsequent biopsy is otherwise warranted after previous negative biopsies (273). Urine from post digital rectal examination is used for Progensa assay and a PCA3 score is obtained from the ratio of PCA3 RNA to PSA RNA detected. PCA scores of <25 are considered low risk of PCa whereas PCA3 scores of ≥25 are considered high risk with more than 25% chance of a positive biopsy result (274). The sensitivity and specificity depend on the cut off value of the PCA3 score. For instance, Leyton *et al.* showed that a PCA3 score of 25 would provide a sensitivity of 82% and specificity of 50.8%, however with a PCA3 score of 35 the sensitivity would decrease to 68.4% but specificity would increase to 58.3% (265). Recently, a meta-analysis of 46 clinical trials consisting of a total of 12,295 participants who used urinary PCA3 for diagnosing PCa reported that the pooled sensitivity was 0.65 (95% confidence interval [CI]: 0.63–0.66) and specificity was 0.73 (95% CI: 0.72–

0.74) (275). Although PCA3 has improved specificity, it is not sensitive enough as a standalone diagnostic biopsy decision tool.

Metastasis associated lung adenocarcinoma transcript 1 (MALAT 1), a lncRNA initially investigated in lung cancer, is also expressed in PCa tissues and cell lines, with the expression level associated with high Gleason score, PSA score, and tumour size reflective of a poor risk subgroup (276). Furthermore, the level of MALAT 1 increases during the transition from castration-sensitive to castration-resistant as reported by Ren *et al.* (276). The group also found that MALAT 1 suppression in cell lines led to a reduction in cell growth and invasion as well as inducing cell cycle arrest and promoting apoptosis (276). When suppressed in PCa xenografts, in castrated nude mice, it reduced tumour growth and metastatic progression thus demonstrating its capability of acting as a potential therapeutic target (276). The same group examined MALAT 1 derived from plasma (MD-miniRNA) as a means to detect PCa. The levels were significantly raised in 196 people with PCa and had a sensitivity of 58.6% and specificity of 84.8% in distinguishing a person with PCa from a healthy control making it a potential non-invasive diagnostic biomarker (266). The diagnostic accuracy to distinguish people with PCa compared to healthy cohort was further demonstrated by Xue *et al.* showing AUC 0.86 (95% CI: 0.80–0.93) and 0.79 (95% CI: 0.70–0.88), respectively (277). MALAT 1 also has the potential of being a predictive biomarker. Wang *et al.* determined that enzalutamide resistant PCa cell lines have increased levels of MALAT 1 and SF2 activity, whereas MALAT 1 may enhance AR-V7 splicing by forming a MALAT 1-SF2 complex leading to enzalutamide resistance (169). In addition, Sebastian *et al.* reported that MALAT 1 might promote PCa bone metastasis through down-regulation of Sost pathway (278). The diagnostic capability of urinary MALAT 1 was evaluated in a retrospective-prospective study of 434 men (279). Wang *et al.* showed that by using the MALAT 1 model, unnecessary biopsy could be safely avoided in up to 46.5% of diagnostic grey zone cohorts where their PSA lies between 4–10 ng/mL (279).

1.4.3 circRNA as a biomarker in PCa

circRNA is a class of endogenous RNA that is produced from backsplicing of exons, introns, or both to form exonic or intronic circRNAs, which were first discovered in the early 1990's (220). However, they were initially thought to represent by-products of splicing error until recently (220, 280-282), when the appeal of circRNA research was resurrected by Salzman

et al. (283). In 2012, during an effort to find genomic rearrangements in RNA-seq samples of paediatric acute lymphoblastic leukaemia, the group found an excessive number of RNA transcripts in which the exons were arranged non-canonically (283). These excessive RNA transcripts were then validated as circRNA by quantitative PCR (RT-qPCR). This substantial amount of circRNAs in RNA sequenced samples suggested that they may be more abundant and of significant importance than previously perceived (283). Two other groups further developed the methods of circRNA detection by locating specific backsplice junction *de novo* from RNA-seq libraries using bioinformatics analyses, which strengthen the foundation of circRNA detection (220, 284). Since then, numerous biochemical devices have been added to the armamentarium with the addition of bioinformatics analyses, which enhances the ability to detect and quantify the expression of new circRNAs. circRNA has been proven to represent a distinct class of ncRNAs, with the 3' and 5' ends connected together resulting in the formation of covalently closed continuous loop, which makes it resistant to degradation by RNA exonucleases (220, 285). Thus, circRNA is present abundantly in the cytoplasm owing to its stability and cellular levels may be regulated by either removal by exosomes or endonucleic activity (286). This triad of stability, abundance and evolutionary preservation between species indicates that circRNA may have significant regulatory function (287). In addition, circRNA is expressed in pathological conditions coupled with tissue specificity, which further begs the question of their role in malignancy and other human diseases (288).

1.4.3.1 Biogenesis and general functions of circRNA

circRNA, are generated by low efficient backsplicing, which disregard the canonical 5' to 3' polarity (289, 290) in contrast to linear RNA transcripts with a 5' to 3' polarity that is formed by high efficiency canonical pre-mRNA splicing, whereby the introns are removed leading to the joining of exons catalysed by the spliceosomal system (289). This low efficient backsplicing can be catalysed by either the spliceosomal machinery or by group 1 and 2 ribozymes (289, 290). A covalently closed circRNA accompanied by a spliced linear RNA with a skipped exon is formed when backsplicing ligates the downstream splice donor site reversely with an upstream splice acceptor site (289). The unique features that distinguish circRNA from linear RNA is the absence of a terminal structure such as a 5' cap or polyadenylated A (poly A) tail as a result of covalently closed loop (284). Backsplicing

usually works in tandem with canonical splicing, leading to production of circRNAs that contain multiple exons derived from internal exons of pre-mRNAs (291). The role of spliceosome in circRNA biogenesis can be proven where inhibition of canonical spliceosome by utilising isoginkgetin, a pre-mRNA splicing inhibitor decreases circRNA levels as well as linear RNA (292). There are three different types of circRNA depending on whether they arise from exons or introns; exonic, intronic and exon-intronic circRNA (Figure 1.6). Exonic circRNA arises when 3' splice donor joins to 5' splice acceptor during pre-mRNA splicing. Exon-intronic circRNA arises when the intron between exons is retained. Intronic circRNAs arise from intron lariats, which are unaffected by debranching enzymes and it is different from exonic circRNA due to expression of 2' to 5' linkage (220, 285). Both cis-elements and trans-factor are needed to direct the downstream donor and upstream acceptor sites to close proximity in order to facilitate spliceosome assembly during backsplicing thus improving the catalytic efficacy of spliceosomal system (289).

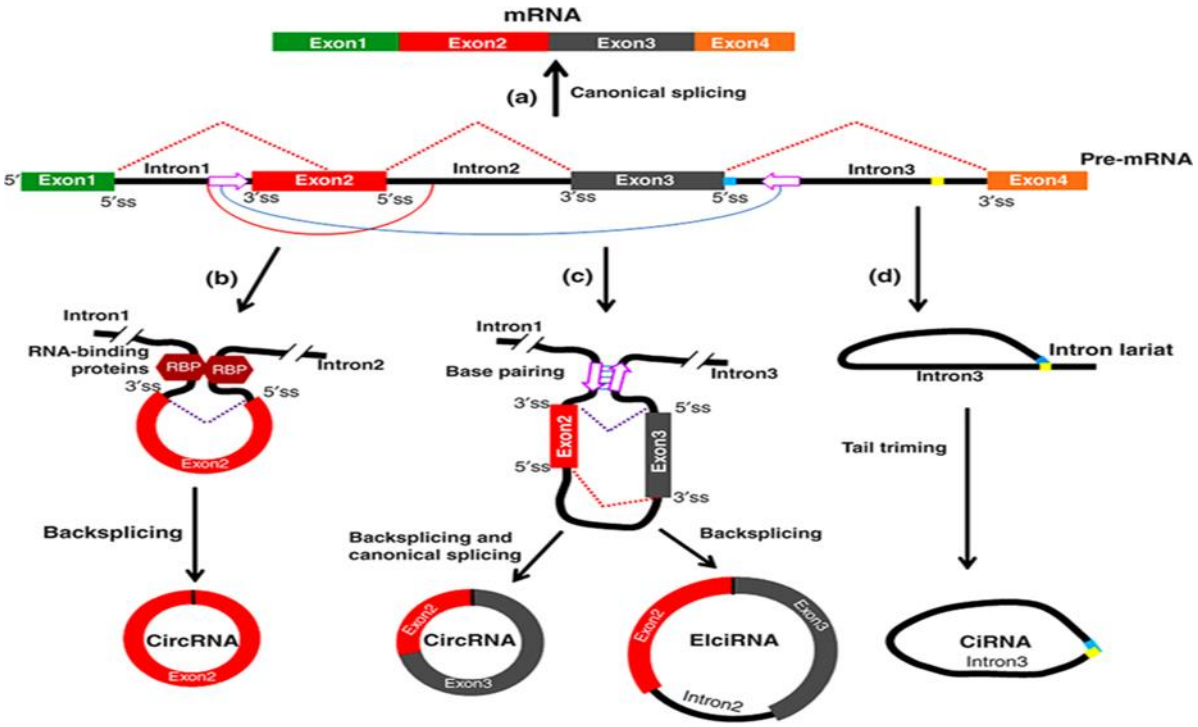

Figure 1.6. Schematic representation of splicing events leading to the generation of circRNA. (a) The canonical splicing machinery conventionally generates normal mRNA. (b) Exonic circRNA is generated through non-canonical splicing (backsplicing) through the unique 'head-to-tail' joining of the 5' splice site (ss) donor site to a 3' ss acceptor site. RNA-binding proteins (RBPs) or transacting factors can bridge two flanking introns close together. The introns are then removed to form a circRNA. (c) Reverse complementary sequences (purple arrows) in Intron1 and Intron3 can pair and bring the 5' ss of Exon3 close to 3' ss of Exon2, promote circularization of Exon2 and Exon3 with a retained intron, and form an exon–intron circRNA (EIciRNA). In addition, backsplicing in combination with canonical splicing may lead to the formation of circRNA with Exon2 and Exon3 only. (d) The circular intronic RNA (ciRNA) is derived from the lariat intron excised from pre-mRNA by canonical splicing machinery and depends on the presence of consensus RNA sequences (yellow bars) to avoid debranching of the lariat intron to form stable ciRNAs. The red and blue dotted lines indicate linear and head-to-tail backsplicing, respectively.

Image taken from Panda *et al.* (293)

RNA binding proteins (RBPs) are another important component in circRNA formation where they may serve as regulatory activators or inhibitors (294). For instance, muscle-blind (MBL) protein, which is a type of RBP found in fruit fly can bind to pre-mRNA and induce backsplicing resulting in the promotion of circRNA production (295, 296). Additionally, Quaking (QKI) protein is another RBP known to regulate circRNA by affecting pre-mRNA, mRNA turnover and translation, which has been associated with cancer and other diseases (294, 297). Interestingly, even though circRNAs have been categorised as non-coding RNA, a recent report suggested that eukaryotic ribosomes have the ability to initiate translation on circRNA that contains internal ribosomal entry sites (IRES) through a rolling circular amplification mechanism (281, 298). On the other hand, circRNA can also be translated into protein even without an IRES sequence or poly A, indicating the possibility of other translational mechanisms (299, 300). The classically described role of miRNA sponging to regulate mRNA stability and translation is but just one of the many other potential functions of circRNAs (Table 1.4) (287). Many studies have shown that circRNAs play a crucial regulatory role as miRNA sponges with ciRS-7 being one of the best examples (226, 287). ciRS-7 contains more than 70 miR-7 targets sites that can inhibit the activity of this specific miRNA leading to an increased level of miR-7 target genes (287). Apart from acting as molecular sponges, circRNA have also been shown to stabilize miRNAs (301). For instance, circCSNK1G3 interaction with miR-181b/d does not inhibit the activity of the specific miRNA, however, a reduction in the level of the circRNA expression prevents miR-181b/d from inhibiting its target genes (*CBX7, CDK1, and CDC25A*) (301). circRNAs can regulate transcript splicing and parental gene transcription by binding to RBPs (295). For instance, circMbl could sponge MBL protein when the protein is in excess and decreases the production of its own mRNA by promoting more circMbl production through negative feedback regulation (295). Another study showed that circEF3J and circPAIP2, which are confined primarily in the nucleus, interact with the U1 small nuclear ribonucleoprotein (U1 snRNP) and RNA Pol II to increase the transcription of their parental genes and knockout of the circRNAs reduced the transcript levels (302). circRNAs can also bind to RBPs to regulate translation where a study has shown that circMYBL2 recruits RBP PTBP1 to regulate the mRNA translation of the oncogene FMS-like tyrosine kinase-3 (FLT3) resulting in the development of white blood cells harbouring FLT3-internal tandem duplication mutations (303). Additionally, circRNA may act as a protein scaffold by binding to multiple RBPs, which

enables stable interactions (304). For instance, circAmotl1 can bind to 3-phosphoinositide-dependent protein kinase 1 (PDK1) and protein kinase B (AKT1) to promote PDK1-dependent AKT1 phosphorylation (304). Furthermore, circRNA containing AUG sites and open reading frame (ORF) could be driven by the IRES and translated into the functional protein (298). circRNA may be involved in the tumor autophagy affecting occurrence and progression of human cancer where reduced expression of circHIPK3 was shown to act as an autophagy regulator in STK11 mutant lung cancer cells through regulating the miR124-3p/signal transducer and activator of transcription 3 (STAT3)/protein kinase AMP-activated catalytic subunit alpha 2 (PRKAA)/AMP-activated protein kinase (AMPKα) signaling regulatory pathways (305).

Table 1.4. General functions of circRNA.

Function	**Reference**
Act as miRNA sponges	(287)
Regulate gene splicing, transcription and translation	(295, 298, 302, 303)
Interact with RBPs and act as protein scaffolds	(304)
Act as autophagy regulator	(305)

1.4.3.2 Methods of detection and sensitivity

1.4.3.2.1 Biochemical Methods

A RNA exonuclease enrichment procedure can be performed as part of circRNA enrichment and to assess whether RNA is indeed circular where the 5’ and 3’ ends are linked covalently with the absence of poly-A tail. Ribonuclease R (RNAse R), an exoribonuclease that digests all linear RNAs from its 3’ to 5’ end but does not degrade circRNAs due to lack of free ends is a helpful tool, however, it may introduce technical artefacts from circle degradation in some instances and some linear RNA are resistant to degradation (306, 307). XRN1 is an alternative 5’ to 3’ exoribonuclease similar to RNAse R that can be used (308). RNAse H, which is an endoribonuclease can also be used to assess for circularity (309). Tabak *et al.* showed that 2D polyacrylamide gel electrophoresis can differentiate circRNA from linear RNA whereby circRNA travels in an arc on the gel compared to linear RNA, which travels diagonally (310). Other methods for circRNA enrichment in sequencing libraries other than exoribonuclease and 2D gel strategy includes the use of ribosomal RNA (rRNA) and poly-A

depletion, however none can provide full certainty that the enriched RNA are purely circular (311).

Reverse Transcription-PCR (RT-PCR) is the primary tool that can be used for circRNA identification. circRNA, which is converted to cDNA through reverse transcription harbour a unique diagnostic exon-exon junctional sequence that differs from canonically spliced mRNA enabling specific primer creation. These specific primers used to detect diagnostic junction are also known as outward-facing primers due to the fact that their 3' end face away from each other thus averting amplification of transcript without diagnostic junction such as linear mRNA. circRNA can then be quantified using RT-qPCR. The phenomena of template switching may occur during reverse transcription step giving rise to false template leading to production of false PCR product despite using outward-facing primer would be a drawback of RT-PCR (312, 313).

Northern Blotting is another method that can be used to identify circRNA whereby the diagnostic junctional sequence can be detected using a specially designed probe (309).

The advancement in NGS has enabled the identification of large numbers of circRNAs (314). For instance cANRIL (antisense non-coding RNA in the INK4 locus) was one of the first circRNA identified through genome-wide RNA assessment for circRNA in cell lines, where it is associated with INK4a/ARF locus, leading to increased risk of atherosclerosis (220, 315). Recently, Bahn *et al.* reported and validated more than 400 circRNAs in human extracellular body fluid using high-throughput RNA sequencing (RNA-Seq) for the first time (316). However, the RNA-Seq data sets remain inconsistent due to non-standardization of circRNA enrichment strategy in data generation on top of the relatively low quantity of circRNA compared to linear RNA (311).

1.4.3.2.2 Bioinformatics approaches

Generally, chimeric reads (5'sequence in the read is downstream of 3' sequence) are searched for in order to identify circRNAs in RNA-seq data. In addition, numerous bioinformatic algorithms have been developed to predict or identify the expression of circRNA (283, 288). Salzman *et al.* first developed the method of RNA circle identification using the alignment of reads in reference to a customized database of annotated exon boundaries which was further refined by incorporating a false discovery rate (FDR)-controlled filtration (283, 288). Following on from this, a variety of algorithms have been

developed such as Burrows-Wheeler Aligner (BWA-MEM) and Segemehl software, Circle Seq, CircRNA Identifier (CIRI) and Mapsplice (317-320). However, studies comparing the performance of some of these published algorithms found striking differences between sensitivity and specificity whereby choice of algorithm used, greatly affects the false positive and false negative rates of circRNA detection (321). Currently, there is no 'gold standard' method to validate the algorithm's performance in circRNA identification (311, 321). Online circRNA databases are available for investigators use such as CircBase, Circ2Traits and CircInteractome (314, 322, 323).

1.4.3.3 circRNAs as a biomarker for PCa

circRNAs could potentially be an ideal biomarker owing to their universal expression patterns accompanied by unique characteristics such as tissue specificity, stability and evolutionary conservation (288, 324, 325). This is also reflected by the findings of circRNAs dysregulation across different types of malignancy (326). Thus, circRNA may be an ideal diagnostic biomarker as they demonstrate a high degree of tissue and disease specificity. The presence of circRNA in human bodily fluid such as saliva, blood and gastric fluid further supports its possibility as disease biomarker (316, 327, 328). Bahn *et al.* has shown that salivary circRNAs are associated with inflammatory response and intercellular signalling (316). Memczak *et al.* found that circRNA can be easily detected in blood and the results are reproducible, apart from its relatively higher level compared to linear counterpart highlighting the fact that blood circRNA may be a better biomarker candidate than linear RNA (327). Furthermore, Yan Li *et al.* demonstrated that circRNA is enriched by at least two fold and stable in exosomes making it a promising biomarker (329) whereas Shao *et al.* confirmed the stability of circRNA in gastric fluid despite freeze-thaw and incubation processes (328). With all these elements combined, circRNA could be an ideal tumour biomarker candidate.

circRNA has been recently discovered to exhibit a functional role in regulating cancer development and progression (330). The role of miRNA in cancer pathogenesis on the other hand, is well established (331). The interest in circRNA as a biomarker was further amplified when circRNA was discovered to act as miRNA sponges thereby regulating specific miRNA target genes responsible for cancer initiation or progression (287). Many studies have described the importance of the circRNA-miRNA-mRNA network in the

pathogenesis of cancer (Table 1.5). Other alternative routes that circRNA may regulate gene expression is by acting as a protein sponge or decoy (332).

A number of circRNA biomarkers have been investigated in PCa, however, there are few studies in the literature describing the role of circRNA in enzalutamide resistance and as a biomarker to inform drug resistance. Kong *et al.* have identified the up-regulation of circSRAMRCA5 (hsa_circ_0001445) across four PCa cell lines (LNCAP, 22RV1, DU145 and PC-3) compared to a normal prostate cell line (WPMY-1) and in 21 paired PCa tissue samples compared with corresponding normal prostate tissue (227). Interestingly, this study also found that circSMARCA5 expression level could be affected by androgens, as circSMARCA5 level increases according to DHT level in a dose dependent manner. Other work demonstrated the possibility of circSMARCA5 to act as a potential pro-oncogenic circRNA *in vitro* affecting cell cycle and apoptosis (227). Recently, Dai *et al.* found circRNA-MYLK (hsa_circ_0141940) was significantly up-regulated in both PCa cell lines (LNCAP, DU145, PC-3 and PC-3MIE8) and 17 paired PCa tissues in comparison to normal prostate cell lines (WPMY-1) and corresponding normal prostate tissues, respectively. The group has shown that the up-regulation of circRNA-MYLK could promote PCa cell proliferation, colony formation, invasion and migration and inhibit tumour apoptosis as a result of miR29a inhibition whereby circRNA-MYLK acted as a miRNA sponge in down-regulating miR29a (333). Greene *et al.* found more circRNAs were down-regulated than up-regulated using microarray screening in enzalutamide-resistant PCa cells (334). One of the down-regulated circRNA, has_circ_0004870 was validated and hypothesised to promote the expression of AR-V7 via U2AF65 leading to enzalutamide resistance (334). Wu *et al.* demonstrated that circRNA17/miR-181c-5p/AR-V7 signalling axis alters enzalutamide resistance (335). AR-V7 level is increased by circRNA17 suppression. circRNA17 up-regulates miR-181c-5p by maintaining its stability instead of acting as a sponge and the miRNA can bind the 3'-UTR of AR-V7 to decrease its expression (335). Xiang *et al.* found circUCK2 to be down-regulated in enzalutamide-resistant PCa cells and showed that the circRNA can sponge miR-767-5p to up-regulate *TET1*, which inhibits proliferation and invasion (336). On the other hand, Cao *et al.* identified 13 AR related circRNAs through analysis of exome-capture RNA-seq from 47 mCRPC samples, patient derived xenograft (PDXs) and cell models (337). The group found that these 13 circRNAs were overexpressed during progression of PCa to CRPC and

were detectable in serum samples from people with CRPC, suggestive of their potential roles as biomarkers (337).

These studies further strengthen the potential role of circRNA, not only as a diagnostic biomarker but also as a therapeutic biomarker for PCa. Even though there is paucity of literature describing the role of circRNA in PCa and drug resistance, it may be important in this disease given that there is abundant evidence demonstrating a role for circRNA in other malignancies (Table 1.5).

Table 1.5. circRNA-miRNA pathway in cancer.

Tumour	Associated circRNA	Target miRNA	Hypothesized miRNA Function	Regulatory Role of circRNA on miRNA	circRNA Expression in Tumour	Potential circRNA Biomarker	Ref
Bladder carcinoma	circTCF25	miR-103a-3p/miR-107	Tumour supressor-miR	Negative	↑	na	(338)
Bladder carcinoma	cir-ITCH	miR-17/miR-224	Onco-miR	Negative	↓	prognostic	(339)
Bladder carcinoma	circRNA-Cdr1as	miR-135a	Onco-miR	Negative	↓	na	(340)
Breast carcinoma	circ-ABCB10	miR-1271	Tumour supressor-miR	Negative	↑	na	(341)
Breast carcinoma	circRNA-000911	miR-449a	Onco-miR	Negative	↓	prognostic	(342)
Colorectal carcinoma	hsa_circ_000984	miR-106b	Onco-miR	Positive	↑	na	(343)
Colorectal carcinoma	hsa_circ_001569	miR-145	Tumour suppressor-miR	Negative	↑	na	(344)
Colorectal carcinoma	circHIPK3	miR-7	Tumour suppressor-miR	Negative	↑	prognostic	(345)
Oesophageal carcinoma	cir-ITCH	miR-7/miR-17/miR-214	Onco-miR	Negative	↓	na	(346)
Gastric carcinoma	circPVT1	miR-125 family	Tumour suppressor-miR	Negative	↑	prognostic	(347)
Hepatocellular carcinoma	circMTO1	miR-9	Onco-miR	Negative	↓	prognostic	(348)
Hepatocellular carcinoma	circRNA-Cdr1as	miR-7	Tumour suppressor-miR	Negative	↑	na	(349)
Lung carcinoma*	hsa_circ_0013958	miR-134	Tumour suppressor-miR	Negative	↑	diagnostic	(350)
Lung carcinoma	cir-ITCH	miR-7/miR-214	Onco-miR	Negative	↓	na	(351)
Osteosarcoma	circUBAP2	miR-143	Tumour suppressor-miR	Negative	↑	prognostic	(352)
Prostate carcinoma	circMYLK	miR-29a	Tumour suppressor-miR	Negative	↑	diagnostic/ therapeutic	(333)
Renal carcinoma	circHIAT1	miR-195-5p/miR-29a-3p/miR-29c-3p	Tumour suppressor-miR	Positive	↓	therapeutic	(353)

na = not available, all samples used were tissues except * = tissues and plasma, ↓=decrease, ↑=increase, Ref = reference

1.5 Aims and Objectives

The aim of this project was to identify novel molecular mechanisms associated with enzalutamide resistance PCa. The data generated will identify predictive biomarkers to therapy and potential therapeutic targets for patients with PCa. The hypothesis is that circRNAs play an important role in the development of enzalutamide resistance in PCa.

The objectives of this project were:

1. To examine the expression of circRNAs across a panel of prostate cell lines consisting of 'normal' (n = 2) and malignant cells (n = 5)
2. To validate the overlapping circRNAs, which are consistently expressed between the normal *vs.* malignant group and androgen dependent *vs.* androgen independent group, allowing for potential identification of circRNA signature reflective of the continuum model of prostate cancer progression
3. To validate the highest up-regulated circRNAs in the enzalutamide resistance clones from the LNCaP model of enzalutamide resistance (n=3) and examine their role in the development of enzalutamide resistance by evaluating predicted corresponding miRNAs and mRNA network
4. To evaluate the potential of circRNAs investigated in the enzalutamide resistant clones as a disease biomarker in clinical samples from the Phase II trial of radium-223 in combination with enzalutamide (CTRIAL-IE 13-21, NCT02225704) (354)
5. To examine the transcriptomic landscape of enzalutamide resistant PCa *in vitro* through NGS analysis of enzalutamide resistant panel and evaluate the potential mechanism associated with the development of enzalutamide resistance
6. To examine the landscape of actionable gene mutations in Irish people with mCRPC through targeted NGS

Chapter 2 - Methods and Materials

2.0 Materials and Methods

2.1 Preparation and handling of materials

Reagents and chemicals used in the laboratory were of analytical grade and stored in accordance with manufacturers' instructions. All chemicals and waste were disposed of according to local guidelines. Chemicals were purchased from Merck KGaA (Darmstadt, Germany) or Sigma-Aldrich (MO, USA) unless stated otherwise.

2.2 Cell culture

Cell culture was performed aseptically in accordance with good laboratory practice in an ABS optimal 18 laminar air flow unit (Aulnay Sous Bois, France). The LAF was exposed to UV light for approximately 30 min, and subsequently sanitised using 70% industrial methylated spirits (IMS) pre and post use. Cell culture reagents were warmed to 37°C prior to use, unless stated otherwise. All cells were cultured in vented tissue culture treated flasks (Corning®, NY, USA) and maintained at 37°C with 5% CO_2 in a humidified atmosphere.

2.2.1 Cell Culture reagents

All supplemental cell culture reagents, including fetal bovine serum (FBS), L-glutamine (200 mM) and antibiotic antimycotic solution (100X) (10,000 U penicillin, 10 mg/mL streptomycin and 25 µg/mL amphotericin b) were purchased from Sigma-Aldrich. RPMI-1640, Minimum Essential Medium Eagle (MEM) and Dulbecco's Modified Eagle's Medium (DMEM) were also obtained from Sigma-Aldrich. F-12K Nut Mix media was obtained from Life Technologies Corporation (WA, USA). Keratinocyte serum free media (KSFM) and associated supplements (2.5 µg EGF, 25 mg bovine pituitary extract) were obtained from Invitrogen (GIBCO) (Biosciences, Dublin, Ireland). All media were supplemented with 10% FBS, 1% penicillin-streptomycin-amphotericin unless stated otherwise (Table 2.1). MEM was additionally supplemented with 1% L-glutamine and 0.01 mg/mL human recombinant insulin.

2.2.2 Cell lines

Ten prostate cell lines were used in this project; five malignant prostate cell lines, two non-malignant prostate cell lines (Table 2.1) and three isogenic LNCaP clones (Table 2.2). Four

additional cell lines were used for control purposes in various experiments (Table 2.3). All cell lines were obtained from American Tissue Culture Collection (ATCC) (VA, USA) except the three LNCaP clones, which were gifted from Novartis (Dublin, Ireland). These age matched isogenic LNCaP clones were generated from mixed clones as described by Korpal *et al*. (138). This model consisted of three aged-matched cell lines; the Control (drug sensitive), Clone 1 (highly drug resistant) and Clone 9 (weakly drug resistant) (Figure 2.1).

Table 2.1. Prostate cancer cell lines with AR status, site of origin and culture medium used.

Cell line	**AR status**	**Site of origin**	**Media used**
LNCaP clone FGC (ATCC® CRL-1740™)	Positive	Lymph node metastasis	Complete RPMI-1640
22Rv1 (ATCC® CRL-2505™	Positive	Androgen dependent CWR22 xenograft	Complete RPMI-1640
VCAP (ATCC® CRL-2876™)	Positive	Vertebral bone metastasis	Completed DMEM
DU145 (ATCC® HTB-81™)	Negative	Brain metastasis	Complete MEM without insulin
PC-3 (ATCC® CRL-1435™)	Negative	Brain metastasis	Complete F-12K
RWPE-1 (ATCC®CRL-11609™)	Positive	Peripheral zone of normal prostate transfected with a single copy of human papilloma virus 18 (HPV-18)	KSFM without 10% FBS
PWR-1E (ATCC ® CRL-11611™)	Positive	Normal prostate with mild hyperplasia immortalised with an adenovirus 12-SV40	KSFM without 10% FBS

Table 2.2. Isogenic model of enzalutamide resistance and culture medium used.

Isogenic LNCaP clones	**Enzalutamide resistance**	**Media used**
Control	Sensitive	Complete RPMI-1640
Clone 1	Highly resistant	Complete RPMI-1640
Clone 9	Weakly resistant	Complete RPMI-1640

Table 2.3. Non-prostate cell lines.

Cell line	**Site of origin**	**Media used**
HeLa (ATCC® CCL-2™)	Cervical adenocarcinoma	Complete MEM without insulin
HEK-293 (ATCC® CRL-1573™)	Embryonic kidney	Complete MEM without insulin
MCF7 (ATCC® HTB-22™)	Breast adenocarcinoma derived from metastatic site: pleural effusion	Complete MEM
NCI-H460 (ATCC® HTB-177™)	Lung large cell carcinoma derived from metastatic pleural effusion	Complete RPMI-1641

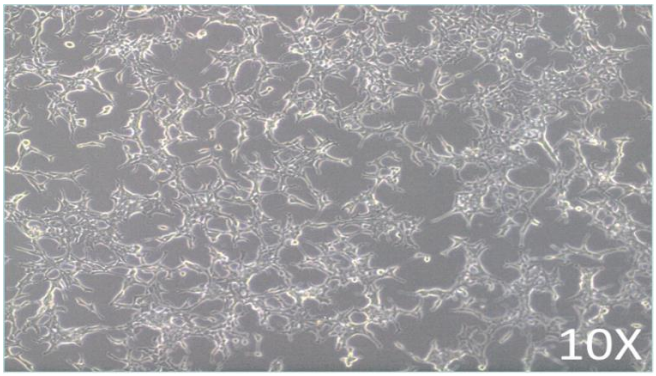

(A)

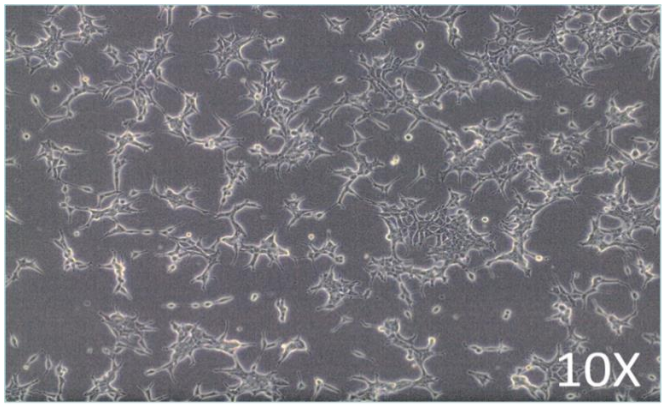

(B)

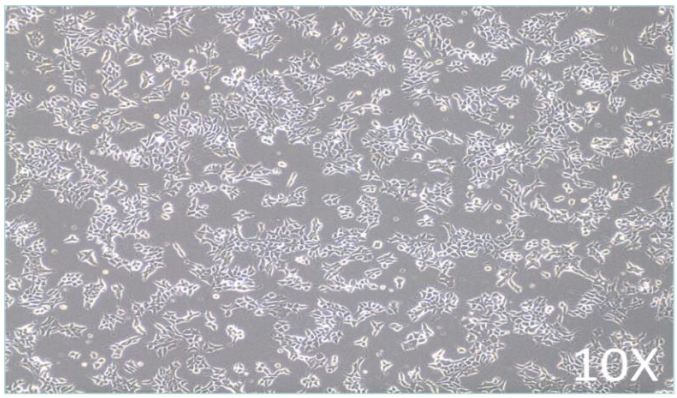

(C)

Figure 2.1: Bright-phase microscopy of cell lines. Morphology of (A) LNCaP Control cells (B) LNCaP Clone 9 cells (C) LNCaP Clone 1 cells. Morphological changes in Clone 1 cells compared to Control cells and Clone 9 cells such as loss of spread-out spindle like morphology with scattered growth.

2.2.3 Propagation of cell lines

Cells were removed from long term storage and thawed rapidly at 37°C for 2 min. Once thawed, the cells were mixed gently and added to 5 mL pre-warmed complete media in a T25 cm^3 tissue culture flask.

2.2.4 Cell subculture

Cells were visualised daily using an inverted phase-contrast microscope (Nikon Corp., Tokyo, Japan). Sub-culturing was performed when cell cultures reached approximately 80% confluency. Cell culture medium was decanted, and the cells were washed with 5 mL 1X PBS (HyClone™, MA, USA) to remove residual FBS. Two mL trypsin ethylene-diamine tetra-acetic acid (EDTA) (Sigma-Aldrich) was added to the flasks. Flasks were incubated at 37°C for approximately 3 min to allow the trypsin to detach the cells from the flask surface. Five mL complete medium was added to the flasks to inactivate the trypsin, cells were dislodged from the surface of the flask, transferred to a sterile 15 mL tube and pelleted by centrifugation at 1300 rpm for 3 min in an Eppendorf™ 5804 centrifuge (Eppendorf). The supernatant was discarded, and the cell pellet re-suspended in 10 mL complete medium. This suspension was used to seed fresh T75 cm^3 flasks at several different densities.

2.2.5 Cryopreservation

Cells were trypsinised (as per section 2.2.4). Resulting pellets were re-suspended in Cellbanker® cryopreservation media (AMS Biotechnology, Abingdon, UK) at a concentration of 1-1.5x10^6 cells/mL. Aliquots were stored at -80°C.

2.2.6 Mycoplasma testing

Cells were tested for mycoplasma infection every 12 weeks. At approximately 80% confluence, the supernatant was removed from T75 cm^3 flasks. The supernatant was centrifuged at 300 χ g to remove cellular debris and a PCR based reaction, adapted from Young *et al.* (355) was used to determine the presence or absence of mycoplasma. The primers were designed to encompass common mycoplasma species (Appendix - Table 1). The PCR reaction consisted of the following: 12.5 µL Green 2X GoTaq (Promega, WI, USA), 0.5 µL FWD primer (10 µM), 0.5 µL REV primer (10 µM) and 10.5 µL DNase free H_2O (Sigma-

Aldrich). Total reaction volume was 25 µL, which included 1 µL cell culture supernatant. The PCR cycling conditions are given in Table 2.4.

Table 2.4. PCR conditions for mycoplasma testing.

Temperature	Time	
95°C	5 min	
94°C	30 sec	40 cycles
55°C	30 sec	
72°C	1 min	
72°C	10 min	

The resulting PCR products were electrophoresed on a 2% agarose gel (as per section 2.3.4). A PCR negative control and a known mycoplasma positive control were included. A band at 270 bp was indicative of a positive result.

2.2.7 STR Profiling

The genomic DNA was extracted (as per section 2.3.1) and prepared according to Source BioScience STR profiling specifications: > 20 ng/µL in total volume of > 20 µL. The ATCC STR database algorithm (https://www.atcc.org/search-str-database) was used for STR analysis of the cell lines. The matching criterion was based on an algorithm that compares the number of shared alleles between two cell line samples, expressed as a percentage. Cell lines with ≥80% match are considered to be related; derived from a common ancestry. Cell lines with between a 55% to 80% match require further analysis for authentication of relatedness. STR profile (Appendix - Table 2) was queried using the following STR criteria: (AMEL) + the following loci: D5S818, D13S317, D7S820, D16S539, vWA, TH01, TPOX, CSF1PO. The results for identity using the ATCC algorithm were as follows: LNCAP Control: 94% (Pass), LNCaP C1: 94% (Pass), LNCaP C9: 94% (Pass), 22RV1: 100% (Pass), PC-3: 100% (Pass), DU145: 94% (Pass), RWPE-1: 94% (Pass), PWR-1E: 83% (Pass).

2.2.8 Cell counting

Cells were seeded at specific densities depending on the experimental set up. A bright line haemocytometer (Hausser Scientific, PA, USA) was used in conjunction with Trypan Blue (GIBCO) (0.4% v/v) for cell counting and viability. Cells were pelleted as above (as per

section 2.2.3) and re-suspended in a specific volume of media until a single cell suspension was obtained. A 20 µL aliquot of suspension was added to 180 µL Trypan Blue and mixed gently. The haemocytometer was cleaned using 70% EtOH and a glass cover slip was placed over the chamber. The edge of the cover slip was touched gently by a pipette tip and the chamber filled by capillary action. Viable cell number per mL was calculated using the following equation:

Average no. of cells counted per large square x 10,000 x 10 = no. of cells/mL

Where, 10,000 accounts for the µL volume under the cover slip and 10 equals the dilution factor.

2.2.9 Drug treatment

Enzalutamide (MDV3100) was purchased from Selleckchem (Stratech Scientific Ltd, Suffolk, UK), dissolved in DMSO at a concentration of 10 mM and stored at -20°C. Cells were treated with a range of enzalutamide concentrations (0 – 60 µM) for a period of 7 days. DMSO was used as the vehicle control.

2.2.10 BrdU proliferation assay

Cell proliferation was measured using a Cell Proliferation ELISA, BrdU (Roche Diagnostics Ltd., Sussex, UK). This is a colorimetric method to quantify cell proliferation based on the measurement of BrdU (5-bromo-2'-deoxyuridine- a pyrimidine analogue) incorporation (instead of thymidine) during DNA synthesis in proliferating cells. Cells were seeded at 1 x 10^3/well in a final volume of 100 µL/well in a 96-well plate. Cells were treated with appropriate drug for a specified period (as per section 2.2.9). Following culture, 10 µL/well of a 1:1000 dilution of BrdU labelling solution (final concentration – 10 µM) was added into each well and incubated for 4 h at 37°C. Following BrdU labelling, the media was removed, and cells fixed and denatured with 200 µL fixative solution for 30 min at room temperature (RT). One hundred µL anti-BrdU-POD (mouse monoclonal antibody, peroxidase-conjugated) working solution was added to each well and incubated for 90 min at RT. Cells were washed 3 times with wash buffer and 100 µL substrate solution was added for 5-10 min (or until colour change was sufficient for photometric detection). Twenty five µL 1 mM H_2SO_4 was added to each well to stop the reaction. Absorbance was measured on a Vesamax tunable microplate reader (Molecular Devices, CA, US) at 450 nm with reference

wavelength set to 690 nm. Untreated controls were set to 100% and treatments compared to the untreated controls.

2.3 Nucleic Acid isolation

2.3.1 Genomic DNA isolation from cell lines

Media was decanted from the tissue culture flask and 1 mL lysis buffer (10 mM Tris pH 8.0, 100 mM NaCl, 10 mM EDTA pH 8.0 and 0.5% SDS) and 5 µL (20 mg/ml stock) Proteinase K (ThermoFisher scientific, Massachusetts, USA) added. Flasks were agitated then incubated at room temperature (RT), for 3 h, after which time cells were scraped into a microfuge tube using a cell scraper (Fisherbrand™, Loughborough, UK). One mL isopropanol was added and the samples were mixed and incubated at RT for 10 min. The samples were centrifuged at 13500 χ g at RT for 10 min and supernatant discarded. The DNA pellets were air dried for 5 min and re-suspended in 500 µL molecular grade H_2O (Accugene, Cambrex Bioscience, IA, USA) and incubated at 37°C for 1 h. Genomic DNA was stored at -20°C until use.

2.3.2 RNA isolation from cell lines

2.3.2.1 RNA isolation using miRNeasy Mini Kit

The miRNeasy Mini Kit (Qiagen, Sussex, UK) was used to isolate RNA for circRNA and miRNA experiments. The cell culture supernatant was discarded, and cells were directly lysed by the addition of 2 mL QIAzol lysis reagent (Qiagen) to the flask surface. Cells were dislodged with a cell scraper and the cell lysate mixed several times using a pipette tip. For phase separation, 140 µL chloroform (Sigma-Aldrich) was added to the cell lysate, and the sample was shaken vigorously for 15 sec and incubated at RT for 3 min. The samples were centrifuged at 12,000 χ g for 15 min at 4°C. The upper aqueous phase was transferred into a fresh tube without disturbing the interphase. The RNA was precipitated from the aqueous phase using 525 µL 100% EtOH (Sigma-Aldrich), which was added to the sample and mixed thoroughly. Seven-hundred µL mix was pipetted onto the centre of a RNeasy mini spin column and centrifuged for 15 sec at 8000 χ g at RT. The flow through was discarded. Genomic DNA contamination was eliminated as follows: 350 µL RW1 buffer was added to the miRNeasy mini spin column and centrifuged at 8000 χ g with flow through discarded.

Next, 10 µL DNase 1 solution was added to 70 µL buffer RDD and mixed by gentle inversion. The DNase 1 mix was added directly to the RNeasy spin mini column membrane and incubated at RT for 15 min. Following incubation, 350 µL RWT buffer was added to the spin column and centrifuged for 15 sec at 8000 χ g. Next 500 µL RPE buffer was added to the spin column and centrifuged for 15 sec at 8000 χ g to wash the column. The flow through was discarded. An additional wash with 500 µL RPE buffer was added to the spin column and centrifuged for 2 min at 8000 χ g. The spin column was then placed into a fresh 2 mL collection tube and centrifuged for 1 min at full speed to avoid any carry-over of RPE buffer. The spin column was placed in a new 1.5 mL collection tube and 30-50 µL RNase-free H_2O was added directly onto the column membrane. The assembly was centrifuged for 1 min at 8000 χ g to elute the RNA. RNA was stored at -80°C until use.

2.3.2.2 RNA isolation using TRI reagent®

Media was decanted from the tissue culture flask and 1 mL TRI reagent® (Molecular Research Center, OH, USA) added. Flasks were incubated, with agitation, for 5 min, after which time cells were scraped into a microfuge tube using a cell scraper. RNA was isolated as follows: 100 µL 1-bromo-chloro-propane (BCP), was added to each sample, with samples inverted for 15 sec and incubated at RT for 10 min. The samples were centrifuged at 13500 χ g at 4°C for 15 min. Following centrifugation, the upper aqueous phase (containing RNA) was removed to a fresh 1.5 mL microfuge tube. Five hundred µL isopropanol was added, and the samples were mixed and incubated at RT for 10 min. Following centrifugation at 13500 χ g at 4°C for 8 min, the supernatant was discarded, and the pellet washed with 70% EtOH for 5 min. The samples were centrifuged again at 13500 χ g at 4°C for 5 min and the EtOH wash discarded. The RNA pellet was air dried for 5 min and re-suspended in 50 µL molecular grade H_2O (Accugene, Cambrex Bioscience). RNA was stored at -80°C until use.

2.3.2.3 RNA quantification using Nano drop

RNA was quantified using the NanoDrop 1000 spectrophotometer (ThermoFisher scientific). The instrument was first initialised and then blanked with 1 µL molecular grade H_2O. One µL each sample was loaded individually onto the NanoDrop. The instrument was cleaned between each sample. The NanoDrop returned the nucleic acid concentration in ng/µL and also the 260:280 and 260:230 purity ratios. A 260:280 of approximately 1.8 is

generally considered as pure for DNA and a ratio of approximately 2.0 is generally considered as pure for RNA.

2.3.2.4 RNA quality assessment

Each RNA sample was electrophoresed on a 2% agarose gel (section 2.3.2.5) to determine RNA quality. Bands for the 18S and 28S ribosomal subunits were an indication of good indication of RNA integrity.

2.3.2.5 Agarose gel electrophoresis

A 2% agarose gel (Sigma-Aldrich) was prepared in 100 mL 1X Tris-acetate EDTA (TAE) buffer (Sigma-Aldrich). The agarose was dissolved by heating in a microwave for 2-3 min. Five µL SYBR Safe DNA gel stain (Invitrogen, CA, USA) was added to the solution and the mixture was poured into a gel tray with well forming combs and allowed to set. Once set, the comb was removed, and the gel was covered with 1X TAE buffer. Six µL appropriate ladder (Fisher Scientific) was added to the first well and 15 µL sample was added to subsequent wells. If required, samples were mixed with 2 µL 6X loading dye (Fisher Scientific) before loading on to the gel. Gels were electrophoresed at 120V for 60 min. Gels were visualised using a Bio-Rad (CA, USA) gel imaging system.

2.3.3 RNA isolation from plasma

The miRNeasy Plasma/Serum Kit (Qiagen) was used to isolate RNA from plasma samples for the determination of circRNA expression. Plasma was thawed at RT and 200 µL was directly lysed by the addition of 1 mL QIAzol lysis reagent (Qiagen) to the sample and mixture vortexed briefly. The homogenate was incubated for 5 min at RT and 200 µL chloroform (equal volume to the starting sample) was added to the homogenate followed by 15 sec of vigorous shaking. The sample was incubated at RT for 3 min and centrifuged at 12,000 χ g at 4°C for 15 min. Next, 600 µL upper aqueous phase was transferred to a new collection tube followed by addition of 900 µL (1.5 volumes to aqueous phase) 100% EtOH and thoroughly mixed by pipetting. Up to 700 µL sample was pipetted into an RNeasy MinElute spin column in a 2 mL collection tube and centrifuged at 8000 χ g for 15 sec at RT then the flow-through discarded. This step was repeated for the remainder of the sample. Then, 700 µL RWT buffer was added to the RNeasy MinElute spin column and centrifuged

at 8000 χ g for 15 sec with the flow-through discarded. Next, 500 µL RPE buffer was added onto the RNeasy MinElute spin column and centrifuged at 8000 χ g for 15 sec with flow-through discarded. Five hundred µL 80% EtOH was added to the RNeasy MinElute spin column and centrifuged at 8000 χ g for 2 min with the flow-through and collection tube discarded. The RNeasy MinElute spin column was placed in a new 2 mL collection tube and centrifuged at full speed for 5 min with the lid of the spin column open to dry the membrane. The flow-through and collection tube were discarded. The RNeasy MinElute spin column was placed in a new 1.5 mL collection tube. Finally, 14 µL RNase-free H_2O was added directly to the centre of the spin column membrane and centrifuged at full speed for 1 min to elute the RNA. RNA was quantified using the NanoDrop spectrophotometer (section 2.3.2.3). RNA was stored at -80°C until use.

2.4 Real-time qPCR

2.4.1. cDNA synthesis for gene and circRNA expression analysis

cDNA was synthesized using the High Capacity cDNA Reverse Transcription Kit (Applied Biosystems, CA, USA). The following components were pipetted into a sterile, nuclease-free tube on ice; 1 µg (cell lines) or 0.1 µg (plasma) total RNA, 2 µL 10X RT buffer, 0.8 µL 25X dNTP Mix, 2.0 µL RT Random Primers, 1.0 µL MultiScribe™ Reverse Transcriptase and 1.0 µL RNase inhibitor. The reaction volume was made up to a final volume of 20 µL using molecular grade H_2O. The thermal cycling conditions are given in Table 2.5. cDNA was stored at -20°C until use.

Table 2.5. cDNA PCR conditions.

Temperature (°C)	Time (min)
25	10
37	120
85	5
4	5

2.4.2 SYBR Green-based gene expression analysis

Each PCR reaction was in a final volume of 20 µL: 10 µL 2X SYBR Green Master Mix, 1 µL FWD primer (10 mM), 1 µL REV primer (10 mM) (Appendix - Table 1), 7 µL molecular grade H_2O and 1 µL cDNA. PCR was performed over 40 cycles using the 7500 Fast Real-Time PCR

System (Applied Biosystems) with the cycling conditions as shown in Table 2.6, with technical triplicates for each sample. Data were normalised to GAPDH and fold change (FC) calculated using the ΔΔ Ct method.

Table 2.6. SYBR Green cycling conditions.

Cycling step	Temperature, °C	Time	Number of cycles
Initial denaturation	95	10 min	1
Denaturation	95	15 sec	40
Annealing	60	1 min	
Melting curve	95	15 sec	1
	60	1 min	
	95	30 sec	

2.4.3 SYBR Green-based circRNA expression analysis

The expression of target circRNA was determined using a SYBR Green PCR Master Mix and circRNA specific primers (Appendix - Table 3). Each PCR reaction was in a final volume of 20 µL containing 10 µL 2X SYBR Green Master Mix, 1 µL custom made FWD primer (10 mM), 1 µL custom made REV primer (10 mM) (Appendix - Table 3), 7 µL molecular grade H_2O and 1 µL cDNA. PCR amplification was performed over 40 cycles using conditions shown in Table 2.7. Data were normalised to GAPDH and FC calculated using the ΔΔ Ct method.

Table 2.7. SYBR Green reaction conditions for circRNA.

Cycling step	Temperature, °C	Time	Number of cycles
Initial denaturation	95	10 min	1
Denaturation	95	15 sec	40
Annealing	60	30 sec	
Melting curve	95	15 sec	1
	60	1 min	
	95	30 sec	

2.4.4 miRNA expression using TaqMan®

2.4.4.1 cDNA synthesis

cDNA synthesis was performed over four steps starting with (i) poly A tail reaction, followed by (ii) adaptor ligation, (iii) RT and (iv) miR-Amp as the final step. Two µL RNA (total 10 ng) was used per reaction. For poly A tail reaction, the following components were added in a

reaction tube; 2 µL RNA, 0.5 µL 10X poly (A) buffer, 0.5 µL ATP, 0.3 µL poly (A) enzyme, 1.7 µL molecular grade H_2O to a final volume of 5 µL per reaction, and vortexed briefly. The reaction tubes were then centrifuged briefly to eliminate air bubbles and incubated in a thermal cycler using the following conditions: polyadenylation at 37°C for 45 min, reaction was stopped at 65°C for 10 min and cooled to 4°C. Next, for the adaptor ligation reaction, the following components were added; 5 µL sample from poly A tail reaction, 3 µL 5X DNA ligase buffer, 4.5 µL 50% PEG 8000, 0.6 µL 25X ligation adaptor, 1.5 µL RNA ligase, 0.4 µL molecular grade H_2O to a total volume of 15 µL per reaction. The reaction tube was then vortexed, and centrifuged briefly followed by incubation in a thermal cycler using the following conditions: ligation at 16°C for 60 min then cooled to 4°C. Next, for the RT reaction, the following components were added to the reaction tube; 15 µL sample post adaptor ligation, 6 µL 5X RT buffer, 1.2 µL dNTP mix (25 mM), 1.5 µL 20X universal RT primer, 3 µL 10X RT enzyme mix and 3.3 µL molecular grade H_2O to a final volume of 30 µL per reaction, and vortexed briefly. The reaction was centrifuged briefly and incubated in a thermal cycler using the following conditions: RT at 42°C for 15 min, reaction was stopped at 85°C for 5 min. Finally for miR-Amp reaction, the following components were added; 5 µL sample from previous RT reaction, 25 µL 2X miR-Amp master mix, 2.5 µL 20x miR-Amp primer mix and 17.5 µL molecular grade H_2O to a final volume of 50 µL per reaction. The reaction tube was vortexed, centrifuged briefly and incubated in a thermal cycler using the conditions outlined in Table 2.8.

Table 2.8. PCR conditions for miR-Amp reaction.

Step	**Temperature**	**Time**	**Cycles**
Enzyme activation	95°C	5 min	1
Denature	95°C	3 sec	14
Anneal/extend	60°C	30 sec	
Stop reaction	99°C	10 min	1

2.4.4.2 TaqMan® miRNA expression analysis

Total miRNA was extracted from cultured cells using the miRNeasy mini kit (section 2.3.2.1). The expression level of miRNA of interest were determined using TaqMan® Advanced miRNA assays (ThermoFisher scientific). The cDNA template (section 2.4.4.1) was diluted 1:10 in 0.1X TE buffer. For the PCR reaction, the following components were added to each

reaction; 5 µL diluted cDNA template, 10 µL TaqMan® fast advanced master mix (2X), 1 µL TaqMan® advanced miRNA assay (20x) (Assay information provided in Appendix - Table 4) and 4 µL molecular grade H_2O to a final volume of 20 µL per reaction. The plates were sealed with an adhesive cover, vortexed and centrifuged briefly. PCR amplification was performed using the 7500 Fast Systems PCR machine (Applied Biosystems) using the conditions outlined in Table 2.9. miR-1228-3p served as an endogenous control. Data were normalised to miR-1228-3p and FC calculated using the ΔΔCt method.

Table 2.9. Real-time PCR conditions for TaqMan® miRNA expression.

Step	Temperature	Time	Cycles
Enzyme activation	95°C	20 sec	1
Denature	95°C	3 sec	40
Anneal/extend	60°C	30 sec	

2.4.5 Standard curve method

gBlocks® gene fragments (Integrated DNA Technologies, CA, US) were designed for hsa_circ_0001275 and hsa_circ_0001721 (Appendix - Table 5). A standard dilution curve was prepared using known quantities of custom designed gBlocks® gene fragments of respective circRNA through serial dilution which allows for calculation of absolute transcript copy numbers. Threshold cycle numbers in quantitative PCR reactions were determined for cDNA specific to gene copy number at 6 dilutions (1×10^7 copies, 1×10^6 copies, 1×10^5 copies, 1×10^4 copies, 1×10^3 copies, and 1×10^2 copies) containing the indicated number of copies of each transcript. Formulas were derived to quantify the absolute copy numbers on the basis of Ct values.

2.5 Molecular Cloning

All media and reagents were obtained from Invivogen (CA, USA) and restriction enzymes and buffers were purchased from either Roche Diagnostics Ltd. or New England Biolabs (MA, USA) unless stated otherwise. Vectors were purchased from Geneseed Biotech (Guangzhou, China) and Invitrogen. pCD25-ciR is a circRNA overexpression vector which carries optimized flanking loop frameworks containing modified Alu elements, Quaking (QKI) and other RNA binding protein (RBP) binding sites with circularization mediation

sequence to ensure accurate and efficient circularization of the inserted circRNA (Appendix - Figure 1). It also contains copGFP sequence which encodes the copGFP fluorescent protein. The cloning site contains EcoRI and BamHI restriction sites. The PCD25-ciR vector (Geneseed Biotech) (Appendix - Figure 1) and pCR™2.1-TOPO® vector (Invitrogen) (Appendix - Figure 2) were kanamycin resistant. pCR™2.1-TOPO® Vector is covalently bound with topoisomerase I for fast cloning and recombinants. pCR™2.1-TOPO® Vectors include a 3´-T overhangs for direct ligation of Taq-amplified PCR products and T7 promoters for *in vitro* RNA transcription and sequencing. pCR™2.1-TOPO® Vectors also contains M13 forward and reverse primer sites for sequencing.

2.5.1 Sanger sequencing

Fifteen µL post-PCR reaction product was mixed with 6 µL ExoSAPIT™ reagent (Applied Biosystems). The mixture was incubated at 37°C for 15 min to degrade remaining primers and nucleotides, followed by incubation at 80°C for 15 min to inactivate ExoSAP-IT™ reagent. The PCR products were prepared according to Source BioScience purified PCR product specifications: 10 ng/µL in a total volume of 5 µL. Primers were used at 3.2 pmol/µL in a total volume of 5µl per reaction.

2.5.2 Preparation of broth and agar plates

E.coli Fast-Media® Kan Agar (Invivogen) was dissolved in 200 mL sterile H_2O and microwaved for 3 min with periodic mixing. The solution was cooled, poured into petri dishes using aseptic technique and allowed to solidify. The plates were dried at 37°C, sealed and stored at 4°C. The LB Fast-Media® Kan broth (Invivogen) was prepared in the same manner as the agar plates and was aseptically aliquot into sterile 50 mL tubes which were sealed and stored at 4°C.

2.5.3 Restriction Digests

2.5.3.1 pCD25-ciR vector

Preparation of pCD25-ciR for ligation with circRNA was carried out as follows:

One µg pCD25-ciR underwent double digestion with 0.5 µL (10U) EcoRI, 0.5 µL (10U) BamHI (Roche Diagnostics Ltd.), 5 µL SuRE/Cut™ Buffer B (Roche Diagnostics Ltd.) and made up to 50 µL with molecular grade H_2O. The sample was digested at 37°C overnight. The digest

was then heat inactivated at 65°C for 15 min. The sample was purified using Wizard® SV Gel and PCR Clean-Up System Promega (Madison, USA). Briefly, an equal volume of membrane binding solution was added to the sample, vortexed, and transferred into an SV minicolumn collection tube assembly and incubated for 1 min at RT. The assembly tube was centrifuged at 14000 rpm for 1 min, with the flow-through discarded. Seven hundred µL membrane wash solution was added to the SV minicolumn and centrifuged for 1 min, with flow-through discarded. Five hundred µL membrane washing solution was added into the column and centrifuged for 5 min. The collection tube was emptied, and the SV minicolumn assembly was centrifuged for 1 min to allow evaporation of any residual EtOH. The SV minicolumn was transferred to a clean 1.5 mL Eppendorf tube and 50 µL molecular grade H_2O was added into the SV minicolumn. The assembly was centrifuged for 1 min. The purified digested pCD25-ciR vector was stored at -20°C until further use.

2.5.3.2 Preparation of circRNA insert

The purified circRNA (1260 ng) underwent two serial digestions. Initially, it was digested overnight as follows: 0.5 µL EcoRI, 5 µL SuRE/Cut™ Buffer B and made up to 50 µL with molecular grade H_2O. The digest was precipitated as follows: 2 µL Polyacryl Carrier (Molecular Research Center), 1 volume 5 M ammonium acetate (50 µL), 3 volumes absolute EtOH (150 µL) was added to the digest, vortexed briefly and incubated at -80°C for 20 min. The tube was centrifuged at 14000 rpm at 4°C for 10 min. The supernatant was discarded, and pellet was washed with 70% EtOH by vortexing briefly, and centrifuged at 14000 rpm for 10 min. The supernatant was discarded and the pellet re-suspended in 30 µL molecular grade H_2O. A second overnight digest was performed as follows: 0.5 µL BamHI, 5 µL SuRE/Cut™ Buffer B and made up to 50 µL with molecular grade H_2O. When the digest was completed, the enzyme was heat inactivated at 65°C for 15 min.

2.5.3.3 DNA isolation and purification

The digested products (section 2.5.3.2) were electrophoresed on a 2% agarose gel and visualised under UV light. The appropriate band was identified and cut out using a sterile scalpel. The isolated band was placed in a separate Eppendorf and weighed (weight conversion to volume was based on 100 mg = 100 µL). The Qiaquick® Gel Extraction Kit (Qiagen) was utilised to purify the band. Briefly, three volumes buffer QG to 1 volume gel

was added to the gel fragment and heated to 50°C for 10 min until the gel dissolved fully. One volume isopropanol was added to the sample and mixed. The mixture was transferred into QiaQuick spin column and centrifuged at 13000 rpm for 1 min. The flow-through was discarded and 500 µL buffer QG was added to the column and centrifuged for 1 min. The column was washed as follows: 750 µL buffer PE was added, and incubated for 5 min at RT. The column was centrifuged for 1 min, the flow-through discarded, and the column was placed into a new collection tube and centrifuged for a further 1 min to remove residual wash buffer. The DNA was eluted using 50 µL buffer EB and incubated for 4 min at RT to increase DNA yield prior to centrifugation. The column was centrifuged for 1 min. All centrifugation steps were undertaken at 13000 rpm. The purified digested DNA product was stored at -20°C until further use.

2.5.3.4 Ligation of circRNA insert into pCD25-ciR

Once the insert was isolated and purified (section 2.5.3.3), ligations were performed to clone the insert into the pCD25-ciR vector. The ligation reaction was prepared as follows: for each ligation a molar ratio of 5:1 insert:vector were added to 2 µL 10 X ligation buffer (Takara Bio, CA, USA), 1 µL pCD25-ciR vector (50 ng/ µL), 1 µL T4 DNA ligase (Takara Bio) and molecular grade H_2O to a final volume of 20 µL. The ligation reaction was incubated at RT for 2 h then heat inactivated at 60°C for 10 min. The sample was stored at -20°C until further use.

2.6 Transfection of mammalian cells

2.6.1 Transient transfection

A number of transfection reagents were evaluated to determine which reagent would provide the optimal transfection efficiency while maintaining cell viability.

2.6.1.1 TurboFect™ Transfection reagent

TurboFect™ (Pierce Biotechnology, IL, US) consists of cationic polymers which form compact, stable, positively charged complexes with DNA, protecting the DNA from degradation and facilitating gene delivery into mammalian cells. Cells were seeded at 2 x 10^5/ well in a 6 well plate in 4 mL complete media and incubated between 24 h to 48 h until 70% confluency was reached. Four µg plasmid DNA was diluted in 400 µL serum-

free/antibiotic-free RPMI-1640. Transfection reagent was added to the diluted plasmid DNA (Table 2.10) and briefly vortexed. The mixture was incubated 20 min at RT. Following incubation, 400 µL transfection reagent/plasmid DNA mixture was transferred in a drop-wise manner to each well. The plate was rocked gently to achieve even distribution of the complexes immediately after adding the transfection reagent. The cells were incubated for 48 h and examined under EVOS™ Digital Colour Fluorescence Microscope (Life Technologies Corporation), which excites the green fluorescent protein (GFP). The transfection efficiency was subsequently estimated by eye.

Table 2.10. TurboFect™ Transfection reactions.

Tube	RPMI-1640 (µl)	TurboFect™ (µl)	Plasmid DNA (µg)
1	400	6	4
2	400	7	4
3	400	8	4

2.6.1.2 Lipofectamine® 3000 reagent

Lipofectamine® 3000 (Life Technologies Corporation), is a cationic-lipid transfection reagent that forms a complex with DNA and then transports it into mammalian cells. Cells were seeded as in section 2.6.1.1 and allowed to reach 70% confluency. Plasmid DNA and Lipofectamine® 3000 reagent were diluted separately in serum-free/antibiotic-free RPMI-1640 (Table 2.11), and mixed well. P3000™ reagent (2 µL/µg DNA) was added to the diluted plasmid DNA and vortexed briefly. The diluted plasmid DNA mixture was added to each tube of diluted Lipofectamine® 3000 Reagent in a 1:1 ratio and incubated for 5 min at RT. The plasmid DNA-lipid complex was added to cells in a drop-wise manner and the 6 well plates rocked to ensure even distribution. The cells were incubated for 48 h and examined as before (section 2.6.1.1).

Table 2.11. Lipofectamine® 3000 reactions.

Tube	RPMI-1640 (µl)	Lipofectamine® 3000 (µl)	-
1	125	3.75	-
2	125	7.5	-
Tube	RPMI-1640 (µl)	P3000™ (µl)	Plasmid DNA (µg)
1	250	10	5

2.6.2 Stable Transfection

2.6.2.1 Geneticin killing curves

The pCD25-ciR vector is under the control of the *neo* gene, which infers Neomycin antibiotic resistance. G418 (Invivogen) also known as geneticin is a broad-spectrum antibiotic that will select mammalian cells expressing neomycin. Kill curves were set-up using LNCaP cells with a range of G418 concentrations (0 - 700 µg) to establish the optimum concentration of the antibiotic required to kill the cells within 7 days. Cells were seeded at 2 x 10^5/well in a 6 well plate in 5 mL complete media and incubated between 24 h to 48 h until 70% confluency was reached. The cells were then treated with G418 at a range of concentrations (0-700 µg/mL). G418 was added directly to the culture medium and the antibiotic was replaced every 4 days. The lowest concentration (450 µg/mL defined as the optimal dose from a G418 killing curve) of antibiotic that resulted in near complete cell death at the end of the 7 days of culture was recorded and used for future transfection experiments (Appendix - Figure 3).

2.6.2.2 Transfection

Transfection was undertaken according to the Lipofectamine® 3000 protocol (section 2.6.1.2). After 48 h, the cells were examined under the microscope to gauge transfection efficiency. Lipofectamine® 3000 Reagent at the transfection-reagent/DNA ratio of 7.5 µl:5 µg gave superior transfection efficiency while protecting cellular health. The cells were trypsinised with 1 mL trypsin (section 2.2.4) and seeded into T25 cm^3 tissue culture flasks. The cells were supplemented with fresh media containing 400 µg G418 every 4 days. After approximately 2 weeks, colonies were visible and sub-cultured to obtain a mixed population of clones. Subsequently, cells expressing GFP were further selected using the BD FACSMelody™ (BD Biosciences, CA, US) as per section 2.6.2.2. Cells were trypsinised with 1 mL trypsin and the pellet collected as described in section 2.2.4. The cell pellet was re-suspended in 3 mL complete RPMI-1640 without FBS at approximately 1 x 10^6 cells/mL and then transferred into 5 mL sterile Falcon collection tube (Becton Dickinson Labware, NJ, USA) and assistance was provided by the flow cytometry core (TTMI, Trinity College Dublin). The total GFP positive cells yielded were between 1 x 10^6 to 1.2 x 10^6 cells. The sorted GFP positive cells were cultured in T25 cm^3 tissue culture flasks with fresh media containing G418.

2.7 Western Blotting

2.7.1 Isolation of proteins by TRI reagent®

Media was decanted and cells were homogenised with 1 mL TRI reagent® (section 2.3.2.2). The samples were centrifuged at 13500 χ g at 4°C for 15 min. Following centrifugation, the upper aqueous phase (containing RNA) was removed to a fresh 1.5 mL microfuge tube for RNA extraction (section 2.3.2.2). After removal of the aqueous phase, 0.3 mL 100% EtOH per 1 mL Tri reagent used for initial homogenisation was added to the interphase and organic phase to precipitate DNA prior to protein precipitation. The sample was mixed by inversion and incubated for 3 min at RT followed by 5 min centrifugation at 2000 χ g at 4°C to precipitate DNA. Protein was isolated from the phenol-ethanol supernatant after the precipitation of DNA. Firstly, to precipitate proteins from the phenol-ethanol supernatant, 3 volumes acetone to 1 volume supernatant was added to 0.5 mL sample, and mixed by inversion for 15 sec then incubated for 10 min at RT. The mixture was centrifuged at 12000 χ g for 10 min at 4°C and the phenol-ethanol supernatant decanted. Secondly, the protein pellet was dispersed and washed in 0.5 mL Protein wash I (0.3 M guanidine hydrochloride, 95% EtOH and 2.5% glycerol) using a pipette tip followed by the addition of another 0.5 mL Protein wash I and incubated for 10 min at RT. The protein was centrifuged at 2000 χ g for 3 min and the wash solution decanted followed by 2 more washes in 1 mL Protein wash I to remove residual phenol. The final wash was performed in 1 mL Protein wash II (95% EtOH and 2.5% glycerol) and centrifuged at 3000 χ g at 4°C. The protein wash was decanted, and the tube was inverted to dry the pellet for 10 min at RT. Lastly, for protein solubilisation, 500 µL protein solvent (1% Sodium dodecyl sulphate (SDS), 10 µL sodium orthovanadair (NA_3SO_4), 100 µL Protein inhibitory cocktail (PIC)) was added to the pellet and gently dispersed by pipetting. Solubilised proteins were stored at -80°C until further use.

2.7.2 Isolation of proteins by RIPA

Media was decanted and cells were washed with 10 mL cold PBS. The PBS wash was discarded. Cells were scraped into a fresh aliquot of cold PBS, transferred into a 2 mL Eppendorf tube. Samples were centrifuged at 1300 rpm at 4°C for 3 min and the

supernatant discarded. The resulting pellet was stored on ice and re-suspended in 100 µL cold 1X RIPA lysis buffer (Cell Signalling Technology, MA, USA) supplemented with 1 µL 100 mM phenylmethylsulfonyl fluoride (PMSF) (Sigma-Aldrich) and 2 µL PIC (2 mM AEBSF, 1 mM EDTA, 130 µM Bestatin, 14 µM E-64, 1 µM Leupepin, 0.3 µM Aprotinin). Samples were then incubated on ice for 30 min to aid lysis. The protein lysate was vortexed, briefly centrifuged at 7500 rpm at 4°C for 5 min. The supernatant containing soluble protein was transferred to a new 1.5 mL Eppendorf tube and stored at -80°C.

2.7.2 Protein Quantification

2.7.2.1 Preparation of diluted albumin (BSA) standards

Protein concentrations were determined using the bicinhoninic acid assay (BCA) (Pierce, IL, US). This assay utilises the principle that Cu^{2+} is oxidised to Cu^{+} in the presence of protein in an alkaline medium. The BCA reagent reacts with the Cu^{+}, yielding a coloured product. A stock solution of BSA was diluted in PBS to prepare a range of standards. BSA standards (0 to 2000 µg/mL) were prepared (Appendix - Table 6). A working solution of the BCA reagent was prepared by mixing 50 parts BCA reagent A with 1 part of BCA reagent B (50:1 ratio of alkaline bicarbonate solution to copper sulphate solution, respectively). Each unknown protein sample was diluted 1:10, and 10 µL was then pipetted in duplicate onto a 96 well plate. Ten µL each BSA standards were pipetted onto the same 96 well plate in duplicate. Two hundred µL working solution was added to each well and incubated at 37°C for 30 min. Following incubation, the absorbance was measured at 595 nm on a Vesamax tuneable microplate reader (Molecular Devices, CA, US). Protein concentrations were determined by interpolation from a standard curve of known concentrations of BSA, ranging from 0 to 2000 µg/mL (Appendix - Figure 4).

2.7.3 SDS PAGE

Glass plates (Atto Corp., Tokyo, Japan) were cleaned with 70% EtOH and assembled in an upright position with rubber seal in place. A 12% (v/v), resolving gel was made using 9.2 mL 30% acrylamide:bisacrylamide, 4.5 mL 1.875 M Tris HCL-pH 8.8, 8.3 mL SDW, 176 µL 10% (w/v) SDS, 120 µL 10% (w/v), fresh ammonium persulfate (APS) and 10 µL N,N,N',N'-tetramethylethylenediamine (TEMED). The solution was mixed gently to avoid bubble formation and pipetted into the upright glass plates. Once set, a 5% (w/v) stacking gel was

prepared containing 1.7 mL 30% (w/v) acrylamide:bisacrylamide, 2 mL 0.6 M Tris HCL-pH 6.8, 6 mL SDW, 100 µL 10% (w/v) SDS, 150 µL 10% (w/v) APS and 10 µL TEMED. A 12 well comb was inserted into the stacking gel and the gel left to set. A total of 30 µg protein were diluted (1:1) with 2X LaemLi buffer (Bio-Rad) and denatured by incubating at 95°C for 10 min. Ten µL trichrome pre-stained protein marker (Pierce) was also loaded onto each gel. Samples were separated by electrophoresis at 25 mA per gel in electrode buffer (50 mM Trizma base, 384 mM Glycine, 0.1% (w/v) SDS) for 90 min or until the dye front reached the end of the gel.

2.7.4 Protein transfer

Separated proteins were transferred onto a 0.45 µM polyvinylidene fluoride (PVDF) membrane (ThermoFisher scientific) using a wet Mini Trans Blot Cell (Bio-Rad). A pre-activated (1 min in 100% MeOH) PVDF membrane and Whatman filter paper (Whatman Laboratory Division, Kent UK) were soaked in cold transfer buffer (0.15 M glycine, 20 mM Trizma base, 0.1% (w/v) SDS, 20% (v/v) MeOH), prior to use. The layers in the transfer cassette are outlined in Figure 2.2. The cassette was then placed in a cooled electrode tank and topped up with cold buffer and run at 100 V and 400 mA for 1 h.

Figure 2.2. Wet transfer layout. Current ran from the anode to the cathode.

2.7.5 Antibody probing of membranes

Following the transfer of proteins, membranes were blocked for 1 h with 5% (w/v) non-fat dried milk (Marvel), which was reconstituted in 1X TBST (20 mM Trizma base, 150 mM NaCl, 0.1% (w/v) Tween® 20 detergent). The membrane was incubated with appropriate primary antibody (Table 2.12) in 5% non-fat milk TBST on a shaker. Membranes were washed six

times for 5 min each in TBST before incubation in the appropriate species-specific horseradish peroxidase (HRP) conjugated secondary antibody (1:2000 dilution in 5% non-fat milk TBST) (Cell Signalling Technology) for 1 h. The membranes were washed with 1X TBST for six 5 min washes. The Supersignal West Pico Chemiluminescent substrate kit (ThermoFisher scientific) was used to detect bound antibody complexes. Working reagent was prepared just prior to use and was applied to the membrane for 5 min. Membranes were then exposed to fluorescence imaging using the Odyssey® Fc Imaging System (Li-Cor, Nebraska, USA). Exposure time ranged from 10 sec to 30 min depending on the signal intensity.

Table 2.12. Antibodies used for western blotting.

Antibody	**Supplier**	**Type**	**Isotype**	**Primary**
E-Cadherin	Cell Signaling Technology	monoclonal	rabbit IgG	1:1000 o/n at 4°C
N-Cadherin	Cell Signaling Technology	monoclonal	rabbit IgG	1:1000 o/n at 4°C
β-Actin	Merck Biosciences	monoclonal	mouse IgG	1: 20,000 for 1 h at RT

2.8.6 Membrane stripping

In order for the membrane to be re-probed with a different antibody, the membranes were incubated in 10 mL Restore™ western blot stripping buffer (ThermoFisher scientific) at RT on a shaker for 20 min. The membranes were washed for 10 min in TBST and stored at 4°C until use. Stripped membranes were re-probed as appropriate.

2.9 Droplet Digital PCR (ddPCR)

2.9.1 EvaGreen-based circRNA expression analysis

Total RNA was isolated from plasma using the miRNeasy Serum/Plasma Kit (Qiagen) (section 2.3.2.1), and cDNA was synthesised using total RNA extracted from cell lines or patients plasma samples (CTRIAL-IE 13-21, NCT02225704) as per section 2.4.1. ddPCR was performed using the QX200™ Droplet Digital PCR System (Bio-Rad) (Appendix - Figure 5).

2.9.1.1 ddPCR reaction preparation

Each PCR reaction was prepared in a 96 well twin-tec PCR plate (Eppendorf, Hamburg, Germany). Each PCR reaction was in a final volume of 20 µL containing 10 µL 2X EvaGreen Supermix, 1 µL custom made FWD primer (200 nM) (Appendix - Table 3), 1 µL custom made REV primer (200 nM) (Appendix - Table 3) and 7 µL molecular grade H_2O and 1 µL cDNA. Reactions were performed in triplicate and copy number used for analysis was the average of the three replicates.

2.9.1.2 ddPCR droplet generation

The DG8 cartridge (Bio-Rad) (Figure 2.3) was inserted into the holder and 20 µL PCR reactions from the 96 well plate was transferred to the middle row of DG8 cartridge carefully to avoid introduction of air bubbles as this results in the formation of fewer droplets and reduces data quality. Next, 70 µL Droplet Generation Oil for EvaGreen (Bio-Rad) was added to each bottom well of the cartridge and a DG8 gasket was securely hooked over the cartridge holder to ensure sufficient pressure for droplet generation. Droplet generation was initiated by placing the cartridge assembly into the QX200™ Droplet Generator (Bio-Rad). Following completion of droplet generation, 40 µL droplets from the top well were transferred using a pipet into a clean 96 well plate. The step was repeated for each cartridge and filled each column across the 96 well plate. The PCR plate was sealed with Pierceable Foil Heat Seal (Bio-Rad) using a PX1™ PCR Plate Sealer (Bio-Rad) and the PCR reaction commenced immediately.

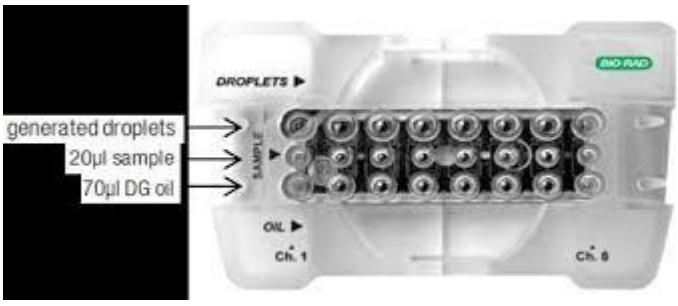

Figure 2.3. Image of DG8 cartridge (Bio-Rad) in the holder.
Image taken from product insert.

2.9.1.3 ddPCR thermal cycling

The sealed PCR plate was placed into the T100™ Thermal Cycler (Bio-Rad) and incubated as shown in Table 2.13. A ramp rate of 2°C/sec was used to avoid droplet instability during rapid temperature alterations and to ensure each individual droplet attained uniform temperature during cycling.

Table 2.13. Cycling conditions for ddPCR.

Cycling step	**Temperature, °C**	**Time**	**Ramp rate**	**Number of cycles**
Enzyme activation	95	5 min	2°C/sec	1
Denaturation	95	30 sec		40
Annealing/extension	60	1 min		40
Signal stabilization	4	5 min		1
	90	5 min		1
Hold	4	Infinite		1

2.9.1.4 ddPCR droplet analysis

The 96-well PCR plate was placed into the QX200 Droplet Reader (Bio-Rad) following completion of the cycling step and the fluorescence intensity of individual droplets was measured. QuantaSoft™ Analysis Pro software (Bio-Rad) was used to analyse the data. The software used Poisson statistics to identify the quantity of starting material present for each amplicon in copies per µL and draw thresholds between droplet populations.

2.10 RNA sequencing of enzalutamide resistance cell lines panel

2.10.1 RNA-Seq Library preparation

Total RNA was isolated from the three isogenic LNCaP clones using the miRNeasy Mini Kit (section 2.3.2.1). The RNA was normalised to 50 ng/µL in 5 µL for quality control (QC) and sequencing. RNA integrity was measured using an Agilent 2100 Bioanalyzer (Agilent, Santa Clara, USA) (Appendix - Figure 6). Samples with a RNA integrity number (RIN) score >7.0 were used for library generation. RNA-Seq libraries were prepared using the TruSeq Stranded mRNA Library Prep Kit (Illumina, San Diego, USA) according to manufacturer's instructions Sequencing was performed on NovaSeq 6000 (Illumina) using paired-end sequencing (75 base pair paired-end reads) with 30 million reads produced per sample.

RNA sequencing was performed in collaboration with Trinseq, Trinity Genomic Sequencing Laboratory and analysis with the School of Mathematics, Statistics & Applied Mathematics, National University of Ireland Galway.

2.11 Statistical analysis

Graphpad PRISM 9 (Graphpad, CA, USA) was used for the statistical analysis. Data is graphed as mean ± SEM or mean ± SD. Significance was determined via one-way or two-way analysis of variance (ANOVA), where the number of groups in the experiment was three or more. A *post hoc* test was required after ANOVA to determine which groups were significantly different to each other. Significance was determined via Mann-Whitney test or Wilcoxon signed rank test where the number of groups did not exceed two. A probability of $p < 0.05$ was considered to signify a significant difference between groups. Spearman correlation coefficient Fisher's exact test was used to determine association between two variables. A probability of $p < 0.05$ was considered to signify a significant association between the variables.

Chapter 3 - Profiling of circRNA as PCa disease biomarkers

3.0 Introduction

There has been a revival of interest in the role of ncRNA, which consists of several different classes including sncRNA and lncRNA (Figure 3.0), both of which have been studied widely in PCa (223). A newly discovered type of ncRNA, termed circRNA, appears to have important roles in cancer initiation, development and progression (224, 226). circRNAs are RNA molecules with covalently joined 3'- and 5'- ends formed by back-splice events, thus presenting as closed continuous loops, which makes them highly stable (283, 284). Recent research suggests they can act as miRNA sponges, bind RBPs and translate peptides (270). miRNAs have been previously shown to have a wide array of biological functions and have an important role in regulating gene expression in cancer (356). For instance, several miRNAs have been identified as direct regulators of AR expression or AR activity such as miR-488 (357) and miR-31 (358). It has been proposed that circRNAs can impair miRNA activity through sequestration, thereby altering the expression of target mRNAs (356). Thus, the discovery of widespread circRNA dysregulation in human malignancy has raised the question of whether circRNA may be utilised to construct a molecular signature of aggressive PCa or serve as a biomarker to inform drug resistance. The well-documented stability of circRNA supports their application as minimally invasive robust biomarkers (283, 284).

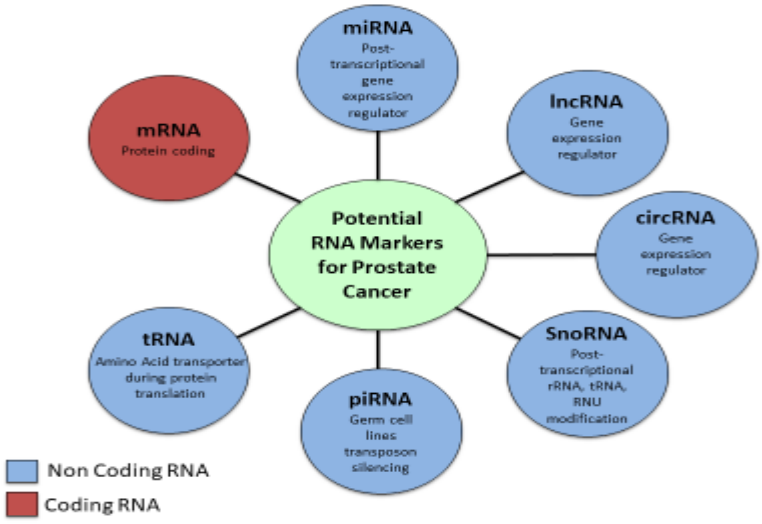

Figure 3.0: Types of RNAs and their associated function.

Image adapted from Lim *et al.* (228).

This study builds on previous work from Green *et al.* (334, 359), which focussed on profiling circRNA in prostate cell lines using microarray technology. Greene's study identified dysregulated circRNAs in PCa cell lines and demonstrated that they were more often down-regulated in enzalutamide resistant cell lines compared with the enzalutamide sensitive cell line.

This chapter will focus on further in-depth study of the differentially expressed circRNAs in a panel of 'normal' prostate cell lines (n=2), PCa cell lines (n=5) and an isogenic cell line of enzalutamide resistance (n=3). The circRNA dataset was generated using microarray technology previously (334, 359). Differentially expressed circRNAs, which were highly up-regulated were selected for further examination to evaluate their potential as disease biomarkers, and determine their role in the development of enzalutamide resistance. The data generated will identify predictive biomarkers to therapy and potential novel therapeutic targets for CRPC.

The aims of this chapter were to:

1. Validate the circRNAs across a panel of prostate cell lines (normal and malignant)
2. Validate the circRNAs across a panel of enzalutamide resistant cell lines
3. Determine the role of circRNA in the development of enzalutamide resistance
4. Examine the circRNA-miRNA-mRNA network in enzalutamide resistant PCa

3.1 Results

3.1.1 Mycoplasma testing

All cell lines used in this project were screened for mycoplasma infection every 3 months. A PCR negative control and a known mycoplasma positive control were included in every testing run. A band at 270 bp was indicative of a positive result. A representative image is outlined in Figure 3.1. No mycoplasma was detected in any of the cell lines used in this project.

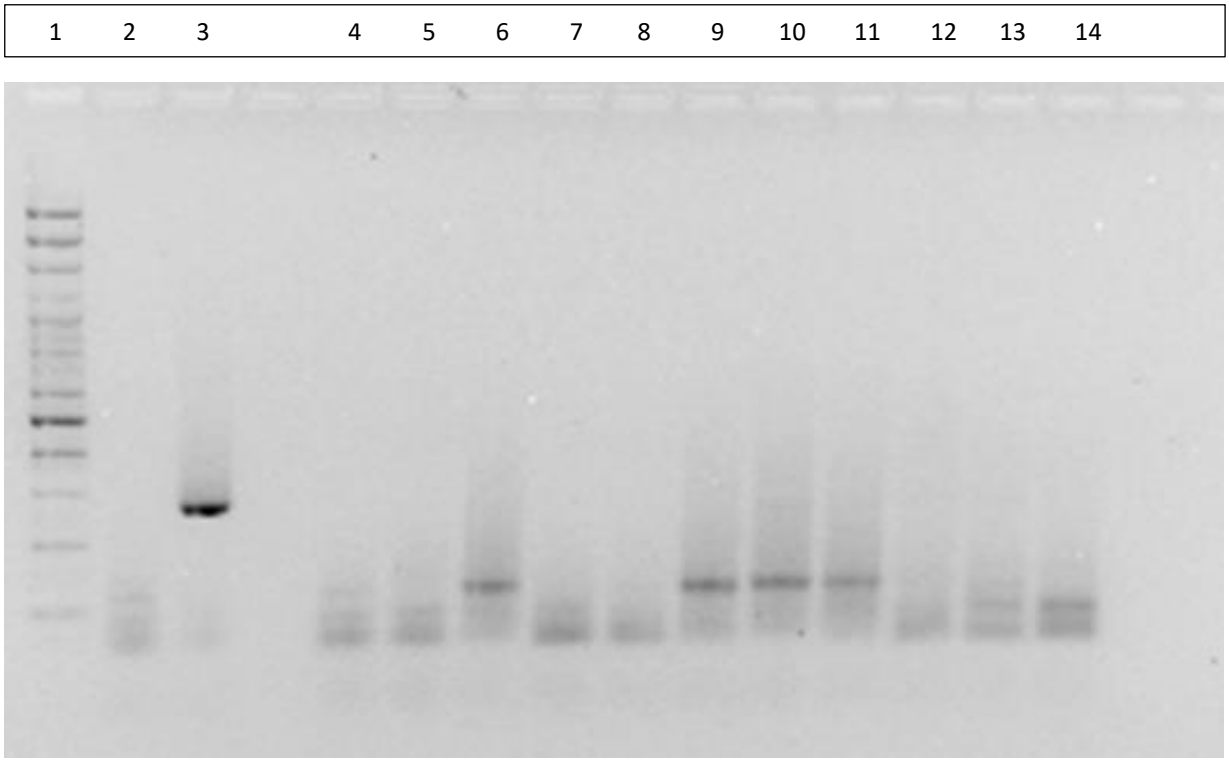

Figure 3.1. Mycoplasma testing of cell lines.

Lane 1: 100 bp DNA ladder, lane 2: negative control, lane 3: positive control (band at 270 bp), lane 4: LNCaP, lane 5: VCaP, lane 6: 22Rv1, lane 7: DU145, lane 9: PC-3, lane 9: Control cell line (CTL), lane 10: Clone 1 cell line (C1), lane 11: Clone 9 cell line (C9), lane 12: BPH-1, lane 13: PWR-1E, lane 14: RWPE-1.

3.1.2 RNA quality assessment

Each RNA sample was electrophoresed on a 2% agarose gel to determine RNA quality. Distinct bands for the 18S and 28S ribosomal subunits were observed in all samples, which indicated good RNA integrity (Figure 3.2).

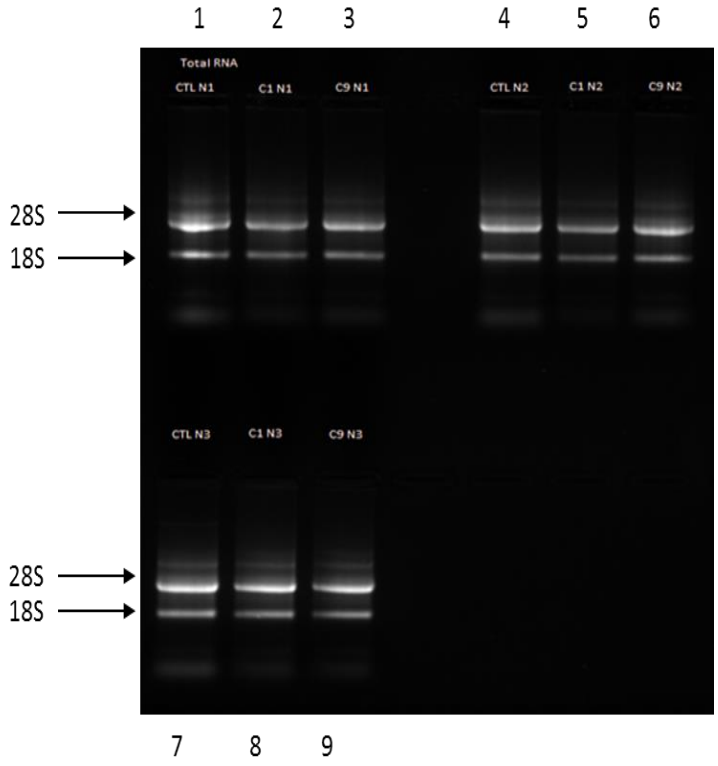

Figure 3.2. Assessment of RNA integrity. Bands at 18S and 28S indicated good RNA integrity. Lane 1: Control 1 n=1, lane 2: Clone 1 n=1, lane 3: Clone9 n=1, lane 4: Control n=2, lane 5: Clone 1 n=2, lane 6: Clone 9 n=2, lane 7: Control n=3, lane 8: Clone 1 n=3, lane 9: Clone 9 n=3.

3.1.3 circRNA profiling of PCa cell lines

A circRNA microarray (Arraystar) was performed across a panel of eight cell lines (22Rv1, VCaP, LNCaP, PC-3, DU 145, BPH-1, PWR-1E and RWPE-1) in triplicate by Greene *et al.* previously (359). The human circRNA microarray version 2.0 covers 13,617 previously discovered human circRNAs. The circRNAs were enriched by treatment with Ribonuclease R (RNase R), which degrades linear RNAs but not circRNAs. Quantile normalization of raw

data and subsequent data processing were performed using R software package (360). In total 9,757 circRNAs were present across the panel of cell lines (359). Differentially expressed circRNAs were examined by computing the fold change (FC) (i.e. the ratio of the group averages) for each circRNA between: normal *vs.* malignant and androgen dependent *vs.* androgen independent cell lines. A student's paired *t* test was then used to identify significantly altered circRNAs between groups. The false discovery rate (FDR) was applied to determine the threshold of p value. An FDR < 0.05 was used. circRNAs with a FC ≥ 1.5 and $p < 0.05$ were considered to be significantly differentially expressed between groups.

3.1.4 circRNAs are differentially expressed in PCa

An overall grouped analysis based on malignancy status was performed between cell line groups. circRNAs expression levels between normal prostate cell lines (PWR-1E and RWPE-1) were compared to malignant prostate cell lines (22RV1, LNCaP, PC-3, DU 145 and VCaP). circRNAs were differentially expressed between these groups according to FC and p value.

3.1.4.1 circRNAs are differentially expressed between normal vs. malignant prostate cell lines

There were 373 circRNAs up-regulated and 186 circRNAs that were down-regulated ($p < 0.05$, normal *vs.* malignant) (Figure 3.3, 3.4A and 3.4B).

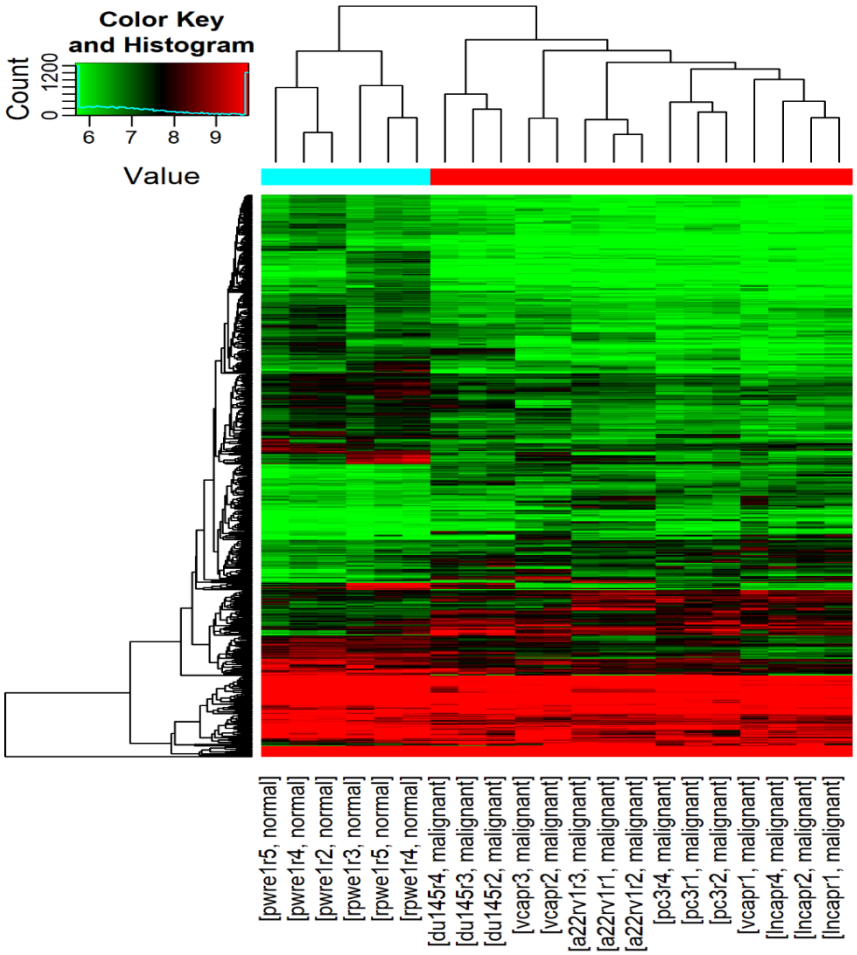

Figure 3.3. Hierarchical clustering of differentially expressed circRNA, normal and malignant prostate cell lines. The clustering heatmap of microarray data showing distinguishable circRNA expression profiling between normal and malignant prostate cell lines. circRNAs were more likely to be up-regulated in normal compared to malignant cell lines. Unsupervised clustering (Euclidean distance measure and the "average" agglomeration method) was used for analysis (n = 3).

Image created by Arraystar.

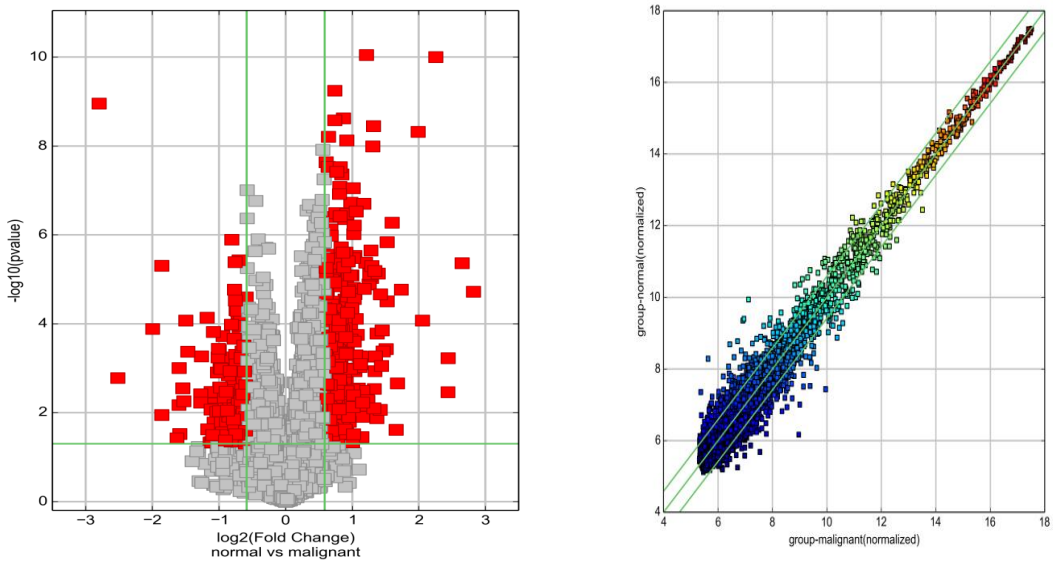

(A) **(B)**

Figure 3.4. Analysis of differentially expressed circRNAs, normal and malignant prostate cell lines. (A) Volcano plot of differentially expressed circRNA. The microarray volcano plot showed the up or down-regulated circRNA between normal and malignant prostate cell lines. The green vertical lines correspond to 1.5-fold up and down, respectively, and the green horizontal line represents a p-value of 0.05 with points above the line having $p < 0.05$ and points below the line having $p > 0.05$. The red point in the plot represents the differentially expressed circRNAs with statistical significance. The grey point in the plot represents the differentially expressed circRNAs without statistical significance. X axis represents FC and Y axis represents -log10 of p value. (B) Scatter plot of differentially expressed circRNA. The scatter plot showed differential expression of circRNA between normal and malignant prostate cell lines. The values of X and Y axes in the Scatter-Plot are the normalized signal values of the samples (log2 scaled) or the averaged normalized signal values of groups of samples (log2 scaled). The green lines are FC Lines. The circRNAs above the top green line and below the bottom green line indicated more than 1.5 fold change of circRNAs between the two compared samples.

Image created by Arraystar.

3.1.4.2 circRNAs are differentially expressed between androgen dependent vs. androgen independent prostate cell lines

There were 333 circRNAs up-regulated and 474 circRNAs that were down-regulated ($p < 0.05$, androgen dependent *vs.* androgen independent) (Figure 3.5, 3.6A and 3.6B).

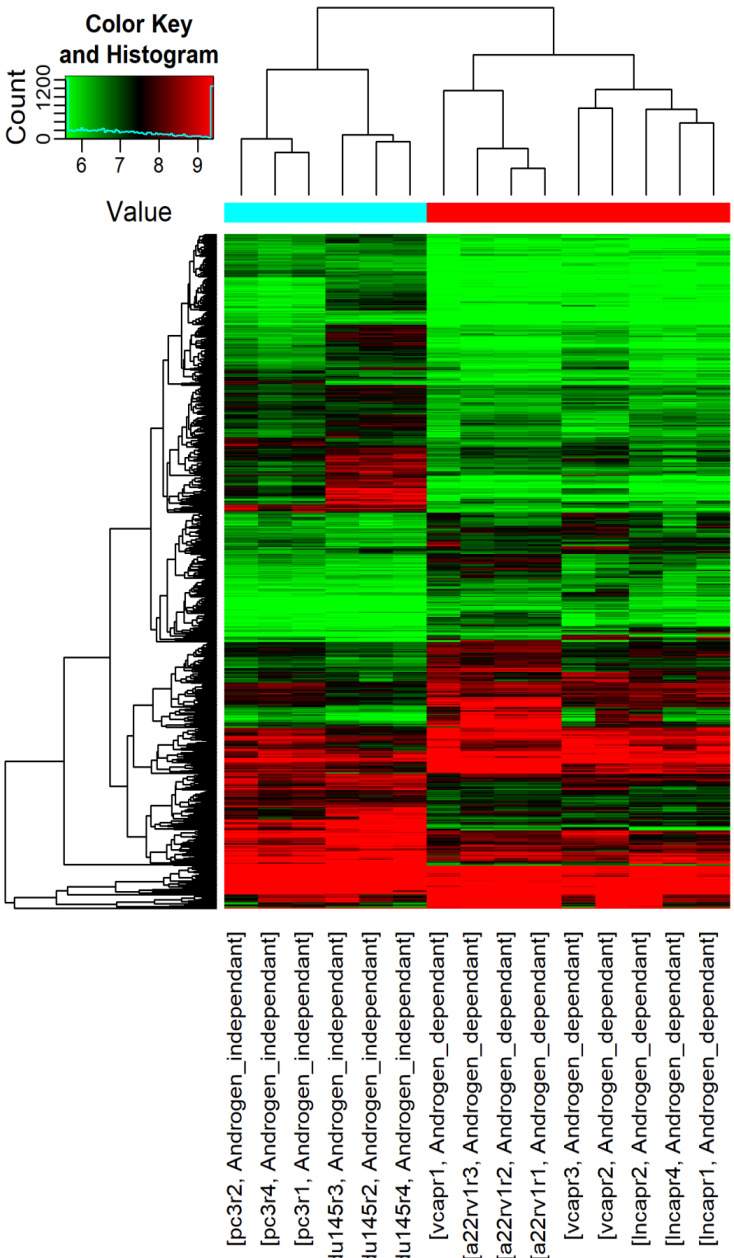

Figure 3.5. Hierarchical clustering of differentially expressed circRNA, androgen dependent and androgen independent prostate cell lines. The clustering heatmap of microarray data showing distinguishable circRNA expression profiling between androgen dependent and androgen independent prostate cell lines. circRNAs were more likely to be down-regulated in androgen dependent compared to androgen independent cell lines. Unsupervised clustering (Euclidean distance measure and the "average" agglomeration method) was used for analysis (n = 3).

Image created by Arraystar.

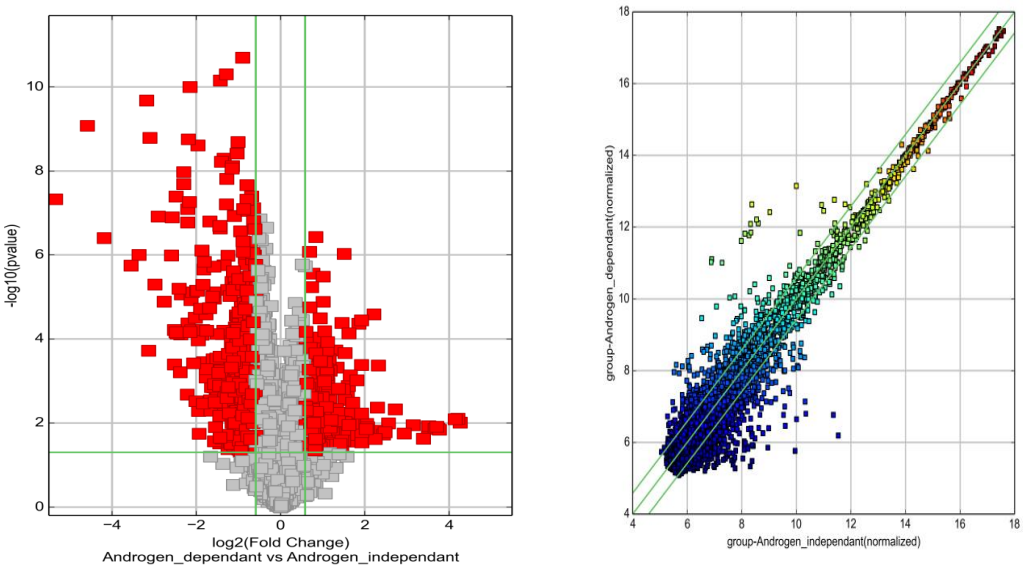

(A) **(B)**

Figure 3.6. Analysis of differentially expressed circRNAs, androgen dependent and androgen independent prostate cell lines. (A) Volcano plot of differentially expressed circRNA. The microarray volcano plot showed the up or down-regulated circRNA between androgen dependent and androgen independent prostate cell lines. The green vertical lines correspond to 1.5-fold up and down, respectively, and the green horizontal line represents a p-value of 0.05 with points above the line having $p < 0.05$ and points below the line having $p > 0.05$. The red point in the plot represents the differentially expressed circRNAs with statistical significance. The grey point in the plot represents the differentially expressed circRNAs without statistical significance. X axis represents FC and Y axis represents -log10 of p value. (B) Scatter plot of differentially expressed circRNA. The scatter plot showed differential expression of circRNA between androgen dependent and androgen independent prostate cell lines. The values of X and Y axes in the Scatter-Plot are the normalized signal values of the samples (log2 scaled) or the averaged normalized signal values of groups of samples (log2 scaled). The green lines are FC Lines. The circRNAs above

the top green line and below the bottom green line indicated more than 1.5 fold change of circRNAs between the two compared samples.

Image created by Arraystar.

3.1.4.3 Identification of overlapping circRNAs in the panel of prostate cell lines.

The differentially expressed and overlapping circRNAs between the two groups (normal *vs.* malignant and androgen dependent *vs.* androgen independent) are represented by a Venn diagram (Figure 3.7). Venn intersection analysis determined 116 overlapping circRNA in normal *vs.* malignant cell lines and androgen dependent *vs.* androgen independent cell lines.

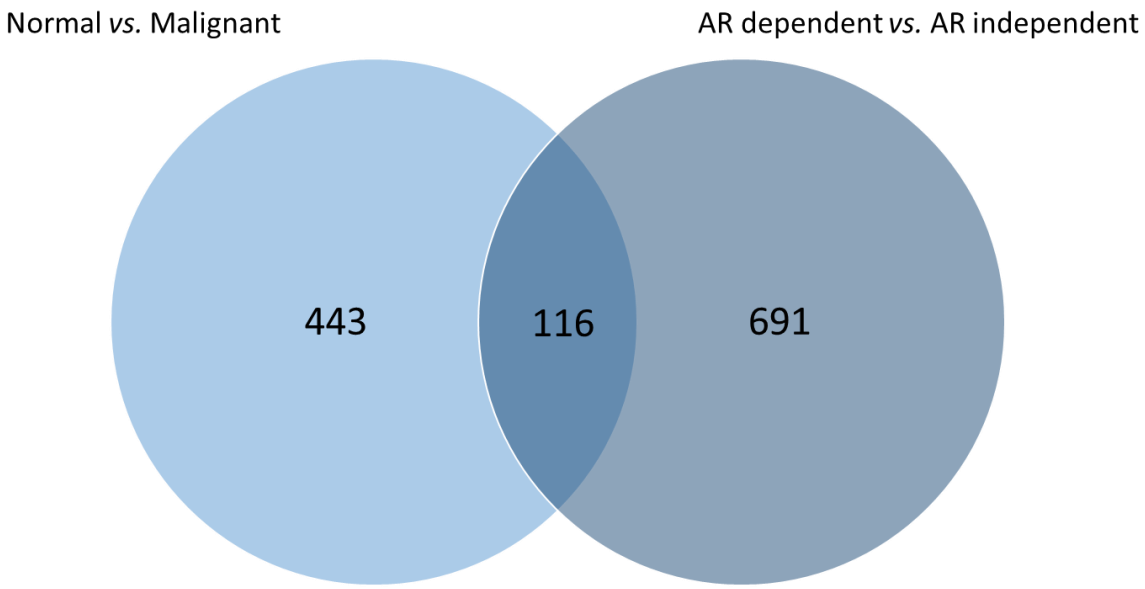

Figure 3.7. Venn diagram displaying differentially expressed and overlapping circRNAs between the cell line groupings.

3.1.5 RT-qPCR validation of selected circRNAs with their associated parental genes

Five out of 116 overlapping circRNAs listed in section 3.1.4.3 were selected for validation (Table 3.1) as they were consistently expressed across the two groups (normal *vs.* malignant and androgen dependent *vs.* androgen independent) thus allowing for potential identification of a circRNA signature reflective of pathological progression from normal to

malignant androgen dependent and malignant androgen independent status. Custom designed outward facing primers were used for validation via RT-qPCR (Appendix -Table 3).

Table 3.1. Five circRNAs that were consistently expressed across the groups of prostate cell lines.

circRNA	**Normal *vs.* malignant FC/(p value)**	**Androgen dependent *vs.* independent FC/(p value)**	**Parental Gene**	**Parental Gene function**
hsa_circ_0066631	1.66 (p = 0.008)	-2.01 (p < 0.0001)	*DCBLD2*	EGFR phosphorylation of *DCBLD2* recruits TRAF6 and stimulates AKT-promoted tumorigenesis in glioblastomas (361).
hsa_circ_0007058	2.35 (p = 0.005)	-2.51 (p = 0.002)	*TEAD1*	Novel prostate basal cell marker that correlate with poor clinical outcome in PCa (362).
hsa_circ_0007365	1.58 (p = 0.008)	-1.53 (p = 0.01)	*RPRD1B*	Promotes tumour growth by accelerating the cell cycle in endometrial cancer (363).
hsa_circ_0005087	2.68 (p < 0.0001)	-1.74 (p = 0.007)	*NUDC*	Inhibition of prostate tumour growth by overexpression of NUDC, a microtubule motor-associated protein (364).
hsa_circ_0005320	1.53 (p = 0.04)	-2.17 (p < 0.0001)	*SEPT9*	Repression of Septin9 suppresses tumour growth of human glioblastoma cells (365).

3.1.5.1 hsa_circ_0066631

hsa_circ_0066631 was significantly down-regulated in LNCaP *vs.* RWPE-1 (FC 0.007 ± SEM 0.001, p = 0.001), VCaP *vs.* RWPE-1 (FC 0.19 ± SEM 0.01, p = 0.004) and 22RV1 *vs.* RWPE-1 (FC 0.06 ± SEM 0.002, p = 0.001) however was significantly up-regulated in DU145 *vs.*

RWPE-1 (FC 1.64 ± SEM 0.29, p = 0.028) (Figure 3.8A). The other AR independent PCa cell lines, PC-3 had higher hsa_circ_0066631 expression compared to RWPE-1 but this was not significant (FC 1.48 ± SEM 0.11, p = 0.11) (Figure 3.8A). Its associated parental gene, *DCBLD2* was significantly down-regulated in AR dependent PCa cell lines compared to RWPE-1 (LNCaP *vs.* RWPE-1 (FC 0.013 ± SEM 0.003, p = 0.0004), VCaP *vs.* RWPE-1 (FC 0.074 ± SEM 0.001, p = 0.0008) and 22RV1 *vs.* RWPE-1 (FC 0.07 ± SEM 0.003, p = 0.0007)) however was significantly up-regulated in PC-3 *vs.* RWPE-1 (FC 2.09 ± SEM 0.24, p = 0.028) (Figure 3.8B). In DU145, *DCBLD2* was up-regulated compared to RWPE-1 but not statistically significant (FC 1.37 ± SEM 0.17, p = 0.19) (Figure 3.8B).

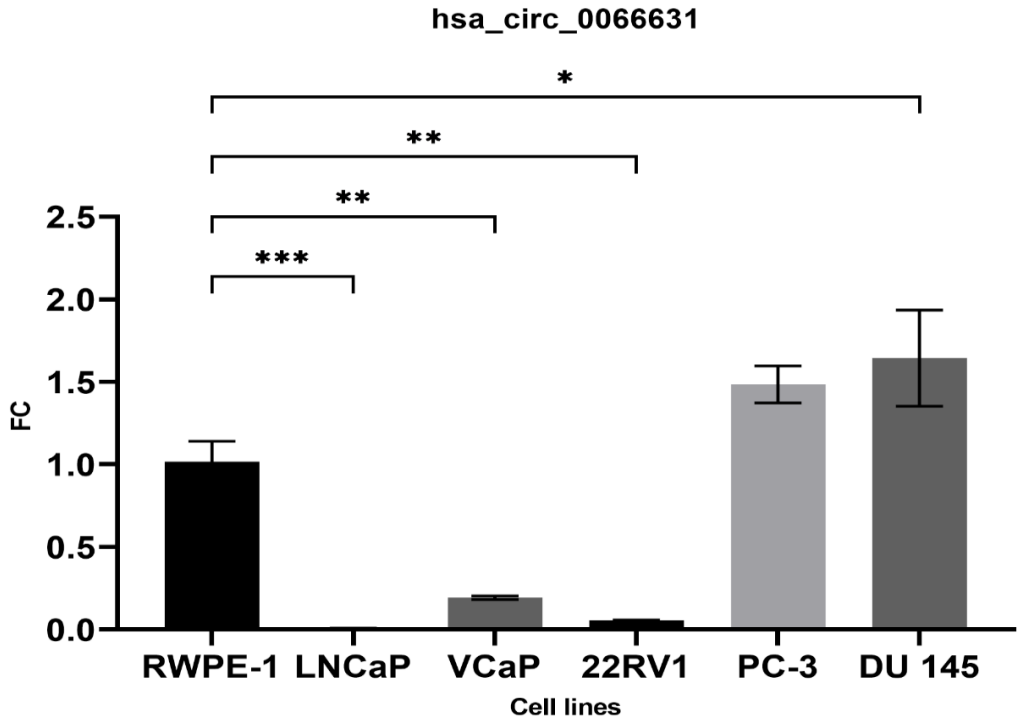

(A)

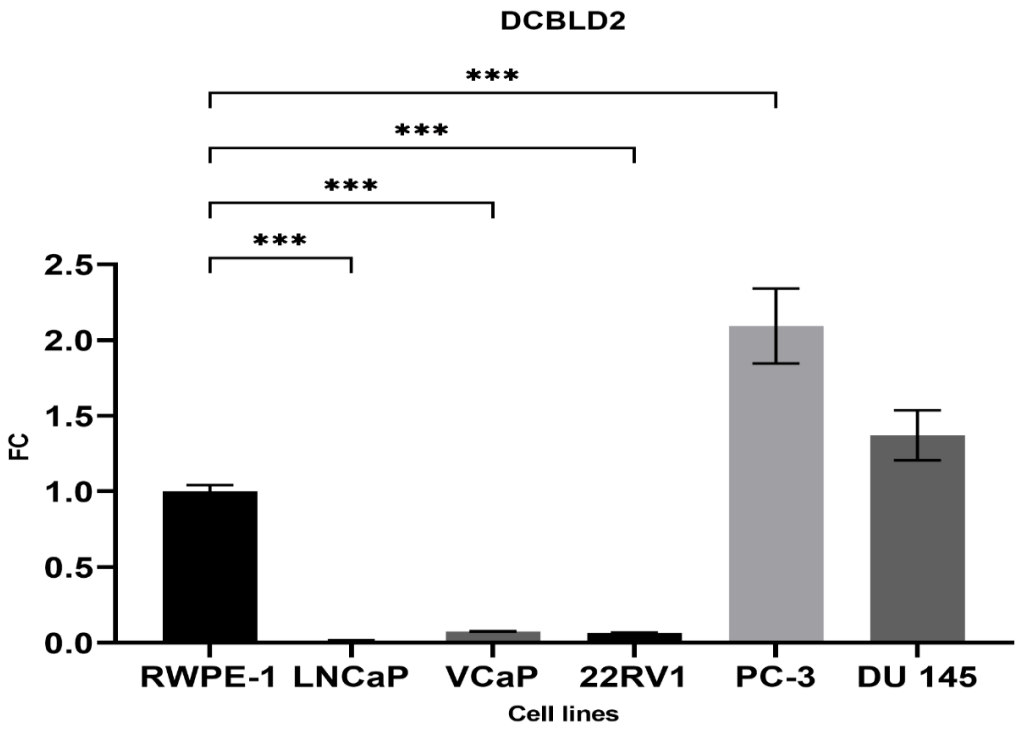

(B)

Figure 3.8. Validation of hsa_circ_0066631 and associated parental gene, *DCBLD2* in the panel of normal and malignant cell lines. (A) hsa_circ_0066631 and (B) *DCBLD2* in RWPE-1, LNCaP, VCaP, 22RV1, PC-3 and DU145. Data graphed as mean ± SEM (n=3). Data analysed using an ordinary one-way ANOVA followed by a Dunnett's *post hoc* test. (*p ≤ 0.05, **p ≤ 0.01, ***p ≤ 0.001).

3.1.5.2 hsa_circ_0007058

hsa_circ_0007058 was significantly up-regulated in DU145 *vs.* RWPE-1 (FC 5.75 ± SEM 1.44, p = 0.0007) (Figure 3.9A). The three AR dependent PCa cell lines (LNCaP, VCaP and 22RV1) had relatively lower hsa_circ_0007058 expression compared to RWPE-1, however, this was not statistically significant (FC 0.41 ± SEM 0.11, p = 0.9), (FC 0.69 ± SEM 0.06, p = 0.9) and (FC 0.22 ± SEM 0.02, p = 0.8) respectively (Figure 3.9A). The expression of hsa_circ_0007058 in PC-3 was similar to RWPE-1 (FC 1.1 ± SEM 0.08, p > 0.9) (Figure 3.9A). There was no statistical significant difference in the expression of its associated parental gene *TEAD1* between the malignant (LNCaP, VCaP, 22RV1, PC-3 and DU145) and normal cell lines (FC 0.95 ± SEM 0.29, p = 0.9), (FC 0.41 ± SEM 0.44, p = 0.2), (FC 0.41 ± SEM 0.19, p = 0.9), (FC 0.69 ± SEM 0.06, p = 0.9) and (FC 0.22 ± SEM 0.27, p = 0.9) respectively (Figure 3.9B).

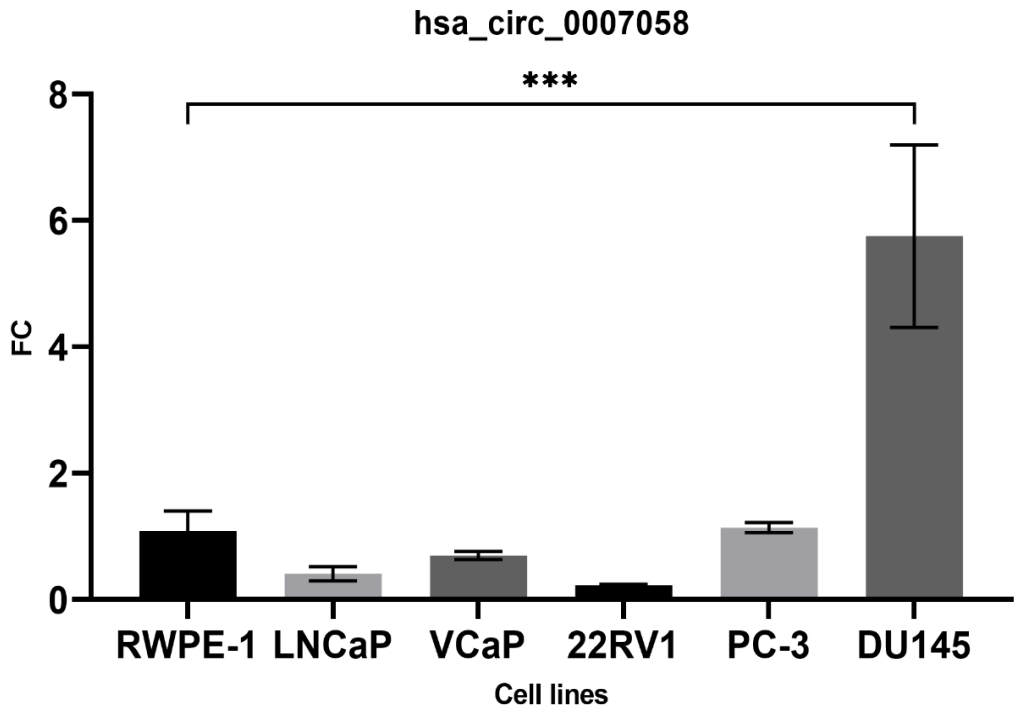

(A)

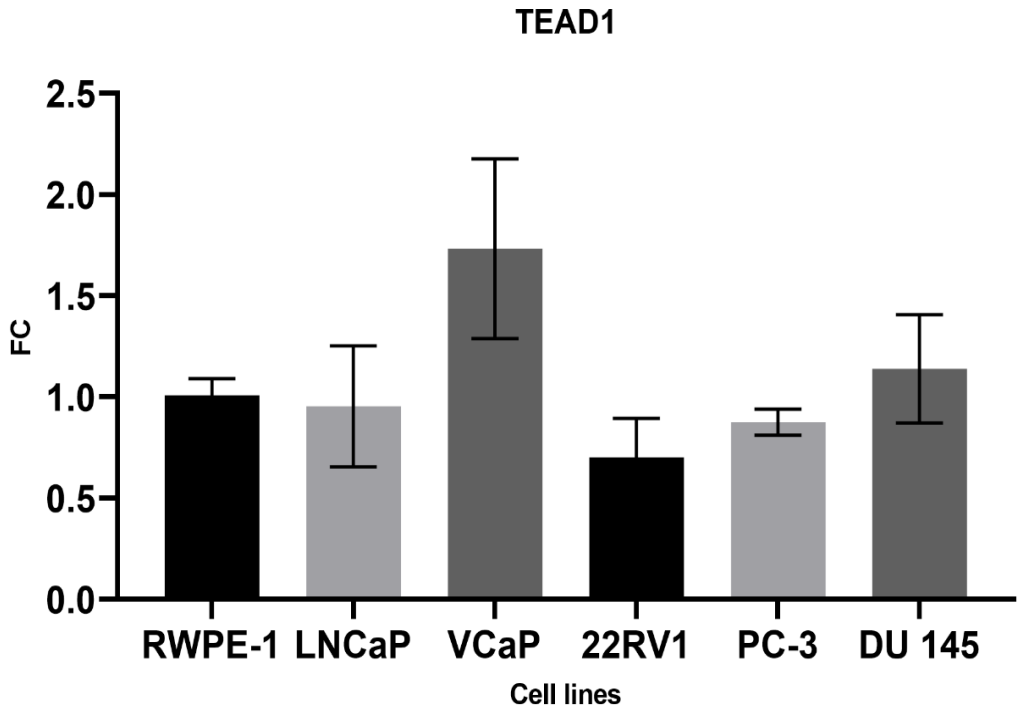

(B)

Figure 3.9. Validation of hsa_circ_0007058 and associated parental gene, *TEAD1* in the panel of normal and malignant cell lines. (A) hsa_circ_0007058 and (B) *TEAD1* in RWPE-1,

LNCaP, VCaP, 22RV1, PC-3 and DU145. Data graphed as mean ± SEM (n=3). Data analysed using an ordinary one-way ANOVA followed by a Dunnett's *post hoc* test. (***p ≤ 0.001).

3.1.5.3 hsa_circ_0007365

hsa_circ_0007365 was significantly up-regulated in VCaP *vs.* RWPE-1 (FC 6.93 ± SEM 0.79, p < 0.0001) (Figure 3.10A). The expression of hsa_circ_0007365 was not statistically significant in other AR dependent (LNCaP and 22RV1) or AR independent (PC-3 and DU145) PCa cell lines compared to RWPE-1 (FC 0.87 ± SEM 0.04, p = 0.9), (FC 2.5 ± SEM 0.28, p = 0.1), (FC 2.3 ± SEM 0.19, p = 0.2) and (FC 2.2 ± SEM 0.53, p = 0.2) respectively (Figure 3.10A). There was no statistical significant difference in the expression of its associated parental gene *RPRD1B* between the malignant (LNCaP, VCaP, 22RV1, PC-3 and DU145) and normal cell lines (FC 1.2 ± SEM 0.22, p = 0.7), (FC 1.54 ± SEM 0.12, p = 0.08), (FC 1.11 ± SEM 0.06, p = 0.9), (FC 0.92 ± SEM 0.13, p = 0.9) and (FC 0.85 ± SEM 0.22, p = 0.9) respectively (Figure 3.10B).

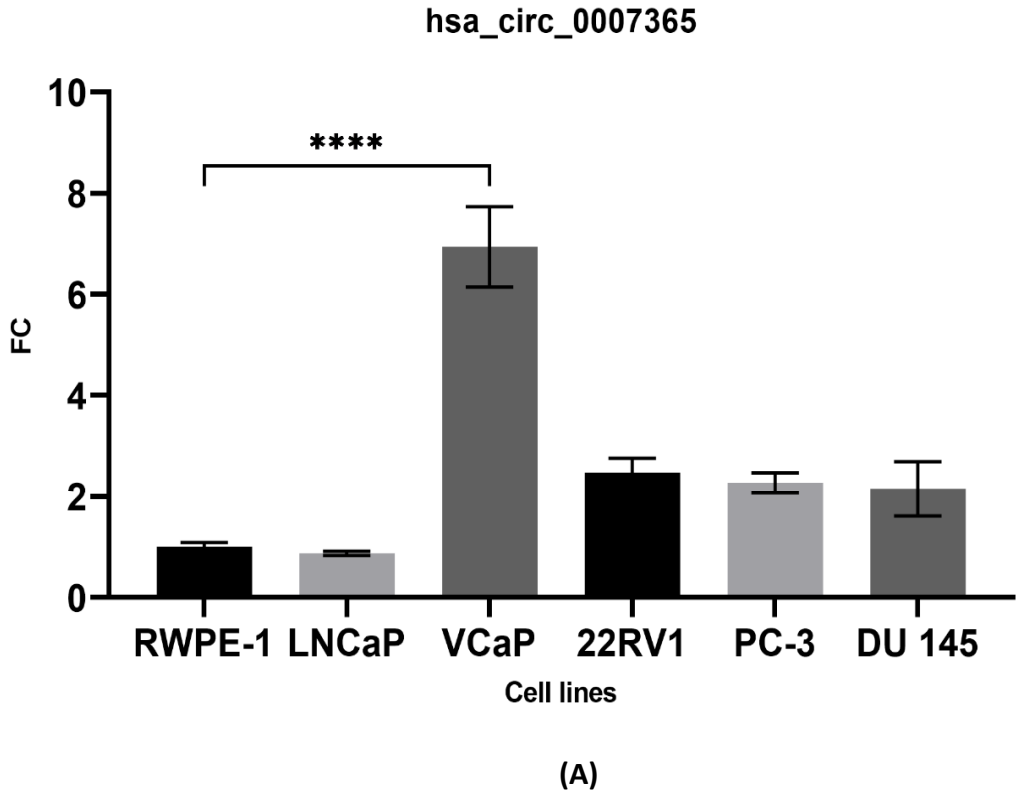

(A)

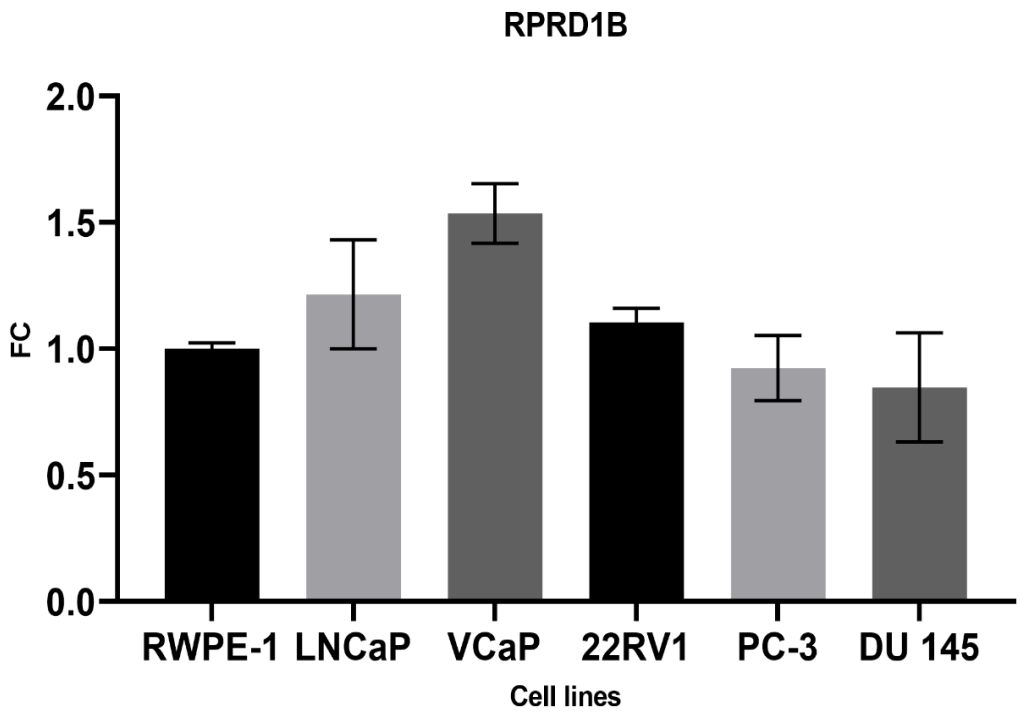

(B)

Figure 3.10. Validation of hsa_circ_0007365 and associated parental gene, *RPRD1B* in the panel of normal and malignant cell lines. (A) hsa_circ_0007365 and (B) *RPRD1B* in RWPE-1, LNCaP, VCaP, 22RV1, PC-3 and DU145. Data graphed as mean ± SEM (n=3). Data analysed using an ordinary one-way ANOVA followed by a Dunnett's *post hoc* test. (****p ≤ 0.0001).

3.1.5.4 hsa_circ_0005087

hsa_circ_0005087 was significantly up-regulated in VCaP *vs.* RWPE-1 (FC 2.37 ± SEM 0.58, p = 0.02) and PC-3 *vs.* RWPE-1 (FC 2.91 ± SEM 0.19, p = 0.001) (Figure 3.11A). There was no statistical significant difference between other malignant cell lines (LNCaP, 22RV1 and DU145) compared to RWPE-1 (FC 2.05 ± SEM 0.16, p = 0.07), (FC 1.06 ± SEM 0.12, p = 0.9) and (FC 0.86 ± SEM 0.2, p = 0.9) respectively (Figure 3.11A). Its associated parental gene *NUDC* was down-regulated in all AR dependent cell lines (LNCaP, VCaP and 22RV1) *vs.* RWPE-1 (FC 0.73 ± SEM 0.06, p = 0.02), (FC 0.4 ± SEM 0.02, p < 0.0001) and (FC 0.5 ± SEM 0.01, p = 0.0003) respectively (Figure 3.11B). *NUDC* was also down-regulated in DU145 compared to RWPE-1 (FC 0.4 ± SEM 0.02, p < 0.0001) with similar expression in PC-3 *vs.* RWPE-1 (FC 0.89 ± SEM 0.1, p = 0.52) (Figure 3.11B).

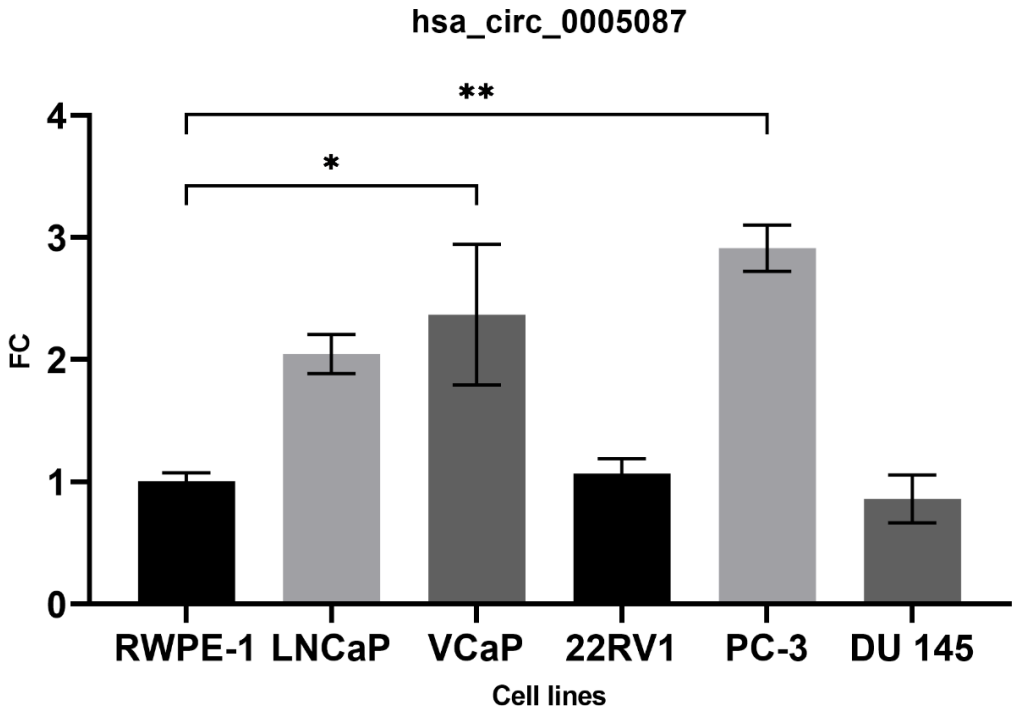
hsa_circ_0005087
**
*
4
3
2
1
0
FC
RWPE-1
LNCaP
VCaP
22RV1
PC-3
DU 145
Cell lines

(A)

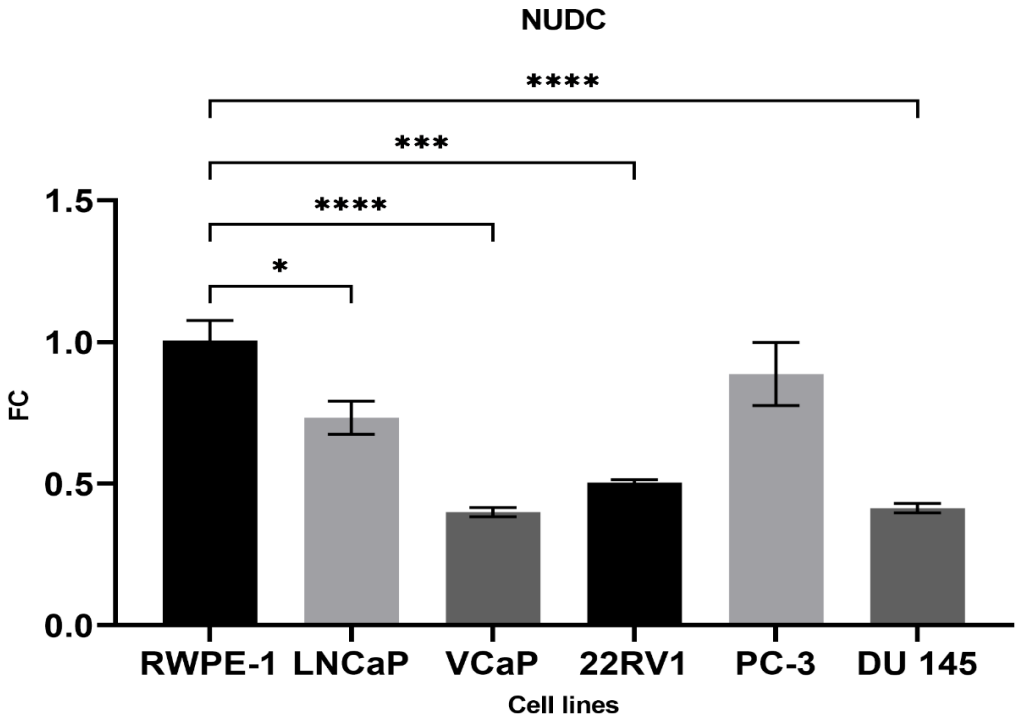
NUDC
****
***
****
*
1.5
1.0
0.5
0.0
FC
RWPE-1
LNCaP
VCaP
22RV1
PC-3
DU 145
Cell lines

(B)

Figure 3.11. Validation of hsa_circ_0005087 and associated parental gene, *NUDC* in the panel of normal and malignant cell lines. (A) hsa_circ_0005087 and (B) *NUDC* in RWPE-1, LNCaP, VCaP, 22RV1, PC-3 and DU145. Data graphed as mean ± SEM (n=3). Data analysed using an ordinary one-way ANOVA followed by a Dunnett's *post hoc* test. (*p ≤ 0.05, **p ≤ 0.01, ***p ≤ 0.001, ****p ≤ 0.0001).

3.1.5.5 hsa_circ_0005320

hsa_circ_0005320 was significantly up-regulated in DU145 *vs.* RWPE-1 (FC 2.11 ± SEM 0.55, p = 0.04) (Figure 3.12A). The expression of hsa_circ_0005320 was not statistically significant in all AR dependent (LNCaP, VCaP and 22RV1) and AR independent (PC-3) PCa cell lines compared to RWPE-1 (FC 1.28 ± SEM 0.07, p = 0.9), (FC 1.9 ± SEM 0.23, p = 0.09), (FC 0.42 ± SEM 0.001, p = 0.3) and (FC 1.3 ± SEM 0.13, p = 0.9) respectively (Figure 3.12A). Its associated parental gene *SEPT9* was down-regulated in both LNCaP and 22RV1 *vs.* RWPE-1 (FC 0.48 ± SEM 0.037, p = 0.0001) and (FC 0.36 ± SEM 0.04, p < 0.0001) respectively with similar expression in VCaP *vs.* RWPE-1 (FC 0.97 ± SEM 0.01, p = 0.9) (Figure 3.12B). *SEPT9* was significantly up-regulated in PC-3 *vs.* RWPE-1 (FC 1.53 ± SEM 0.05, p = 0.0001) but significantly down-regulated in DU145 *vs.* RWPE-1 (FC 0.51 ± SEM 0.02, p = 0.0002) (Figure 3.12B).

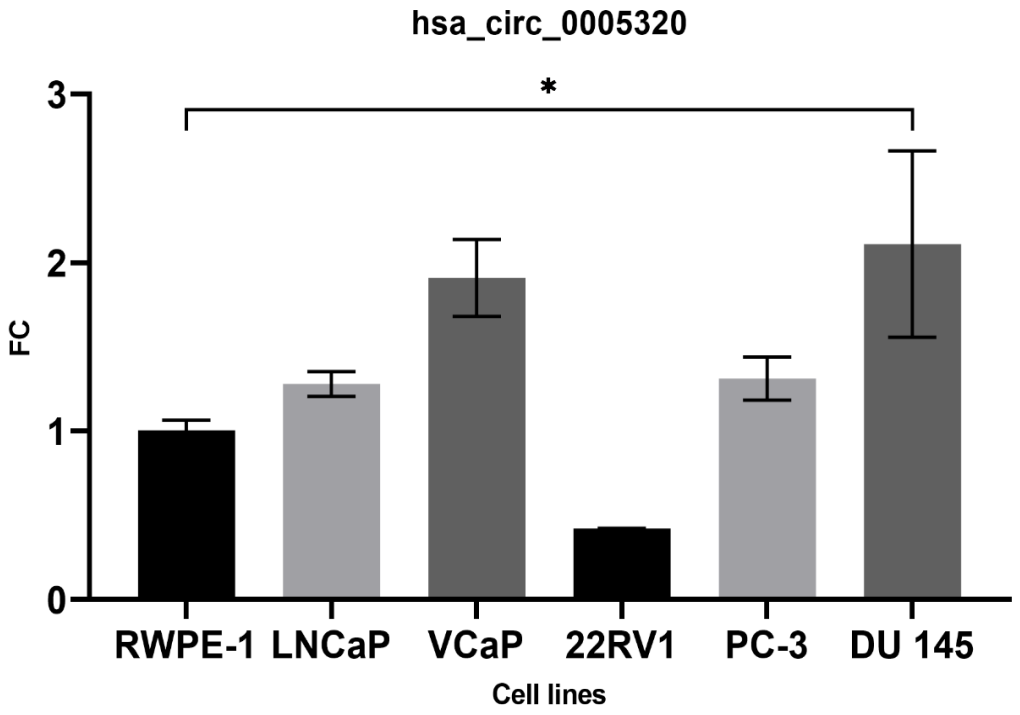

(A)

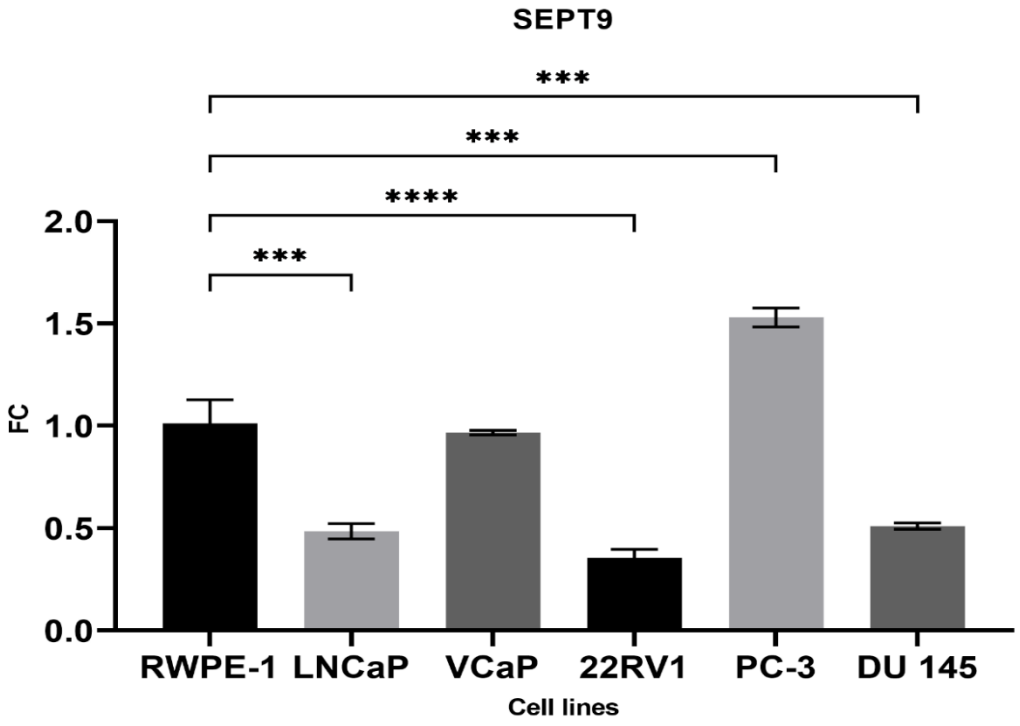

(B)

Figure 3.12. Validation of hsa_circ_0005320 and associated parental gene, *SEPT9* in the panel of normal and malignant cell lines. (A) hsa_circ_0005320 and (B) *SEPT9* in RWPE-1,

LNCaP, VCaP, 22RV1, PC-3 and DU145. Data graphed as mean ± SEM (n=3). Data analysed using an ordinary one-way ANOVA followed by a Dunnett's *post hoc* test. (*p ≤ 0.05, ***p ≤ 0.001, ****p ≤ 0.0001).

3.1.6 circRNAs in enzalutamide resistance PCa cell lines

3.1.6.1 circRNA profiling of isogenic model of enzalutamide resistance cell lines

circRNA microarray analysis was performed across a panel, which consisted of a Control cell line, Clone 1 cell line and Clone 9 cell line (366). Differentially expressed circRNAs were identified within the isogenic model. circRNA with a FC ≥ 1.5 and $p < 0.05$ were considered significantly differentially expressed. There were 230 circRNAs up-regulated in Clone 1 *vs.* Control ($p < 0.05$) and 465 circRNAs that were down-regulated in Clone 1 *vs.* Control ($p < 0.05$). There were 60 circRNAs up-regulated in Clone 9 *vs.* Control ($p < 0.05$) and 175 circRNAs that were down-regulated in Clone 9 *vs.* Control ($p < 0.05$) (366). The top 5 up-regulated circRNAs in Clone 1 *vs.* Control ranked by FC are shown in Table 3.2.

Table 3.2. Top five up-regulated circRNAs with its associated parental gene in Clone 1 *vs.* Control based on FC.

circRNA	**FC/(p value)**	**Parental Gene**	**Parental Gene Function**
hsa_circ_0001275	5.8 (p = 0.047)	*PLCL2*	Part of a 23-gene signature, which predicted metastatic lethal PCa outcomes (367).
hsa_circ_0026462	5.7 (p = 0.026)	*KRT1*	Target receptor overexpressed in breast cancer cells (368).
hsa_circ_0033144	5.2 (p = 0.012)	*BCL11B*	Methylation occurs in PCa (369).
hsa_circ_0000673	4.2 (p = 0.038)	*RSL1D1*	Associated with an aggressive phenotype and a poor prognosis in patients with PCa (370).

hsa_circ_0000129	3.9 (p = 0.039)	*VPS72*	May have role in regulating haematopoietic stem cell activity (371).

3.1.6.2 RT-qPCR validation of top five up-regulated circRNAs with their associated parental genes in the isogenic model of enzalutamide resistance cell lines

Custom designed outward facing primers were used for validation via RT-qPCR for selected top five up-regulated circRNAs (Table 3.2). Out of the five circRNAs, two (hsa_circ_0001275 and hsa_circ_0000129) were in line with the microarray data.

hsa_circ_0001275 was significantly up-regulated in Clone 1 *vs.* Control (FC 5.02 ± SEM 0.74, p = 0.006) (Figure 3.13A). This circRNA was also up-regulated in Clone 9 *vs.* Control but was not statistically significant (FC 2.86 ± SEM 0.4, p = 0.14) (Figure 3.13A). The associated parental gene *PLCL2* was significantly up-regulated in Clone 1 *vs.* Control and Clone 9 *vs.* Control (FC 7.17 ± SEM 0.03, p = 0.0026 and FC 8.33 ± SEM 1.19, p = 0.001, respectively) (Figure 3.13B). The second validated circRNA, hsa_circ_0000129 was up-regulated in Clone 1 *vs.* Control (FC 2.71 ± SEM 0.2, p = 0.023), however, the associated parental gene, *VPS72*, showed no difference between both cell lines (FC 0.81 ± SEM 0.009, p = 0.36) (Figure 3.13C and 3.13D, respectively).

hsa_circ_0000673 was significantly down-regulated in Clone 1 *vs.* Control (FC 0.31 ± SEM 0.05, p = 0.023) (Figure 3.13E), which was in contrast to the microarray result. The associated parental gene RSL1D1 was not significantly different in Clone 1 *vs.* Control (FC 0.49 ± SEM 0.003, p = 0.096) (Figure 3.13F). There was no significant difference in the expression of hsa_circ_0033144 in Clone 1 *vs.* Control (FC 1.15 ± SEM 0.05, p = 0.75) (Figure 3.13G). The expression of the associated parental gene *BCL11B* was also not significant in Clone 1 *vs.* Control (FC 0.38 ± SEM 0.13, p = 0.32) (Figure 3.13H). However, this circRNA expression and its associated parental gene was significantly up-regulated in Clone 9 *vs.* Control (FC 5.0 ± SEM 0.2, p < 0.0001 and FC 3.6 ± SEM 0.29, p = 0.008, respectively) (Figure 3.13G and 3.13H respectively).

The expression of hsa_circ_0026462 and associated parental gene *KRT1* was not significantly different in Clone 1 *vs.* Control or Clone 9 *vs.* Control (FC 0.81 ± SEM 0.05, p = 0.60 and FC 1.57 ± SEM 0.14, p = 0.77, respectively) (Figure 3.13I and 3.13J, respectively).

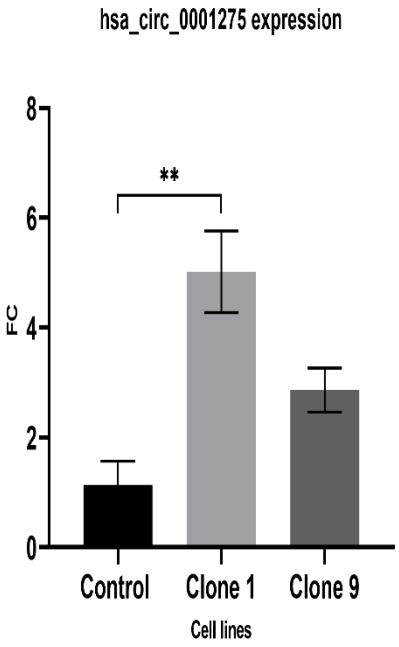
hsa_circ_0001275 expression
FC
8
6
4
2
0
**
Control
Clone 1
Clone 9
Cell lines

(A)

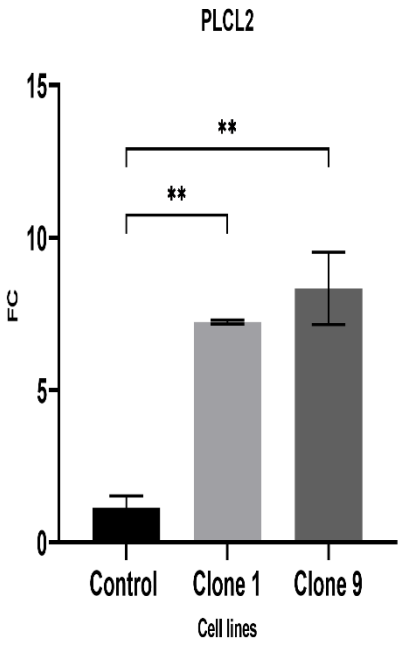
PLCL2
FC
15
10
5
0
**
**
Control
Clone 1
Clone 9
Cell lines

(B)

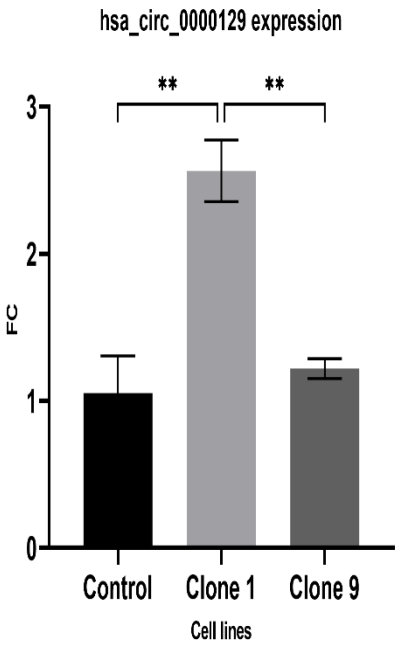
hsa_circ_0000129 expression
FC
3
2
1
0
**
**
Control
Clone 1
Clone 9
Cell lines

(C)

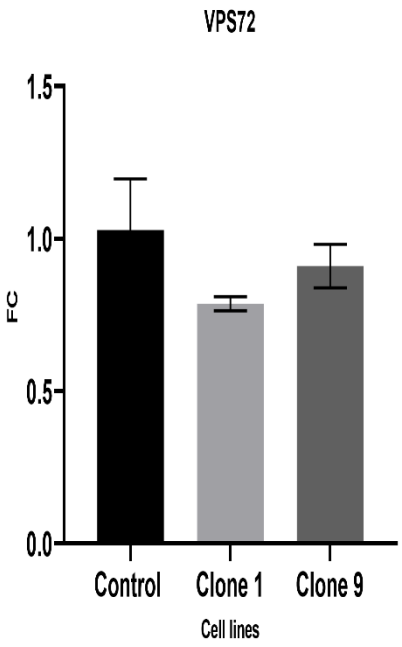
VPS72
FC
1.5
1.0
0.5
0.0
Control
Clone 1
Clone 9
Cell lines

(D)

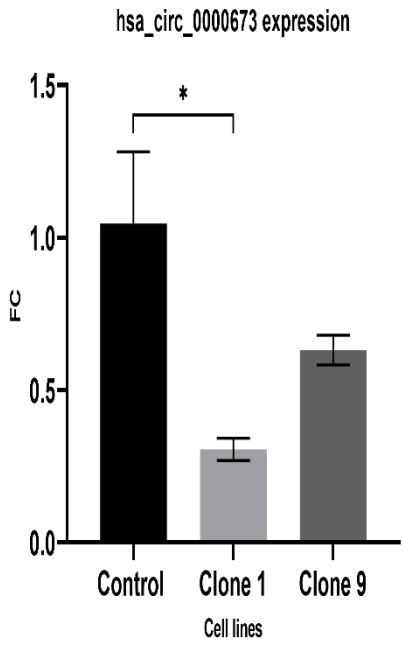
hsa_circ_0000673 expression
*
1.5
1.0
0.5
0.0
FC
Control
Clone 1
Clone 9
Cell lines

(E)

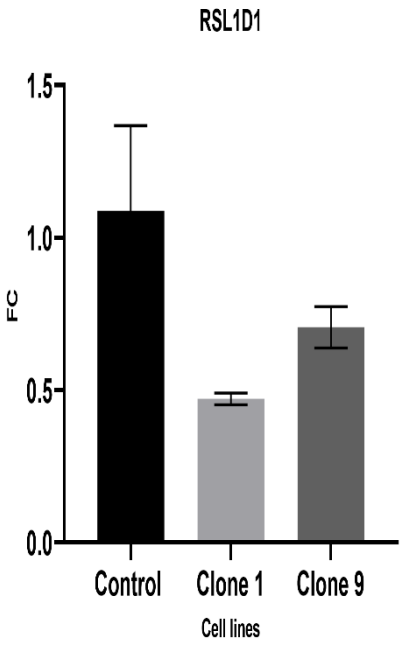
RSL1D1
1.5
1.0
0.5
0.0
FC
Control
Clone 1
Clone 9
Cell lines

(F)

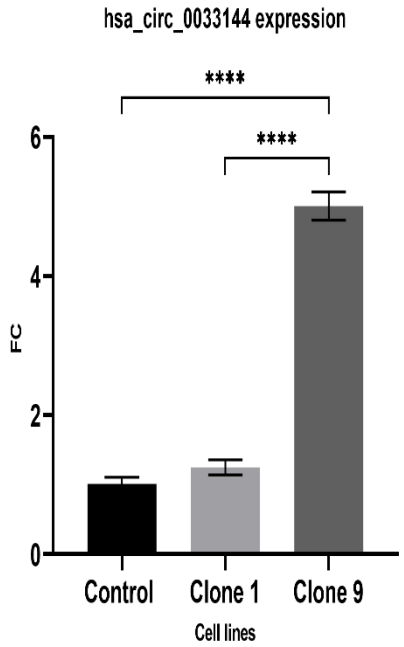
hsa_circ_0033144 expression
****
****
6
4
2
0
FC
Control
Clone 1
Clone 9
Cell lines

(G)

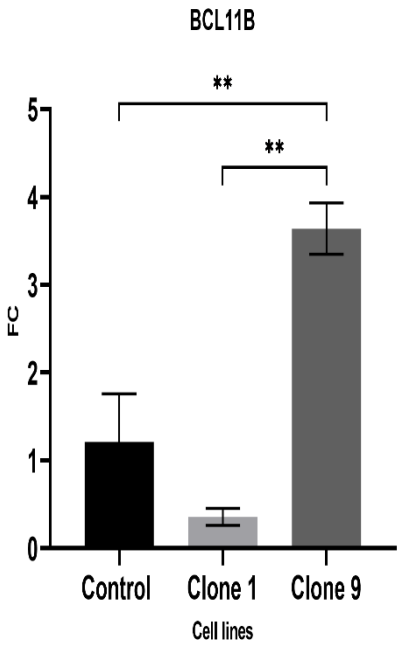
BCL11B
**
**
5
4
3
2
1
0
FC
Control
Clone 1
Clone 9
Cell lines

(H)

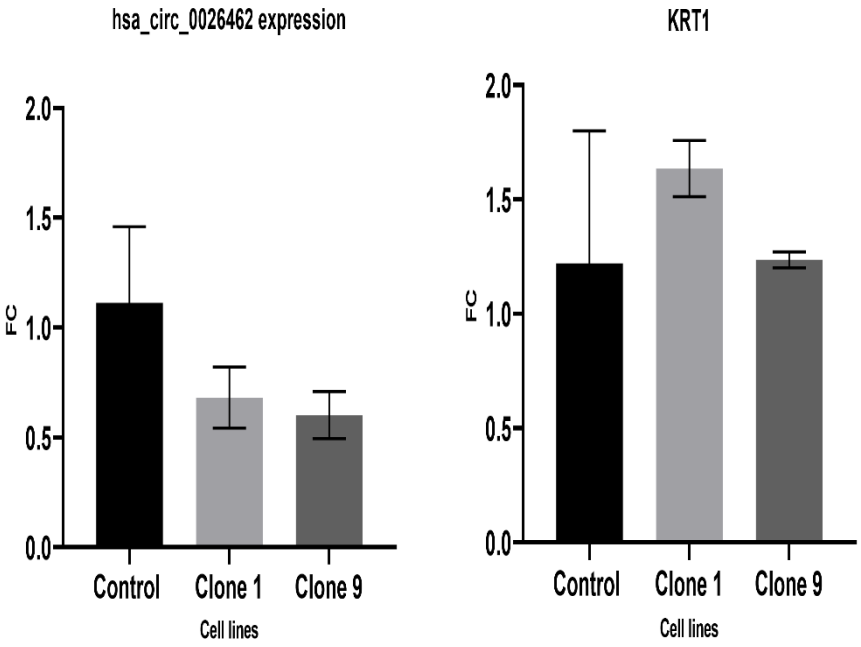

(I) **(J)**

Figure 3.13. Validation of circRNAs and associated parental gene in the enzalutamide panel. (A) hsa_circ_0001275, (B) *PLCL2* parental gene, (C) hsa_circ_0000129, (D) *VPS72* parental gene, (E) hsa_circ_0000673, (F) *RSL1D1* parental gene, (G) hsa_circ_0033144, (H) *BCL11B* parental gene, (I) hsa_circ_0026462, (J) *KRT1* parental gene. Data graphed as mean ± SEM (n=3). Data analysed using an ordinary one-way ANOVA followed by a Tukey's *post hoc* test. (*p ≤ 0.05, **p ≤ 0.01, ***p ≤ 0.001, ****p ≤ 0.0001).

3.1.6.2.1 RT-qPCR validation of hsa_circ_0001721 associated parental genes, CDK14 in the isogenic model of enzalutamide resistance cell lines

Our group has previously shown that the hsa_circ_0001721 was up-regulated in the highly resistant clone compared to Control using RT-qPCR (334) (Figure 3.14A). Its parental gene, *CDK14* was also up-regulated in Clone 1 *vs.* Control (FC 3.51 ± SEM 0.64, p = 0.009) (Figure 3.14B).

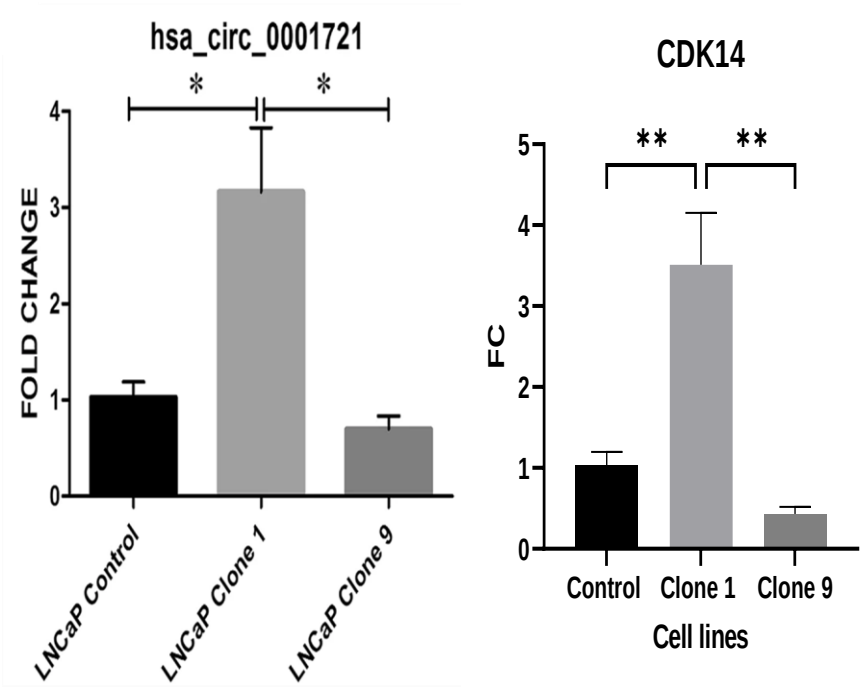

(A) **(B)**

Figure 3.14. hsa_circ_0001721 and *CDK14* in the enzalutamide resistant panel. (A) hsa_circ_0001721 RT-qPCR validation (image adapted from Greene *et al.)* (334), (B) *CDK14* parental gene RT-qPCR validation. Data graphed as mean ± SEM (n=3). Data analysed using an ordinary one-way ANOVA followed by a Tukey's *post hoc* test. (*p ≤ 0.05, **p ≤ 0.01).

3.1.6.3 Additional methods for validation of the hsa_circ_0001275 and hsa_circ_0001721

Both hsa_circ_0001275 and hsa_circ_0001721 were selected for further studies on the basis that their parental gene were also up-regulated in the strongly resistant clone compared to Control. To verify the characteristics of stability, circRNAs were treated with RNase R. RNAse R was used to degrade linear RNAs and thus enrich for circRNAs. RNAse R was used as a proof of concept to confirm circRNA expression during RT-qPCR validation. As expected, the circRNAs were resistant to RNase R treatment in contrast to linear control (Figure 3.15). The RT-qPCR products of circRNAs were electrophoresed on an agarose gel for sequencing purposes (Figure 3.16). The identity of hsa_circ_0001275 and hsa_circ_0001721 were confirmed by Sanger sequencing (Figure 3.17).

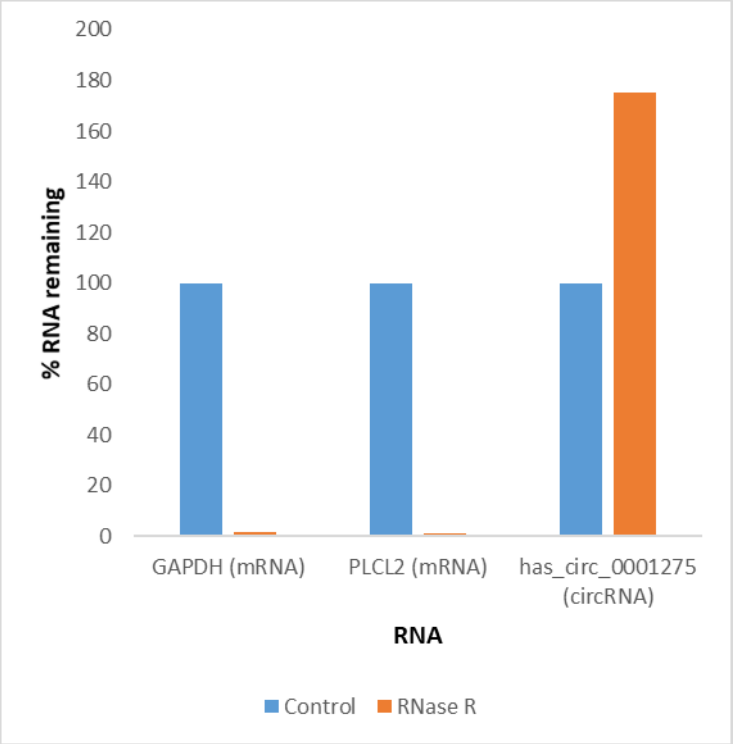

Figure 3.15. hsa_circ_0001275 enrichment using RNase R treatment. RT-qPCR data showing the resistance of circRNA to RNase R treatment as reflected by the levels of circRNA and linear RNAs in RNase R (orange) treated sample compared with control (blue) treatment. (n=1)

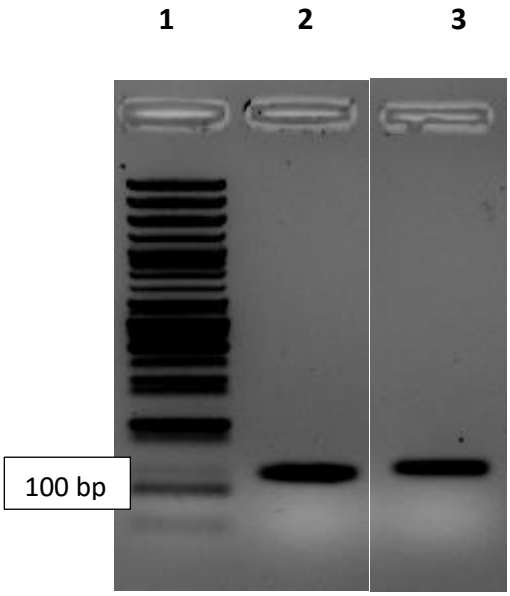

Figure 3.16. Agarose gel electrophoresis results of RT-qPCR amplified products from circRNA validation. Lane 1: 50 bp DNA ladder, lane 2: hsa_circ_0001275 product (122bp), lane 3: hsa_circ_0001721 product (130bp).

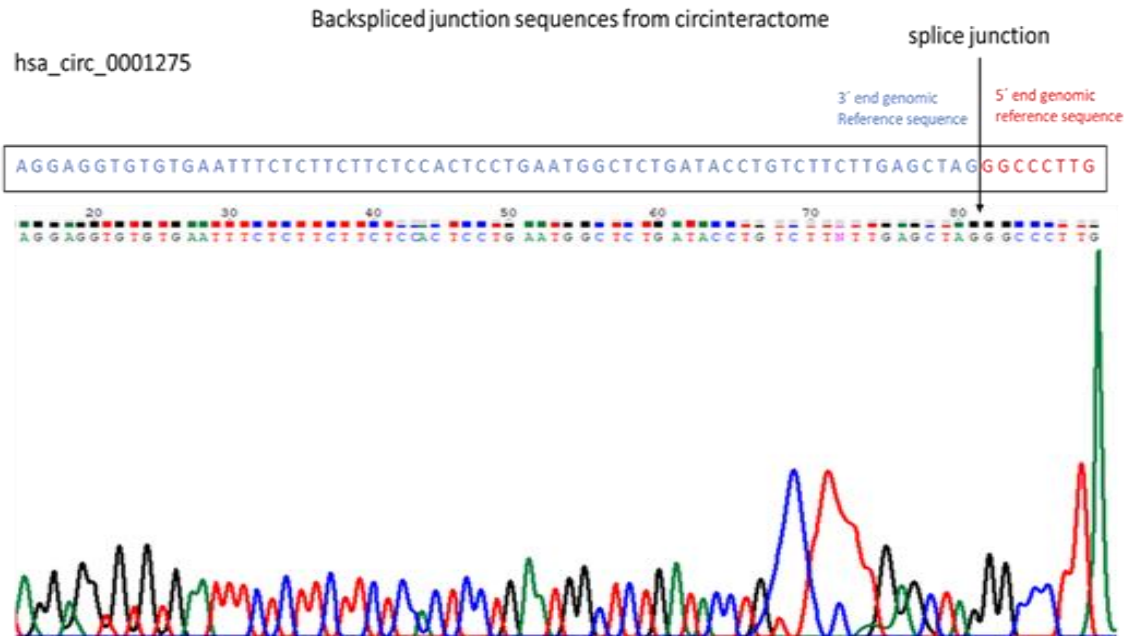

(A)

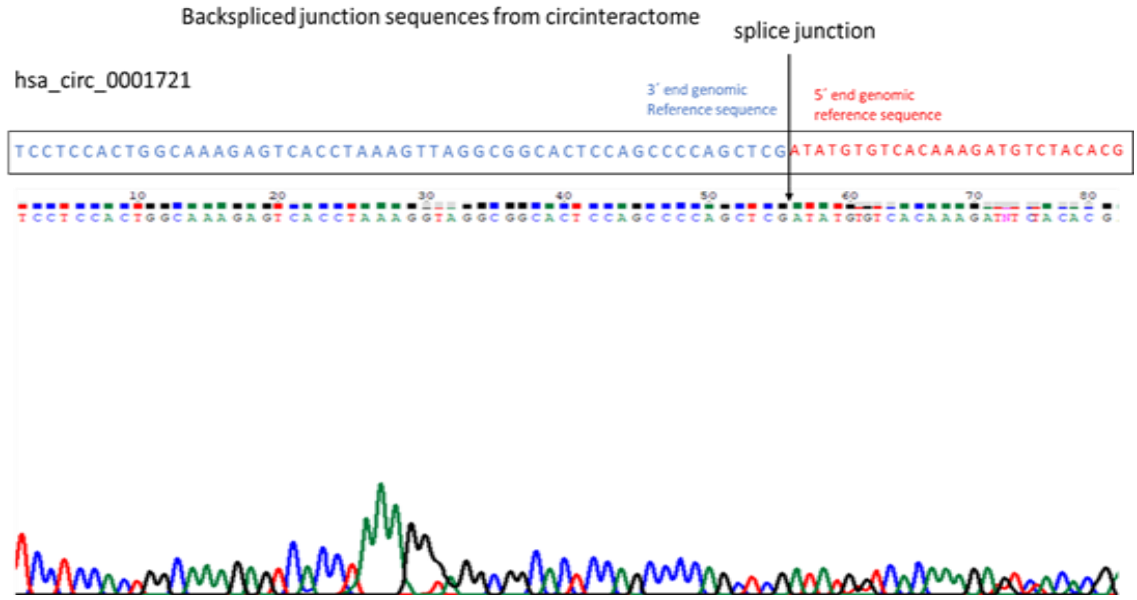

(B)

Figure 3.17. Confirmation of circRNA by Sanger sequencing. (A) hsa_circ_0001275 and (B) hsa_circ_0001721 by Sanger sequencing. Both RT-qPCR product sequence aligned to respective backspliced junction sequence obtained from circinteractome database.

3.1.6.4 miRNA associated with circRNA

miRNA response elements (MREs) are miRNA binding sites on circRNAs that were predicted using TargetScan (372) and miRanda (373) bioinformatic platforms based on the circRNA-miRNA-mRNA network. hsa_circ_0001275 was chosen for further studies following validation steps. All five of the predicted miRNAs for hsa_circ_0001275 using Arraystar's miRNA prediction software (Figure 3.18) were selected for validation studies (Table 3.3). The expression of three out of the five selected miRNA were significantly different between the isogenic cell lines. miR-361-5p was significantly up-regulated in both Clone 1 *vs.* Control ($p < 0.0001$) and in Clone 9 *vs.* Control ($p < 0.0001$) (Figure 3.19Ai). miR-422a and miR-378a-3p was significantly up-regulated only in Clone 1 *vs.* Control ($p = 0.046$ and $p = 0.0087$ respectively) (Figure 3.19Bi and 3.19Ci, respectively). There was no significant difference in expression of miR-370-3p and miR-506-3p between the cell lines (Figure 3.19D and 3.19E respectively). The hypothesized associated target genes of the target miRNA as listed on Table 3.3 were validated using RT-qPCR. Target genes of miR-370-3p and miR-506-3p were not investigated further as there were no significant differences in expression of these miRNA within the cell line panel. The expression of *STAT6* was significantly up-regulated in Clone 1 *vs.* Control and Clone 9 *vs.* Control (FC 68.4 ± SEM 2.33, $p = 0.0226$ and FC 153 ± SEM 21.9, $p = 0.0004$, respectively) (Figure 3.19Aii). Whereas *KLK4* was significantly down-regulated only in Clone 9 *vs.* Control (FC 0.1735 ± SEM 0.0438, $p = 0.0007$) (Figure 3.19Bii). There was no significant difference in expression of *PDK2* between the cell lines (Figure 3.19Cii).

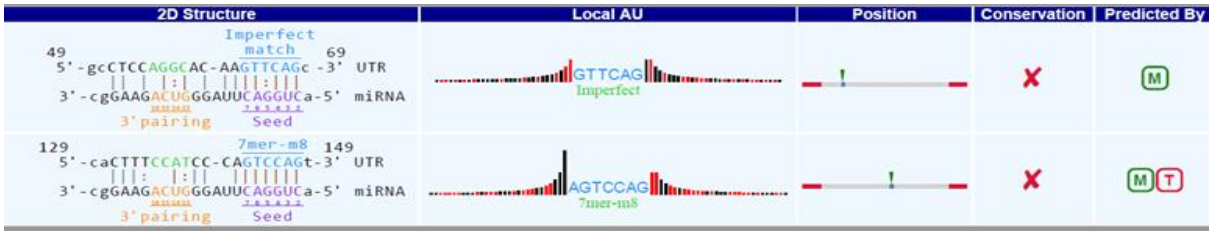

(A)

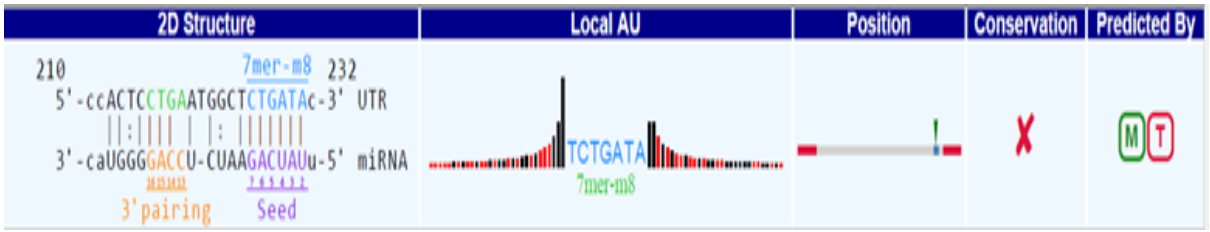

(B)

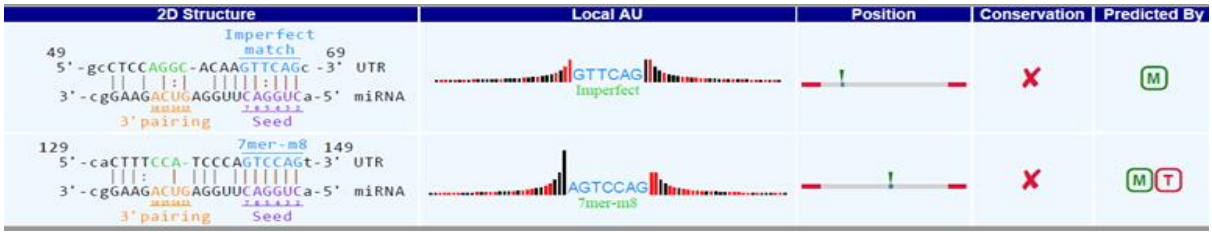

(C)

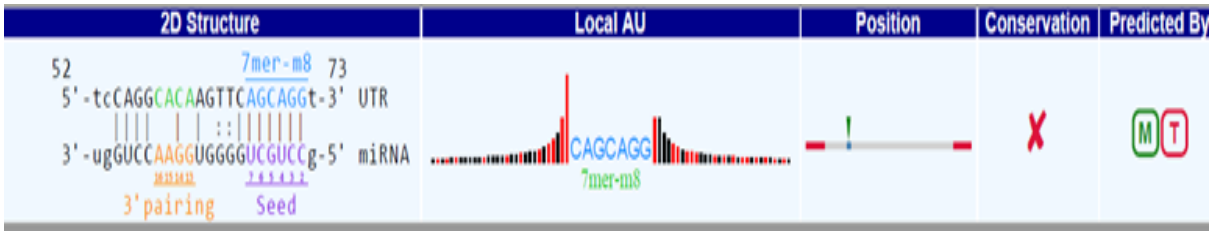

(D)

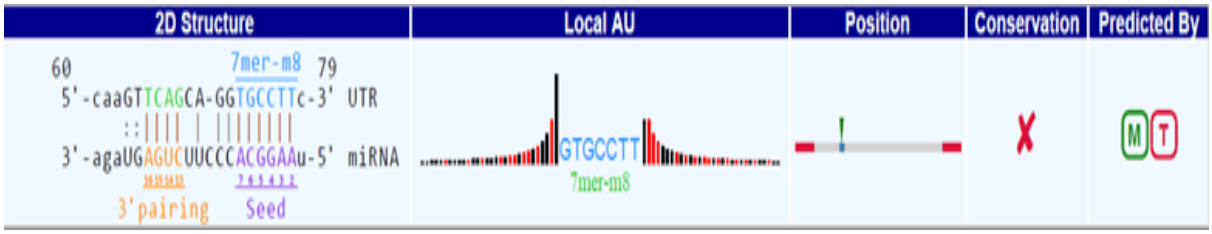

(E)

Figure 3.18. Detailed annotation for predicting circRNA-miRNA interaction. This was performed for hsa_circ_0001275 using Arraystar's integrated TargetScan and miRanda bioinformatic platforms (372, 373). The top five hsa_circ_0001275 target miRNAs were predicted as follows: (A) miR-361-5p, (B) miR-422a, (C) miR-378a-3p, (D) miR-370-3p and (E) miR-506-3p.

Image created by Arraystar.

Table 3.3. Top five target miRNAs predicted for hsa_circ_0001275 with its hypothesised function and associated target gene.

Predicted target miRNAs for hsa_circ_0001275	**Hypothesized miRNA function**	**Hypothesized associated target gene**	**Hypothesized gene function**	**Reference**
miR-361-5p	Tumour suppressor-miR. Suppress cell growth and proliferation. Expression lower in CRPC *vs.* CSPC tissues.	*STAT6*	Oncogene. Expression higher in PCa *vs* normal tissue. Prognostic factor in CRPC. Regulates *BCL-XL* at transcriptional level in CRPC.	(374)
miR-422a	Tumour suppressor-miR. Expression reduced in PCa *vs.* normal cell lines. Suppress Warburg effect by targeting PDK2	*PDK2*	Oncogene. Promotes proliferation and Warburg effect.	(375)
miR-378a-3p	Tumour suppressor-miR. Expression reduced in PCa *vs.* BPH tissues. Prognostic marker for relapse.	*KLK4*	Oncogene. Increase tumorigenesis and metastasis.	(376)
miR-506-3p	Tumour suppressor-miR. Suppress cell growth, proliferation, and invasion. Induced cell cycle arrest and apoptosis.	*ITGB1, ITGB3 and ITGA3*	Oncogene. Interacts with multiple extracellular matrix protein and mediate survival signalling in cancer.	(377)
miR-370-3p	Onco-miR. Expression increase in PCa *vs.* normal cells.	*FOXO1*	Tumour suppressor. Supress cell growth and angiogenesis. Pro-apoptosis.	(378)

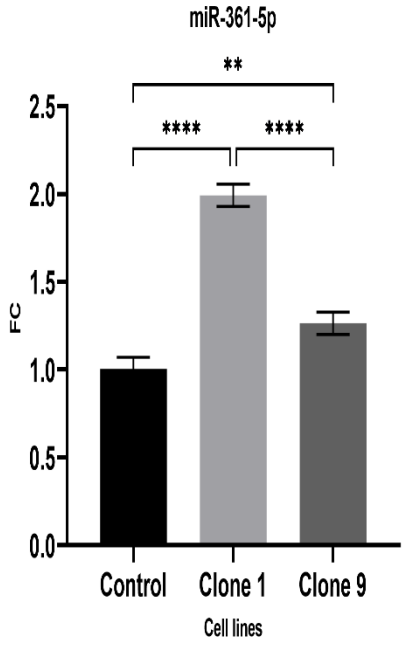
miR-361-5p
**
****
****
2.5
2.0
1.5
1.0
0.5
0.0
FC
Control
Clone 1
Clone 9
Cell lines

(Ai)

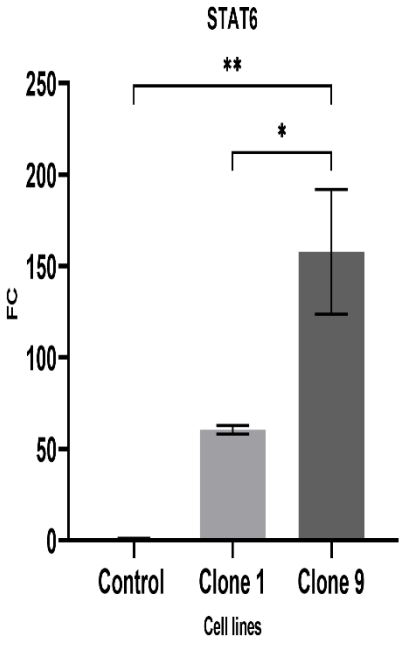
STAT6
**
*
250
200
150
100
50
0
FC
Control
Clone 1
Clone 9
Cell lines

(Aii)

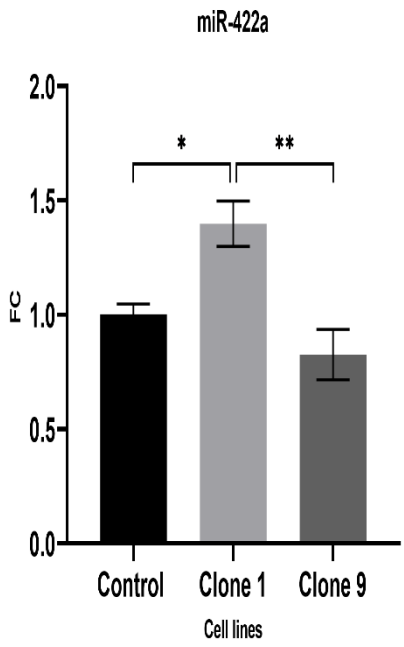
miR-422a
*
**
2.0
1.5
1.0
0.5
0.0
FC
Control
Clone 1
Clone 9
Cell lines

(Bi)

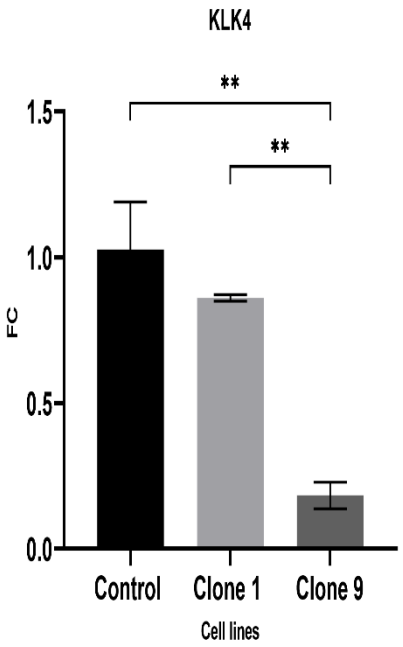
KLK4
**
**
1.5
1.0
0.5
0.0
FC
Control
Clone 1
Clone 9
Cell lines

(Bii)

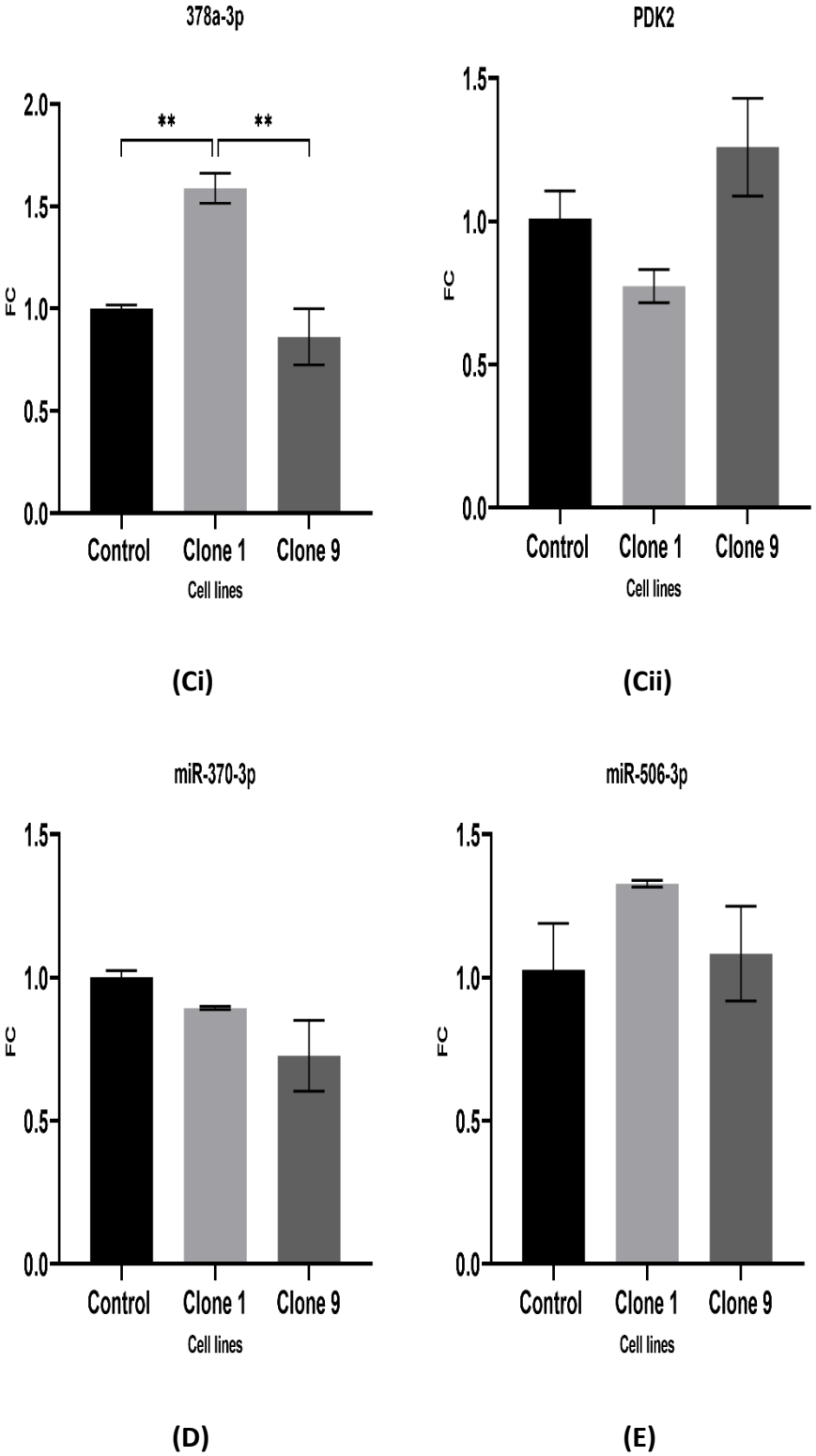

Figure 3.19. Expression of miRNAs associated with hsa_circ_0001275 in enzalutamide resistant cell lines and its associated target mRNA. (Ai) miR-361-5p, (Aii) *STAT6*; (Bi) miR-422a, (Bii) *KLK4*; (Ci) miR-378a-3p, (Cii) *PDK2*; (D) miR-370-3p; and (E) miR-506-3p. Data

graphed as mean ± SEM (n=3). Data analysed using an ordinary one-way ANOVA followed by a Tukey's *post hoc* test. (*p ≤ 0.05, **p ≤ 0.01, ***p ≤ 0.001, ****p ≤ 0.0001).

3.1.7 Functional assessment of circRNA

3.1.7.1 Stable over expression of circRNA in Control cell line

3.1.7.1.1 Overexpression of hsa_circ_0001275 and hsa_circ_0001721

A geneticin kill curve was first performed (section 2.6.2.1).The Control cell line was transfected using Lipofectamine 3000 (section 2.6.2.2). After 2 weeks, several clones were evident and further subjected to flow cytometry for GFP positive cell selection (Figure 3.20). The clones were classified as stable over expression clones for (i) EVC, (ii) hsa_circ_1275 and (iii) hsa_circ_1721 in Control cell line.

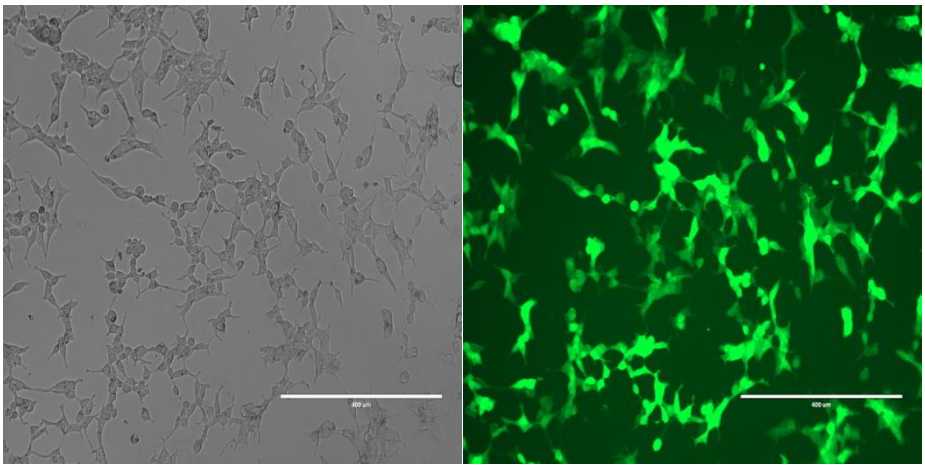

(A) **(B)**

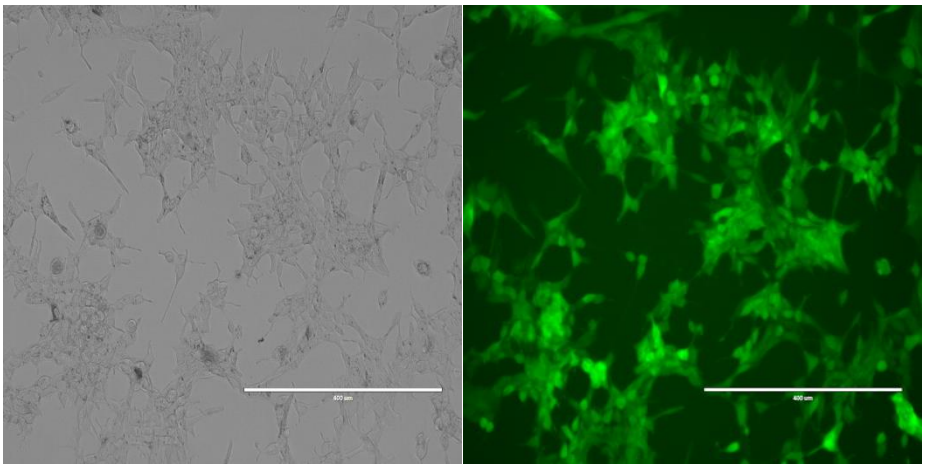

(C) **(D)**

Figure 3.20. Representative images of Control cell line transfected with hsa_circ_0001275. Images generate using (A) bright field and (B) fluorescence microscopy and hsa_circ_0001721 using (C) bright field and (D) fluorescence microscopy. All scale bars are 400 µm. All images are X10 magnification.

3.1.7.1.2 Validation of stable clones

A mixed population of stable clones were selected for the remainder of the experiments in this project. To verify that the stable clones contained the inserts of interest RNA was isolated from each of the over expression cell lines (EVC, pCD25-ciRhsa_circ_0001275 and pCD25-ciRhsa_circ_0001721) (n=3) and circRNA expression was determined using RT-qPCR. hsa_circ_0001275 was significantly up-regulated in Control cell lines, which were stably transfected with pCD25-ciR hsa_circ_0001275 (*1275 Stable*) *vs.* Control and *1275 Stable vs.* EVC (FC 21.7± SEM 5.32, p = 0.0074 and FC 33.4± SEM 8.2, p = 0.0069 respectively) (Figure 3.21A). Whereas, hsa_circ_000721 was significantly up-regulated in Control cell lines stably transfected with pCD25-ciR hsa_circ_0001721 (*1721 Stable*) *vs.* Control and *1721 Stable vs.* EVC (FC 18.82± SEM 2.75, p = 0.0005 and FC 17.0± SEM 2.49, p = 0.0006 respectively) (Figure 3.21B).

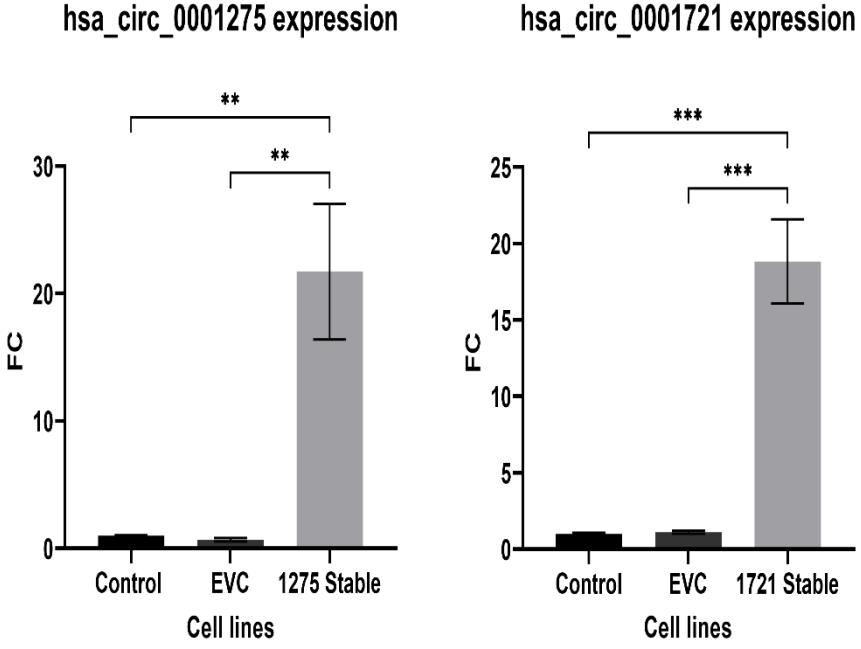

Figure 3.21. RT-qPCR expression of circRNA in the stably transfected cell lines. (A) hsa_circ_0001275 and (B) hsa_circ_0001721. Data graphed as mean ± SEM (n=3). Data analysed using an ordinary one-way ANOVA followed by a Tukey's *post hoc* test. (**p ≤ 0.01, ***p ≤ 0.001).

3.1.7.2 Expression of parental gene associated to circRNA in Stable clones

Clone 1 had high expression of both hsa_circ_0001275 and hsa_circ_0001721 including their associated parental genes compared to Control. RT-qPCR validation of circRNA parental genes in both *1275 Stable* and *1721 Stable* showed no significant up-regulation of their respective circRNA parental genes, suggesting that alteration of circRNA expression does not affect the expression of the parental gene in this instance (Figure 3.22A and 3.22B).

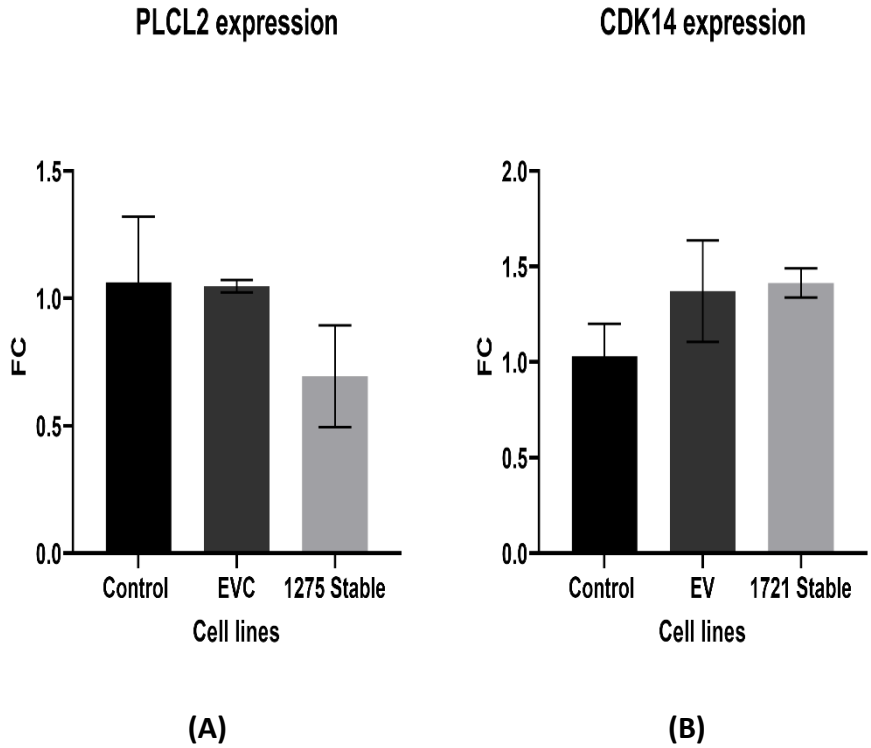

Figure 3.22. RT-qPCR expression of PLCL2 and *CDK14* in stably transfected cell lines. (A) PLCL2 in the hsa_circ_0001275 stably transfected cell line and (B) *CDK14* in the hsa_circ_0001721 stably transfected cell line. Data graphed as mean ± SEM (n=3). Data analysed using an ordinary one-way ANOVA followed by a Tukey's *post hoc* test.

3.1.7.3 hsa_circ_0001275 overexpression contributed to enzalutamide resistance

Cells were seeded at 1 x 10^3/well in a 96 well plate and treated with various doses of enzalutamide. The treated cell lines were incubated for 1 week and proliferation quantified using a BrdU ELISA. The proliferative capacity of *1275 Stable* and *1721 Stable* in comparison to Control and EVC in the absence of drug were evaluated. The untreated control was set to 100%. There were no significant differences between *1275 Stable vs.* Control (107% *vs.* 100%) ($p < 0.05$) and EVC *vs.* Control (99% *vs.* 100%) ($p < 0.05$) in the absence of enzalutamide treatment (untreated) (Figure 3.23A). Additionally, there were no significant differences in the proliferative capacity between *1721 Stable vs.* Control (110% *vs.* 100%) ($p < 0.05$) and EVC *vs.* Control (102% *vs.* 100%) ($p < 0.05$) in the absence of enzalutamide treatment (untreated) (Figure 3.23B).

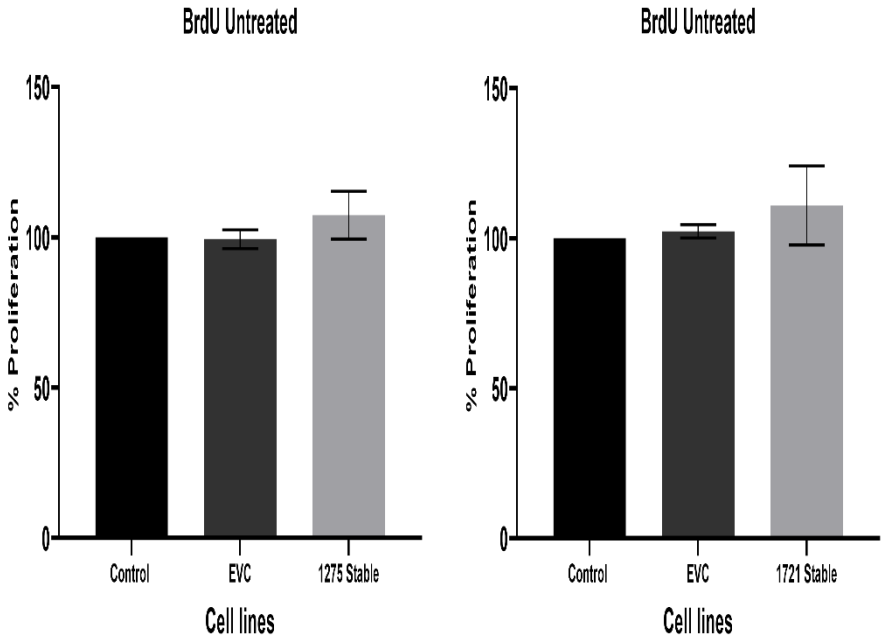

(A) **(B)**

Figure 3.23. The proliferative rate of Control, EVC and stable cell lines. Proliferative capacity of (A) hsa_circ_0001275 (1275 Stable) and (B) hsa_circ_0001721 (1721 Stable) in the absence of enzalutamide. Proliferation was measured using BrdU ELISA. Data graphed as mean ± SEM (n=3). Data analysed using an ordinary one-way ANOVA followed by a Tukey's *post hoc* test.

The DMSO vehicle control served as untreated and was set to 100%. The *1275 Stable* cell line showed a significant increase in resistance to enzalutamide at every concentration tested ($p < 0.05$) except for 80 µM compared to EVC (Figure 3.24A), as judged by the proliferative capacity of the cell lines. The *1275 Stable* cell line showed significant increased resistance to enzalutamide at every concentration tested ($p < 0.05$) except for 2 µM and 80 µM compared to Control cell line (Figure 3.24B), when comparing the proliferative capacity of the cell lines. There was no significant difference in *1721 Stable* compared to EVC at every enzalutamide concentration tested (Figure 3.24C), however, there was significant resistance to enzalutamide at 2, 5, 15 and 20 µM concentration range ($p < 0.05$) compared to Control cell line (Figure 3.24D), based on cellular proliferation capacity.

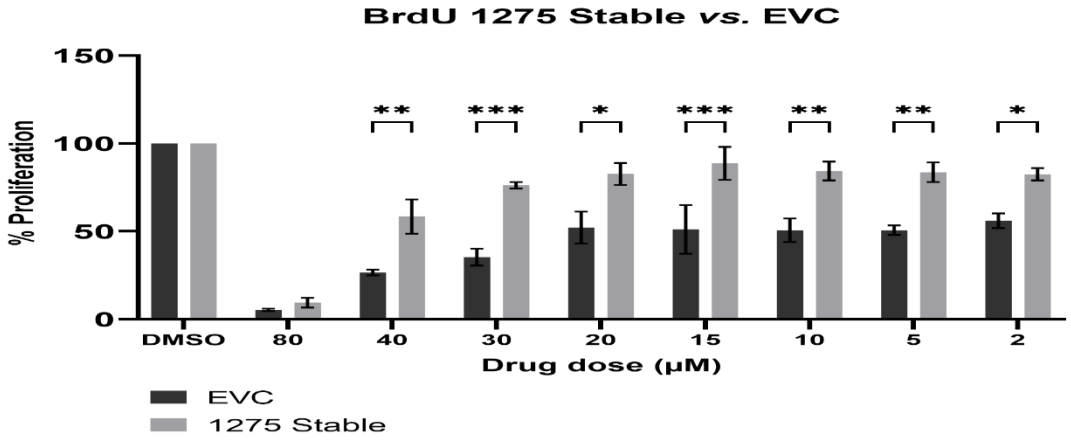

(A)

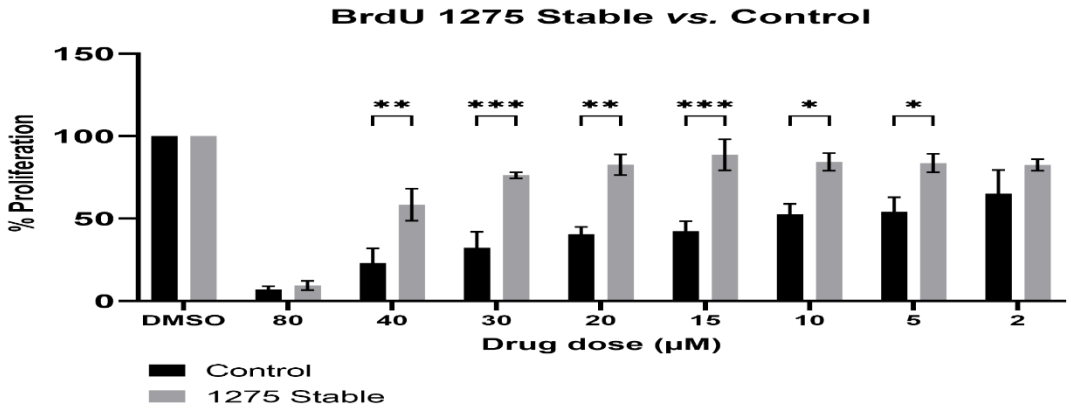

(B)

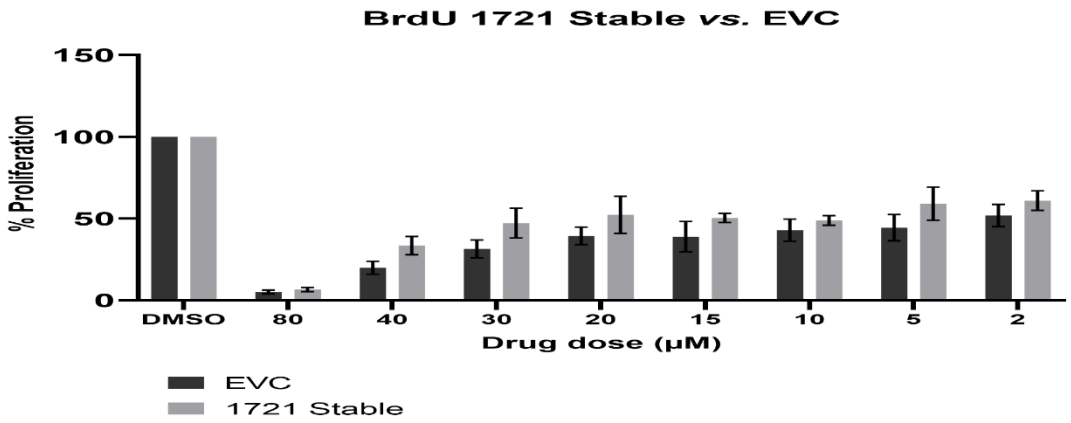

(C)

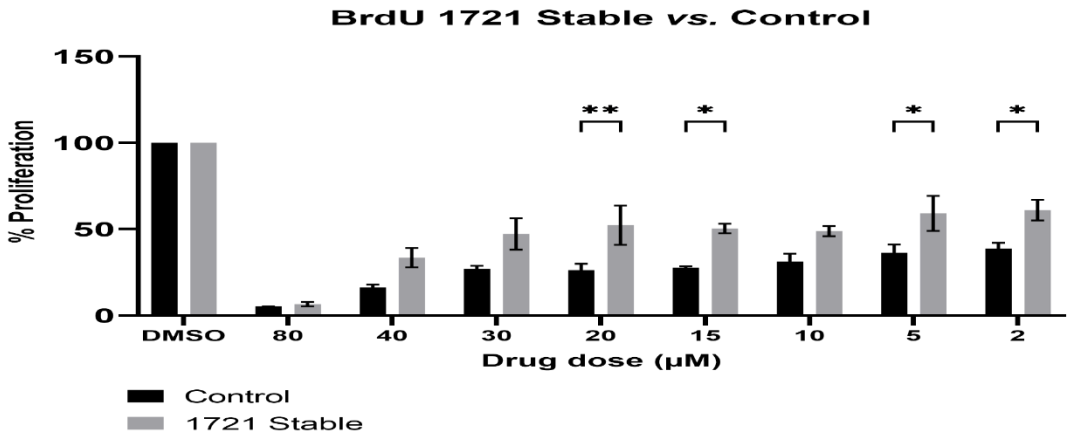

(D)

Figure 3.24. The effect of enzalutamide on the proliferative rate of cell lines. EVC and cell line overexpressing (A) hsa_circ_0001275 (*1275 Stable*) and (C) hsa_circ_0001721 (*1721 Stable*). The effect of enzalutamide on the proliferative rate of Control and cell line overexpressing (B) hsa_circ_0001275 (*1275 Stable*) and (D) hsa_circ_0001721 (*1721 Stable*). Proliferation was measured using BrdU ELISA. Data graphed as mean ± SEM (n=3). Analysis was performed using a Two-way ANOVA followed by a Šídák's *post hoc* test. (*p ≤ 0.05, **p ≤ 0.01, ***p ≤ 0.001). Dimethyl Sulfoxide (DMSO).

3.2 Discussion

Although circRNAs were discovered three decades ago, they have remained a novel RNA since they were originally thought to be part of the by-products of splicing error (220). It was only in the last decade when Salzman *et al.* identified circRNAs in RNA-seq data from samples of paediatric acute lymphoblastic leukaemia, that suggested that they may have more significant importance than formerly perceived (283). Recently, circRNAs have been identified in numerous malignancies including PCa. Their role in cancer remains to be fully elucidated but appears to have importance in cancer initiation, development and progression (226, 335) through mechanisms such as acting as miRNA sponges (287), RBPs and peptide translation (294, 299). Previously, Green *et al.* discovered a number of circRNAs, which were differentially expressed in a model of enzalutamide resistance, further supporting the notion that circRNAs play a role in development of resistance and may be used to monitor for the emergence of enzalutamide resistance and disease progression (334).

Firstly, this study aimed to examine the expression of circRNAs across a panel of prostate cell lines consisting of normal and malignant cells thus, allowing for potential identification of a circRNA signature reflective of the continuum model of PCa progression from normal prostate cells to androgen dependent PCa cells and androgen independent PCa cells. The circRNA microarray profiles in the panel of prostate cell lines were validated using RT-qPCR. The prostate cell lines panel were separated into two groups (normal and malignant) and analysed according to malignancy status and androgen dependency status. The circRNAs were differentially expressed between these groups. Universally, the normal group had the highest number of up-regulated circRNAs compared to the malignant group. Numerous studies have shown that circRNAs are generally reduced in highly proliferative cells across various cancer subtypes due to rapid cell division, thus diluting the circRNA concentration (224, 379, 380), which was consistent with the findings of circRNA expression in the malignant group in this study. The concept of this circRNA dilution effect, however, was in contrast to the findings of Rong *et al.* where the group found high expression of circDcbld1 in vessels intimal hyperplasia and demonstrated a reduction in intimal hyperplasia when the circRNA was silenced suggesting a potential therapeutic approach for the disease (381).

Venn intersection analysis was performed to determine overlapping differentially expressed circRNAs between normal *vs.* malignant compares and androgen dependent *vs.* androgen independent compares. Hundred and sixteen circRNAs were found to be consistently expressed in these two compares. Five of the circRNAs were validated to confirm their expression in the prostate cell line panel. The expression of one out of five validated circRNAs, hsa_circ_0066631 was of particular interest. While the expression of hsa_circ_0066631 was significantly up-regulated in DU145 (androgen independent) *vs.* RWPE-1 (normal) (FC 1.64 ± SEM 0.29, p = 0.028), its expression was significantly down-regulated in each androgen dependent cell line (LNCaP, VCaP and 22RV1) *vs.* RWPE-1 (normal) (FC 0.007 ± SEM 0.001, p = 0.001), (FC 0.19 ± SEM 0.01, p = 0.004) and (FC 0.06 ± SEM 0.002, p = 0.001) respectively. Though not statistically significant, the other androgen independent PCa cell lines, PC-3 had higher hsa_circ_0066631 expression compared to RWPE-1 (FC 1.48 ± SEM 0.11, p = 0.11). Its associated parental gene, DCBLD2 was also significantly down-regulated in all three androgen dependent PCa cell lines (LNCaP, VCaP and 22RV1) compared to RWPE-1 ($p \leq 0.05$) (FC 0.013 ± SEM 0.003, p = 0.0004), (FC 0.074 ± SEM 0.001, p = 0.0008) and (FC 0.07 ± SEM 0.003, p = 0.0007) respectively but was up-regulated in PC-3 (FC 2.09 ± SEM 0.24, p = 0.028) and DU145 (FC 1.37 ± SEM 0.17, p = 0.19) compared to RWPE-1 though not did not reach statistical significance in DU145.

RT-qPCR validation of this consistently expressed circRNA demonstrated a notable configuration of differential expression across the prostate disease spectrum. The expression of hsa_circ_0066631 decreased during early malignancy, where PCa cells were still AR dependent, but increased as the disease progressed to the AR independent stage based on the cell line models of disease. A recent study has shown that hsa_circ_0066631 was highly up-regulated in colorectal cancer spherical cells, which harbour features of cancer stem cells, hence it may be involved in the recurrence and metastasis of colorectal cancer (382). This circRNA was believed to play vital role in the stemness network by acting as an miRNA sponge in down-regulating miR-140–3p, miR-224, miR-382, miR-548c-3p and miR-579 (382). These miRNAs regulate stemness associated pathways such as TGF-β/SMAD and Wnt/β-catenin through mRNA that encode proteins such as ACVR1C/ALK7, FZD3, IL6ST/GP130, SKIL/ SNON, SMAD2, and WNT5 (382). Additionally, in colorectal cancer, *DCBLD2* overexpression has been linked with tumour progression and poor prognosis (361, 383). Another study in glioblastoma showed that EGFR phosphorylation of *DCBLD2* recruits

TRAF6 and stimulates AKT-promoted tumorigenesis (361). *DCBLD2* was down-regulated in AR dependent PCa cell lines but up-regulated in AR independent PCa cell lines in parallel with the expression of hsa_circ_0066631, suggesting possibility that the mechanism of malignant progression or PCa resistance requires the synergistic effect of circRNA and its parental gene. It is also worth noting that hsa_circ_00066631 expression was significantly different between the normal and malignant cell lines, hence it may potentially be an excellent biomarker candidate in complementing PSA to discriminate between normal prostate and PCa, as PSA alone is not adequately specific to discriminate between both disease states especially at intermediate values (384).

Numerous studies in the literature have shown that circRNAs are differentially expressed in a number of human diseases (283, 334). Despite this, there is a scarcity of studies that have examined circRNAs' molecular function (227), and even less have investigated the role of circRNA in drug resistance (335). This study also aimed to investigate circRNAs in the enzalutamide resistant PCa setting. The top 5 circRNAs from the initial array results, ranked by highest FC in the strongly resistant cell line ($p < 0.05$, Clone 1 *vs.* Control) were examined and validated along with their associated parental genes via RT-qPCR. Consistent with the array results, both hsa_circ_0001275 and its parental gene, *PLCL2* were confirmed as up-regulated in the strongly resistant cell line compared to Control ($p < 0.05$). *PLCL2* was part of a 23-gene expression panel that predicts poor prognosis in people with localised PCa in previous studies (367). Thus, further reinforces the possible association of this circRNA with PCa. hsa_circ_0001275 and hsa_circ_0001721 were separately overexpressed in the Control cell line (sensitive to enzalutamide) in order to study the effects of circRNA on enzalutamide resistance. Both hsa_circ_0001275 and hsa_circ_0001721 were selected for overexpression as these circRNAs and their associated parental genes were highly up-regulated in the strongly resistant clone ($p < 0.05$, Clone 1 *vs.* Control) and also associated with invasion and metastasis (a known hallmark in cancer) (367, 385). Cells stably overexpressed with hsa_circ_0001275 were shown to be associated with increased resistance to enzalutamide ($p < 0.05$), based on cellular proliferation. However, cells overexpressing hsa_circ_0001721 did not demonstrate the same proliferative effect, suggesting that increased hsa_circ_0001721 does not contribute to enzalutamide resistance. This infers that only certain up-regulated circRNAs may contribute to resistance by acting as a key regulator through possibly the ceRNAs network. This was

evident from previous studies that have shown a historical role of miRNA "sponging" in circRNA-miRNA-mRNA networks, thus playing important roles in both gene regulation and carcinogenesis (226). For example, in an effort to discover new treatments for osteoporosis, Xu *et al.* recently showed that dexamethasone-induced osteoblast growth inhibition can be reversed by down-regulating hsa_circ_0001275, which mediates the miR-377/CDKN1B axis (386).

miRNA is categorized as sncRNA, comprising approximately 22 nucleotides with the capability to regulate genes post-transcriptionally (229). miRNA can be designated as either an Onco-miR or a tumour suppressor-miR if it inhibits proto-oncogenes (234). The top five most likely miRNA binding sites for hsa_circ_0001275 were predicted using Arraystar's miRNA prediction software and subsequently validated. Out of the five miRNAs, three (miR-361-5p, miR-422a and miR-378a-3p) were significantly up-regulated and two (miR-370-3p and miR-506-3p) showed no significant difference in the highly resistant cell line. These findings were in contrast to the early concept of miRNA sponging, whereby these miRNAs should be down-regulated when circRNA was up-regulated. However, studies that are more recent have shown that rather than acting as a sponge, circRNA may serve as a sanctuary for miRNA stabilisation. For instance, circRNA17 increased the expression of miR-181c-5p by maintaining its stability and in turn, the miRNA decreased the expression of AR-V7 in PCa cells (335). Since circRNAs and miRNAs interact in the ceRNAs network, it is possible that despite the increased expression of miRNA witnessed in our study, these miRNAs might not be able to act on their target mRNA since they are bound to circRNAs. Even though all three up-regulated miRNAs have been described as tumour suppressor-miRs in the literature, they were also described as onco-miR depending on the cancer subtypes (374-376, 387). For instance, Liu *et al.* found that the expression of miR-361-5p was lower in CRPC compared to CSPC tissues by performing miRNA microarray analysis, with an miR-361-5p mimic acting as a tumour suppressor by reducing DU145 proliferation and triggering apoptosis by targeting *STAT6* (374). On the other hand, Wu *et al.* reported that miR-361-5p promotes cervical cancer progression by acting as an onco-miR to enhance cell proliferation and promote cell invasion through the mediation of EMT (387). Thus, hsa_circ_0001275 may contribute to development of enzalutamide resistance through these ceRNAs network. However, further investigations are required to fully delineate the circRNA-miRNA-mRNA network.

This study showed that expression of hsa_circ_0001275 was increased along with its parental gene *PLCL2* in Clone 1 (*vs.* Control) and previous literature described *PLCL2* as associated with aggressive PCa (367). This begs the question of what the parental gene's contribution to the development of enzalutamide resistance is. In the hsa_circ_0001275 (*1275 Stable*) overexpressed cell line, which was more resistant to enzalutamide, there was no difference in the expression of *PLCL2* compared to Control. Therefore, *PLCL2* alone does not contribute to the increase in resistance, based on proliferative capacity. The variability of circRNA expression is not reliant on its parental gene expression as shown by Vo *et al.* (379). In this circRNA overexpression study, the level of circRNA parental gene was not significantly altered when its circRNA was up-regulated. Numerous studies have demonstrated that circRNAs are globally down-regulated in proliferative cells across different cancer subtypes, which may be a result of circRNA concentration dilution upon fast cell division as suggested by Bachmayr-Heyda *et al.* (224) and further supported by findings from Gruner *et al.* (380) displaying accumulation of circRNAs in non-proliferative cells such as ageing nervous tissue. Additionally, Vo *et al.* showed that the universal abundance of circRNAs in LNCaP increased because of decreased cell growth due to a reduction in cellular proliferation from potent kinase inhibition (379). As such, from this supporting literature, the enzalutamide resistance demonstrated in this study was not due to increased malignancy/proliferation in general, however, the precise role of this circRNA on an enzalutamide mechanism of action would require further investigation.

In conclusion, this study demonstrated that hsa_circ_0001275 was highly expressed in enzalutamide resistant cell lines with data suggesting a protective role against enzalutamide *in vitro*. While this current research suggests that hsa_circ_0001275 plays a part in resistance to enzalutamide, the exact functional mechanisms underpinning this have yet to be elucidated. This study provides a valuable foundation for further exploration of circRNAs as therapeutic targets for drug resistant PCa.

Chapter 4 - circRNAs in plasma of patients with enzalutamide resistance PCa

4.0 Introduction

circRNAs are believed to be a novel stable plasma biomarker due to their resistance to degradation by RNA exonucleases (220, 285), presence in cytoplasm and can be partitioned into exosomes (286, 329). A number of circRNA biomarkers have been studied in PCa (388), however, there are few studies in the literature describing the role of circRNA in enzalutamide resistance (334, 335). Furthermore, the molecular function of circRNAs in drug resistant PCa and their potential as biomarkers to inform treatment strategies remain elusive.

The aims of this chapter were to:

1. Examine the accuracy between RT-ddPCR and RT-qPCR for detection of circRNA in plasma samples
2. Examine different methods of RT-ddPCR for detection of circRNA in plasma samples
3. Determine the levels of candidate circRNAs in clinical samples from the Radium-223/Enzalutamide clinical trial (ClinicalTrials.gov Identifier: NCT02225704) (354) and correlate with clinico-pathological data

4.1 RT-qPCR validation of hsa_circ_0001275 and hsa_circ_0001721 in plasma of people with PCa treated with enzalutamide

hsa_circ_0001275 and hsa_circ_0001721 were further investigated in clinical samples using RT-qPCR as the *in vitro* data demonstrated a potential biomarker of enzalutamide resistance. For the pilot study, hsa_circ_0001275 and hsa_circ_0001721 expression were quantified in the plasma of 5 participants with metastatic CRPC (mCRPC). These samples were part of a Phase II trial examining radium-223 in combination with enzalutamide in metastatic castration-resistant PCa (CTRIAL-IE 13-21, NCT02225704). Participants received 6 cycles of radium-223 in combination with enzalutamide followed by enzalutamide alone until disease progression or treatment intolerance (Figure 4.0) (354). The plasma from three different time points were selected according to PSA level. This consisted of baseline (prior to treatment, TP1), PSA nadir (absolute lowest PSA level on treatment, TP2), first PSA progression (an increase of ≥ 25% and absolute increase of ≥ 2 ng/ mL of PSA level from the nadir, TP3). The circRNA quantification was performed using a standard curve method. Serial dilutions of a custom designed gBlock was used in order to determine circRNA copy number within the samples (Figure 4.1A and 4.1B). The expression of hsa_circ_0001275 (Figure 4.2A) and hsa_circ_0001721 (Figure 4.2B) in plasma samples showed a similar trend to PSA level (Figure 4.2C) according to the three time points, however, this was not statistically significant. The mean average copies/ 20 µL of hsa_circ_0001275 at TP2 (9.93 copies/ 20 µL) (plasma at time of PSA nadir) were lower than baseline TP1 (24.8 copies/ 20 µL) (prior to enzalutamide treatment) (Figure 4.2A). TP2 was the time point where the disease responded to enzalutamide treatment (Figure 4.2C) as shown by the mean PSA level, which was significantly lower at TP2 (1.68 µg/L) compared to TP1 (33.54 µg/L) ($p \leq 0.01$) (Figure 4.2C). The mean average copies/ 20 µL of hsa_circ_0001275 at TP3 (13.04 copies/ 20 µL) (plasma at time of first PSA progression) were higher than TP2 (9.93 copies/ 20 µL) (Figure 4.2A) and mean PSA level at TP3 (5.94 µg/L) was also higher than TP2 however was not statistically significant ($p > 0.05$) (Figure 4.2C). The mean average copies/ 20 µL of hsa_circ_0001721 at PSA nadir, TP2 (11.76 copies/ 20 µL) was lower compared to TP1 (18.87 copies/ 20 µL) and TP3 (23.29 copies/ 20 µL) however this was not statistically significantly ($p > 0.05$) (Figure 4.2B).

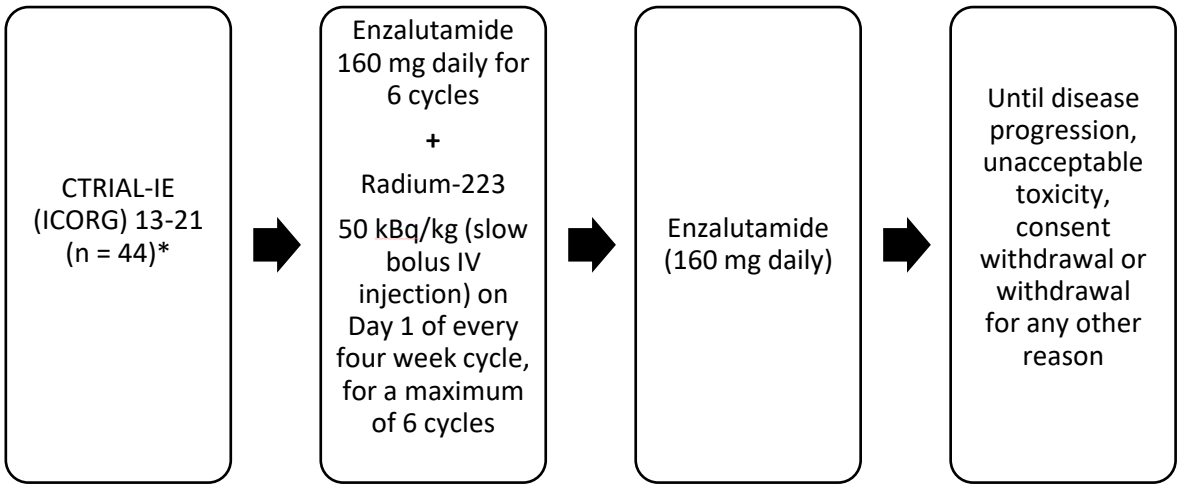

Figure 4.0. Study schema for CTRIAL-IE (ICORG) 13-21 trial. All enrolled patients received six cycles of radium-223 and continuous daily enzalutamide until study discontinuation. *Blood samples were taken at the beginning of Cycle 1, every 4 weeks for the first 6 months and then every 6 weeks during the remainder of study treatment.

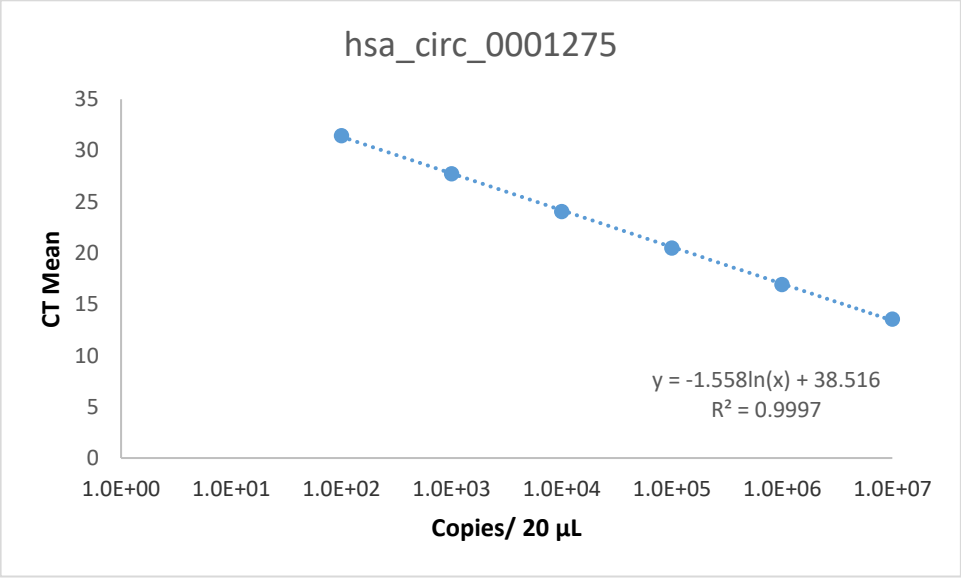

(A)

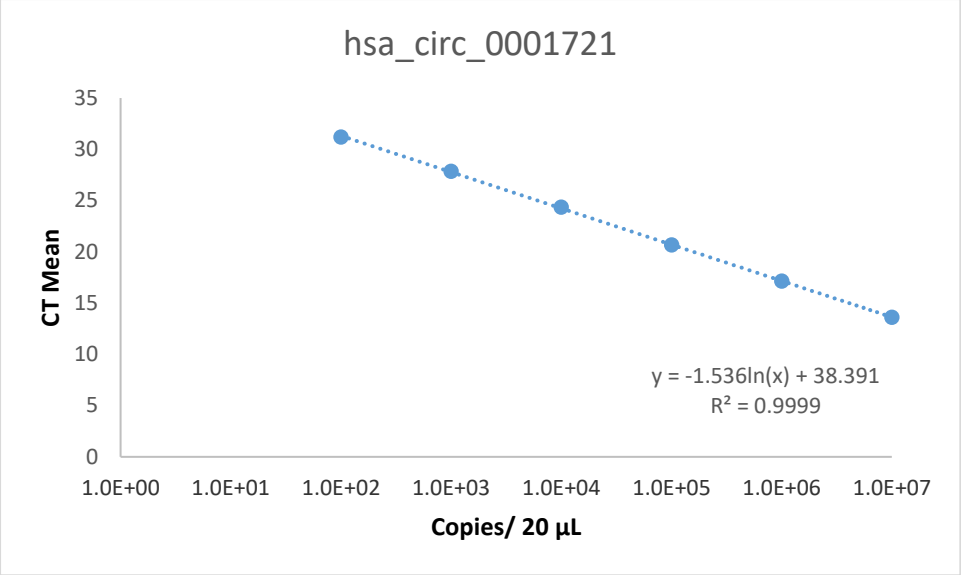

(B)

Figure 4.1. Standard curve method for assessment of circRNA copies. (A) hsa_circ_0001275 and (B) hsa_circ_0001721. Standard dilution curve using gBlock for circRNAs are shown. Threshold cycle numbers (Y axis) in RT-qPCR reactions were determined from gBlock at 6 dilutions containing the indicated number of copies of each transcript (X axis). Formula as shown in both figure was derived to quantify the absolute copy numbers/ 20 µL according to CT values.

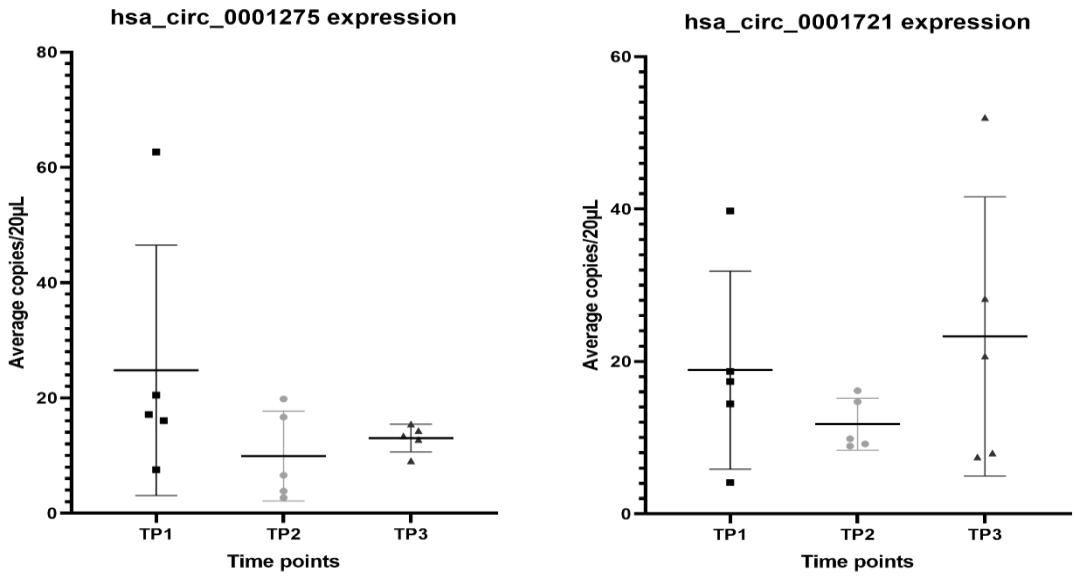

(A) **(B)**

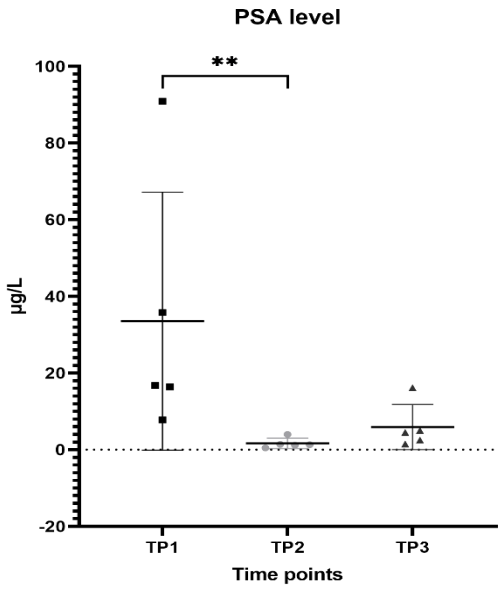

(C)

Figure 4.2. Scatter plots of circRNAs in plasma samples. Scatter plot of (A) hsa_circ_0001275 and (B) hsa_circ_0001721 level in plasma samples and (C) PSA level in all 5 participants. Data graphed as mean ± SD (n=5) and analysed using one-way ANOVA with Friedman *post hoc* test. (**p ≤ 0.01). Plasma at TP1 was selected as baseline prior to enzalutamide treatment, plasma at TP2 was selected during PSA nadir, and plasma at TP3 was selected when PSA first progressed as defined by Prostate Cancer Working Group 2 (PCWG2).

4.2 Validation of circRNAs in the isogenic cell lines and plasma samples using different methods of RT-ddPCR.

4.2.1 Probe-based multiplex RT-ddPCR

As circRNA was lowly expressed, RT-ddPCR was then employed. Assay optimisation was achieved using optimized primers/probe concentration and a custom designed gBlock (Appendix -Table 5) as a positive control under a range of temperatures (Figure 4.3A). This step demonstrated that multiplexing using probe-based absolute quantification can accurately detect the expression of both hsa_circ_0001721 and hsa_circ_0001275 as shown by clear separation of positive droplets from the negative droplet background (Figure 4.3B and 4.3C, respectively). The optimal temperature at 60 °C was selected for further experiments.

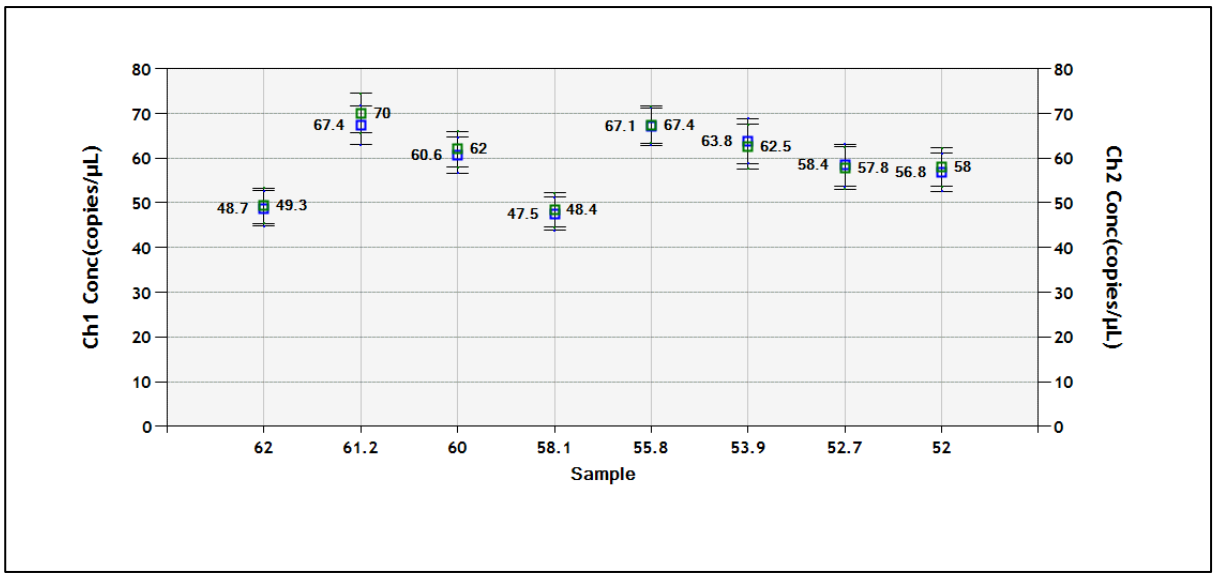
Ch1 Conc(copies/µL)
Ch2 Conc(copies/µL)
Sample
62
61.2
60
58.1
55.8
53.9
52.7
52
48.7
49.3
67.4
70
60.6
62
47.5
48.4
67.1
67.4
63.8
62.5
58.4
57.8
56.8
58

(A)

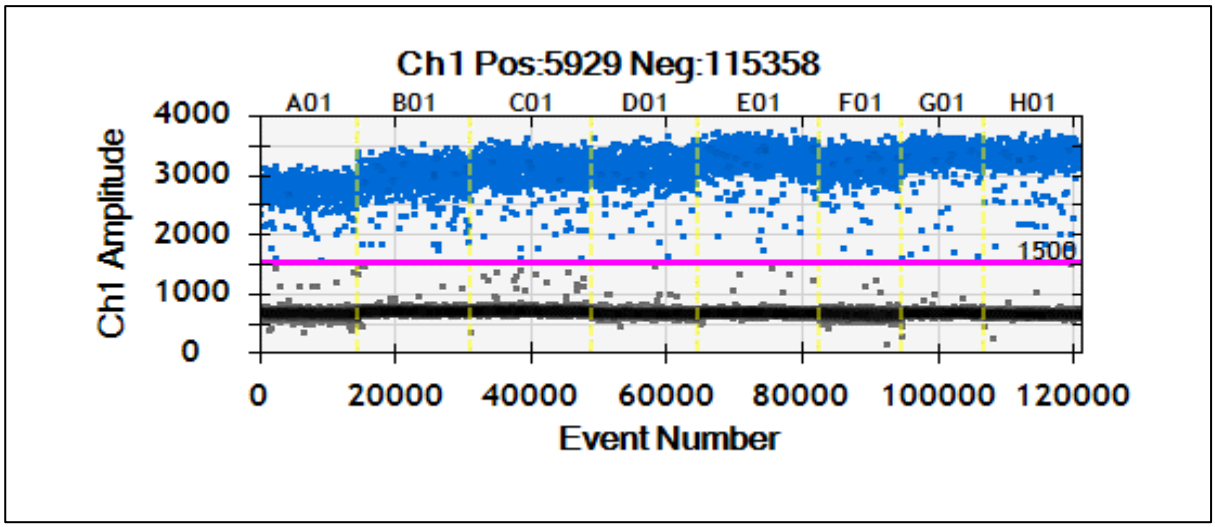
Ch1 Pos:5929 Neg:115358
A01
B01
C01
D01
E01
F01
G01
H01
Ch1 Amplitude
1500
Event Number

(B)

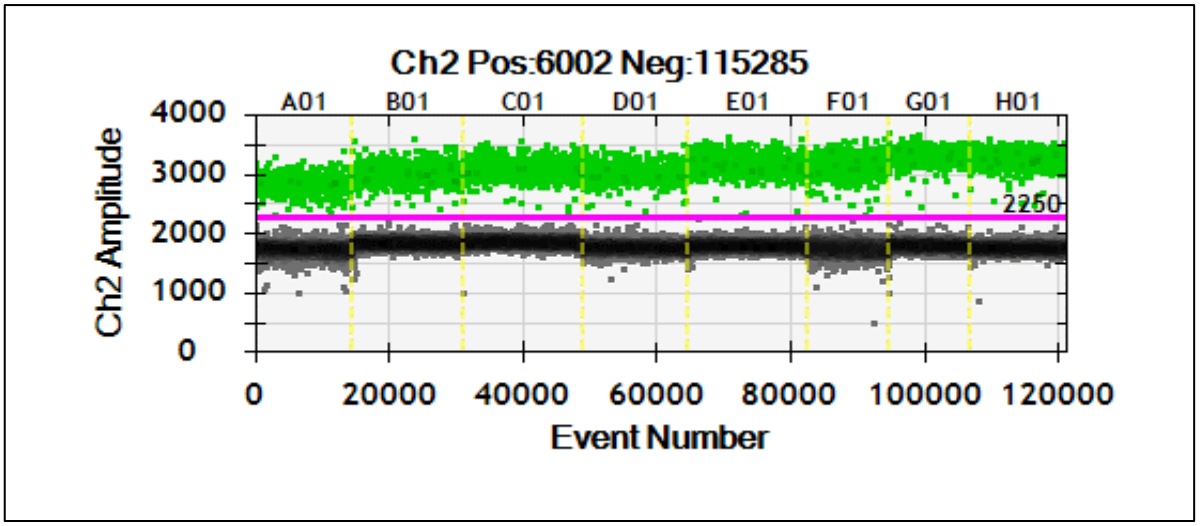

(C)

Figure 4.3. Probe-based RT-ddPCR detection of circRNA. (A) RT-ddPCR assay optimisation of hsa_circ_0001721 and hsa_circ_0001275 using optimised primers/probe and gBlock as positive control under a range of different temperatures (52 °C to 62 °C). Precise detection of (B) hsa_circ_0001721 and (C) hsa_circ_0001275 levels by RT-ddPCR multiplex with probe using gBlock positive control.

The expression of hsa_circ_0001721 and hsa_circ_0001275 were firstly examined in the isogenic LNCaP clones. The expression of hsa_circ_0001721 were detected in the isogenic clones (Control, 87.33 average copies/ 20 µL; Clone 1, 76.67 average copies/ 20 µL and Clone 9, 11.87 average copies/ 20 µL), however, the expression levels were not significantly different ($p > 0.05$) (Figure 4.4A) in contrast to previous RT-qPCR results for this specific circRNA. The expression of hsa_circ_0001275 was significantly up-regulated in the strongly enzalutamide resistant clone (1445.33 average copies/ 20 µL) compared to Control (154.42 average copies/ 20 µL) ($p = 0.039$), further confirming initial RT-qPCR results for this specific circRNA (Figure 4.4B).

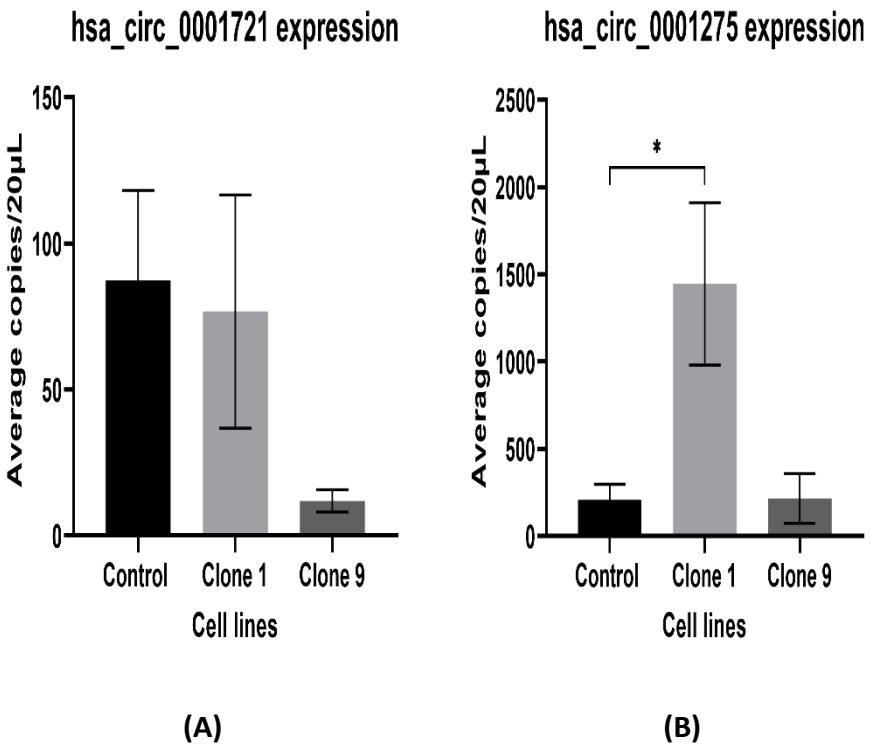

Figure 4.4. Probe based absolute quantification of circRNAs. (A) hsa_circ_0001721 and (B) hsa_circ_0001275 in enzalutamide resistant panel. Data graphed as mean ± SEM (n=3). Ordinary one-way ANOVA followed by a Tukey's *post hoc* test. (*p ≤ 0.05).

4.2.2 Dye-based RT-ddPCR

Assay optimisation was achieved using optimised primer concentration and a custom designed gBlock (Appendix - Table 5) as a positive control under a range of temperatures (Figure 4.5A). This step demonstrated that dye-based (EvaGreen) absolute quantification can accurately detect the expression of hsa_circ_0001275 as shown by clear separation of positive droplets from the negative droplet background (Figure 4.5B). An optimal temperature at 60 °C was selected for further experiments.

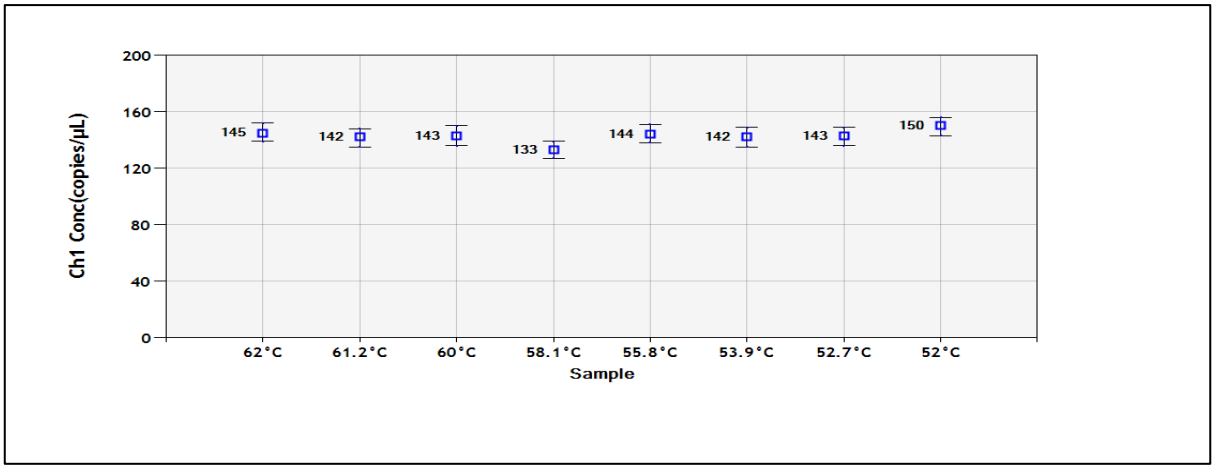

(A)

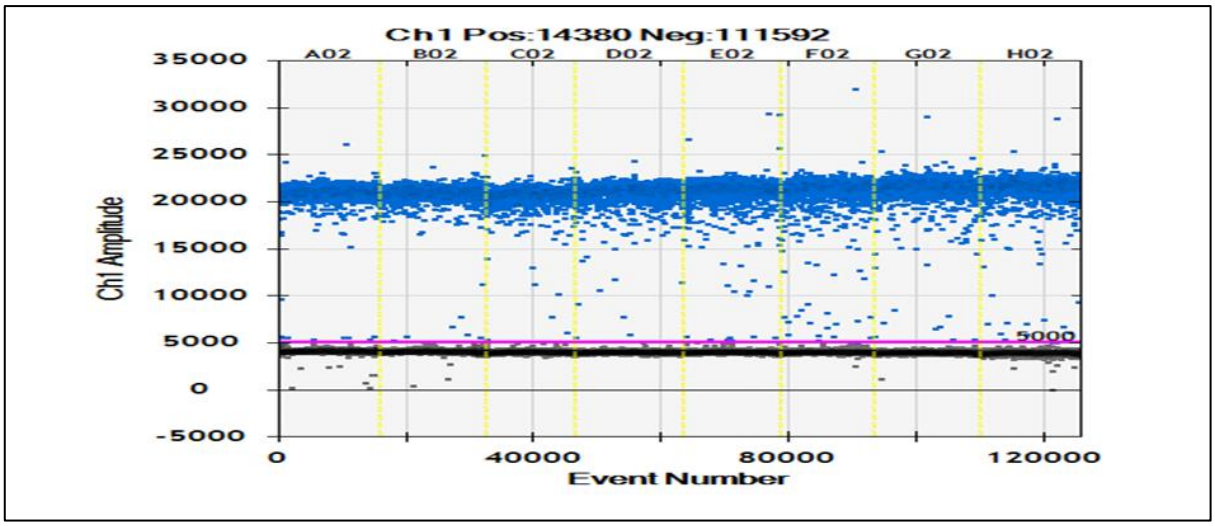

(B)

Figure 4.5. EvaGreen RT-ddPCR detection of circRNA. (A) RT-ddPCR assay optimisation of hsa_circ_0001275 using optimised primers and gBlock as positive control under a range of different temperatures (52 °C to 62 °C). (B) Precise detection of hsa_circ_0001275 levels by RT-ddPCR with EvaGreen dye using gBlock positive control.

Reverse transcription methods using gene specific priming (GSP) and random priming (RP) were evaluated to ensure no significant discrepancy in circRNA quantification. The mean average copies/ 20 µL of hsa_circ_0001275 using GSP (13.5 copies/ 20 µL) were higher than RP (10.04 copies/ 20 µL) but not statistically significant ($p > 0.05$) (Figure 4.6). As there was no significant difference between the two reverse transcription methods, RP was chosen for subsequent experiments as RT-qPCR had been used previously.

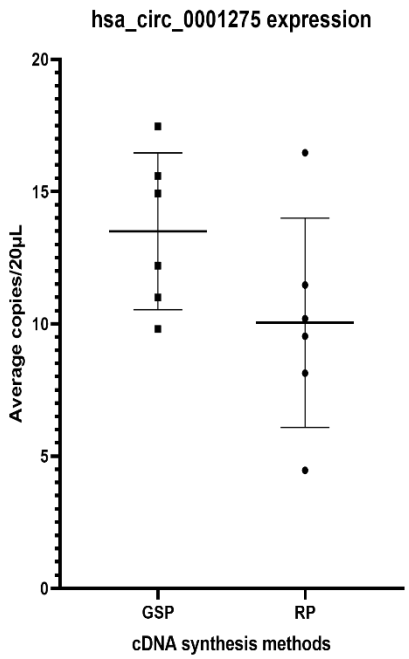

Figure 4.6. Comparison of hsa_circ_0001275 level in plasma samples using GSP and RP methods. Data graphed as mean ± SD (n=6) and analysed using the Wilcoxon signed rank test.

The expression of hsa_circ_0001721 and hsa_circ_0001275 in the isogenic LNCaP clones were examined. hsa_circ_0001721 was highly expressed in Clone 1 (2373.33 average copies/ 20 µL) compared to Control (710.67 average copies/ 20 µL) ($p \leq 0.0001$) (Figure 4.7A). hsa_circ_0001275 was also significantly up-regulated in the strongly enzalutamide resistant clone (200.67 average copies/ 20 µL) compared to Control (37.33 average copies/ 20 µL) ($p = 0.019$) (Figure 4.7B) further confirming initial RT-qPCR results.

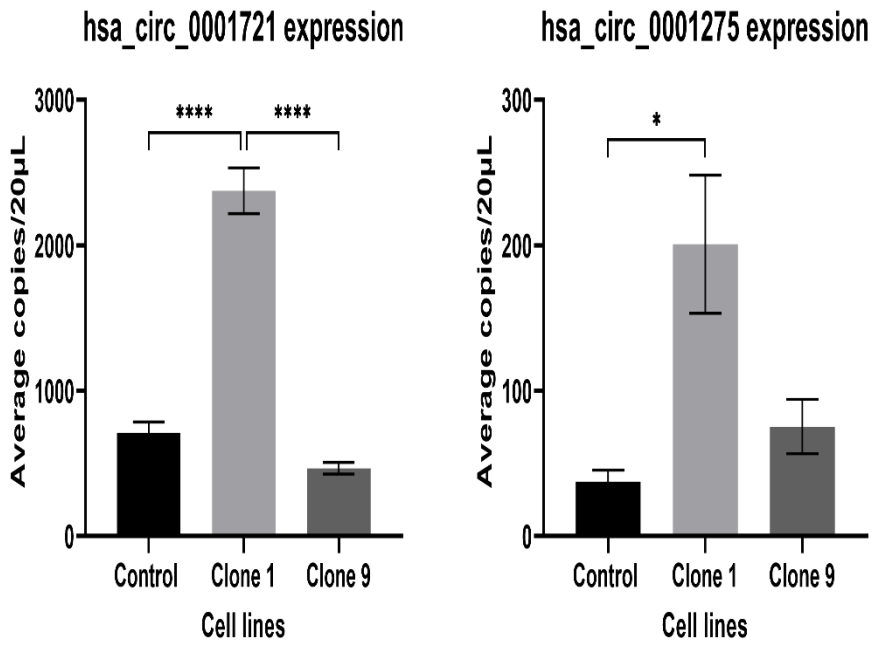

Figure 4.7. EvaGreen absolute quantification of circRNAs. Quantification of (A) hsa_circ_0001721 and (B) hsa_circ_0001275 in enzalutamide resistant panel. Data graphed as mean ± SEM (n=3). Ordinary one-way ANOVA followed by a Tukey's *post hoc* test. (*p ≤ 0.05, **** P ≤ 0.0001).

4.2.3 Comparison of of probe based RT-ddPCR, EvaGreen RT-ddPCR and RT-qPCR validation of circRNAs

4.2.3.1 Probe-based RT-ddPCR vs. dye-based RT-ddPCR

Both probe-based and EvaGreen methods were evaluated for the detection of circRNA expression in cell lines and plasma samples. A probe-based approach in cell line samples yielded a significantly higher number of hsa_circ_0001275 transcripts (623.11 copies/ 20 µL) compared to the EvaGreen approach (104.44 copies/ 20 µL) (p = 0.038) (Figure 4.8A) however, were not statistically significant when tested in plasma samples (p > 0.05) (Figure 4.8B). The hsa_circ_0001275 expression in cell lines from both methods significantly correlated with each other (r = 0.845, p = 0.0062) (Figure 4.9A). Likewise, in plasma samples, a correlation was evident in the hsa_circ_0001275 expression from both methods (r = 0.748, p = 0.0019) (Figure 3.35B).

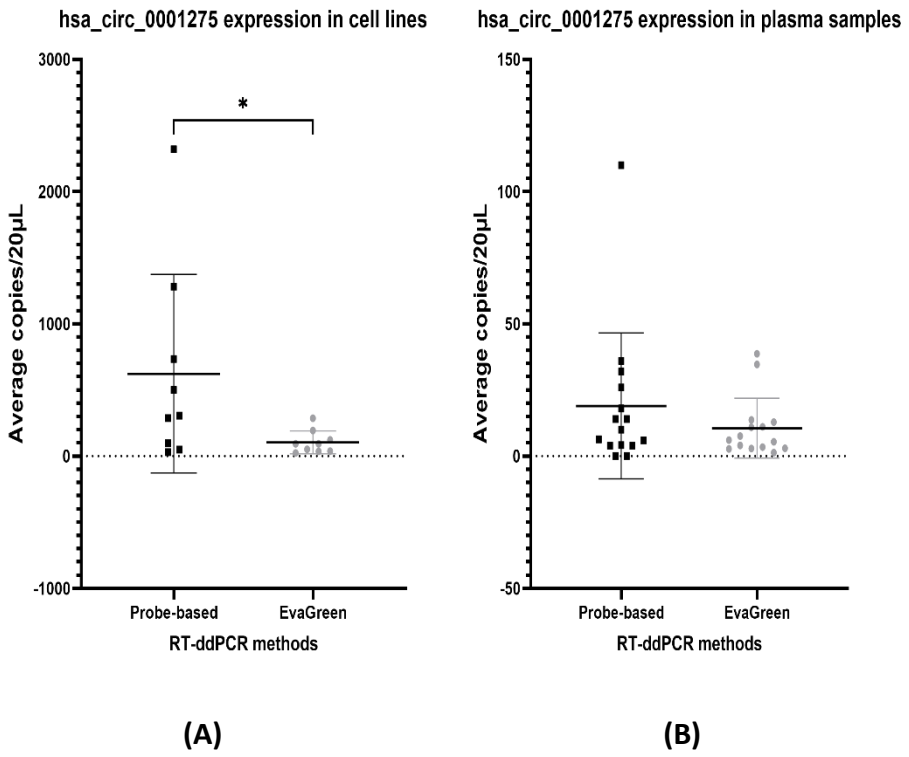

Figure 4.8. Scatter plot of hsa_circ_0001275 level in cell lines and plasma samples detected using probe-based and EvaGreen RT-ddPCR. (A) Comparison of hsa_circ_0001275 level in enzalutamide resistant panel. Data graphed as mean ± SD (n=9) and analysed using the Mann-Whitney test. (B) Comparison of hsa_circ_0001275 level in plasma samples of 5 partcipants, with each having three time points. Data graphed as mean ± SD (n=15) and analysed using the Wilcoxon signed rank test.

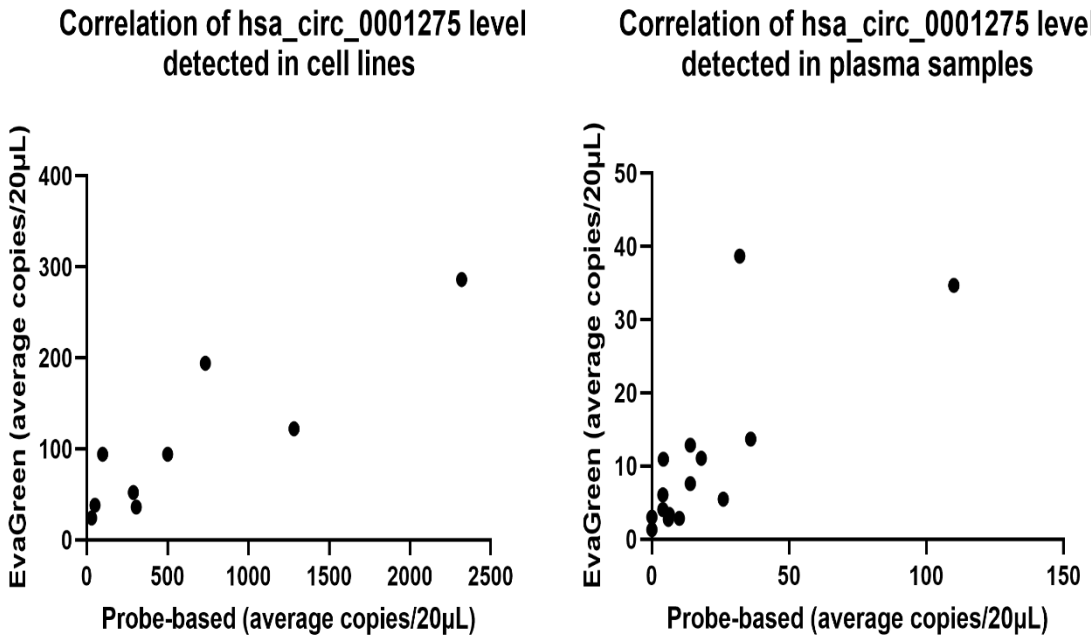

(A) **(B)**

Figure 4.9. XY scatter plot showing positive correlation of hsa_circ_0001275 level detected using probe-based *vs.* EvaGreen RT-ddPCR. (A) cell lines (Spearman correlation coefficient r = 0.845, p (two-tailed) < 0.01) and (B) plasma samples (Spearman correlation coefficient r = 0.748, p (two-tailed) < 0.01).

4.2.3.2 Comparison of probe-based RT-ddPCR and dye-based RT-ddPCR vs. RT-qPCR (gBlock standard curve method)

To estimate the accuracy between RT-ddPCR and RT-qPCR, the average copies/ 20 µL of hsa_circ_0001275 in plasma samples of 5 partcipants (each had three time points) were quantified and compared using the two methodologies. Probe-based RT-ddPCR yielded the highest copies of hsa_circ_0001275 followed by RT-qPCR (gBlock) and EvaGreen RT-ddPCR (18.97, 15.92 and 10.56 mean average copies/ 20 µL, respectively). The difference in the detection rate of circRNA between the two methodologies were not statistically significant ($p > 0.05$) (Figure 4.10A and 4.10B). hsa_circ_0001275 expression in plasma from both methods did not correlates with each other ($p > 0.05$) (Figure 4.11A and 4.11B).

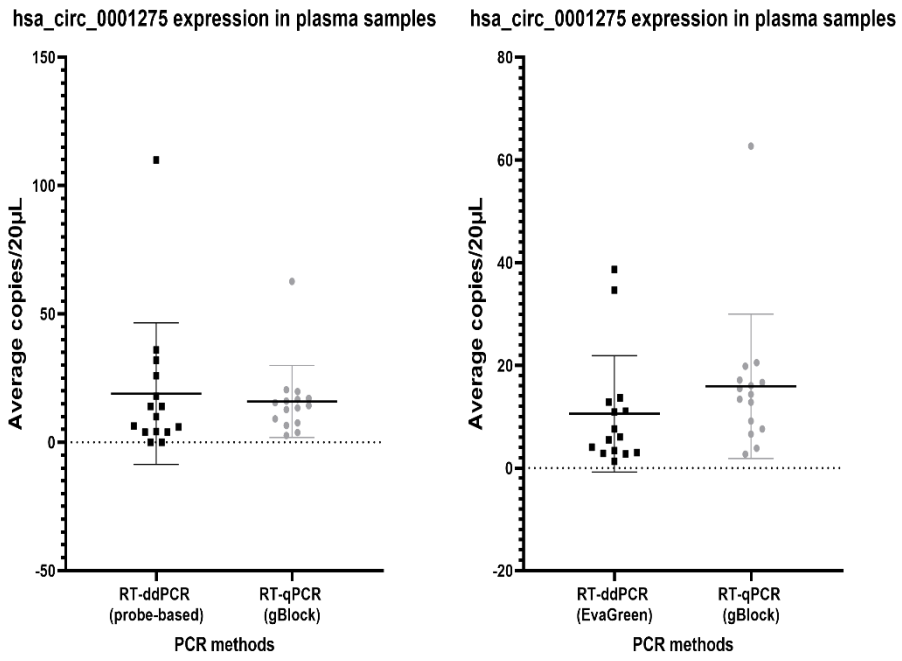

(A) **(B)**

Figure 4.10. Scatter plot of hsa_circ_0001275 level in plasma samples using different methodologies. The 5 each had three time points, with circRNA detected using probe-based RT-ddPCR, EvaGreen RT-ddPCR and RT-qPCR (standard curve method-gBlock). (A) Comparison of hsa_circ_0001275 level between probe-based RT-ddPCR and RT-qPCR. (B) Comparison of hsa_circ_0001275 level between EvaGreen RT-ddPCR and RT-qPCR. Data graphed as mean ± SD (n=15) and analysed using the Wilcoxon signed rank test.

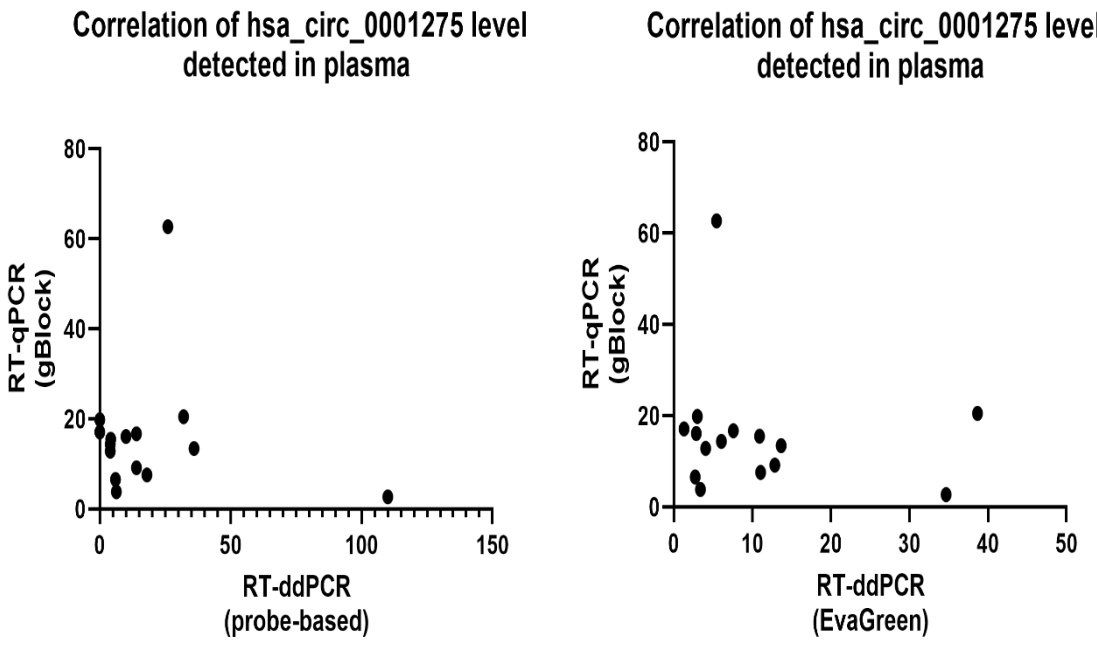

(A) **(B)**

Figure 4.11. XY plot showing no correlation of plasma hsa_circ_0001275 level detected using RT-ddPCR and RT-qPCR. (A) Probe-based RT-ddPCR *vs.* RT-qPCR (gBlock) (Spearman correlation coefficient r = -0.163, p (two-tailed) > 0.05) and (B) Evagreen RT-ddPCR *vs.* RT-qPCR (gBlock) (Spearman correlation coefficient r = -0.132, p (two-tailed) > 0.05).

4.2.4 RT-ddPCR validation of circRNAs in plasma of patients with PCa treated with enzalutamide

4.2.4.1 EvaGreen RT-ddPCR of hsa_circ_0001275

Following the pilot study of circRNA in plasma samples of participants using RT-qPCR, which showed encouraging results, these circRNAs were further evaluated as a biomarker of enzalutamide resistance clinically via RT-ddPCR detection. hsa_circ_0001275 was selected as the candidate for further investigations as both probe based and EvaGreen based absolute quantification in the enzalutamide resistant panel demonstrated consistent results and confirmed initial RT-qPCR results. hsa_circ_0001275 expression was quantified in the plasma of all 44 participants with mCRPC on the phase II trial (CTRIAL-IE 13-21, NCT02225704). The plasma from four different time points were selected according to PSA level where the first 3 time points were defined previously (section 3.2.1). The fourth time point was defined as second PSA progression (PSA level higher than first PSA progression,

TP4). Plasma were available for both TP1 and TP2 time points for all 44 cases. Not all cases had PSA progression at the time of this study and thus only 21 had plasma for all 4 time points. The expression of hsa_circ_0001275 in plasma samples showed a trend that mirrored the activity of the disease status according to PSA level, however, this was not statistically significant (Figure 4.12A-D). All 44 had the first two time points available and their mean average copies/ 20 µL of hsa_circ_0001275 at TP2 (4 copies/ 20 µL) (plasma at time of PSA nadir) were lower than baseline TP1 (6 copies/ 20 µL) (prior to enzalutamide treatment) (Figure 4.12A). TP2 was the time point where the disease responded to enzalutamide treatment (Figure 4.12A) as shown by the mean PSA level, which was significantly lower at TP2 (75 µg/L) compared to TP1 (10 µg/L) ($p < 0.05$) (Figure 4.12B). A subgroup analysis of 21 cases who had four available time points available showed a similar trend. The mean average copies/ 20 µL of hsa_circ_0001275 was high at TP1 (9 copies/ 20 µL) then reduced at TP2 (6 copies/ 20 µL) but remained unchanged at TP3 (6 copies/ 20 µL) and increased again upon further PSA progression at TP4 (12 copies/ 20 µL) (Figure 4.12C). The mean PSA at nadir, TP2 (20 µg/L) was significantly lower compared to TP1 (94 µg/L) and TP4 (186 µg/L) ($p < 0.05$). However, compared to TP3 (90 µg/L) it was significantly less (Figure 4.12D). This indicated that the disease at TP3 was biochemically less resistant to enzalutamide compared to TP4.

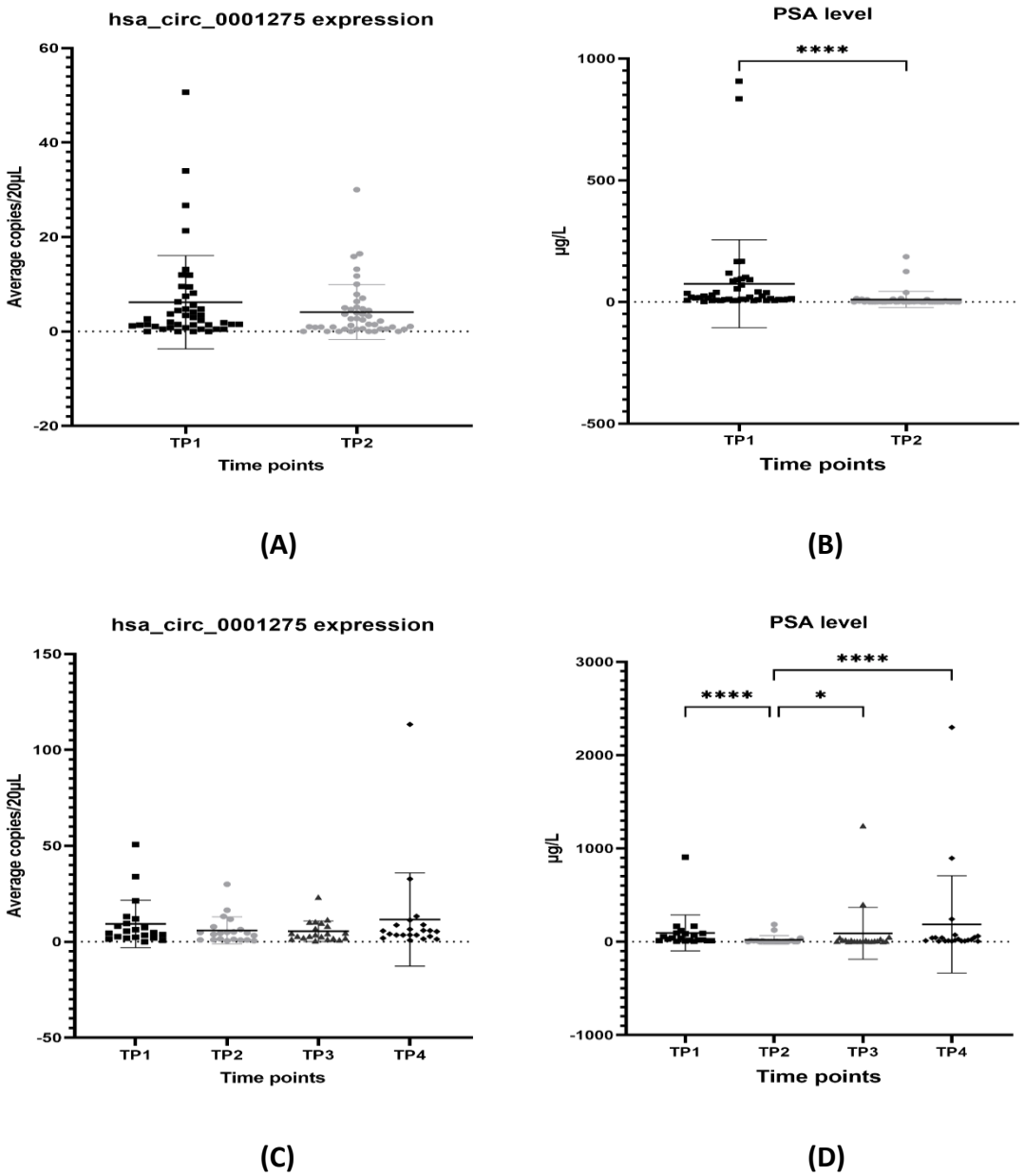

Figure 4.12. Scatter plot of hsa_circ_0001275 level in plasma samples and PSA level. (A) hsa_circ_0001275 level in plasma samples and (B) PSA level of all 44 cases with first 2 available time points. Data graphed as mean ± SD (n=44) and analysed using the Wilcoxon signed rank test. (C) hsa_circ_0001275 level in plasma samples and (D) PSA level of 21 cases with all 4 time points available. Data graphed as mean ± SD (n=21) and analysed using one-way ANOVA with Friedman *post hoc* test. (***p ≤ 0.001, ****p ≤ 0.0001). Plasma at TP1 was selected as baseline prior to enzalutamide treatment, plasma at TP2 was selected

during PSA nadir, plasma at TP3 was selected when PSA first progressed and plasma at TP4 was selected on second PSA progression.

4.2.4.2 Probe-based RT-ddPCR of hsa_circ_0001275 and hsa_circ_0001721

Probe-based duplexing was performed for hsa_circ_0001275 and hsa_circ_0001721 in plasma of all 44 participants with mCRPC on the phase II trial (CTRIAL-IE 13-21, NCT02225704). All 44 cases had the first two time points available and their mean average copies/ 20 µL of both hsa_circ_0001275 and hsa_circ_0001721 at TP2 (11.82 and 15.68 copies/ 20 µL respectively) (plasma at time of PSA nadir) were lower than baseline TP1 (22.39 and 13.16 copies/ 20 µL, respectively) (prior to enzalutamide treatment). These were not statistically significant ($p > 0.05$) (Figure 4.13A and 4.13C). A subgroup analysis of 21 cases, who had four available time points available showed a trend similar to PSA. The mean average copies/ 20 µL of hsa_circ_0001275 was high at TP1 (22.77 copies/ 20 µL) then reduced at TP2 (16.44 copies/ 20 µL) and at TP3 (9.92 copies/ 20 µL) but increased again upon further PSA progression at TP4 (58.71 copies/ 20 µL) (Figure 4.13C). In contrast, there was no similar trend to PSA observed for hsa_circ_0001721 in the subgroup analysis of 21 cases (TP1: 26.61 copies/ 20 µL, TP2: 21.41 copies/ 20 µL, TP3 10.46 copies/ 20 µL, and TP4 7.85 copies/ 20 µL) (Figure 4.13D).

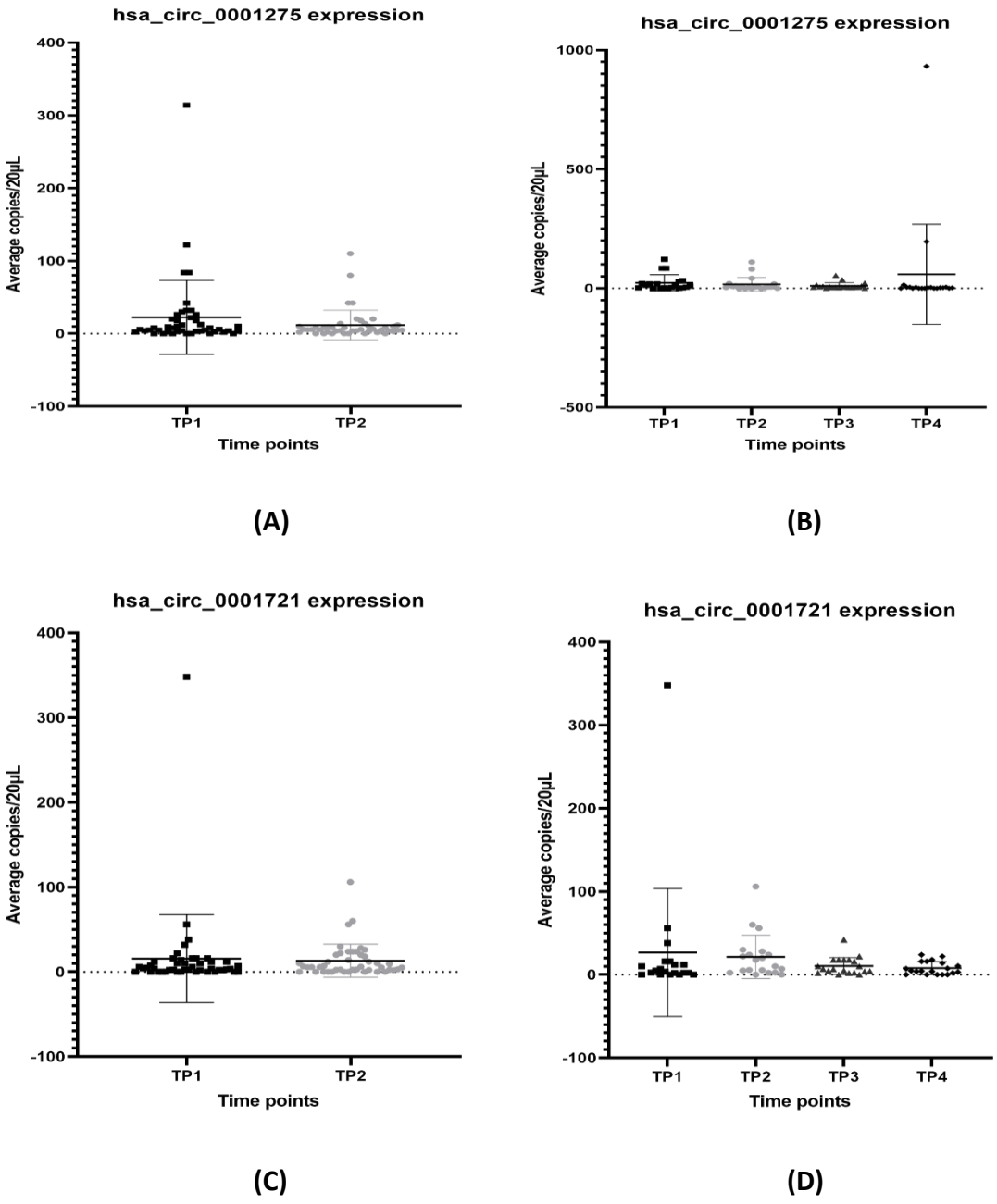

Figure 4.13. Scatter plot of hsa_circ_0001275 and hsa_circ_0001721 level in plasma samples. (A) hsa_circ_0001275 and (C) hsa_circ_0001721 level in plasma samples all 44 cases with the first 2 available time points. Data graphed as mean ± SD (n=44) and analysed using the Wilcoxon signed rank test. (B) hsa_circ_0001275 and (D) hsa_circ_0001721 level in plasma samples of 21 cases with all 4 time points available. Data graphed as mean ± SD (n=21) and analysed using one-way ANOVA with Friedman *post hoc* test. Plasma at TP1 was selected as baseline prior to enzalutamide treatment, plasma at TP2 was selected during PSA nadir, plasma at TP3 was selected when PSA first progressed and plasma at TP4 was selected on second PSA progression.

4.3 Discussion

circRNA has recently been the centre of attention owing to their known dysregulation across different tumour subtypes (326), as well as the ability to detect them in human bodily fluids such as saliva, and blood (316, 327, 328). The level of hsa_circ_0001275 and hsa_circ_0001721 were examined in the plasma samples from a clinical trial (CTRIAL-IE 13-21, NCT02225704) (354). The aim was to further investigate the value of circRNA as a candidate biomarker to inform drug resistance. The expression of both circRNAs were initially quantified using RT-qPCR through a standard curve method in a pilot study of 5 samples, following which RT-ddPCR was employed to examine the circRNA expression in plasma samples of all 44 cases.

In the pilot study using RT-qPCR, the expression of both hsa_circ_0001275 and hsa_circ_0001721 showed a similar trend to PSA level according to disease activity, however, this was not statistically significant ($p > 0.05$). This study also attempted to examine levels between RT-ddPCR and RT-qPCR. The average copies/ 20 µL of hsa_circ_0001275 in plasma samples of 5 cases were quantified and compared using the different methodologies. Probe-based RT-ddPCR yielded the highest copies of hsa_circ_0001275 followed by RT-qPCR (standard curve method) and EvaGreen RT-ddPCR (18.97, 15.92 and 10.56 mean average copies/ 20 µL, respectively). However, the difference in the detection rate of circRNA between the three methodologies were not statistically significant ($p > 0.05$). There was a correlation between plasma hsa_circ_0001275 expression, probe-based and EvaGreen RT-ddPCR ($p < 0.05$), however, no correlation was found when both RT-ddPCR methods were compared to RT-qPCR ($p > 0.05$) suggesting that RT-qPCR may not be a sensitive enough method for low circRNA transcript detection. Furthermore, it has been reported by Chen *et al.* that RT-qPCR may overestimate the actual abundance of circRNA due to multiple PCR products of circRNA caused by rolling cDNA during reverse transcription (389). The main advantages of probe-based RT-ddPCR compared to EvaGreen RT-ddPCR was the ability to multiplex and detect a higher transcript yield, which was attributed to the Hot-start Reverse Transcriptase which enabled RNA to be reverse transcribed and amplified in the same reaction tube. Additionally, a high temperature reverse transcription reaction at 55°C further improved the specificity and efficiency of primer mediated cDNA synthesis.

Both probe-based and EvaGreen RT-ddPCR results of hsa_circ_0001275 suggested a trend that corresponded to the activity of the disease as defined by the PSA level of participants on enzalutamide treatment, however, it did not reach statistical significance. This is likely due to small cohorts and/or copy numbers were close to the limit of detection for RT-ddPCR. Previous studies have described that circRNAs are tissue specific (325) and therefore may explain the low abundance of hsa_circ_0001275 in plasma particularly if it is not actively secreted by tumour tissue. This study demonstrated that hsa_circ_0001275 was not expressed abundantly in plasma, which presently limits its potential use as a liquid-based predictive biomarker of enzalutamide resistance. In future, a panel of circRNAs may be used to increase its sensitivity.

There are several limitations in this study. The study used a single isogenic cell line model of enzalutamide resistance developed by Korpal *et al.* (138). It would be valuable to explore the overexpression of hsa_circ_0001275 in addition enzalutamide sensitive PCa cell lines to further explore its association with drug resistance. Another limitation was the relatively small cohort of cases in this study. Initial statistical analysis revealed that circRNA data was positively skewed and thus further analysis was performed using the Wilcoxon signed rank test for those with two time points, and the Friedman test for those with four time points. It has been debated that a sample size of more than five in each group is sufficient, nonetheless, the hsa_circ_0001275 value difference across groups was also important. It is difficult to ascertain the statistical significance in particular to confidence interval and p-values due to small sample size used in this study. Additionally, even with RT-ddPCR, only low copy numbers of hsa_circ_0001275 were present in plasma samples. This could have contributed to a large variation across groups. A pre-amplification step described by Karousi *et al.* (390), may have helped in the detection of circRNAs but this approach can cause problems such as multiple PCR products caused by rolling cDNA during reverse transcription (389). Going forward, it may be essential to first evaluate the circRNAs expression using an explant or organoid based protocol to establish whether the circRNAs of interest can be detected within the conditioned media, which may offer a more robust foundation for circRNA testing in plasma samples. Second, PSA was the only surrogate marker used to select plasma samples for time-point analysis. It is known that PSA level is not the only surrogate maker to inform disease progression, however, rising PSA is often the initial signal of tumour regrowth, which is then succeeded by disease progression on

imaging and eventually symptomatic clinical presentations (391). Consequently, the time points selected may not be a concrete reflection of disease status and tumour burden. Third, this study encompassed a combination of six cycles of alpha-radium and enzalutamide followed by enzalutamide maintenance until disease progression. Ideally, the results obtained in this study should be investigated in a larger cohort with participants on enzalutamide alone. Fourth, tissue sample circRNA expression was not examined because they were not available, as tissue biopsy upon disease progression was not performed routinely as part of the trial.

In conclusion, the clinical data in this study showed that hsa_circ_0001275 was not expressed abundantly in this cohort of plasma samples. Though the trend of expression mirrored disease activity according to PSA level, it does suggest an association with enzalutamide resistance. However, further studies are warranted. The therapeutic landscape of PCa has advanced rapidly in the last decade due to better availability and accessibility of therapeutics. Despite this growing battery of therapeutic options, most people eventually progress due to drug resistance, which poses a clinically challenging conundrum. This study provides a valuable foundation for further exploration of circRNAs as biomarkers in PCa.

Chapter 5 - Evaluating the transcriptomic landscape of enzalutamide resistant PCa

5.0 Introduction

NGS is the blanket term used to describe several different sequencing technologies. NGS is a promising molecular diagnostic technique for informing clinical practice due to its ability to detect genomic and transcriptomic alterations (392, 393). NGS can be applied in the form of large-scale sequencing to detect genetic alterations such as gene mutation and amplification by sequencing the whole genome, exome or transcriptome. On the other hand, NGS can also be applied in the form of targeted sequencing to detect genome alterations related to cancer genes by performing deep sequencing on genomic regions of interest (394, 395).

PCa is the second major cause of cancer-related deaths among males (396). Several recent large-scale sequencing efforts have contributed to the better understanding of the diverse genomic landscapes of primary PCa and CRPC (397-400). Alterations common in CRPC includes adaptive AR amplifications and mutations, as well as increased incidence of germline or somatic changes in DNA repair pathway genes (397-400). Comprehensive RNA sequencing of advanced PCa has built upon previous expression profiling studies of CRPC (400, 401).

PCa morbidity remains high despite recent breakthroughs in treatment. While enzalutamide has been shown to increase survival, the use of this drug is complicated by the development of resistance. Several mechanisms of enzalutamide resistance in PCa have been identified such as AR splice variants and F876L mutations that may switch the antagonistic effect of enzalutamide to an agonistic effect (138, 142). Approximately 20% of those with mCRPC who progressed on enzalutamide were reported to harbour F876L or other enzalutamide resistance-associated mutations (132, 133). However, these are non-targetable with current drugs. The molecular mechanism of enzalutamide resistance is still largely unknown. Thus, a greater understanding of the transcriptomic basis of enzalutamide resistance may provide better molecular stratification for PCa treatment.

5.1 Experimental aims

The aim of this chapter was to evaluate the transcriptomic alterations that may underpin enzalutamide resistant PCa. Paired-end, RNA sequencing was performed on the enzalutamide resistance panel in this study.

5.2 Results

5.2.1 High throughput sequencing of enzalutamide resistance panel

Global gene expression was analysed in Control, Clone 1 and Clone 9 (n=3) on the Illumina® NovaSeq™ 6000 Sequencing System (TrinSeq, TTMI, Trinity College Dublin).

5.2.1.1 Quality control

The quality of RNA from the enzalutamide cell line panel was examined using a bioanalyser, with all samples achieving a RIN score of more than eight except for Clone 1 (N2) and Clone 9 (N3). However, the18S and 28S bands appeared intact on electrophoresis (Appendix - Figure 7A and 7B). The RNA samples were sequenced to a depth of at least 30 million reads/sample. Illumina® RNA-Seq Alignment (version: 1.1.1) software was used to align the reads. The summary is shown in Table 5.0, Figure 5.0 and Figure 5.1. The reads were mapped to the reference genome (Homo sapiens NCBI GRCh58Decoy) using the STAR aligner and sequences were annotated based on their overlap with publicly available mRNA transcripts. More than 80 % of the reads generated from each sample matched the genome (Table 5.0, Figure 5.0). The mean insert length of the cell lines ranged between 150 bp to 250 bp (Figure 5.1), which was acceptable as the NovaSeq flow cell works optimally with libraries containing an insert size that ranges between 50 and 700 bp. The transcript coverage plot of each cell line formed a Poisson-like distribution suggestive of good sequencing coverage (Figure 5.2). The number of reads that mapped to loci of known transcripts were used to calculate abundances, and therefore infer the expression levels of those transcripts within a given sample. Read counts were calculated across all transcripts using Salmon and were subsequently used to determine differential expression patterns between samples through DESeq2 software (402).

Table 5.0. Summary of RNA-Seq alignment.

Sample ID	Read Length	Number of Reads	% Total Aligned	% Abundant	% Unaligned	Median CV Coverage Uniformity	% Stranded
LNCaP_Clone_1_N1	76/76	29,035,681	88.96%	7.04%	11.04%	0.51	98.62%
LNCaP_Clone_1_N2	76/76	29,466,982	88.33%	5.74%	11.67%	0.52	97.99%
LNCaP_Clone_1_N3	76/76	28,367,106	87.95%	6.43%	12.05%	0.51	99.00%
LNCaP_Clone_9_N1	76/76	13,246,401	87.54%	10.16%	12.46%	0.52	99.11%
LNCaP_Clone_9_N2	76/76	3,475,115	85.06%	7.27%	14.94%	0.58	98.83%
LNCaP_Clone_9_N3	76/76	16,571,868	89.84%	8.17%	10.16%	0.51	98.81%
LNCaP_cntrl_N1	76/76	30,954,840	87.32%	9.96%	12.68%	0.5	97.99%
LNCaP_cntrl_N2	76/76	26,805,037	83.93%	8.80%	16.07%	0.51	98.91%
LNCaP_cntrl_N3	76/76	32,119,273	90.40%	7.28%	9.60%	0.51	99.14%

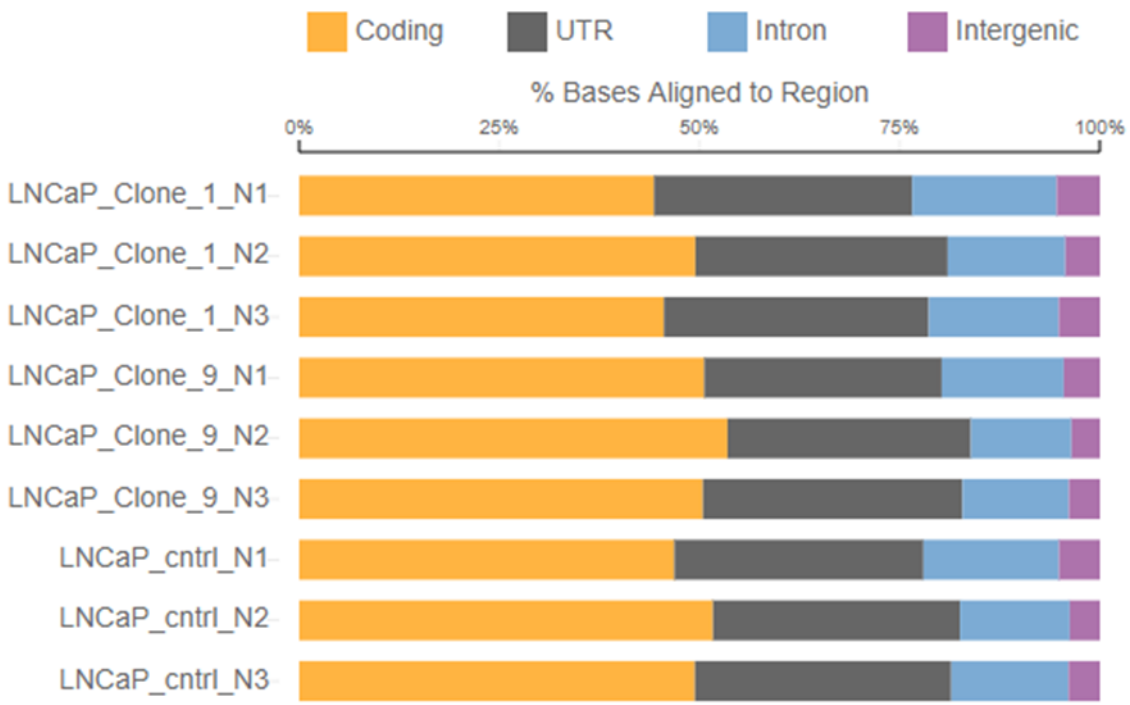

Figure 5.0. Alignment distribution of the enzalutamide resistance panel. The distribution showed more than 75 % of the data generated aligned to transcripts (coding and UTRs) in each cell line.

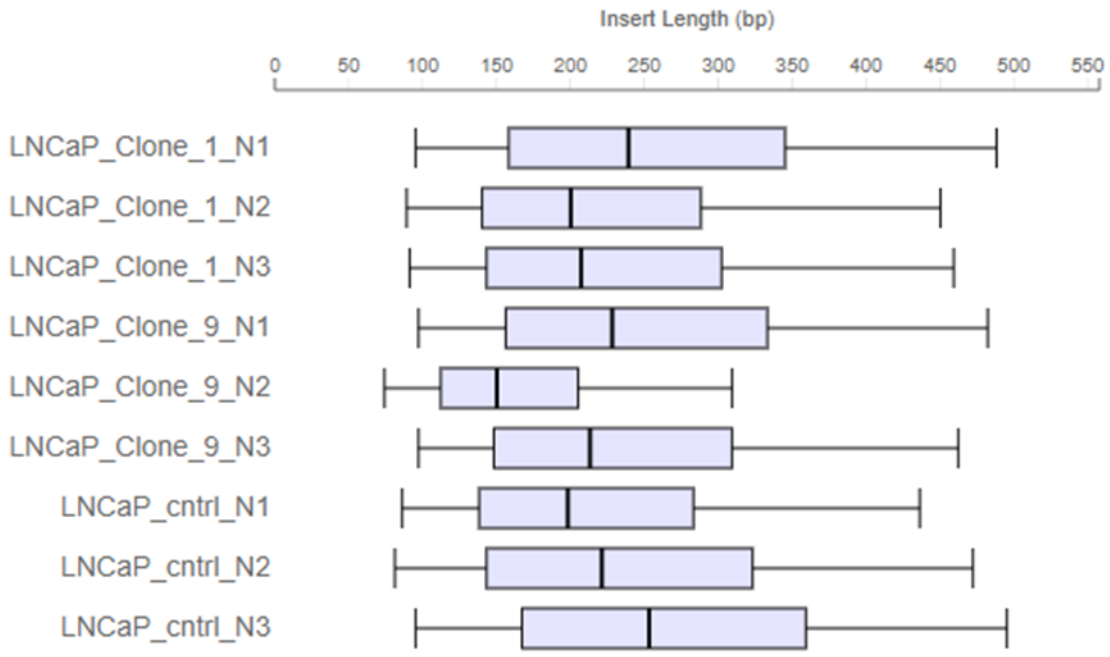

Figure 5.1. Insert length distribution in the enzalutamide resistance panel. The mean insert length of the cell lines ranged between 150 bp to 250 bp.

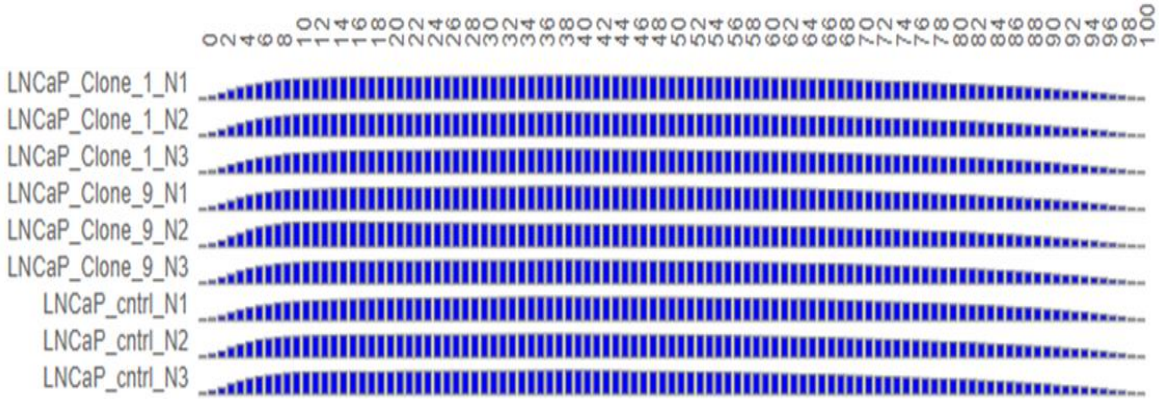

Figure 5.2. Transcript coverage in the enzalutamide resistance panel. The plot of each cell line formed a Poisson-like distribution suggestive of a good sequencing coverage histogram.

5.2.1.2 Gene expression exploratory analysis

Gene expression counts were normalised using DESeq2 median of ratios method and transformed using log2 for visualisation. Samples were clustered by appropriate replicate. The generated heatmap showed that there were no outliers in the dataset and Clone 1 had the largest distance in latent space (Figure 5.3). The scree plot showed approximately 70% variation in principal component 1 (PC1) analysis (Figure 5.4) suggesting that PC1 was responsible for most variation in the data set. Principal component analysis (PCA) was performed on the log2 transformed counts using the PCA tools package BiocSingular (Lun 2019). PCA bi-plot demonstrated clustering of samples and confirmed the quality of the experimental design, where each replicate clustered according to their resistance to enzalutamide (Figure 5.5). Furthermore, it was determined that the variation observed in PC1 in the scree plot was accounted for by Clone 1, as it clustered further from Clone 9 and Control in PC1 (69.14%). Separation of Clone 9 and Control samples was evident in principal component 2 (PC2) (11.99% variation). Due to the small variation present in Clone 9 and Control replicates in the PCA bi-plot, the coefficient “replicates” were accounted for when fitting the generalised linear model in DESeq2 to remove technical variation from the differential gene analysis.

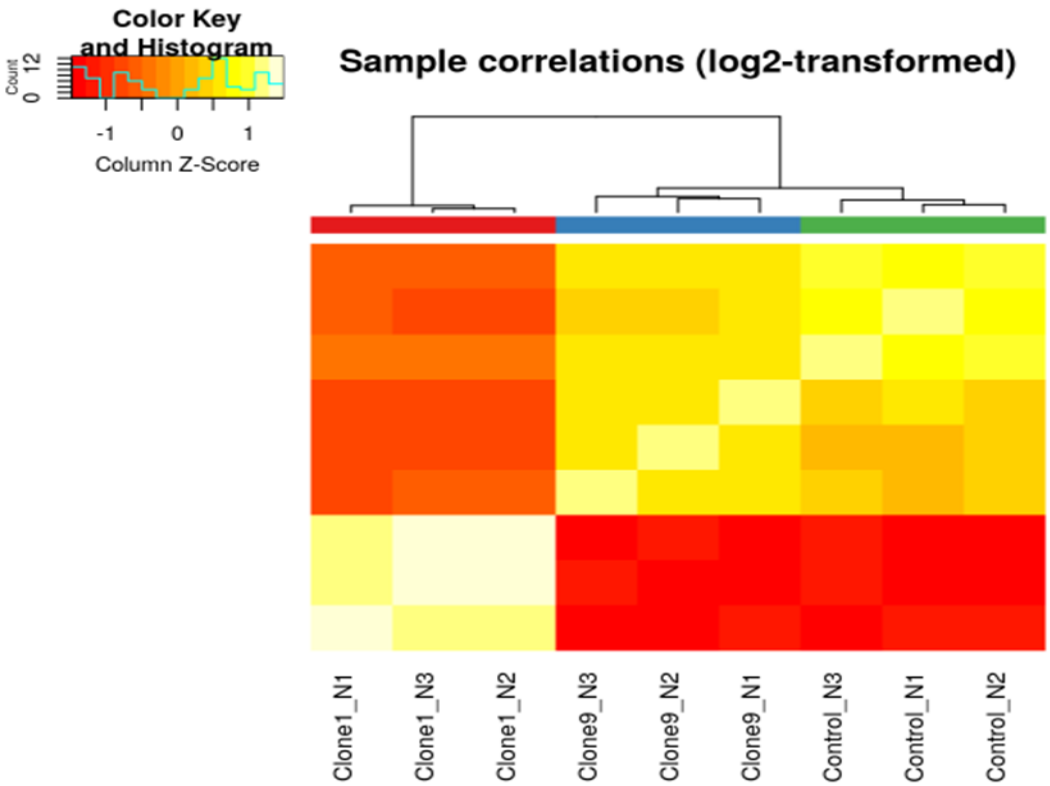

Figure 5.3. Heatmap of sample to sample distances. Samples were clustered by replicate according to their degree of enzalutamide resistance. The heatmap shows there were no outliers in the dataset and Clone 1 had the largest distance in latent space. The heatmap was built using the heatmap.2 package using log2 transformed gene expression data. Image created by Barry Digby.

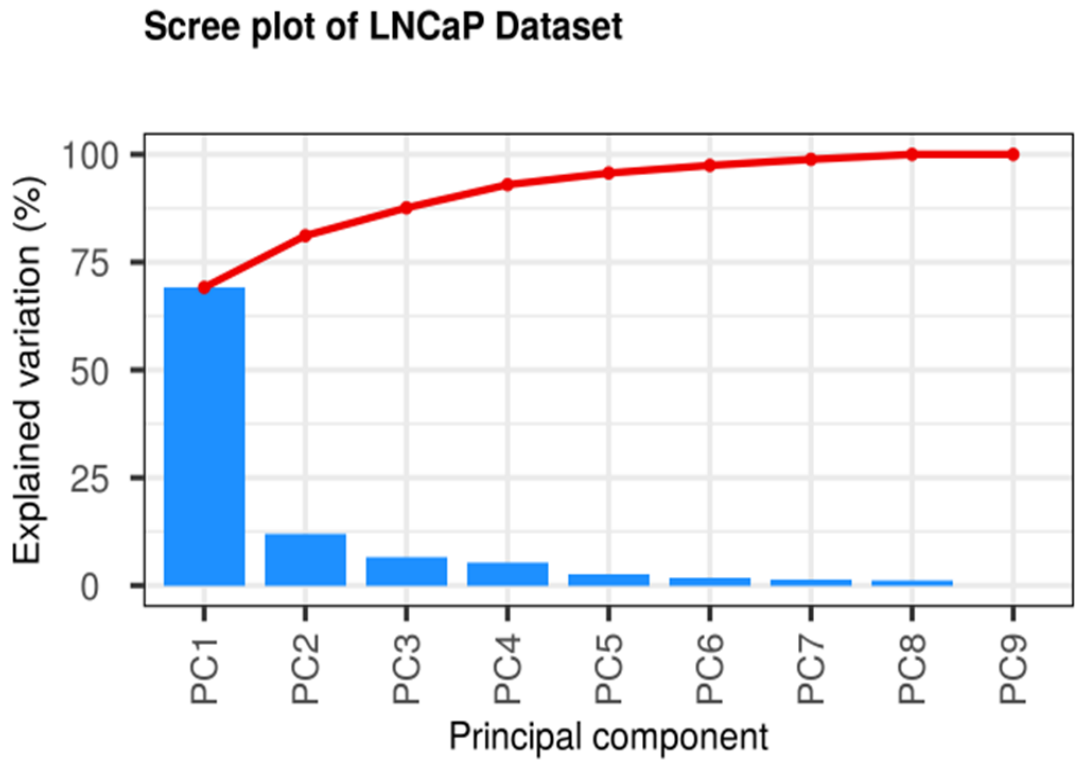

Figure 5.4. Scree plot of enzalutamide resistant panel. The plot showed that principal component 1 (PC1) explained ~70% of the variation present in the dataset.

Image created by Barry Digby.

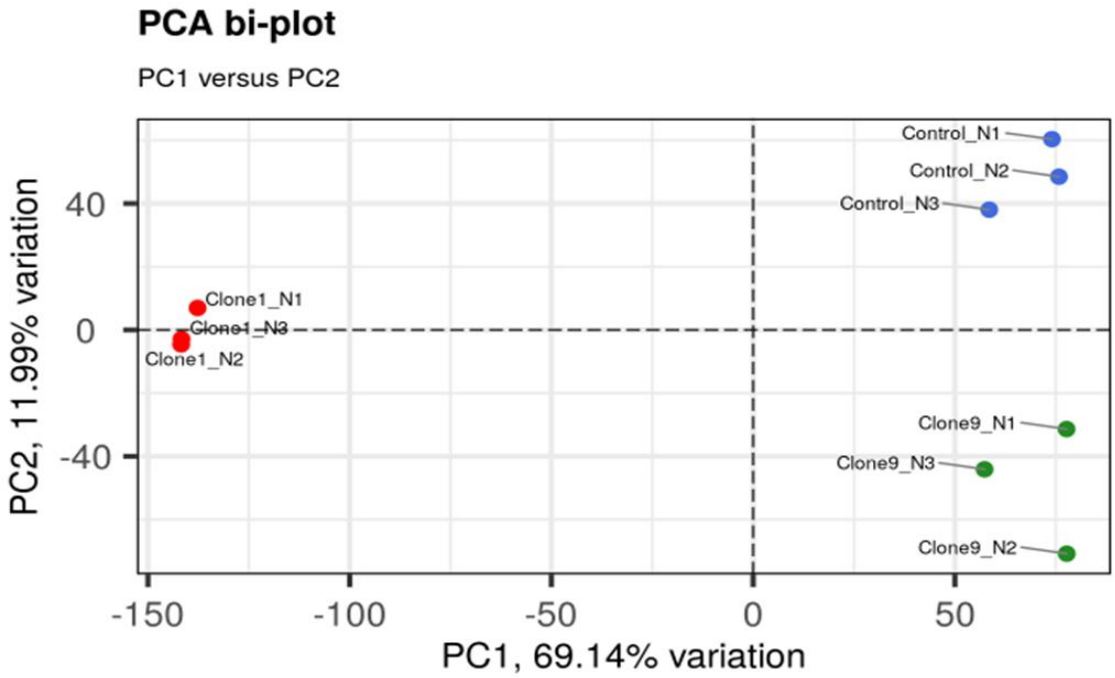

Figure 5.5. PCA bi-plot of enzalutamide resistance panel. This plot demonstrated clustering of samples and confirmed the quality of the experiment design.

Image created by Barry Digby.

5.2.2 Differential gene expression analysis

Differential gene tests were conducted using the DESeq2 package. DESeq2 fits negative binomial generalised linear models for each gene and uses the Wald test for significance testing, returning a table of differentially expressed genes. Multiple testing correction was performed using the independent hypothesis weighting (IHW) package, with the significance threshold for genes set at P-value < 0.05. Genes were annotated using the BiomaRt package. Initial results showed a subset of genes with extremely high/low Log2 FC in the order of +/- 20. This was due to the high variability witnessed within these gene counts. When the read counts were low or highly variable, the maximum likelihood estimates for the Log2 FC had high variance, leading to large estimates not representative of true differences. Lowly expressed genes were filtered out using the rowSums function, where the threshold was set to 20. Inevitably, highly variable genes exceeded this filtering threshold and introduced outliers in the results. Thus, heavy-tailed Cauchy prior distribution for effect sizes was used as part of DESeq2 analysis. The method, approximate posterior estimation for GLM (apeglm), has lower bias than shrinkage estimators, while still reducing variance for those genes with little information for statistical inference. The rowSums function to filter lowly expressed genes was used in conjunction with the apeglm function to shrink the effect size of genes with high variance, returning a robust set of gene. Results of the differentially expressed genes were filtered according to an adjusted P-value of < 0.05 and a log2 FC ≥ 1/ ≤ -1, returning statistically significant genes.

5.2.2.1 Differential gene expression in Clone 1 vs. Control

There were 2,584 up-regulated genes and 1,825 down-regulated genes in Clone 1 *vs.* Control (Figure 5.6 and 5.7). The top 10 highly up-regulated genes ranked by FC for Clone 1 *vs.* Control were *CNTN1*, *VSTM2A*, *RTBDN*, *SKIDA1*, *PCDH10*, *TLX2*, *MIA2*, *SRMS*, *ENPEP* and *PCDH19* with their associated functions in relation to malignancy are listed in Table 5.1. Two of the highly expressed genes, *CNTN1* and *PCDH10* were previously described in PCa

studies. *CNTN1* was reported to promote cell invasion through AKT activation and down-regulates E-cadherin expression (403), while *PCDH10* methylation was frequently observed in people with high risk localised PCa or advanced clinical stage (404).

The top 10 highly down-regulated genes as ranked by FC for Clone 1 *vs.* Control were *DNASE2B, CYP4F11, GRK1, LRRTM3, ZNF204P, SV2C, GRIK1, JAKMIP1, ADAM7 and TRPM8* with their associated functions in relation to malignancy are listed in Table 5.2. Two of the highly down-regulated genes *LRRTM3* and *TRPM8* were previously described in PCa studies. *LRRTM3* was demonstrated to be suppressed in LNCaP cells treated with androgen therapy (405), while *TRPM8* has been reported to play an important role in calcium homeostasis regulated by androgen signalling (406).

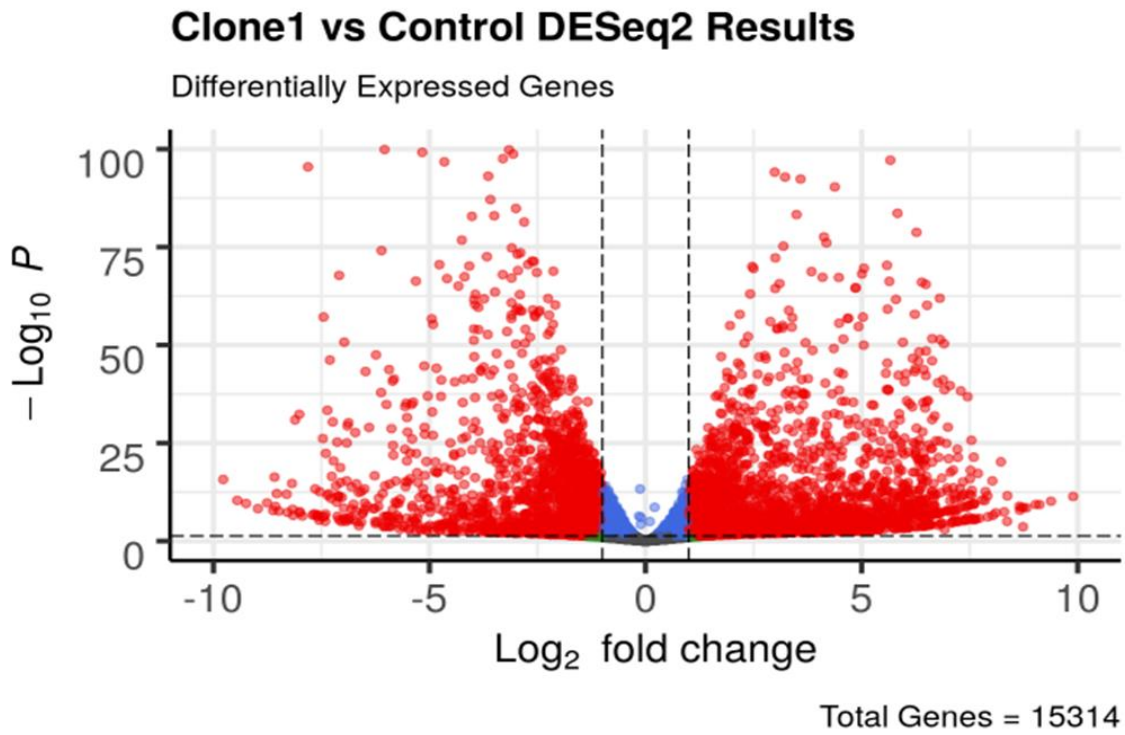

Figure 5.6. The RNA-Seq scatter plot of Clone 1 *vs.* Control. The plot showed the up-regulated (right side) or down-regulated (left side) genes between Clone 1 *vs.* Control. The horizontal line indicated the significance threshold ($p < 0.05$), and the vertical lines indicated the FC threshold ($\geq 1/ \leq -1$). Non-differentially expressed genes were indicated with blue dots and differentially expressed genes were indicated with red dots.

Image created by Barry Digby.

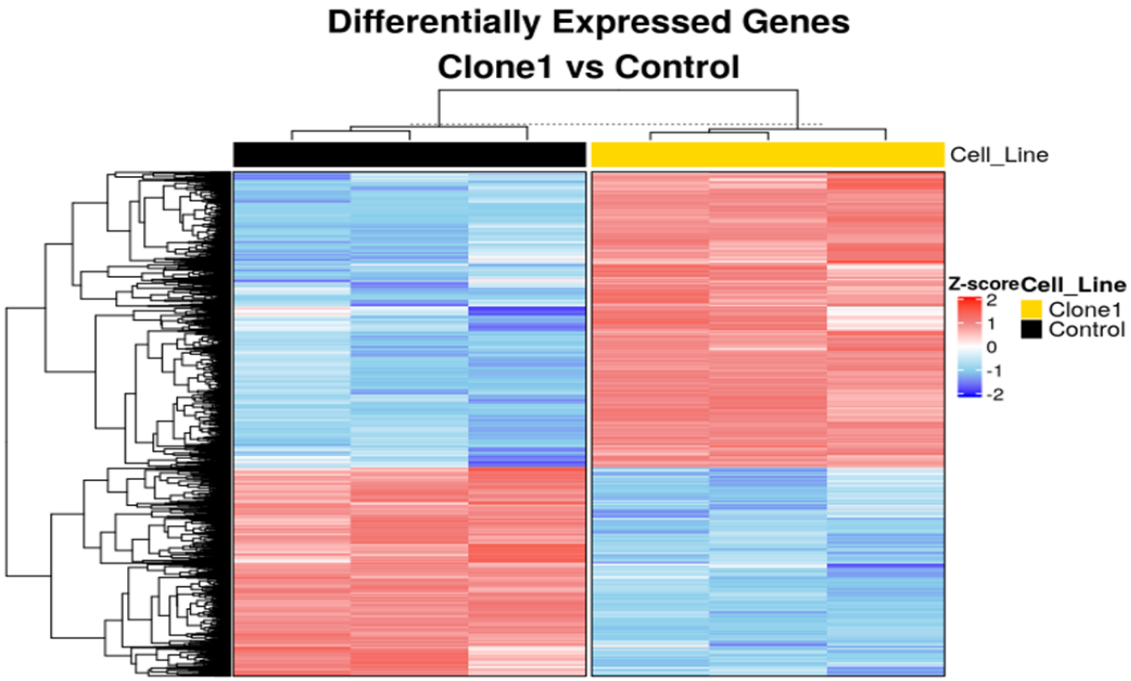

Figure 5.7. The RNA-Seq heatmap of Clone 1 *vs.* Control. The heatmap showed differentially expressed genes in Clone 1 *vs.* Control. Red indicated high expression, blue indicated low expression and white indicated no significant difference between Clone 1 *vs.* Control.

Image created by Barry Digby.

Table 5.1. Top 10 up-regulated genes in Clone 1 *vs.* Control.

Gene	Chromosome	Description	Log2 FC	Adj P-value	Functions
CNTN1	12	contactin 1	9.89435	4.16E-12	Up-regulation of contactin-1 expression promotes PCa progression (403, 407).
VSTM2A	7	V-set and transmembrane domain containing 2A	9.382442	6.96E-11	*VSTM2A* overexpression is a sensitive and specific biomarker for mucinous tubular and spindle cell carcinoma of the kidney (408).
RTBDN	19	retbindin	9.115892	4.91E-10	Lowly expressed in PCa according to TCGA (397).
SKIDA1	10	SKI/DACH domain containing 1	9.025758	4.55E-10	Lowly expressed in PCa according to TCGA (397).
PCDH10	4	protocadherin 10	8.819282	3.27E-09	Promoter methylation-mediated inactivation of *PCDH10* in acute lymphoblastic leukaemia contributes to chemotherapy resistance (409). Frequently observed in patients with high risk localised PCa or advanced clinical stage (404).
TLX2	2	T cell leukaemia homeobox 2	8.742505	2.94E-09	Lowly expressed in PCa according to TCGA (397).
MIA2	14	MIA SH3 domain ER export factor 2	8.734867	0.0002258	Expression was strongly correlated with tumour progression and nodal metastasis in oral squamous cell carcinoma (410).
SRMS	20	src-related kinase lacking C-terminal regulatory tyrosine and N-terminal myristylation sites	8.703573	2.92E-09	Low cancer specificity according to TCGA (397).
ENPEP	4	glutamyl aminopeptidase	8.660357	1.33E-08	Over expressed in CRC tissues and cells (411).
PCDH19	X	protocadherin 19	8.648951	1.29E-09	Methylation of *PCDH19* predicts poor prognosis of hepatocellular carcinoma (412).

Table 5.2. Top 10 down-regulated genes in Clone 1 *vs.* Control.

Gene	Chromosome	Description	Log2 FC	Adj P-value	Functions
DNASE2B	1	deoxyribonuclease 2 beta	-10.6333	1.17E-13	*DNASE2B* silencing suppresses proliferation and induces cell cycle arrest in non-small cell lung cancer cells (413).
CYP4F11	19	cytochrome P450 family 4 subfamily F member 11	-10.324	6.40E-13	NF-κB signalling pathways negatively regulate the *CYP4F11* gene (414).
GRK1	13	G protein-coupled receptor kinase 1	-10.1882	1.81E-12	Hyperactivation of G protein-coupled receptors (GPCRs) may result in loss of normal cell physiological properties. GRK-mediated phosphorylation terminates GPCR hyperactivation (415).
LRRTM3	10	leucine rich repeat transmembrane neuronal 3	-9.77373	3.00E-15	Supressed in LNCaP cells treated with androgen therapy (405).
ZNF204P	6	zinc finger protein 204	-9.44674	7.41E-10	Part of a 5-gene signature that is closely related to tumour immune microenvironment and predicts the prognosis of patients with non-small cell lung cancer (416).
SV2C	5	synaptic vesicle glycoprotein 2C	-9.24417	4.09E-09	Dysregulation of SV2 can regulate transporter and transmembrane transporter activity and provide the necessary nutrients for tumour cell proliferation (417).
GRIK1	21	glutamate ionotropic receptor kainate type subunit 1	-8.97094	3.55E-08	Involved in post-transcriptional deleterious substitutions in cancer (418).
JAKMIP1	4	janus kinase and microtubule interacting protein 1	-8.75733	1.75E-09	Overexpression of *JAKMIP1* associates with Wnt/β-catenin pathway activation and promotes cancer cell proliferation in vitro (419).
ADAM7	8	ADAM metallopeptidase domain 7	-8.61862	1.07E-07	Part of a 7 gene signature prognostic biomarker panel in high-risk PCa patients (400).
TRPM8	2	transient receptor potential cation channel subfamily M member 8	-8.586	8.23E-16	Plays a key role in processes such as the proliferation, viability and cell migration of PCa cells. *TRPM8* have a protective anti-invasive effect (406).

5.2.2.2 Differential gene expression in Clone 9 vs. Control

There were 395 up-regulated genes and 329 down-regulated genes in Clone 9 *vs.* Control (Figure 5.8 and 5.9). The top 10 highly up-regulated genes for Clone 9 *vs.* Control were *PRSS12, FGG, CNTNAP4, ENPP2, PCDH19, SMOC2, UNC5A, ASZ1, CRLF1 and CBLN2* (Table 5.3). Whereas the top 10 highly down-regulated genes for Clone 9 *vs.* Control were *MAGEC2, EFS, SLC22A3, LRRTM3, LPAR3, ADGRG6, ARHGAP6, DDX53, ETV1 and ZNF135* (Table 5.4).

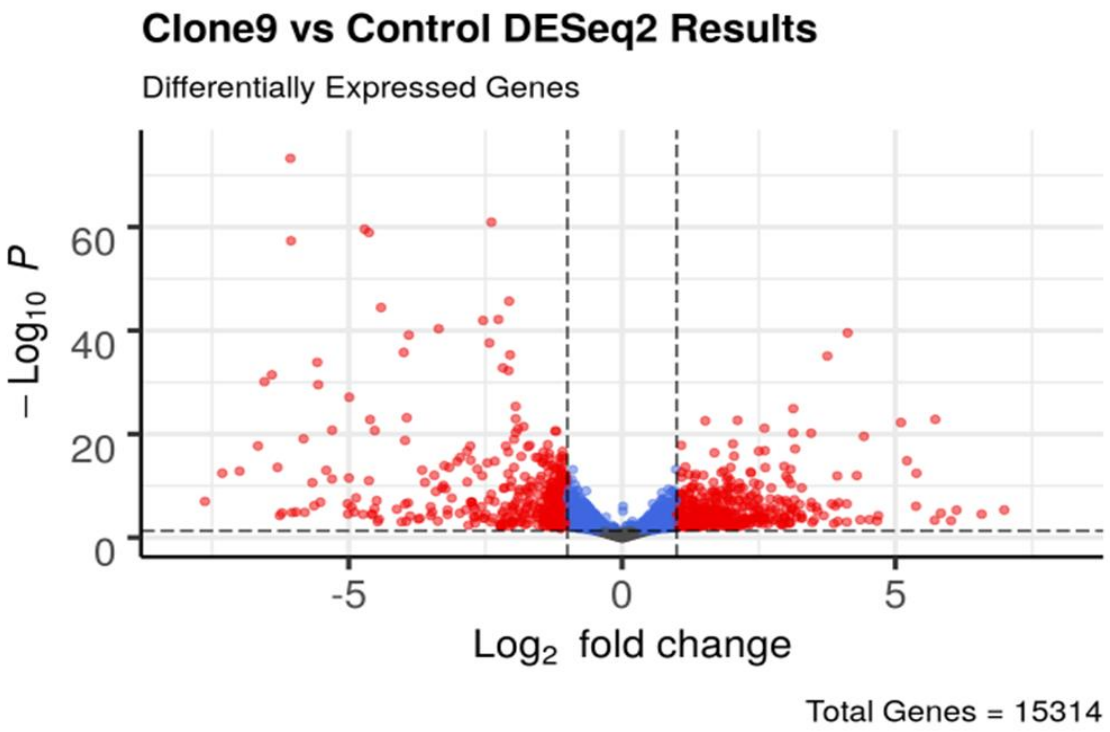

Figure 5.8. The RNA-Seq scatter plot of Clone 9 *vs.* Control. The plot showed the up or down-regulated genes between Clone 9 *vs.* Control. The horizontal line indicated the significance threshold ($p < 0.05$), and the vertical lines indicated the FC threshold ($\geq 1 / \leq -1$). Non-differentially expressed genes were indicated with blue dots and differentially expressed genes were indicated with red dots.

Image created by Barry Digby.

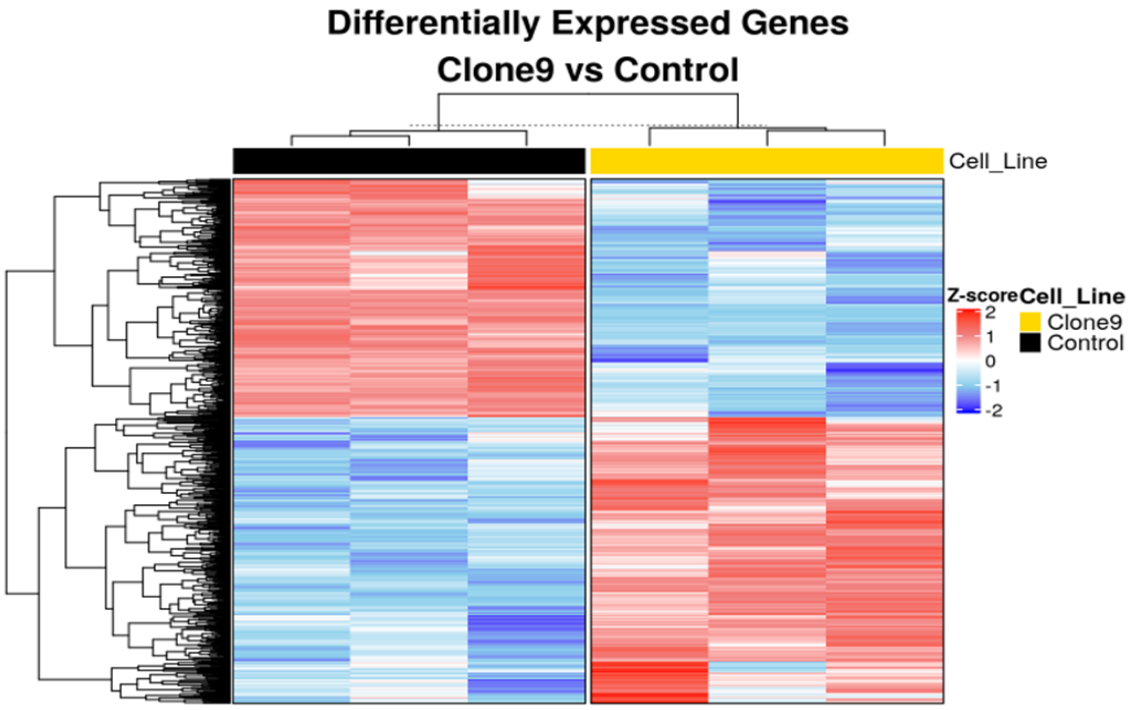

Figure 5.9. The RNA-Seq heatmap of Clone 9 *vs.* Control. The heatmap showed differentially expressed genes in Clone 9 *vs.* Control. Red indicated high expression, blue indicated low expression and white indicated no significant difference between Clone 9 *vs.* Control. Image created by Barry Digby.

Table 5.3. Top 10 up-regulated genes in Clone 9 *vs.* Control.

Gene	Chromosome	Description	Log2FC	Adj P-value
PRSS12	4	serine protease 12	6.991097	0.000338529
FGG	4	fibrinogen gamma chain	6.577454	0.001118071
CNTNAP4	16	contactin associated protein family member 4	6.116741	0.000369852
ENPP2	8	ectonucleotide pyrophosphatase/phosphodiesterase 2	6.017777	0.014043428
PCDH19	X	protocadherin 19	5.830747	0.001109461
SMOC2	6	SPARC related modular calcium binding 2	5.728052	8.67E-21
UNC5A	5	unc-5 netrin receptor A	5.384148	4.74E-11
ASZ1	7	ankyrin repeat, SAM and basic leucine zipper domain containing 1	5.376614	7.91591E-05
CRLF1	19	cytokine receptor like factor 1	5.210595	2.65E-13
CBLN2	18	cerebellin 2 precursor	5.101316	2.57E-20

Table 5.4. Top 10 down-regulated genes in Clone 9 *vs.* Control.

Gene	Chromosome	Description	Log2FC	Adj P-value
MAGEC2	X	MAGE family member C2	-7.63042	1.19412E-05
EFS	14	embryonal Fyn-associated substrate	-7.31353	5.79E-11
SLC22A3	6	solute carrier family 22 member 3	-6.99765	1.91E-11
LRRTM3	10	leucine rich repeat transmembrane neuronal 3	-6.66016	5.31E-16
LPAR3	1	lysophosphatidic acid receptor 3	-6.54286	4.76E-28
ADGRG6	6	adhesion G protein-coupled receptor G6	-6.43033	1.85E-149
ARHGAP6	X	Rho GTPase activating protein 6	-6.40686	2.15E-29
DDX53	X	DEAD-box helicase 53	-6.25997	0.001803226
ETV1	7	ETS variant transcription factor 1	-6.05531	8.37E-55
ZNF135	19	zinc finger protein 135	-6.03775	0.000369852

5.2.2.3 Differential gene expression in Clone 1 vs. Clone 9

There were 2,429 up-regulated genes and 2,076 down-regulated genes in Clone 1 *vs.* Clone 9 (Figure 5.10 and 5.11). The top 10 highly up-regulated genes for Clone 1 *vs.* Clone 9 were *AVPR1A, PCDHA13, GABRB2, CAND2, GRM8, GUCY2D, PAK6, TPTE, PHYHIPL and SYTL5* (Table 5.5). Whereas the top 10 highly down-regulated genes for Clone 1 *vs.* Clone 9 were *DNASE2B, JAKMIP1, KRT6C, CYP4F11, TFF3, KNDC1, TMPRSS6, AGT, SMOC2 and CAPN13* (Table 5.6).

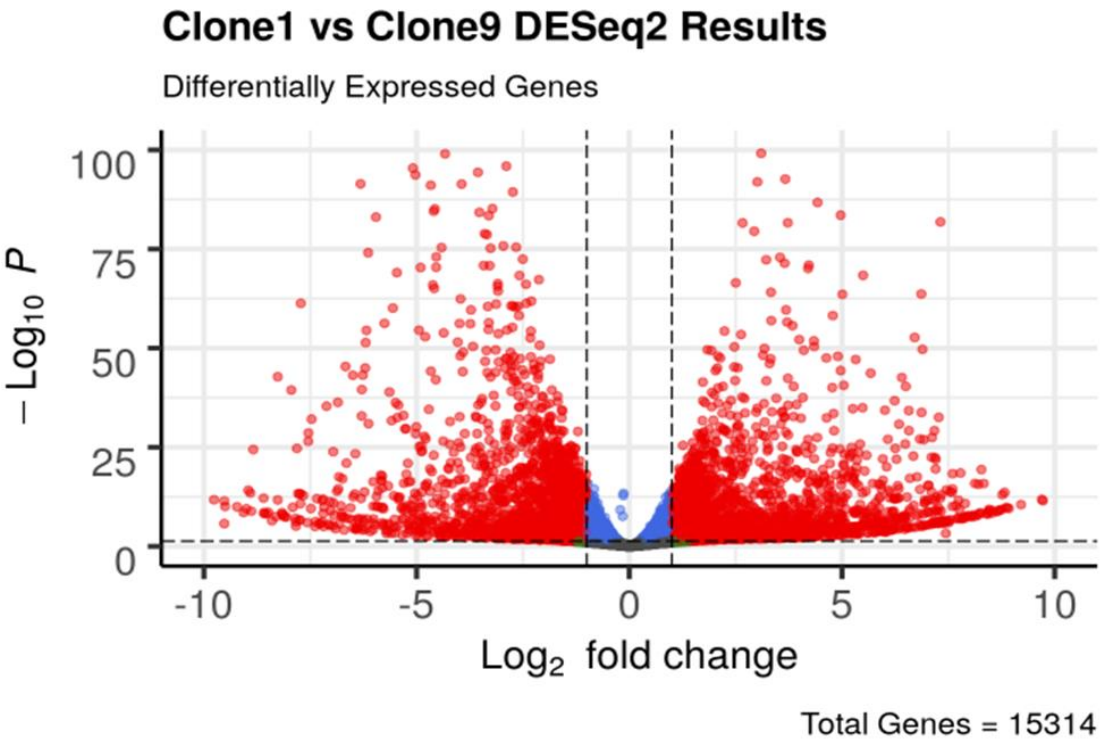

Figure 5.10. The RNA-Seq scatter plot of Clone 1 *vs.* Clone 9. The plot showed the up or down-regulated genes between Clone 1 *vs.* Clone 9. The horizontal line indicated the significance threshold ($p < 0.05$), and the vertical lines indicated the FC threshold ($\geq 1 / \leq -1$). Non-differentially expressed genes were indicated with blue dots and differentially expressed genes were indicated with red dots.

Image created by Barry Digby.

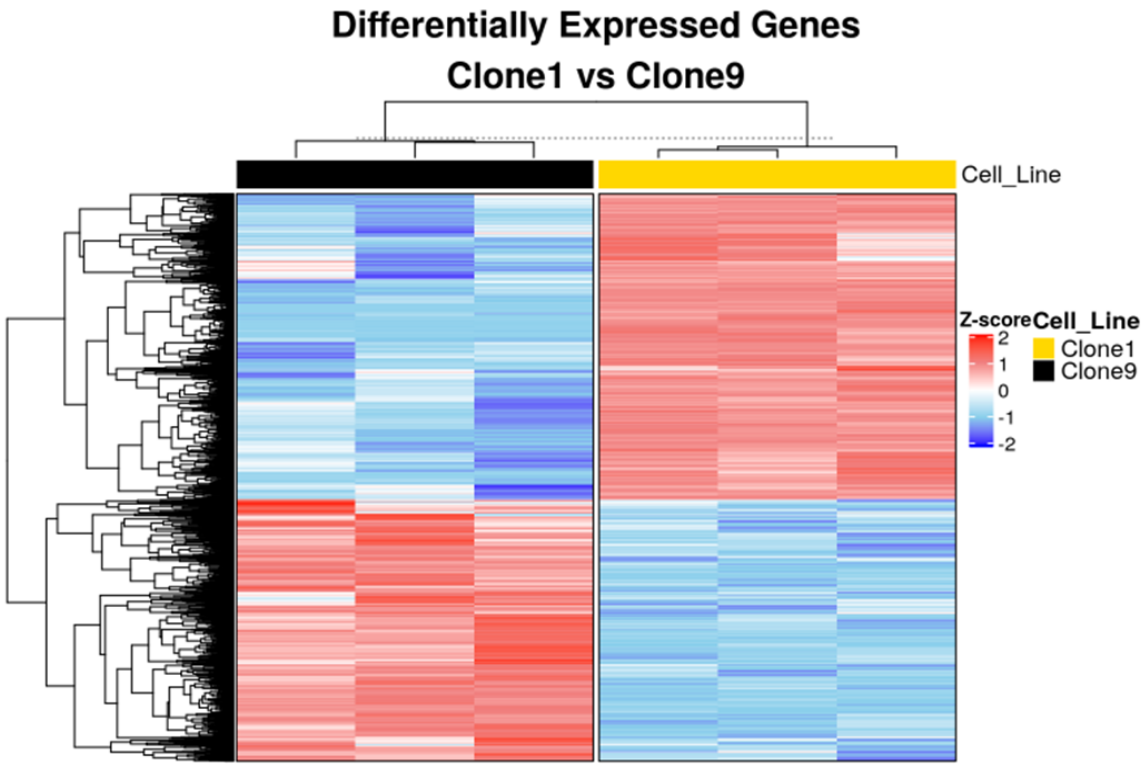

Figure 5.11. The RNA-Seq heatmap of Clone 1 *vs.* Clone 9. The heat map showed differentially expressed genes in Clone 1 *vs.* Clone 9. Red indicated high expression, blue indicated low expression and white indicated no significant difference between Clone 9 *vs.* Control.

Image created by Barry Digby.

Table 5.5. Top 10 up-regulated gene in Clone 1 *vs.* Clone 9.

Gene	Chromosome	Description	Log2FC	Adj P-value
AVPR1A	12	arginine vasopressin receptor 1A	11.14307	1.66E-15
PCDHA13	5	protocadherin alpha 13	9.696594	1.28E-11
GABRB2	5	gamma-aminobutyric acid type A receptor subunit beta2	9.207707	2.56E-10
CAND2	3	cullin associated and neddylation dissociated 2 (putative)	8.924685	2.40E-09
GRM8	7	glutamate metabotropic receptor 8	8.870741	1.34E-09
GUCY2D	17	guanylate cyclase 2D, retinal	8.863316	1.58E-09
PAK6	15	BUB1B-PAK6 readthrough	8.821866	3.16E-13
TPTE	21	transmembrane phosphatase with tensin homology	8.767224	1.11E-12
PHYHIPL	10	phytanoyl-CoA 2-hydroxylase interacting protein like	8.755069	3.83E-09
SYTL5	X	synaptotagmin like 5	8.710789	5.44E-09

Table 5.6. Top 10 down-regulated gene in Clone 1 *vs.* Clone 9.

Gene	Chromosome	Description	Log2FC	Adj P-value
DNASE2B	1	deoxyribonuclease 2 beta	-10.1262	1.55E-12
JAKMIP1	4	janus kinase and microtubule interacting protein 1	-9.76368	2.19E-11
KRT6C	12	keratin 6C	-9.5223	9.41339E-06
CYP4F11	19	cytochrome P450 family 4 subfamily F member 11	-9.52121	3.24E-11
TFF3	21	trefoil factor 3	-9.5026	6.99E-10
KNDC1	10	kinase non-catalytic C-lobe domain containing 1	-9.22146	9.01E-10
TMPRSS6	22	transmembrane serine protease 6	-9.06823	2.30E-08
AGT	1	angiotensinogen	-9.00205	2.97E-09
SMOC2	6	SPARC related modular calcium binding 2	-8.95718	9.83E-14
CAPN13	2	calpain 13	-8.91034	3.70E-13

5.2.3 Gene set enrichment analysis

Gene set enrichment analysis (GSEA) was performed using GSEA software (420). The dataset was normalised using DESeq2 median of ratios method and parsed to .gct format using custom bash scripts as input to GSEA. Parameters that deviate from the default settings are described below:

1. Permutation Type: Gene Set was chosen for this parameter as the number of samples per phenotype was below 7, thus phenotype shuffling was not feasible for this option.
2. Metric for Ranking Genes: T-test uses the difference of means scaled by the standard deviation and number of samples, as opposed to the default signal-to-noise metric that uses the difference of means scaled by the standard deviation, without taking into account the number of samples.

5.2.3.1 Hallmark gene enrichment

Molecular Signatures Database (MSigDB) has comprehensive databases for gene sets and is widely used for GSEA (421). The hallmark gene sets were generated by computational methodology based on identifying overlaps between gene sets in other MSigDB collections and retaining genes that display coordinated expression. These gene sets summarise and represent specific well-defined biological states or processes and display coherent expression. The hallmarks efficiently condense most of the related information from the original founder sets by decreasing both variation and redundancy hence, deliver more refined and concise inputs for GSEA.

5.2.3.1.1 Hallmark gene enrichment in Clone 1 *vs.* Control

GSEA of Clone 1 *vs.* Control revealed positive enrichments of hallmark gene sets for Clone 1 in *'terms'* of proliferation and cell cycle (e.g. E2F_TARGETS, G2M_CHECKPOINT), wound healing, fibrosis and metastasis (e.g. EPITHELIAL_MESENCHYMAL_TRANSITION, APICAL_JUNCTION, TGF_BETA_SIGNALING), cell signalling (e.g. HEDGEHOG_SIGNALING, KRAS_SIGNALING_DN) and DNA repair (e.g. SPERMATOGENESIS) (Table 5.7, Figure 5.12). Whereas the enriched hallmark pathway for the Control cell line was associated with canonical AR functions and luminal differentiation (e.g. ANDROGEN_RESPONSE, FATTY_ACID_METABOLISM, P53_PATHWAY) (Table 5.8, Figure 5.12).

Table 5.7. Clone 1 *vs.* Control hallmark gene sets enrichment pathway for Clone 1.

Name	Normalised Enrichment Score (NES)	NOM.p.val
HALLMARK_E2F_TARGETS	1.7182336	0
HALLMARK_EPITHELIAL_MESENCHYMAL_TRANSITION	1.647743	0
HALLMARK_HEDGEHOG_SIGNALING	1.6068962	0.010835913
HALLMARK_SPERMATOGENESIS	1.596519	0.0027894
HALLMARK_KRAS_SIGNALING_DN	1.533521	0.004
HALLMARK_G2M_CHECKPOINT	1.5132686	0.001283697
HALLMARK_APICAL_JUNCTION	1.4458987	0.006451613
HALLMARK_TGF_BETA_SIGNALING	1.4371105	0.041853514

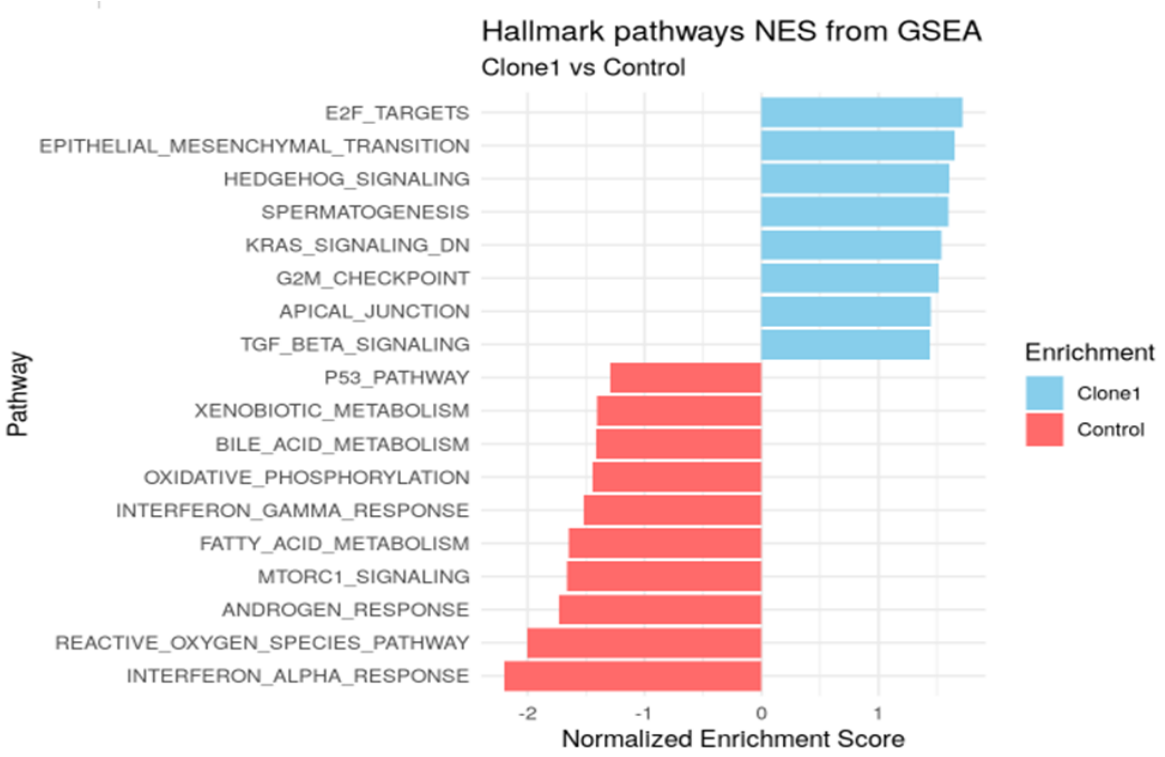

Figure 5.12. Enriched Hallmark pathways plot for both Clone 1 and Control according to normalised enrichment score (NES).

Image created by Barry Digby.

Table 5.8. Clone 1 *vs.* Control hallmark gene sets enrichment pathway for Control.

Name	Normalised Enrichment Score (NES)	NOM.p.val
HALLMARK_INTERFERON_ALPHA_RESPONSE	-2.198988	0
HALLMARK_REACTIVE_OXYGEN_SPECIES_PATHWAY	-2.0053463	0
HALLMARK_ANDROGEN_RESPONSE	-1.7316155	0
HALLMARK_MTORC1_SIGNALING	-1.6639274	0
HALLMARK_FATTY_ACID_METABOLISM	-1.6512092	0
HALLMARK_INTERFERON_GAMMA_RESPONSE	-1.5193813	0.004405286
HALLMARK_OXIDATIVE_PHOSPHORYLATION	-1.44698	0
HALLMARK_BILE_ACID_METABOLISM	-1.4120221	0.039007094
HALLMARK_XENOBIOTIC_METABOLISM	-1.4071633	0.004385965
HALLMARK_P53_PATHWAY	-1.2958128	0.020618556

5.2.3.1.2 Hallmark gene enrichment in Clone 9 *vs.* Control

GSEA of Clone 9 *vs.* Control revealed positive enrichments of hallmark gene sets for Clone 9 in *'terms'* of wound healing, fibrosis and metastasis (e.g. EPITHELIAL_MESENCHYMAL_TRANSITION), and cell signalling (e.g. NOTCH_SIGNALING, KRAS_SIGNALING) (Table 5.9, Figure 5.13). Whereas the enriched hallmark pathway for Control was associated with canonical AR functions (e.g. ANDROGEN_RESPONSE) (Table 5.10, Figure 5.13).

Table 5.9. Clone 9 *vs.* Control hallmark gene sets enrichment pathway for Clone 9.

Name	Normalised Enrichment Score (NES)	NOM.p.val
HALLMARK_NOTCH_SIGNALING	1.8992859	0
HALLMARK_EPITHELIAL_MESENCHYMAL_TRANSITION	1.8033924	0
HALLMARK_INTERFERON_GAMMA_RESPONSE	1.7285744	0
HALLMARK_MYOGENESIS	1.7199115	0
HALLMARK_COAGULATION	1.5855019	0.001972387
HALLMARK_ALLOGRAFT_REJECTION	1.5018028	0.013888889
HALLMARK_KRAS_SIGNALING_DN	1.3872683	0.02636535
HALLMARK_KRAS_SIGNALING_UP	1.3534801	0.03219697
HALLMARK_ESTROGEN_RESPONSE_LATE	1.3402249	0.022132797
HALLMARK_ESTROGEN_RESPONSE_EARLY	1.3242459	0.03137255

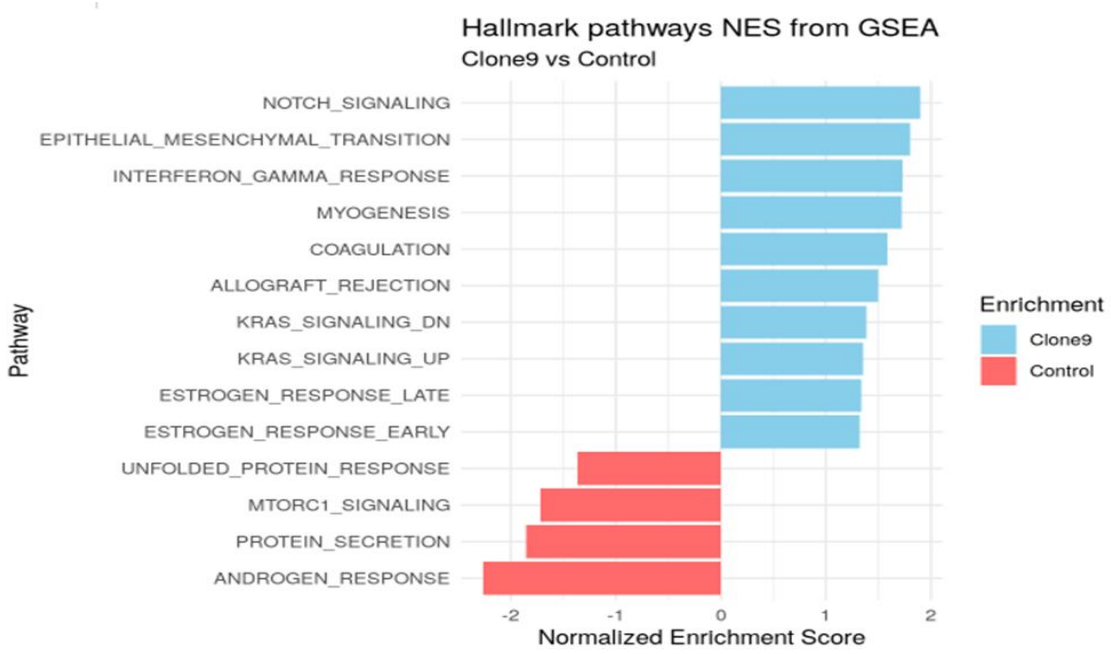

Figure 5.13. Enriched Hallmark pathways plot for both Clone 9 and Control according to NES.

Image created by Barry Digby.

Table 5.10. Clone 9 *vs.* Control hallmark gene sets enrichment pathway for Control.

Name	Normalised Enrichment Score (NES)	NOM.p.val
HALLMARK_ANDROGEN_RESPONSE	-2.2623067	0
HALLMARK_PROTEIN_SECRETION	-1.8531822	0
HALLMARK_MTORC1_SIGNALING	-1.720772	0
HALLMARK_UNFOLDED_PROTEIN_RESPONSE	-1.3650557	0.038854804

5.2.3.1.3 Hallmark gene enrichment in Clone 1 *vs.* Clone 9

GSEA of Clone 1 *vs.* Clone 9 revealed positive enrichments of Hallmark gene sets for Clone 1 in *'terms'* of proliferation and cell cycle (e.g. E2F_TARGETS, G2M_CHECKPOINT), wound healing, fibrosis and metastasis (e.g. APICAL_JUNCTION, TGF_BETA_SIGNALING), cell signalling (e.g. HEDGEHOG_SIGNALING, KRAS_SIGNALING_DN) and DNA repair (e.g. SPERMATOGENESIS) (Table 5.11, Figure 5.14). Whereas the enriched hallmark pathway for Clone 9 was associated with luminal differentiation (e.g. FATTY_ACID_METABOLISM, P53_PATHWAY) (Table 5.12, Figure 5.14).

Table 5.11. Clone 1 *vs.* Clone 9 hallmark gene sets enrichment pathway for Clone 1.

Name	Normalised Enrichment Score (NES)	NOM.p.val
HALLMARK_E2F_TARGETS	1.7742442	0
HALLMARK_HEDGEHOG_SIGNALING	1.6965327	0.013062409
HALLMARK_TGF_BETA_SIGNALING	1.5920576	0.011204482
HALLMARK_G2M_CHECKPOINT	1.5769154	0.001182033
HALLMARK_SPERMATOGENESIS	1.5304968	0.012
HALLMARK_KRAS_SIGNALING_DN	1.477232	0.01010101
HALLMARK_APICAL_JUNCTION	1.3764853	0.024271844

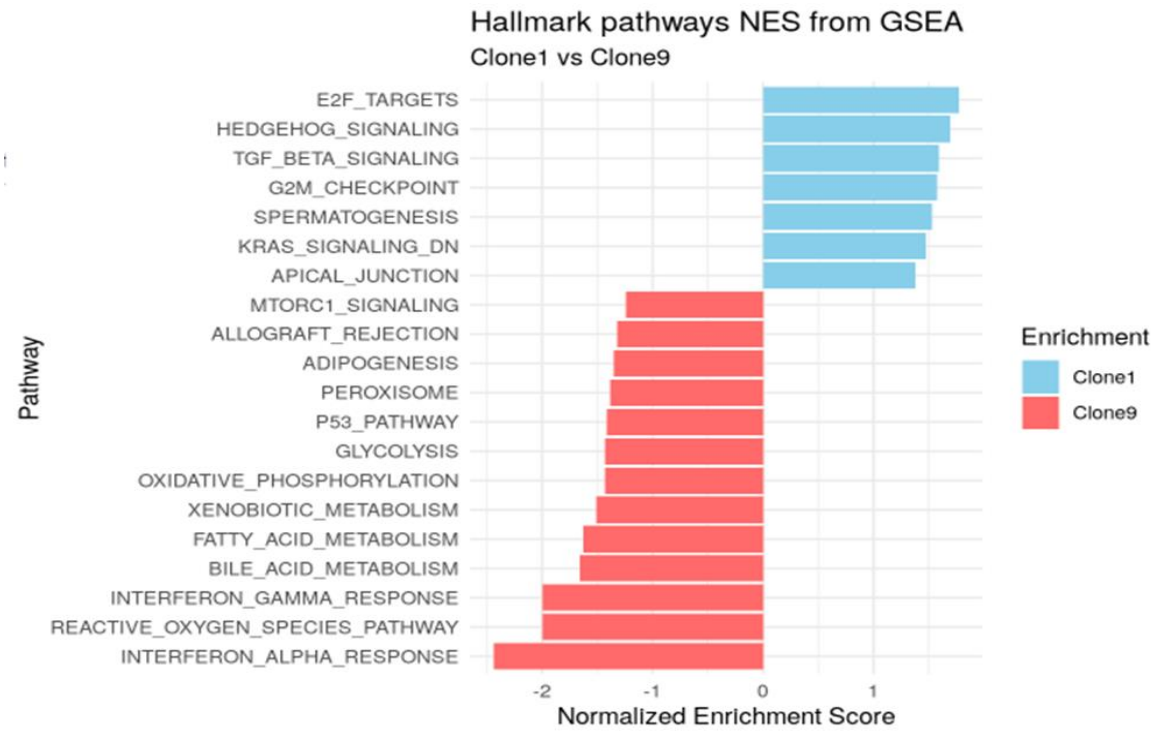

Figure 5.14. Enriched Hallmark pathways plot for both Clone 1 and Clone 9 according to NES.

Image created by Barry Digby.

Table 5.12. Clone 1 *vs.* Clone 9 gene sets enrichment pathway for Clone 9.

Name	Normalised Enrichment Score (NES)	NOM.p.val
HALLMARK_INTERFERON_ALPHA_RESPONSE	-2.4399471	0
HALLMARK_REACTIVE_OXYGEN_SPECIES_PATHWAY	-2.0002444	0
HALLMARK_INTERFERON_GAMMA_RESPONSE	-1.9965045	0

HALLMARK_BILE_ACID_METABOLISM	-1.660734	0
HALLMARK_FATTY_ACID_METABOLISM	-1.6281723	0
HALLMARK_XENOBIOTIC_METABOLISM	-1.5123318	0
HALLMARK_OXIDATIVE_PHOSPHORYLATION	-1.434762	0
HALLMARK_GLYCOLYSIS	-1.433255	0
HALLMARK_P53_PATHWAY	-1.4146837	0.006896552
HALLMARK_PEROXISOME	-1.3843288	0.038961038

5.2.3.2 Integrative Analysis of Kyoto Encyclopaedia of Genes and Genomes (KEEG)

The Kyoto Encyclopaedia of Genes and Genomes (KEGG) database is a resource for understanding high-level functions and utilities of the biological system, such as the cell, the organism and the ecosystem, from molecular-level information, especially large-scale molecular datasets generated by genome sequencing and other high-throughput experimental technologies (422).

5.2.3.2.1 KEGG in Clone 1 *vs.* Control

Analysis of Clone 1 *vs.* Control identified 16 pathways that were significantly enriched for Clone 1 (Table 5.13 and Figure 5.15) and 23 pathways for Control (Table 5.14, Figure 5.15). The majority of Clone 1 KEEG pathways were associated with calcium homeostasis and signalling such as KEGG_ HCM, KEGG_ARVC, KEGG_LONG_TERM_DEPRESSION, KEGG_DILATED_CARDIOMYOPATHY, KEGG_TASTE_TRANSDUCTION and KEGG_CALCIUM_SIGNALIN. Other cancer signal transduction pathways such as KEGG_TGF_BETA_SIGNALING, KEGG_MAPK_SIGNALING and lastly cell coordination such as KEGG_NEUROACTIVE_LIGAND_RECEPTOR_INTERACTION, KEGG_AXON_GUIDANCE, KEGG_CYTOKINE_CYTOKINE_RECEPTOR_INTERACTION and KEGG_REGULATION_OF_ACTIN_CYTOSKELETON were also identified.

Table 5.13. KEGG pathways associated with Clone 1.

Name	**Normalised Enrichment Score (NES)**	**NOM.p.val**
KEGG_HYPERTROPHIC_CARDIOMYOPATHY_HCM	2.1290123	0
KEGG_NEUROACTIVE_LIGAND_RECEPTOR_INTERACTION	2.0008655	0
KEGG_TGF_BETA_SIGNALING_PATHWAY	1.8861989	0
KEGG_ARRHYTHMOGENIC_RIGHT_VENTRICULAR_CARDIOMYOPATHY_ARVC	1.8771864	0

KEGG_LONG_TERM_DEPRESSION	1.7600564	0.001494768
KEGG_DILATED_CARDIOMYOPATHY	1.6765262	0.004580153
KEGG_AXON_GUIDANCE	1.6168513	0
KEGG_CELL_CYCLE	1.6020046	0
KEGG_MELANOGENESIS	1.5440861	0.01010101
KEGG_BASAL_CELL_CARCINOMA	1.5192964	0.010752688
KEGG_MATURITY_ONSET_DIABETES_OF_THE_YOUNG	1.519197	0.045075126
KEGG_CYTOKINE_CYTOKINE_RECEPTOR_INTERACTION	1.4974877	0.010781671
KEGG_TASTE_TRANSDUCTION	1.472757	0.045813587
KEGG_REGULATION_OF_ACTIN_CYTOSKELETON	1.4368652	0.011627907
KEGG_CALCIUM_SIGNALING_PATHWAY	1.4330951	0.010738255
KEGG_MAPK_SIGNALING_PATHWAY	1.3138214	0.03566879

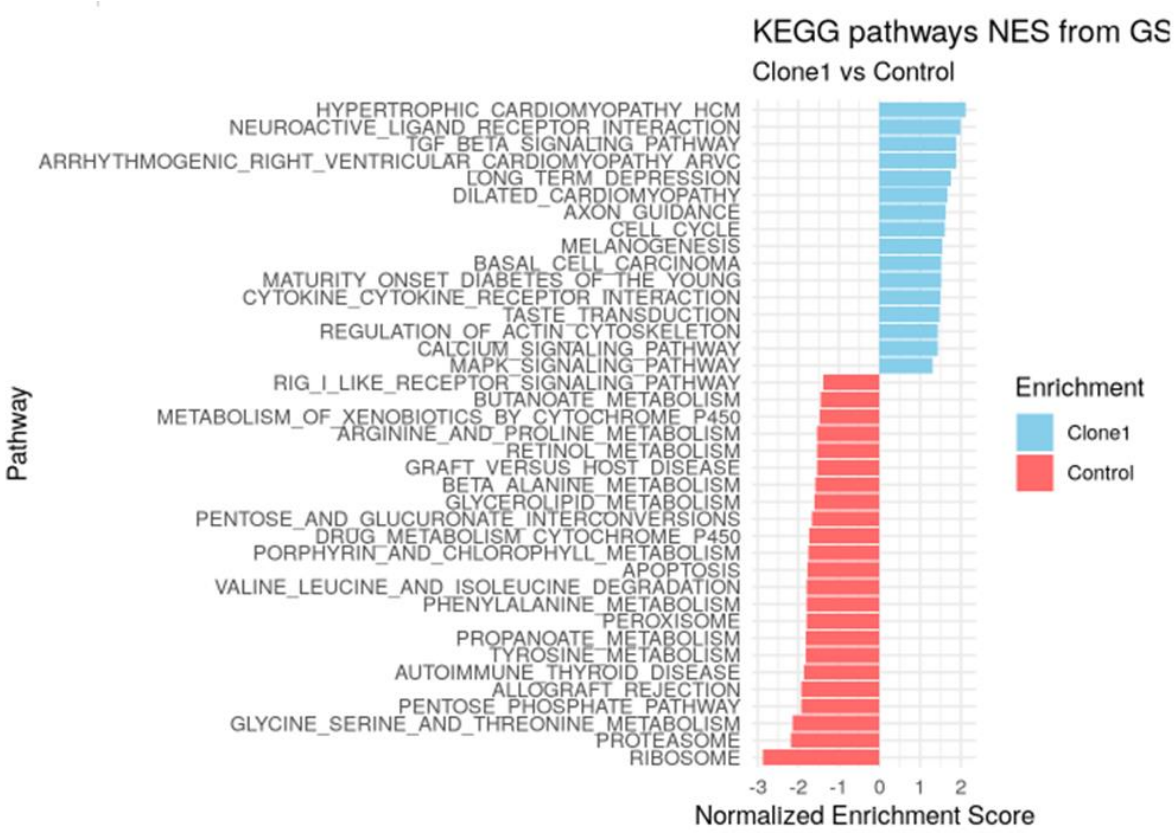

Figure 5.15. Enriched KEGG pathways plot for both Clone 1 and Control according to NES.

Image created by Barry Digby.

Table 5.14. KEGG pathways associated with Control.

Name	Normalised Enrichment Score (NES)	NOM.p.val
KEGG_RIBOSOME	-2.8774042	0
KEGG_PROTEASOME	-2.174453	0
KEGG_GLYCINE_SERINE_AND_THREONINE_METABOLISM	-2.1290758	0
KEGG_PENTOSE_PHOSPHATE_PATHWAY	-1.9183646	0.005
KEGG_ALLOGRAFT_REJECTION	-1.9174867	0
KEGG_AUTOIMMUNE_THYROID_DISEASE	-1.8542013	0
KEGG_TYROSINE_METABOLISM	-1.814152	0.005540166
KEGG_PROPANOATE_METABOLISM	-1.8096485	0.007633588
KEGG_PEROXISOME	-1.8008882	0
KEGG_PHENYLALANINE_METABOLISM	-1.7866994	0.002450981
KEGG_VALINE_LEUCINE_AND_ISOLEUCINE_DEGRADATION	-1.7844507	0.006097561
KEGG_APOPTOSIS	-1.7819197	0
KEGG_PORPHYRIN_AND_CHLOROPHYLL_METABOLISM	-1.7470502	0.00802139
KEGG_DRUG_METABOLISM_CYTOCHROME_P450	-1.7302134	0
KEGG_PENTOSE_AND_GLUCURONATE_INTERCONVERSIONS	-1.6697093	0.015
KEGG_GLYCEROLIPID_METABOLISM	-1.6066929	0.016666668
KEGG_BETA_ALANINE_METABOLISM	-1.5704874	0.033333335
KEGG_GRAFT_VERSUS_HOST_DISEASE	-1.5459976	0.043956045
KEGG_RETINOL_METABOLISM	-1.5437679	0.00867052
KEGG_ARGININE_AND_PROLINE_METABOLISM	-1.541852	0.02616279
KEGG_METABOLISM_OF_XENOBIOTICS_BY_CYTOCHROME_P450	-1.4721928	0.031847134
KEGG_BUTANOATE_METABOLISM	-1.4597449	0.048991356
KEGG_RIG_I_LIKE_RECEPTOR_SIGNALING_PATHWAY	-1.3949547	0.04178273

5.2.3.2.2 KEGG in Clone 9 *vs.* Control

KEGG analysis of Clone 9 *vs.* Control identified 12 pathways that were significantly enriched for Clone 9 (Table 5.15, Figure 5.16) and 9 pathways for Control (Table 5.16, Figure 5.16). The KEEG pathways in Clone 9 were associated with cell coordination (i.e., KEGG_AXON_GUIDANCE, KEGG_CAMS, KEGG_ECM_RECEPTOR_INTERACTION and KEGG_FOCAL_ADHESION) and cancer signal transduction pathways (i.e., KEGG_BASAL_CELL_CARCINOMA, KEGG_MELANOGENESIS and KEGG_HEDGEHOG_SIGNALING).

Table 5.15. KEGG pathways associated with Clone 9.

Name	Normalised Enrichment Score (NES)	NOM.p.val
KEGG_COMPLEMENT_AND_COAGULATION_CASCADES	1.8473225	0
KEGG_BASAL_CELL_CARCINOMA	1.7862694	0
KEGG_MELANOGENESIS	1.7393768	0
KEGG_AXON_GUIDANCE	1.6028252	0.001988072
KEGG_GLYCOSAMINOGLYCAN_DEGRADATION	1.5991979	0.018416205
KEGG_SYSTEMIC_LUPUS_ERYTHEMATOSUS	1.5635294	0.025540275
KEGG_HEDGEHOG_SIGNALING_PATHWAY	1.4705548	0.046153847
KEGG_CELL_ADHESION_MOLECULES_CAMS	1.4610238	0.0295858
KEGG_CYTOKINE_CYTOKINE_RECEPTOR_INTERACTION	1.4229332	0.015841585
KEGG_CALCIUM_SIGNALING_PATHWAY	1.4203799	0.0227704
KEGG_ECM_RECEPTOR_INTERACTION	1.3992882	0.044025157
KEGG_FOCAL_ADHESION	1.3040253	0.03508772

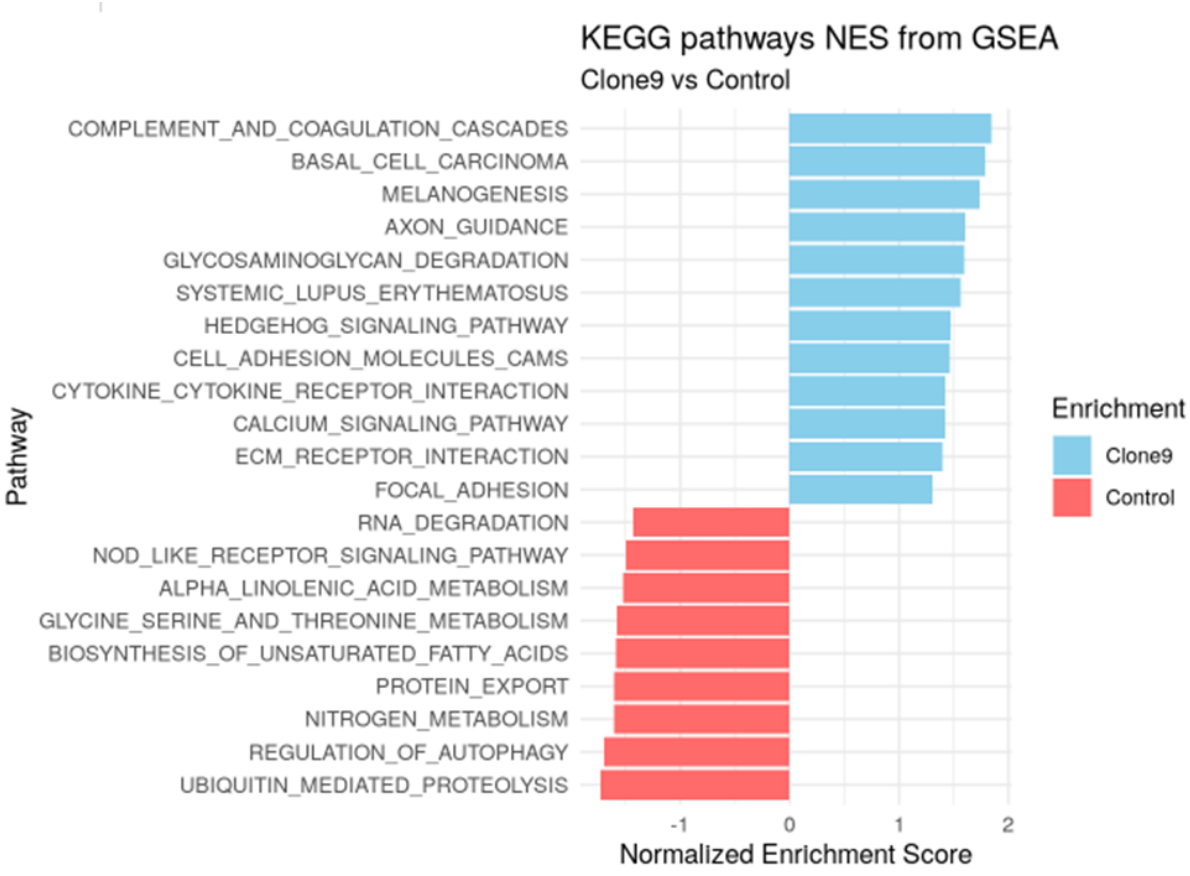

Figure 5.16. Enriched KEGG pathways plot for both Clone 9 and Control according to NES.

Image created by Barry Digby.

Table 5.16. KEGG pathways associated with Control.

Name	Normalised Enrichment Score (NES)	NOM.p.val
KEGG_UBIQUITIN_MEDIATED_PROTEOLYSIS	-1.7308584	0
KEGG_REGULATION_OF_AUTOPHAGY	-1.6981469	0.01629328
KEGG_NITROGEN_METABOLISM	-1.6069914	0.027896997
KEGG_PROTEIN_EXPORT	-1.6056662	0.01268499
KEGG_BIOSYNTHESIS_OF_UNSATURATED_FATTY_ACIDS	-1.5876603	0.027559055
KEGG_GLYCINE_SERINE_AND_THREONINE_METABOLISM	-1.5757413	0.03448276
KEGG_ALPHA_LINOLENIC_ACID_METABOLISM	-1.5206926	0.04742268
KEGG_NOD_LIKE_RECEPTOR_SIGNALING_PATHWAY	-1.4949745	0.021611001
KEGG_RNA_DEGRADATION	-1.426167	0.047058824

5.2.3.2.3 KEGG in Clone 1 *vs.* Clone 9

KEGG analysis of Clone 1 *vs.* Clone 9 identified 12 pathways that were significantly enriched for Clone 1 (Table 5.17, Figure 5.17) and 29 pathways for Clone 9 (Table 5.18, Figure 5.17). The majority of Clone 1 KEGG pathways were associated with calcium homeostasis and signalling (i.e., KEGG_ HCM, KEGG_TASTE_TRANSDUCTION, KEGG_DILATED_CARDIOMYOPATHY, KEGG_LONG_TERM_POTENTIATION, KEGG_LONG_TERM_DEPRESSION and KEGG_CALCIUM_SIGNALING) as well as other cancer signal transduction pathways (i.e., KEGG_TGF_BETA_SIGNALING, KEGG_MAPK_SIGNALING) and cell coordination (i.e., KEGG_NEUROACTIVE_LIGAND_RECEPTOR_INTERACTION and KEGG_AXON_GUIDANCE).

Table 5.17. KEGG pathways associated with Clone 1.

Name	Normalised Enrichment Score (NES)	NOM.p.val
KEGG_NEUROACTIVE_LIGAND_RECEPTOR_INTERACTION	2.044234	0
KEGG_HYPERTROPHIC_CARDIOMYOPATHY_HCM	1.8545351	0.00140056
KEGG_TGF_BETA_SIGNALING_PATHWAY	1.6945947	0.002688172
KEGG_CELL_CYCLE	1.6161737	0
KEGG_MATURITY_ONSET_DIABETES_OF_THE_YOUNG	1.5446388	0.034653466
KEGG_TASTE_TRANSDUCTION	1.5256346	0.03851852
KEGG_DILATED_CARDIOMYOPATHY	1.5037297	0.013642564
KEGG_DNA_REPLICATION	1.4748116	0.03003003
KEGG_LONG_TERM_POTENTIATION	1.4591323	0.034188036
KEGG_LONG_TERM_DEPRESSION	1.4501323	0.039017342
KEGG_CALCIUM_SIGNALING_PATHWAY	1.434515	0.02457956
KEGG_AXON_GUIDANCE	1.3973556	0.019132653

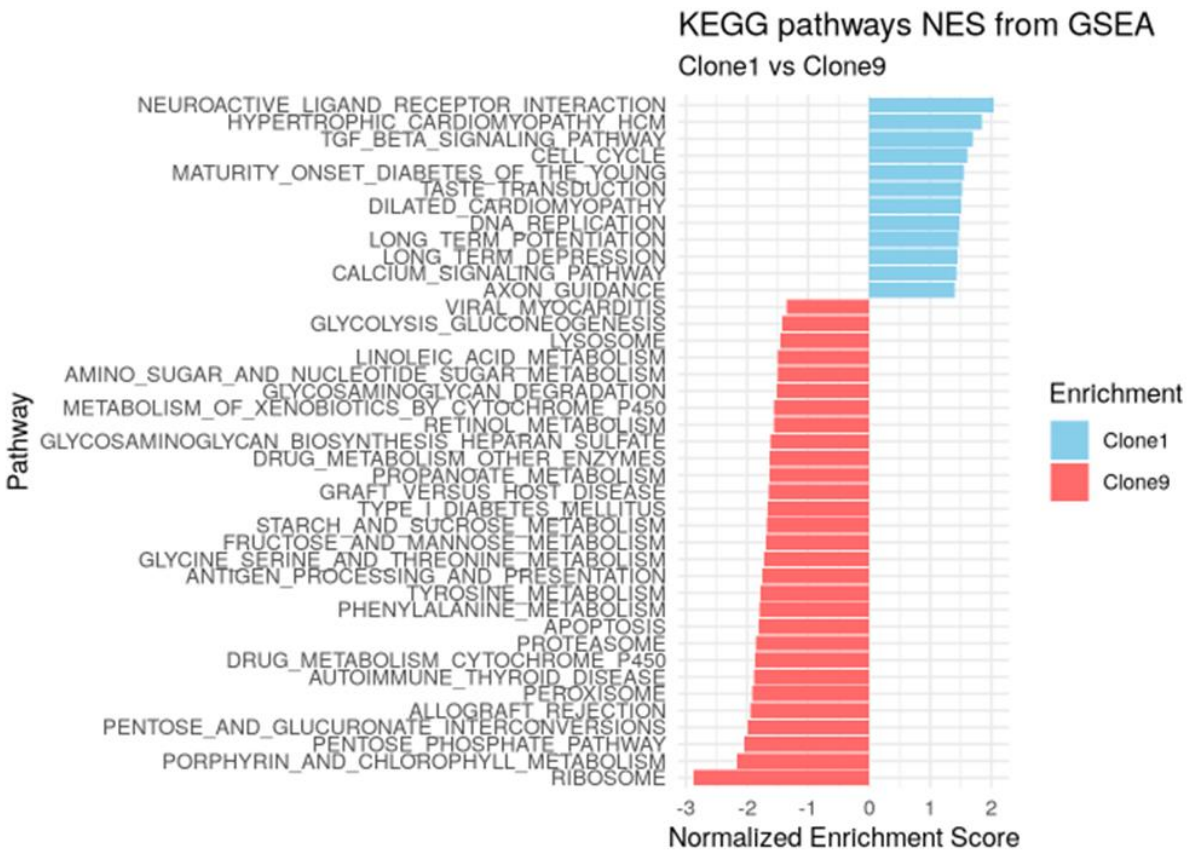

Figure 5.17. Enriched KEGG pathways plot for both Clone 1 and Clone 9 according to NES.

Image created by Barry Digby.

Table 5.18. KEGG pathways associated with Clone 9.

Name	Normalised Enrichment Score (NES)	NOM.p.val
KEGG_RIBOSOME	-2.8810968	0
KEGG_PORPHYRIN_AND_CHLOROPHYLL_METABOLISM	-2.1584315	0
KEGG_PENTOSE_PHOSPHATE_PATHWAY	-2.047728	0
KEGG_PENTOSE_AND_GLUCURONATE_INTERCONVERSIONS	-1.9856925	0.002617801
KEGG_ALLOGRAFT_REJECTION	-1.9493806	0
KEGG_PEROXISOME	-1.9168677	0
KEGG_AUTOIMMUNE_THYROID_DISEASE	-1.8886505	0.002702703
KEGG_DRUG_METABOLISM_CYTOCHROME_P450	-1.8680905	0
KEGG_PROTEASOME	-1.8533373	0.00310559
KEGG_APOPTOSIS	-1.8143264	0
KEGG_PHENYLALANINE_METABOLISM	-1.7966727	0.007751938
KEGG_TYROSINE_METABOLISM	-1.7862295	0.002762431
KEGG_ANTIGEN_PROCESSING_AND_PRESENTATION	-1.7557894	0.003401361
KEGG_GLYCINE_SERINE_AND_THREONINE_METABOLISM	-1.7289603	0.008426966
KEGG_FRUCTOSE_AND_MANNOSE_METABOLISM	-1.6880517	0.00308642
KEGG_STARCH_AND_SUCROSE_METABOLISM	-1.6788396	0.005970149
KEGG_TYPE_I_DIABETES_MELLITUS	-1.6626157	0.016620498
KEGG_GRAFT_VERSUS_HOST_DISEASE	-1.6516978	0.022959184
KEGG_PROPANOATE_METABOLISM	-1.6364313	0.008474576
KEGG_DRUG_METABOLISM_OTHER_ENZYMES	-1.6349679	0.017964073
KEGG_GLYCOSAMINOGLYCAN_BIOSYNTHESIS_HEPARAN_SULFATE	-1.6167312	0.024523161
KEGG_RETINOL_METABOLISM	-1.5591038	0.023809524
KEGG_METABOLISM_OF_XENOBIOTICS_BY_CYTOCHROME_P450	-1.5555222	0
KEGG_GLYCOSAMINOGLYCAN_DEGRADATION	-1.5145516	0.046961326
KEGG_AMINO_SUGAR_AND_NUCLEOTIDE_SUGAR_METABOLISM	-1.5034186	0.02507837
KEGG_LINOLEIC_ACID_METABOLISM	-1.4976913	0.042713568
KEGG_LYSOSOME	-1.459626	0.004694836
KEGG_GLYCOLYSIS_GLUCONEOGENESIS	-1.4295211	0.044217687
KEGG_VIRAL_MYOCARDITIS	-1.3562151	0.045454547

5.2.3.3 Integrative Analysis of Gene Networks by Gene Ontology (GO) classifications

In order to identify enriched biological themes within the dataset, the computationally derived lists of genes dysregulated in the isogenic cell lines were examined by Gene Ontology (GO) classifications.

5.2.3.3.1 GO biological process in Clone 1 *vs.* Control

GO Biological Process describe larger processes, or 'biological programs' accomplished by multiple molecular activities. Examples of broad biological process terms are DNA repair or signal transduction.

GO Biological Process enrichment of Clone 1 *vs.* Control identified 621 *'terms'* that were significantly enriched for Clone 1 and 228 terms for Control. The biological process enriched for Clone 1 were broadly associated with signal transduction. The top 10 GO biological process associated with Clone 1 are listed in Table 5.19. Whereas the biological process enriched for Control were broadly associated with metabolic processes. The top 10 GO biological process associated with Control are listed in Table 5.20.

Table 5.19. Top 10 GO biological process associated with Clone 1.

Name	**Normalised Enrichment Score (NES)**	**NOM.p.val**
GO_NEUROTRANSMITTER_SECRETION	2.2613125	0
GO_REGULATION_OF_POSTSYNAPTIC_MEMBRANE_POTENTIAL	2.2597485	0
GO_GLUTAMATE_RECEPTOR_SIGNALING_PATHWAY	2.2373962	0
GO_SYNAPTIC_TRANSMISSION_GLUTAMATERGIC	2.2147057	0
GO_STARTLE_RESPONSE	2.1895418	0
GO_NEUROMUSCULAR_SYNAPTIC_TRANSMISSION	2.1643927	0
GO_VESICLE_MEDIATED_TRANSPORT_IN_SYNAPSE	2.1391413	0
GO_CELLULAR_RESPONSE_TO_CALCIUM_ION	2.1267343	0
GO_SYNAPTIC_VESICLE_LOCALIZATION	2.1205022	0
GO_REGULATION_OF_SYNAPSE_ASSEMBLY	2.1004996	0

Table 5.20. Top 10 GO biological process associated with Control.

Name	Normalised Enrichment Score (NES)	NOM.p. val
GO_COTRANSLATIONAL_PROTEIN_TARGETING_TO_MEMBRANE	-2.5626125	0
GO_CYTOPLASMIC_TRANSLATION	-2.459897	0
GO_ESTABLISHMENT_OF_PROTEIN_LOCALIZATION_TO_ENDOPLASMIC_RETICULUM	-2.4532323	0
GO_TRANSLATIONAL_INITIATION	-2.4304352	0
GO_SERINE_FAMILY_AMINO_ACID_METABOLIC_PROCESS	-2.4229891	0
GO_NUCLEAR_TRANSCRIBED_MRNA_CATABOLIC_PROCESS_NONSENSE_MEDIATED_DECAY	-2.2042985	0
GO_SERINE_FAMILY_AMINO_ACID_BIOSYNTHETIC_PROCESS	-2.203702	0
GO_L_SERINE_METABOLIC_PROCESS	-2.1370127	0
GO_PROTEIN_LOCALIZATION_TO_ENDOPLASMIC_RETICULUM	-2.1281812	0
GO_CYTOPLASMIC_TRANSLATIONAL_INITIATION	-2.0454428	0

5.2.3.3.2 GO biological process in Clone 9 *vs.* Control

GO Biological Process enrichment of Clone 9 *vs.* Control identified 417 *'terms'* that were significantly enriched for Clone 9 and 102 *'terms'* for Control. Top 10 GO biological process associated with Clone 9 broadly related to signal transduction, and Control were broadly related with metabolic processes as listed on Table 5.21 and Table 5.22, respectively.

Table 5.21. Top 10 GO biological process associated with Clone 9.

Name	Normalised Enrichment Score (NES)	NOM.p.val
GO_ENTEROENDOCRINE_CELL_DIFFERENTIATION	2.162511	0.001897533
GO_GLANDULAR_EPITHELIAL_CELL_DIFFERENTIATION	2.0826008	0
GO_SYNAPTIC_TRANSMISSION_GABAERGIC	2.072216	0
GO_TYPE_B_PANCREATIC_CELL_DEVELOPMENT	2.0456526	0
GO_METANEPHRIC_NEPHRON_DEVELOPMENT	2.0446446	0
GO_GLANDULAR_EPITHELIAL_CELL_DEVELOPMENT	1.9377226	0.001930502
GO_CIRCADIAN_SLEEP_WAKE_CYCLE	1.926538	0
GO_REGULATION_OF_SYNAPTIC_TRANSMISSION_GABAERGIC	1.9151865	0
GO_SYNAPTIC_VESICLE_CLUSTERING	1.9041928	0
GO_REGULATION_OF_CELLULAR_RESPONSE_TO_VASCULAR_ENDOTHELIAL_GROWTH_FACTOR_STIMULUS	1.9036803	0

Table 5.22. Top 10 GO biological process associated with Control.

Name	Normalised Enrichment Score (NES)	NOM .p.val
GO_CELLULAR_RESPONSE_TO_STARVATION	-1.9652334	0
GO_POSITIVE_REGULATION_OF_TRANSCRIPTION_FROM_RNA_POLYMERASE_II_PROMOTER_INVOLVED_IN_CELLULAR_RESPONSE_TO_CHEMICAL_STIMULUS	-1.9472595	0.002016
GO_ALPHA_LINOLENIC_ACID_METABOLIC_PROCESS	-1.8182136	0.001964
GO_MATING_BEHAVIOR	-1.8139457	0.008368
GO_MRNA_METHYLATION	-1.8082647	0.007797
GO_RESPONSE_TO_STARVATION	-1.8022239	0
GO_BRANCHED_CHAIN_AMINO_ACID_METABOLIC_PROCESS	-1.7934711	0.005928
GO_ENDOSOME_TO_PLASMA_MEMBRANE_PROTEIN_TRANSPORT	-1.7865623	0.005893
GO_CYTOPLASMIC_TRANSLATIONAL_INITIATION	-1.7763095	0.004081
GO_CARDIAC_LEFT_VENTRICLE_MORPHOGENESIS	-1.7726148	0.004065

5.2.3.3.3 GO biological process in Clone 1 *vs.* Clone 9

GO Biological Process enrichment of Clone 1 *vs.* Clone 9 identified 460 *'terms'* that were significantly enriched for Clone 1 and 258 terms for Clone 9. Top 10 GO biological process associated with Clone 1 were largely related with signal transduction and Clone 9 were largely related with protein translation as listed in Table 5.23 and Table 5.24, respectively.

Table 5.23. Top 10 GO biological process associated with Clone 1.

Name	Normalised Enrichment Score (NES)	NOM.p.val
GO_NEUROMUSCULAR_SYNAPTIC_TRANSMISSION	2.3338258	0
GO_REGULATION_OF_POSTSYNAPTIC_MEMBRANE_POTENTIAL	2.280913	0
GO_SYNAPTIC_TRANSMISSION_GLUTAMATERGIC	2.1426601	0
GO_NEUROTRANSMITTER_SECRETION	2.1417553	0
GO_GLUTAMATE_RECEPTOR_SIGNALING_PATHWAY	2.1211474	0
GO_STARTLE_RESPONSE	2.0995364	0
GO_CHEMICAL_SYNAPTIC_TRANSMISSION_POSTSYNAPTIC	2.0944338	0
GO_NEUROTRANSMITTER_TRANSPORT	2.064192	0
GO_HOMOPHILIC_CELL_ADHESION_VIA_PLASMA_MEMBRANE_ADHESION_MOLECULES	2.0190928	0
GO_IONOTROPIC_GLUTAMATE_RECEPTOR_SIGNALING_PATHWAY	2.0156271	0

Table 5.24. Top 10 GO biological process associated with Clone 9.

Name	Normalised Enrichment Score (NES)	NOM.p.val
GO_COTRANSLATIONAL_PROTEIN_TARGETING_TO_MEMBRANE	-2.686811	0
GO_ESTABLISHMENT_OF_PROTEIN_LOCALIZATION_TO_ENDOPLASMIC_RETICULUM	-2.4537783	0
GO_TRANSLATIONAL_INITIATION	-2.2959065	0
GO_URONIC_ACID_METABOLIC_PROCESS	-2.1917844	0
GO_ANTIGEN_PROCESSING_AND_PRESENTATION_OF_ENDOGENOUS_ANTIGEN	-2.1823068	0
GO_CYTOPLASMIC_TRANSLATION	-2.169783	0
GO_MITOCHONDRIAL_TRANSLATIONAL_TERMINATION	-2.1679337	0
GO_NUCLEAR_TRANSCRIBED_MRNA_CATABOLIC_PROCESS_NONSENSE_MEDIATED_DECAY	-2.1236372	0
GO_PROTEIN_LOCALIZATION_TO_ENDOPLASMIC_RETICULUM	-2.1138113	0
GO_TRANSLATIONAL_TERMINATION	-2.110328	0

5.2.3.3.4 GO molecular function in Clone 1 *vs.* Control

Molecular-level activities are performed by gene products. Molecular function *'terms'* describe activities that occur at the molecular level, such as "catalysis" or "transport". GO molecular function terms represent activities rather than the entities (molecules or complexes) that perform the actions, and do not specify where, when, or in what context the action takes place. Molecular functions generally correspond to activities that can be performed by individual gene products (i.e. a protein or RNA), but some activities are

performed by molecular complexes composed of multiple gene products. GO molecular function enrichment of Clone 1 *vs.* Control identified 108 *'terms'* that were significantly enriched for Clone 1 and 45 *'terms'* for Control. The top 10 GO molecular function associated with Clone 1 were broadly related with signal transduction, and in Control were broadly related with metabolic processes as listed on Table 5.25 and Table 5.26, respectively.

Table 5.25. Top 10 GO molecular function associated with Clone 1.

Name	**Normalised Enrichment Score (NES)**	**NOM. p.val**
GO_POSTSYNAPTIC_NEUROTRANSMITTER_RECEPTOR_ACTIVITY	2.4377992	0
GO_TRANSMITTER_GATED_CHANNEL_ACTIVITY	2.3398015	0
GO_EXTRACELLULAR_LIGAND_GATED_ION_CHANNEL_ACTIVITY	2.3324316	0
GO_NEUROTRANSMITTER_RECEPTOR_ACTIVITY	2.3128905	0
GO_GLUTAMATE_RECEPTOR_ACTIVITY	2.3025975	0
GO_NEUROTRANSMITTER_RECEPTOR_ACTIVITY_INVOLVED_IN_REGULATION_OF_POSTSYNAPTIC_MEMBRANE_POTENTIAL	2.2969942	0
GO_VOLTAGE_GATED_CATION_CHANNEL_ACTIVITY	2.2263775	0
GO_GATED_CHANNEL_ACTIVITY	2.1813748	0
GO_VOLTAGE_GATED_POTASSIUM_CHANNEL_ACTIVITY	2.1794386	0
GO_VOLTAGE_GATED_ION_CHANNEL_ACTIVITY	2.1438212	0

Table 5.26. Top 10 GO molecular function associated with Control.

Name	**Normalised Enrichment Score (NES)**	**NOM.p.val**
GO_STRUCTURAL_CONSTITUENT_OF_RIBOSOME	-2.6302006	0
GO_COENZYME_BINDING	-1.8721524	0
GO_ACTININ_BINDING	-1.8334183	0.005434783
GO_TRANSLATION_FACTOR_ACTIVITY_RNA_BINDING	-1.8205868	0
GO_OXIDOREDUCTASE_ACTIVITY_ACTING_ON_A_SULFUR_GROUP_OF_DONORS_NAD_P_AS_ACCEPTOR	-1.8103175	0.012562814
GO_SUGAR_TRANSMEMBRANE_TRANSPORTER_ACTIVITY	-1.8001765	0.007281554
GO_TRANSLATION_INITIATION_FACTOR_ACTIVITY	-1.7657048	0
GO_DEAMINASE_ACTIVITY	-1.7564671	0.00954654
GO_LIGASE_ACTIVITY_FORMING_CARBON_NITROGEN_BONDS	-1.7246658	0.006329114
GO_CARBOXYLIC_ESTER_HYDROLASE_ACTIVITY	-1.713199	0

5.2.3.3.5 GO molecular function in Clone 9 *vs.* Control

GO molecular function enrichment of Clone 9 *vs.* Control identified 61 *'terms'* that were significantly enriched for Clone 9 and 24 *'terms'* for Control. The top 10 GO molecular function associated with Clone 9 were broadly related to molecular transport and protein translation, and in Control, these were broadly similar to Clone 9, as listed in Table 5.27 and Table 5.28, respectively.

Table 5.27. Top 10 GO molecular function associated with Clone 9.

Name	**Normalised Enrichment Score (NES)**	**NOM.p.val**
GO_SULFOTRANSFERASE_ACTIVITY	1.9960977	0
GO_G_PROTEIN_BETA_GAMMA_SUBUNIT_COMPLEX_BINDING	1.8512435	0
GO_CARGO_RECEPTOR_ACTIVITY	1.8335103	0.001988072
GO_AMYLOID_BETA_BINDING	1.7631936	0.001964637
GO_SCAVENGER_RECEPTOR_ACTIVITY	1.7446837	0.005905512
GO_CYCLASE_ACTIVITY	1.7409111	0.00952381
GO_EXTRACELLULAR_MATRIX_STRUCTURAL_CONSTITUENT	1.72654	0.001945525
GO_ALDO_KETO_REDUCTASE_NADP_ACTIVITY	1.7254549	0.009363296
GO_NEUROTRANSMITTER_SODIUM_SYMPORTER_ACTIVITY	1.7162696	0.005586592
GO_PEPTIDE_RECEPTOR_ACTIVITY	1.7093205	0.003929273

Table 5.28. Top 10 GO molecular function associated with Control.

Name	**Normalised Enrichment Score (NES)**	**NOM.p.val**
GO_PHOSPHATIDYLINOSITOL_MONOPHOSPHATE_PHOSPHATASE_ACTIVITY	-1.8449166	0.002053388
GO_OLIGOSACCHARYL_TRANSFERASE_ACTIVITY	-1.8135864	0.00407332
GO_RIBOSOME_BINDING	-1.7788503	0.001980198
GO_DYNEIN_HEAVY_CHAIN_BINDING	-1.7067794	0.006302521
GO_PRE_MRNA_INTRONIC_BINDING	-1.7007383	0.01171875
GO_L_AMINO_ACID_TRANSMEMBRANE_TRANSPORTER_ACTIVITY	-1.6994603	0.001992032
GO_METHYLATED_HISTONE_BINDING	-1.6539514	0.00210084
GO_RAN_GTPASE_BINDING	-1.6453956	0.007984032
GO_UBIQUITIN_LIKE_PROTEIN_CONJUGATING_ENZYME_BINDING	-1.6181333	0.001988072
GO_NEUTRAL_AMINO_ACID_TRANSMEMBRANE_TRANSPORTER_ACTIVITY	-1.5978385	0.018518519

5.2.3.3.6 GO molecular function in Clone 1 *vs.* Clone 9

GO molecular function enrichment of Clone 1 *vs.* Clone 9 identified 61 *'terms'* that were significantly enriched for Clone 1 and 24 *'terms'* for Clone 9. The top 10 GO molecular function associated with Clone 1 were broadly related with signal transduction, and in Clone 9 were broadly related with molecular transport and protein translation, as listed in Table 5.29 and Table 5.30, respectively.

Table 5.29. Top 10 GO molecular function associated with Clone 1.

Name	**Normalised Enrichment Score (NES)**	**NOM. p.val**
GO_TRANSMITTER_GATED_CHANNEL_ACTIVITY	2.4510996	0
GO_NEUROTRANSMITTER_RECEPTOR_ACTIVITY_INVOLVED_IN_REGULATION_OF_POSTSYNAPTIC_MEMBRANE_POTENTIAL	2.4056387	0
GO_POSTSYNAPTIC_NEUROTRANSMITTER_RECEPTOR_ACTIVITY	2.398918	0
GO_EXTRACELLULAR_LIGAND_GATED_ION_CHANNEL_ACTIVITY	2.3577325	0
GO_NEUROTRANSMITTER_RECEPTOR_ACTIVITY	2.332242	0
GO_EXCITATORY_EXTRACELLULAR_LIGAND_GATED_ION_CHANNEL_ACTIVITY	2.1747954	0
GO_GLUTAMATE_RECEPTOR_ACTIVITY	2.1449094	0
GO_LIGAND_GATED_ION_CHANNEL_ACTIVITY	2.114721	0
GO_GATED_CHANNEL_ACTIVITY	2.0973275	0
GO_ACETYLCHOLINE_RECEPTOR_ACTIVITY	2.091744	0

Table 5.30. Top 10 GO molecular function associated with Clone 9.

Name	**Normalised Enrichment Score (NES)**	**NOM.p.val**
GO_STRUCTURAL_CONSTITUENT_OF_RIBOSOME	-2.687951	0
GO_ANTIOXIDANT_ACTIVITY	-2.15491	0
GO_OXIDOREDUCTASE_ACTIVITY_ACTING_ON_PEROXIDE_AS_ACCEPTOR	-2.073979	0
GO_FAD_BINDING	-2.0352685	0
GO_COENZYME_BINDING	-2.0183895	0
GO_SUGAR_TRANSMEMBRANE_TRANSPORTER_ACTIVITY	-1.9402193	0.00255102
GO_CARBOXYLIC_ESTER_HYDROLASE_ACTIVITY	-1.9340633	0
GO_COFACTOR_BINDING	-1.9140542	0
GO_MOLECULAR_CARRIER_ACTIVITY	-1.910678	0.005154639
GO_VITAMIN_B6_BINDING	-1.8962508	0

5.3 Discussion

Enzalutamide has been proven to clinically benefit men with PCa (115). However, the response can be temporary and improvement in OS modest, suggestive of rapid development of treatment resistance in some men (90). Although previous studies have identified a number of mechanisms that may be involved in the development of enzalutamide resistance, the exact mechanisms are still poorly understood (423). The advent of NGS has not only broadened the understanding of genomic and transcriptomic architecture of PCa but allowed further means to evaluate the underlying mechanism of drug resistance and disease progression (222). Thus, providing opportunities for novel biomarker and therapeutic discovery. This study aimed to examine the transcriptomic landscape of enzalutamide resistant PCa *in vitro* in order to understand the disease biology in concert with the effort of elucidating the mechanisms involved in the development of enzalutamide resistance.

This study evaluated RNA-Seq data generated from an enzalutamide resistant cell line panel. A large number of DEGs were identified between Clone 1 *vs.* Control (2,584 up-regulated genes and 1,825 down-regulated genes), while less were observed between Clone 9 *vs.* Control (395 up-regulated genes and 329 down-regulated genes). This suggested that Clone 1, the highly resistant clone, was phenotypically very different compared to the Control cell line and the dysregulated genes may be investigated further to identify a clinical signature that could be used as biomarker to inform drug resistance or as a potential for therapeutic targets. A literature search was undertaken to examine the top 10 highest up-regulated and down-regulated genes according to FC in Clone 1 *vs.* Control to evaluate their association with PCa. Two of the highly expressed genes, *CNTN1* and *PCDH10* were previously described in PCa studies. Yan *et al.* demonstrated that *CNTN1* was overexpressed in both androgen independent cell lines, DU145 and PC-3 cell-derived PCa stem-like cells, where it enhanced cell invasion through *AKT* activation and E-cadherin down-regulation (403), which is part of the key features of EMT. Apart from loss of E-cadherin, increased cell adhesion molecules (CAM) principally immunoglobulins-like CAMs (contactins, neural CAM (NCAM), L1CAMs, CAM L1-like (CHL1), neuronal CAM (NrCAM), and neurofascin (NFASC)) plays a vital role in EMT related cancer progression and metastasis (424, 425). In this present study, Contactins, L1CAMS, CHL1, NrCAM and NFASC were up-regulated in Clone 1 *vs.* Control, thus further supporting the role of EMT in

enzalutamide resistance. CNTN1 is a neural cell adhesion protein that plays an essential role in the development of the central nervous system, lineage differentiation, axonal elongation and formation of neuromuscular junction (426-429). *PCDH10*, the other highly expressed gene in Clone 1 *vs.* Control was previously reported to be frequently hypermethylated in the serum of people with PCa and was significantly associated with aggressive disease such as higher Gleason score, lymph node metastasis and advanced clinical stage (404). Elevated PCDH10 expression in the strongly enzalutamide resistant clone compared to drug sensitive cells (used in this study) was in contrast to the traditional view where DNA methylation is accompanied by suppression of gene expression (430, 431). This may be explained by a recent study that showed a strong association between DNA hypermethylation and concurrent gene overexpression in PCa (430).

Two of the highly down-regulated genes in Clone 1 *vs.* Control, Transient Receptor Potential Cation Channel Subfamily M member 8 (*TRPM8*) and Leucine Rich Repeat Transmembrane Neuronal 3 (*LRRTM3*) were previously described in PCa studies (397, 406). Numerous studies in the literature have implicated that alterations in Ca2+ homeostasis are involved in PCa development and metastasis (432, 433). Transient Receptor Potential (TRP) ion channel superfamily are involved in all the hallmarks of cancer, while their expression levels are associated with the development and progression of many epithelial cancers (434, 435). The alteration of TRP expression affects intracellular Ca2+ concentrations and, consequently, processes involved in carcinogenesis, such as proliferation, migration and apoptosis (436). TRPM8 is a non-selective calcium permeable ion channel that is involved in calcium homeostasis directly (406) and can be regulated by androgens or the AR (437). Studies have demonstrated that TRPM8 has a dual role in PCa depending on the androgen sensitivity status (406). Overexpression of TRPM8 has an anti-proliferative effect in androgen independent PCa cells (PC3 and DU-145), but a pro-proliferative effect in androgen dependent PCa cells (LNCaP) (406). Furthermore, studies have also shown that TRPM8 loss of expression was positively correlated with aggressive androgen-independent PCa and the use of TRPM8 blocker exerted anti-proliferative, anti-migratory and anti-apoptotic effects in PCa cells (406). Multiple mechanisms of enzalutamide resistance have been defined, however, studies in the literature on the involvement of calcium homeostasis in enzalutamide resistance are scarce (438). Another highly down-regulated gene in Clone 1, *LRRTM3* was supressed in LNCaP cells treated with

androgen therapy, however, LRRTM3 depletion was shown to have no effect on Androgen independent growth (405).

The hallmarks GSEA condense information across multiple gene sets by highlighting genes that display coordinate expression and denote well-defined biological processes, hence decreasing discrepancy and redundancy resulting in a superior defined biological space for GSEA analysis. Hallmarks enrichment analysis of DEGs in Clone 1 *vs.* Control revealed eight distinct pathways. Interestingly, EMT was one of the hallmark pathways enriched along with other two pathways, which was reported to be closely related to EMT, known as TGF-β signalling and apical junctions. The EMTome serves as a platform and resource to interrogate EMT-signatures across tumour sub-types (439). The EMTome study, identified 314 genes with significant frequency in the literature as being correlated with EMT and performed cancer hallmark enrichment analysis showing that these genes were enriched in *'terms'* related to EMT, angiogenesis, TGF-β signalling pathway and apical junctions (439). Furthermore, DEG analysis for KEGG showed that the DEGs in Clone 1 *vs.* Control were enriched for *'terms'* broadly related to morphological changes since alteration in cell adhesion, cell to cell contact and mobility was involved. This was represented by *'terms'* such as neuroactive ligand receptor interaction, cytokine receptor interaction, axon guidance and regulation of actin cytoskeleton. Additionally, several signalling pathways were identified such as TGF-β pathway and MAP Kinase pathway, which has been described to regulate and mediate EMT previously (440). Additionally, a number of enriched KEGG *'terms'* were broadly related to calcium homeostasis and signalling such as hypertrophic cardiomyopathy, dilated cardiomyopathy, calcium signalling, long term depression and taste transduction. A recent study by O'Reilly and colleagues demonstrated that increased in store-operated calcium entry through voltage gated calcium channels CaV1.3 promoted resistance to bicalutamide in PCa (441). Thus, calcium homeostasis and signalling may be involved in the development of enzalutamide resistant PCa.

The top 10 GO biological process for Clone 1 *vs.* Control were broadly related to cellular processes involving cell communication (neurotransmitter secretion, glutamate receptor signalling, synaptic transmission glutamatergic and neuromuscular synaptic transmission), cellular component organisation, localisation and response to stimulus (regulation of synapse assembly, synaptic vesicle localisation and cellular response to calcium ion) supporting the role of EMT in enzalutamide resistance. Moreover, the top 10

GO molecular process for Clone 1 *vs.* Control were largely related to molecular transducer activity (neurotransmitter receptor activity, postsynaptic neurotransmitter receptor activity, neurotransmitter receptor activity involved in regulation of postsynaptic membrane potential and glutamate receptor activity) and transporter activity (gated channel activity, transmitter gated channel activity, extracellular ligand gated ion channel activity, voltage gated cation channel activity, voltage gated potassium channel activity and voltage gated ion channel activity). The GO molecular transducer activity further suggested that EMT plays a role in the development of enzalutamide resistance in PCa. It is worth noting that the enrichment in transporter activity raised the notion of the possible importance of membrane transporters in enzalutamide resistance. Overexpression of the ATP binding cassette (ABC) transporter superfamily has been well recognised as a reason of multi drug resistance in cancer cells, whereby the chemotherapeutics can be exported out of the cell (442). However, the down-regulation of ABC transporters has also been shown to influence cellular phenotypes associated with differentiation, migration and invasion across tumour subtypes (443, 444). In this study, *ABCC11, ABCC2, ABCA10, ABCA5* and *ABCA3* were up-regulated in Clone 1 *vs.* control while *ABCC4, ABCA12, ABCA4, ABCC1, ABCD1* and *ABCA17P* were down-regulated.

In summary, GO enrichment analysis showed that the DEGs in Clone 1 *vs*. Control were enriched in the regulation of cell communication as well as transducer activity, and KEGG pathway analysis found that the DEGs were closely associated with cell adhesion, cell to cell contact and mobility. This suggests that EMT has an important role in development of enzalutamide resistance. This was further supported by hallmark gene set enrichment, which revealed EMT as one of the major pathways enriched. In addition, GO and KEGG enrichment analysis also showed that the DEGs in Clone 1 *vs*. Control were enriched in transporter activity and calcium signalling, respectively. Overall, this RNA-Seq study of the enzalutamide resistant panel highlighted several pathways that may provide more insight into the molecular mechanism of enzalutamide resistance PCa such as EMT, membrane transporter and Calcium homeostasis. Overall, this study represents an essential first step in understanding the dynamic changes to the transcriptomic nature of enzalutamide resistance PCa *in vitro*.

Chapter 6 - EMT and neuroendocrine differentiation in enzalutamide resistant PCa

6.0 Introduction

The role of the AR signalling axis has served as the foundation for the current understanding of the molecular mechanisms behind the progression of PCa. The progression of PCa to CRPC and subsequent drug resistance may involve the cross talk of the AR with other important signalling pathways (445). The EMT pathway is of particular interest in such cross talk as it has been shown to be a hallmark of metastatic cancer spread and there is evidence demonstrating the involvement of AR signalling pathways in the regulation of EMT (211). Furthermore, recent *in vitro* studies have implicated EMT in inducing PCa resistance to ADT and chemotherapy (446, 447). For instance, gene expression profiling of cabazitaxel resistant PCa cells showed alterations in the expression of EMT marker profiles specifically, the increased expression of mesenchymal markers and decreased expression of the epithelial markers compared to parental controls (446). In addition, Shiota *et al.* reported that Twist is up-regulated during ADT and enzalutamide treatment of PCa cell lines (447). Moreover, there is growing clinical evidence implicating EMT as a cellular mechanism conferring drug resistance and progression of metastases. For instance, Puhr *et al.* have shown that a docetaxel resistant PCa cell line acquired EMT, which was facilitated by reduced expression of miR-200c and miR-205 (448). Apart from the association of EMT with the AR signalling pathway, numerous circRNAs have also been implicated in the regulation of EMT in cancer, however, the mechanisms remain unclear (449). Studies have shown that circRNAs can regulate EMT by affecting EMT-related signalling pathways such as TGF-β and Wnt and certain circRNAs may directly control the expression of cell adhesion molecules and cytoskeletal proteins (449). Such deregulated circRNAs can act as either tumour suppressors or oncogenes to control cell proliferation, migration and metastasis (449).

Besides EMT, neuroendocrine prostate carcinoma (NEPCa) differentiation is an increasingly recognised mechanism of resistance to AR targeted therapy involving epithelial plasticity. These PCa cells show low to absent AR expression accompanied by expression of neuroendocrine features, which arise from divergent clonal evolution of CRPC adenocarcinoma cells because of selective pressure from ADT (450). NEPCa is histologically different from PCa, which is featured by the presence of small round blue neuroendocrine cells that do not secrete PSA, however, they may express neuroendocrine markers such as chromogranin A, synaptophysin, and neuron specific enolase (NSE) (451). Indeed the frequency of NEPCa has been rising steadily due to increased utilisation of more potent

ADTs, with one study showing at least 25% of PCa autopsies with signs of NEPCa (452). The mechanism and molecular transformation to this disease remain incompletely understood (450).

There are however limited studies evaluating the full spectrum of genomic alterations in enzalutamide resistant PCa cell lines and the relationship between EMT, NEPCa and drug resistance. Thus, identifying key signatures in EMT and/or NEPCa-activating signalling pathways in enzalutamide resistant PCa is vital to understanding the functional contribution of EMT and/or NEPCa to the development of enzalutamide failure.

6.1 Experimental aims

To this end, the hypothesis of this work was that unique EMT or NEPCa signatures might play an important role in enzalutamide resistant PCa. Thus, RNA-Seq analysis of the enzalutamide resistant isogenic cell lines to evaluate the transcriptomic landscape changes was performed as part of the effort to identify possible EMT and NEPCa signatures.

This study had the following aims:

1. Determine EMT expression in enzalutamide resistant PCa through the interrogation of RNA-Seq data
2. Validate the changes in gene expression for common EMT regulators
3. Assess the changes in common EMT regulators at the protein level
4. Determine a molecular signature of neuroendocrine expression in enzalutamide resistant PCa through the interrogation of RNA-Seq data
5. Validate the changes in gene expression for common neuroendocrine regulators

6.2. EMT gene expression profile from RNA-Seq of enzalutamide resistance panel

The EMT pathway was investigated further as it was significantly enriched in the Hallmark pathway and is associated with drug resistance. All 1184 EMT genes provided by dbEMT (http://www.dbemt.bioinfo-minzhao.org/download.cgi) (453) were downloaded. Next, differentially expressed genes in Clone 1 *vs.* Control, Clone 9 *vs.* Control and Clone 1 *vs.* Clone 9 that were present in the dbEMT list were selected. This returned a statistically significant set of genes involved in the EMT pathway (adjusted p-value < 0.05).

6.2.1 EMT gene expression profile in Clone 1 *vs.* Control

Of the 1184 EMT genes, there were 177 up-regulated and 118 down-regulated in Clone 1 *vs.* Control (Figure 6.0) and the top 10 up-regulated and down-regulated genes are listed in Table 6.0 and Table 6.1, respectively. A literature search was performed to evaluate the association of the top 10 up-regulated and down-regulated genes in relation to cancer as described in Table 6.0 and Table 6.1. All the top 10 up-regulated genes associated with EMT, were described in the literature as having a role as oncogenes in facilitating tumour migration and aggressiveness. Four out of the top 10 down-regulated genes associated with EMT were described as tumour suppressors, whereas the rest of the six genes were described as oncogenes in the literature.

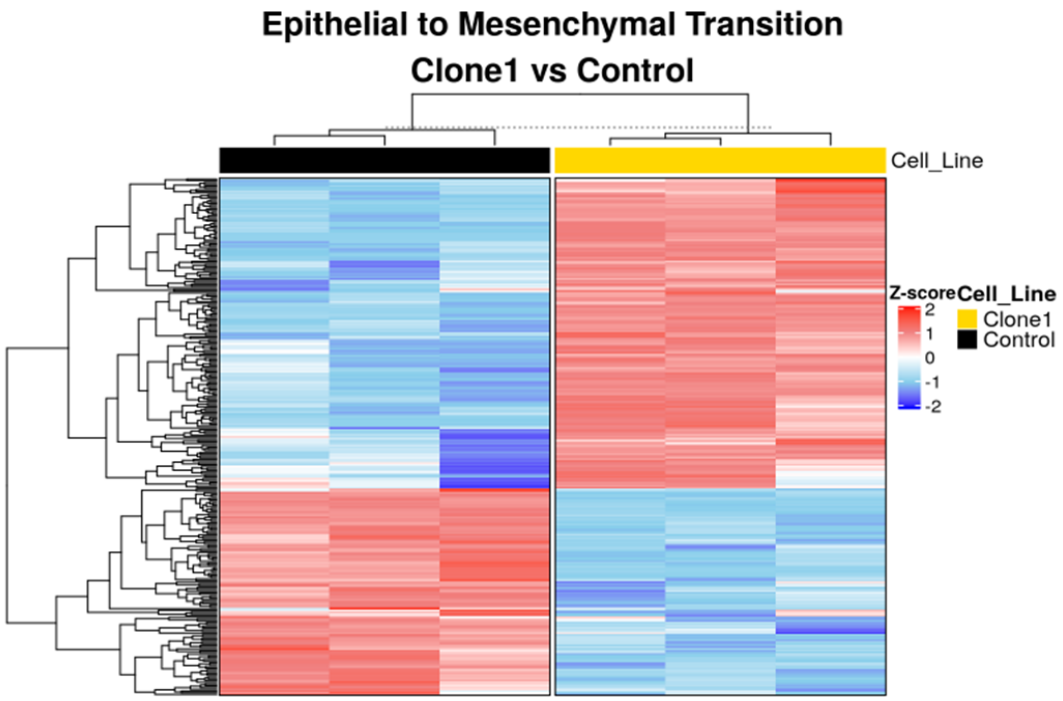

Figure 6.0. The heatmap of RNA-Seq in Clone 1 *vs.* Control. The heatmap shows the upregulation and down-regulation of genes related to EMT in Clone 1 *vs.* Control. Red indicated high expression, blue indicated low expression and white indicated no significant difference between Clone 1 *vs.* Control.

Image created by Barry Digby.

Table 6.0. Top 10 up-regulated EMT associated genes in Clone 1 *vs.* Control.

Gene	Description	Log2 FC	P-value	Functions
CNTN1	contactin 1	9.894	4.16E-12	Promotes tumour cell invasion, migration, and metastasis by inducing EMT through PIK3CA/AKT pathway as well as reducing e-cadherin, increasing n-cadherin and vimentin in PCa (403, 407).
HGF	hepatocyte growth factor	7.452	1.53E-37	The HGF/c-MET signalling pathway plays an important role to epithelial-stromal interactions in PCa, which is essential for invasive growth, metastasis and drug resistance (454).
BMP2	bone morphogenetic protein 2	7.295	4.97E-39	BMP2 increased CD44 expression, facilitated the development of tumour spheroids and amplified the population of CD44+/CD24− cells in MCF-7 breast cancer cells (455).
LGR5	leucine rich repeat containing G protein-coupled receptor 5	7.145	9.92E-09	LGR5 overexpression promoted cancer cell mobility and EMT in breast cancer cells through WNT/β-catenin signalling pathway (456). WNT pathway upregulation will increase β-catenin in the nucleus leading to increased expression of numerous genes, in particular Cyclin D1 (*CCND1*) which influences the G1 phase of the cell division cycle (457).
MGAT3	beta-1,4-mannosyl-glycoprotein 4-beta-N-acetylglucosaminyltransferase	7.006	1.39E-08	*MGAT3* suppression resulted in inhibition of the metastatic properties of lung cancer cell lines likely from regulation of EMT process (458).
PEG10	paternally expressed 10	6.821	6.43E-200	TGF-β1 up-regulates *PEG10* in hepatocellular carcinoma cells (HepG2) and promotes cell migration, invasion and EMT (459).
SOX5	SRY-box transcription factor 5	6.594	2.75E-07	*SOX5* expression increased concordantly with TGF-β-induced EMT in PCa cells (460). Knockdown of SOX5 expression mitigated the EMT process induced by TGF-β signalling and reduced cell migration ability in PCa cells (460). Additionally,

				SOX5 could bind to TWIST1 promoter and increase TWIST1 expression (460).
GRIN1	glutamate ionotropic receptor NMDA type subunit 1	6.511	2.44E-36	GRIN1 is part of the ionotropic glutamate receptors N-methyl-D-aspartate receptors (NMDARs). NMDARs consist of multiple protein subunit complexes that form plasma membrane ion channels allowing for transports of cations such as calcium, which is vital for synaptic communications, cellular migration and survival. It was shown that loss of complex formation between *GRIN1* and *GRIN2A* mutants augmented anchorage-independent growth and increased migration of melanoma cells (461).
SCUBE2	signal peptide, CUB domain and EGF like domain containing 2	6.365	2.25E-21	*SCUBE2* overexpression induced EMT and promoted triple negative breast cancer aggressiveness through notch signalling (462).
HPGD	15-hydroxyprostaglandin dehydrogenase	6.269	1.76E-79	*HPGD* was highly expressed in metastatic breast cancer cells and repression of the gene expression resulted in a decrease in TGF-β signalling mitigating EMT as well as in cell migration (463).

Table 6.1. Top 10 down-regulated EMT associated genes in Clone 1 *vs.* Control.

Gene	Description	Log2 FC	P-value	Functions
TRPM8	transient receptor potential cation channel subfamily M member 8	-8.586	4.83E-17	*TRPM8* has been shown to play a vital role in the regulation of cell migration where the activation suppressed PCa cell migration (464, 465). The loss of TRPM8 expression was also positively correlated with the transition to the androgen-independent aggressive stage of PCa (464).
CYP3A5	cytochrome P450 family 3 subfamily A member 5	-8.282	4.77E-08	CYP3A5 expression have important role in AR signalling as it facilitates AR nuclear translocation and downstream signalling inducing tumour growth however more importantly, its expression variation in tumour cells can be attributed to gene polymorphism which can produce truncated non-functional protein (466).
LCN2	lipocalin 2	-7.413	8.9E-06	*LCN2* down-regulation in PC3 and DU145 cells reduced cell proliferation, colony formation, migration, and invasion (467). Additionally, tumour

				growth was decreased in the *LCN2*-knockdown mice (467).
FGFR2	fibroblast growth factor receptor 2	-6.990	2.94E-06	*FGFR2* was identified as a tumour suppressor (468). FGFR2 could regulate HIF transcriptional activity through inhibition of p300 recruitment by HIF-1/2α hence resulted in a decrease of HIF transcriptional activity leading to a reduction in HIF-induced migration and invasion of PCa cells (469)
PPARG	peroxisome proliferator activated receptor gamma	-6.546	8.24E-08	*PPARG* has tumour suppressive role and PPARG agonists have shown anti-proliferative and pro-apoptotic effect in numerous cancers including PCa and have entered colorectal cancers clinical trials (470-473). PPARG agonists decreased AR levels and inhibited PCa cell growth (472).
JAG1	jagged canonical Notch ligand 1	-5.507	1.56E-28	*JAG1* overexpression correlated with PCa metastasis and recurrence (474). JAG1-mediated Notch activation promoted tumour cell motility by inducing EMT in breast cancer cells (475).
CAMK1D	calcium/calmodulin dependent protein kinase ID	-5.387	1.68E-06	*CAMK1D* overexpression in non-tumorigenic breast epithelial cells promoted molecular and phenotypic alterations suggestive of EMT featuring loss of cell-cell adhesions and increased cell migration and invasion (476).
SNAI2	snail family transcriptional repressor 2	-5.085	0.001078	*SNAI2* overexpression was related to poor prognosis in numerous tumour sub-types (477). *SNAI2* up-regulation has been shown to enhance proliferation, migration and invasiveness via EMT in PCa cells (478).
MSX2	msh homeobox 2	-5.051	1.92E-11	*MSX2* down-regulation was associated with poor prognosis in patients with oral squamous cell cancer and the expression level was inversely correlated with the *SOX2* in oral cancer cell lines (479). *MSX2* has a tumour suppression effect on the cancer stem cell phenotypes of oral squamous cell carcinoma likely via MSX2–SOX2 signalling pathway (479).
LRG1	leucine rich alpha-2-glycoprotein 1	-4.874	1.61E-18	*LRG1* was upregulated in aggressive colorectal cancer tissue where it can promote EMT process through HIF-1α activation hence increasing cell migration as well as invasion ability (480).

6.2.2 EMT gene expression profile in Clone 9 *vs.* Control

There were 29 up-regulated and 21 down-regulated EMT related genes in Clone 9 *vs.* Control (Figure 6.1) and the top 10 up-regulated and down-regulated genes are listed in Table 6.2 and Table 6.3, respectively.

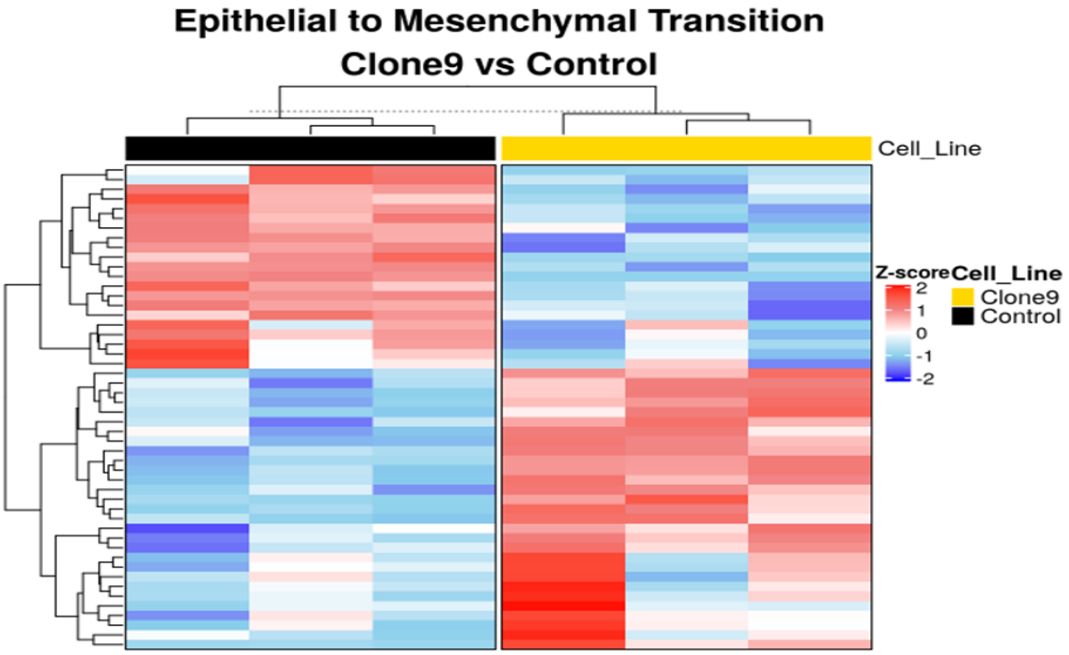

Figure 6.1. The heatmap of RNA-seq in Clone 9 *vs.* Control. The heatmap shows the upregulation and down-regulation of genes related to EMT in Clone 9 *vs.* Control. Red indicated high expression, blue indicated low expression and white indicated no significant difference between Clone 9 *vs.* Control.

Image created by Barry Digby.

Table 6.2. Top 10 up-regulated EMT associated genes in Clone 9 *vs.* Control.

Gene	Description	Log2FC	P-value
EPB41L3	erythrocyte membrane protein band 4.1 like 3	3.276041	0.000165
CAMK1D	calcium/calmodulin dependent protein kinase ID	2.498816	3.28E-08
HES1	hes family bHLH transcription factor 1	1.953345	2.75E-08
EHD2	EH domain containing 2	1.951967	0.001018
SPOCK1	SPARC (osteonectin), cwcv and kazal like domains proteoglycan 1	1.916381	1.69E-10
APBB1	amyloid beta precursor protein binding family B member 1	1.916095	6.42E-12
TNS1	tensin 1	1.913382	1.05E-08
CRYAB	crystallin alpha B	1.877286	3.58E-06

PDE4A	phosphodiesterase 4A	1.841744	9.46E-06
UCP2	uncoupling protein 2	1.834781	0.001592

Table 6.3. Top 10 down-regulated EMT associated genes in Clone 9 *vs.* Control.

Gene	Description	Log2FC	P-value
MAGEC2	MAGE family member C2	-7.63042	1.05E-07
ETV1	ETS variant transcription factor 1	-6.05531	4.65E-58
TRPM8	transient receptor potential cation channel subfamily M member 8	-3.01498	2.11E-15
AQP3	aquaporin 3 (Gill blood group)	-2.96177	3.38E-16
LRG1	leucine rich alpha-2-glycoprotein 1	-2.13766	7.95E-07
TNFSF15	TNF superfamily member 15	-1.7091	7.93E-08
NRP1	neuropilin 1	-1.53489	5.46E-09
MALAT1	metastasis associated lung adenocarcinoma transcript 1	-1.45801	2.57E-15
GLS2	glutaminase 2	-1.44155	4.49E-06
SMAD9	SMAD family member 9	-1.36362	6.10E-09

6.2.3 EMT gene expression profile in Clone 1 *vs.* Clone 9

There were 142 up-regulated and 127 down-regulated EMT related genes in Clone 1 *vs.* Clone 9 (Figure 6.2) and the top 10 up-regulated and down-regulated genes are listed in Table 6.4 and Table 6.5 respectively.

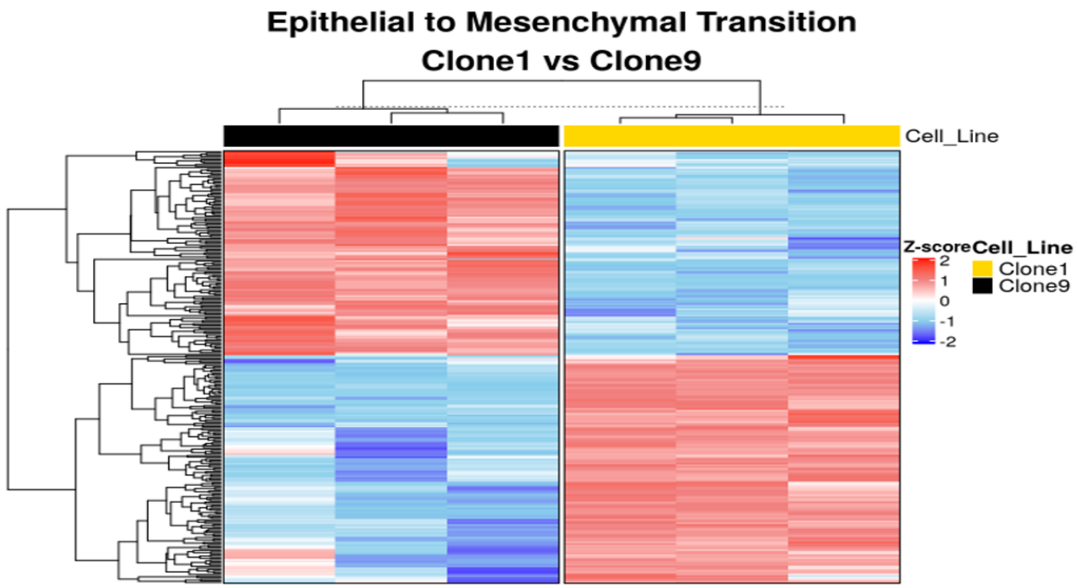

Figure 6.2. The heatmap of RNA-seq data from Clone 1 *vs.* Clone 9. The heatmap shows the upregulation and down-regulation of genes related to EMT in Clone 1 *vs.* Clone 9. Red indicated high expression, blue indicated low expression and white indicated no significant difference between Clone 1 *vs.* Clone 9.

Image created by Barry Digby.

Table 6.4. Top 10 up-regulated EMT associated genes in Clone 1 *vs.* Clone 9.

Gene	Description	Log2FC	P-value
HGF	hepatocyte growth factor	8.123113	1.32E-16
BMP2	bone morphogenetic protein 2	7.78549	3.16E-19
LGR5	leucine rich repeat containing G protein-coupled receptor 5	7.704036	1.19E-07
FOXP2	forkhead box P2	7.40889	7.51E-07
SOX5	SRY-box transcription factor 5	7.143269	2.02E-06
HPGD	15-hydroxyprostaglandin dehydrogenase	6.707749	2.08E-53
CNTN1	contactin 1	6.58521	6.72E-08
HOXA13	homeobox A13	6.531738	2.07E-05
SATB1	SATB homeobox 1	6.349207	1.39E-07
SCUBE2	signal peptide, CUB domain and EGF like domain containing 2	6.330354	7.27E-13

Table 6.5. Top 10 down-regulated EMT associated genes in Clone 1 *vs.* Clone 9.

Gene	Description	Log2FC	P-value
CAMK1D	calcium/calmodulin dependent protein kinase ID	-8.26692	1.96E-12
FGFR2	fibroblast growth factor receptor 2	-7.28842	1.63E-06
LCN2	lipocalin 2	-6.70479	7.45E-05
PPARG	peroxisome proliferator activated receptor gamma	-6.37747	1.91E-07
ROR2	receptor tyrosine kinase like orphan receptor 2	-6.27086	8.63E-05
MSX2	msh homeobox 2	-5.90304	9.54E-15
CYP3A5	cytochrome P450 family 3 subfamily A member 5	-5.71217	0.00012
TRPM8	transient receptor potential cation channel subfamily M member 8	-5.33117	1.08E-07
PEBP4	phosphatidylethanolamine binding protein 4	-5.26151	3.08E-10
CRYAB	crystallin alpha B	-5.19318	5.75E-17

6.2.4 Validation of EMT markers in enzalutamide resistant cell lines at the mRNA level

Custom designed primers (Appendix - Table 1) were used for validation via RT-qPCR for 9 common EMT markers (CDH1/ECAD, CDH2/NCAD, TWIST1, ZEB1, ZEB2, VIM, SNAI2/SLUG, SNAI1/SNAIL and EPCAM) (439). The epithelial junction markers consisted of ECAD and

EPCAM whereas the mesenchymal junction markers consisted of NCAD and VIM. The other five markers are core transcription factors related to EMT (TWIST1, ZEB1, ZEB2, SNAIL and SLUG) (481). TGF-β signalling markers (TGFB1 and TGFB2) (481), which are associated with EMT signalling were also included.

ECAD was significantly down-regulated in Clone 1 *vs.* Control and Clone 9 *vs.* Control (FC 0.56 ± SEM 0.05, p = 0.023 and FC 0.49 ± SEM 0.003, p = 0.096, respectively) (Figure 6.3A). The expression of EPCAM was reduced in Clone 1 *vs.* Control (FC 0.84 ± SEM 0.12, p = 0.32), however, it was not statistically significant. Even though the expression of EPCAM was higher in Clone 9 *vs.* Control (FC 1.7 ± SEM 0.05, p = 0.60), the difference was not significant (Figure 6.3B).

NCAD was significantly up-regulated in Clone 1 *vs.* Control (FC 126 ± SEM 0.03, p = 0.0026) but there was no difference between Clone 9 *vs.* Control (P > 0.05) (Figure 6.4A). VIM was increased in Clone 9 *vs.* Control (FC 18 ± SEM 0.29, p = 0.008) but no difference was observed between Clone 1 *vs.* Control (p > 0.05) (Figure 6.4B).

TWIST and ZEB2 were significantly up-regulated in Clone 1 *vs.* Control (FC 42 ± SEM 1.19, p = 0.001 and FC 2.9 ± SEM 0.2, p= 0.023, respectively) but no difference was identified between Clone 9 *vs.* Control (p > 0.05) (Figure 6.5A and 6.5B). ZEB1 was highly up-regulated in Clone 9 *vs.* Control (FC 498 ± SEM 0.2, p < 0.0001) but no difference was identified between Clone 1 *vs.* Control (p > 0.05) (Figure 6.5C). SNAIL and SLUG was significantly down-regulated in Clone 1 *vs.* Control (FC 0.36 ± SEM 0.14, p = 0.04 and FC 0.81 ± SEM 0.05, p = 0.002, respectively) but there was no difference between Clone 9 *vs.* Control (P > 0.05) (Figure 6.5D and 6.5E).

TGFB1 and TGFB2 were significantly up-regulated in Clone 9 *vs.* Control (FC 886.9 ± SEM 135.6, p = 0.0005 and FC 109.9 ± SEM 31.2, p = 0.0123, respectively) but there was no difference in Clone 1 *vs.* Control for both markers (p > 0.05).

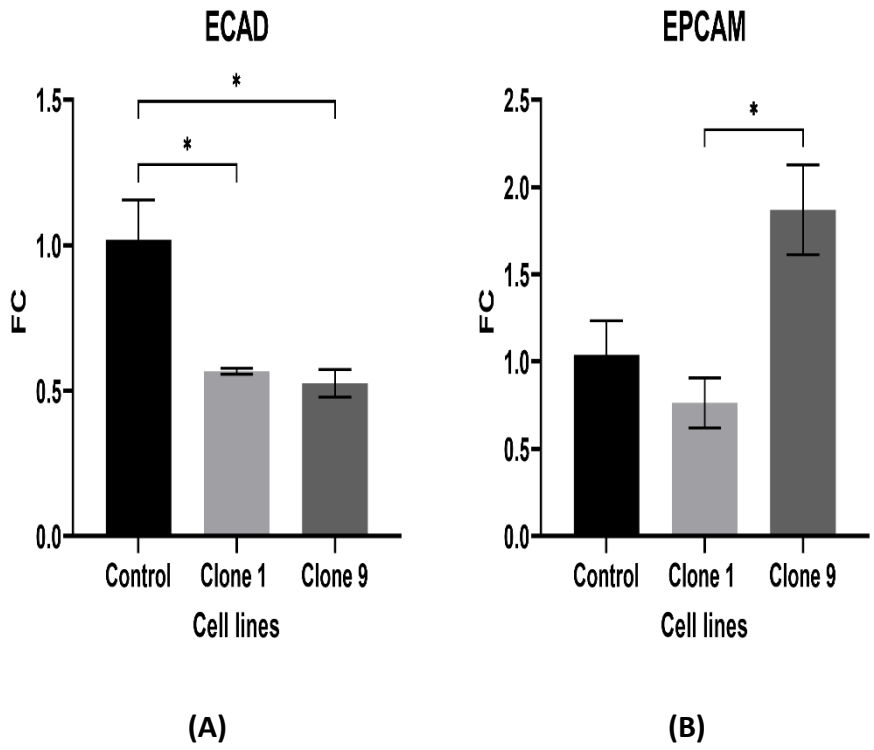

Figure 6.3. mRNA level of epithelial junction marker. (A) CDH1 (ECAD) and (B) EPCAM in enzalutamide resistant panel. Data graphed as mean ± SEM (n=3). Data analysed using an ordinary one-way ANOVA followed by Tukey's *post hoc* test (*p ≤ 0.05).

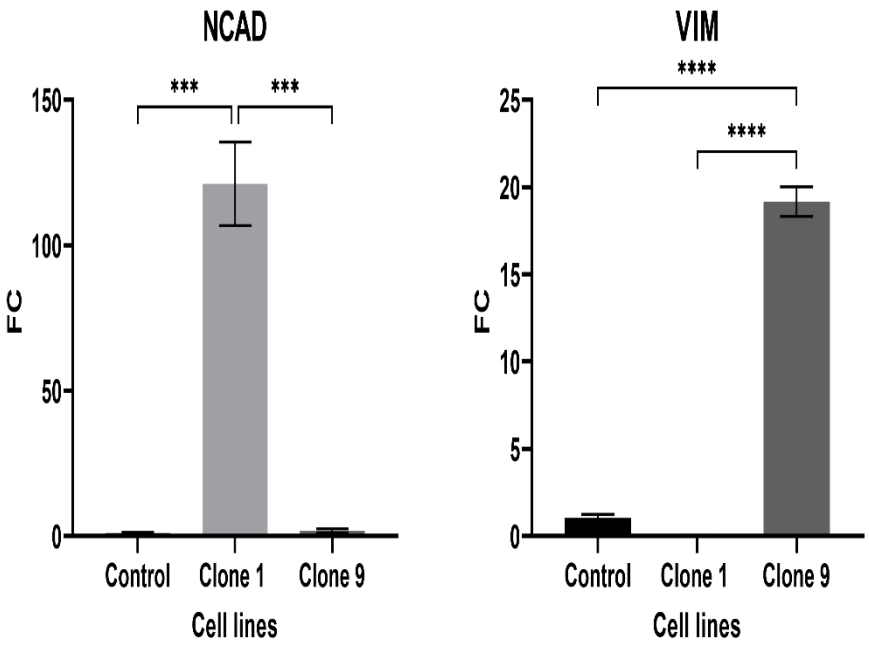

(A) **(B)**

Figure 6.4. mRNA level of mesenchymal junction markers. (A) CDH2 (NCAD), (B) VIM in the enzalutamide resistant panel. Data graphed as mean ± SEM (n=3). Data analysed using an ordinary one-way ANOVA followed by Tukey's *post hoc* test (***p ≤ 0.001, ****p ≤ 0.0001).

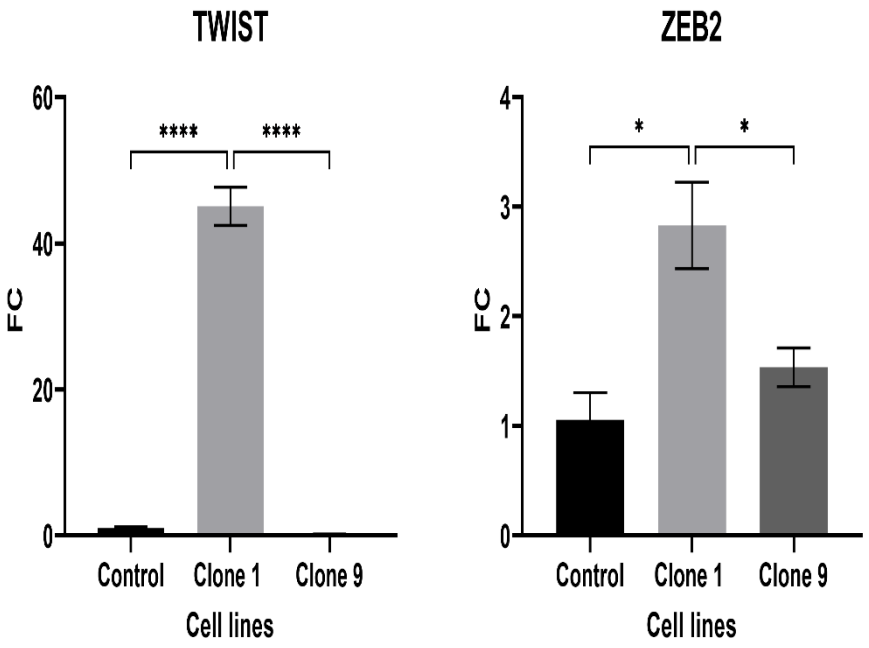

(A) **(B)**

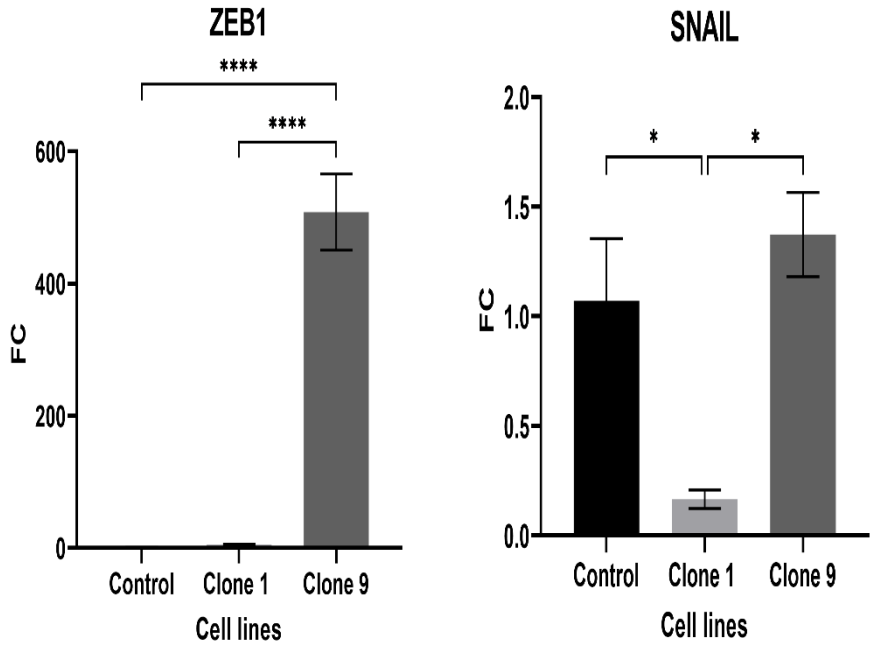

(C)

(D)

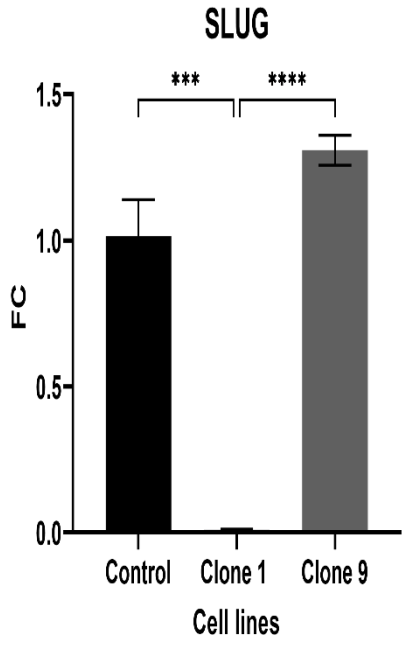

(E)

Figure 6.5. mRNA level of mesenchymal transcription factors. (A) TWIST, (B) ZEB2, (C) ZEB1, (D) SNAI1 (SNAIL) and (E) SNAI2 (SLUG) in enzalutamide resistant panel. Data graphed as mean ± SEM (n=3). Data analysed using an ordinary one-way ANOVA followed by Tukey's *post hoc* test (*p ≤ 0.05, ***p ≤ 0.001, ****p ≤ 0.0001).

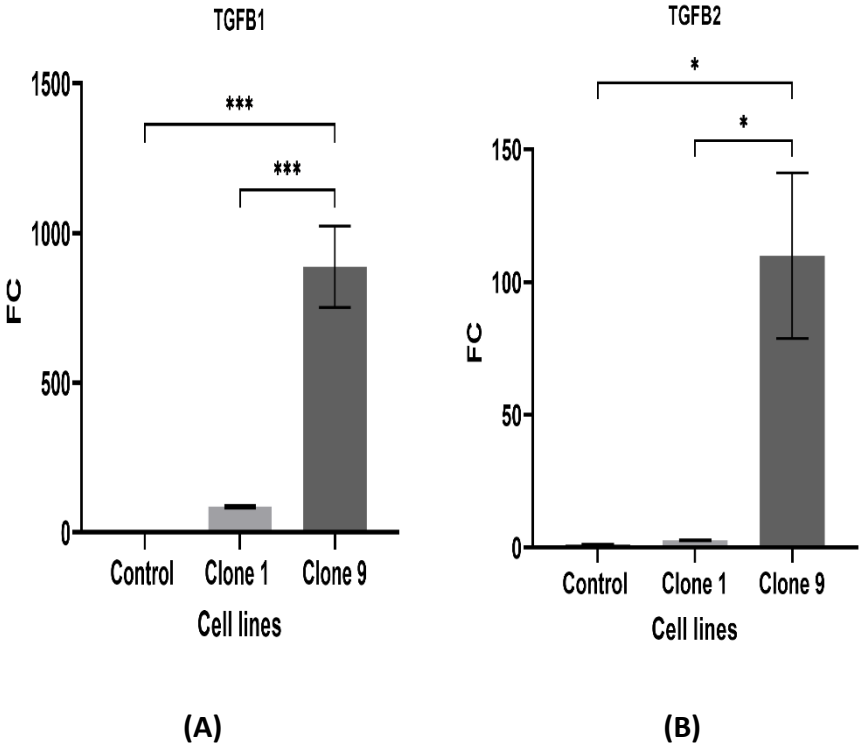

Figure 6.6. mRNA level of TGF-β. (A) TGFB1 and (B) TGFB2 in the enzalutamide resistant panel. Data graphed as mean ± SEM (n=3). Data analysed using an ordinary one-way ANOVA followed by Tukey's *post hoc* test (*p ≤ 0.05, ***p ≤ 0.001).

6.2.5 Western blot analysis of EMT proteins in enzalutamide resistant cell lines

Western blot analysis was performed to detect the differences in the expression of the EMT associated proteins, e-cadherin, n-cadherin and vimentin between the isogenic cell lines. The expression levels of ECAD in Clone 1 and Clone 9 were lower than Control (FC 0.651 ± SD 0.21, p > 0.05 and FC 0.691 ± SD 0.23, p > 0.05) (Figure 6.7A and 6.7B). The trend for ECAD protein expression was, however, consistent with mRNA expression, which was also down-regulated in Clone 1 *vs.* Control and Clone 9 *vs.* Control (Figure 6.3A). The expression levels of NCAD in Clone 1 was significantly higher than Control (FC 26.3 ± SD 1.5, p = 0.0002) (Figure 6.7C and 6.7D). This was consistent with mRNA expression (Figure 6.4A).

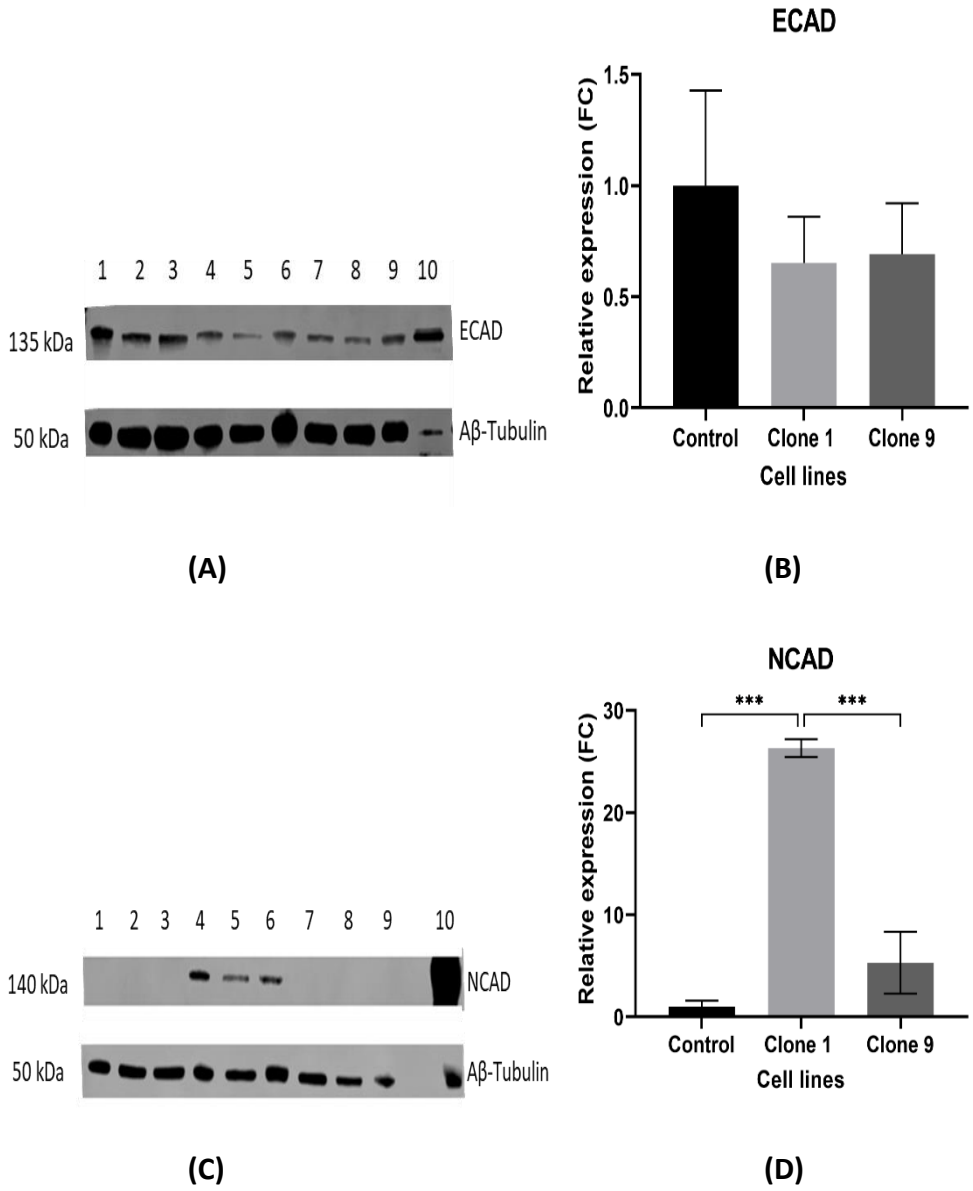

Figure 6.7. Western blot analysis and quantification of EMT related protein expression in the enzalutamide resistant panel. (A) ECAD, (B) quantification of ECAD band intensity, (C) NCAD, and (D) quantification of NCAD band intensity. Data graphed as mean ± SD (n=3). Data analysed using an ordinary one-way ANOVA followed by Tukey's *post hoc* test (***p ≤ 0.001). αβ-Tubulin was used as a loading control, with protein expression normalised to loading control. Lane 1-3: Control (n=3); lane 4-6: Clone 1 (n=3); lane 7-9: Clone 9 (n=3); lane 10: positive control (A = MCF7, C = MCF7).

6.3 NEPCa gene expression profile from RNA-Seq of enzalutamide resistance panel

The data set for analysing the concordance of differentially expressed genes in LNCaP Clone1 *vs.* Control samples and NEPCa gene signature sets were derived from Cheng *et al.* (482) and Beltran *et al.* (450). Cheng *et al.* derived a 12 signature gene set from a literature review of genes involved in NEPCa progression and a 304 gene signature set derived from overlapping differentially expressed genes from 3 microarray studies analysing NEPCa *vs.* prostate adenocarcinoma (482). The two gene sets were merged, resulting in a 310-gene signature set. Beltran *et al.* provided an integrated 70-gene signature NEPCa classifier developed by using expression data of genes that were prioritised by genomic, transcriptomic or epigenomic status (450).

6.3.1 NEPCa gene expression profile in Clone 1 *vs.* Control

The number of differentially expressed genes in Clone1 *vs.* Control that overlapped with the two NEPCa gene lists provided by Cheng *et al.* and Beltran *et al.* were assessed. In total 174 differentially expressed genes in Clone 1 *vs.* Control overlapped with either, one of two NEPCa data sets (Figure 6.8 and 6.9). In total, 10 differentially expressed genes in Clone 1 *vs.* Control were found to be consistently overlapped in both NEPCa data sets (Figure 6.8 and 6.10). The functions of the 10 NEPCa genes in relation to malignant or non-malignant diseases were evaluated through a review of the literature (Table 6.6).

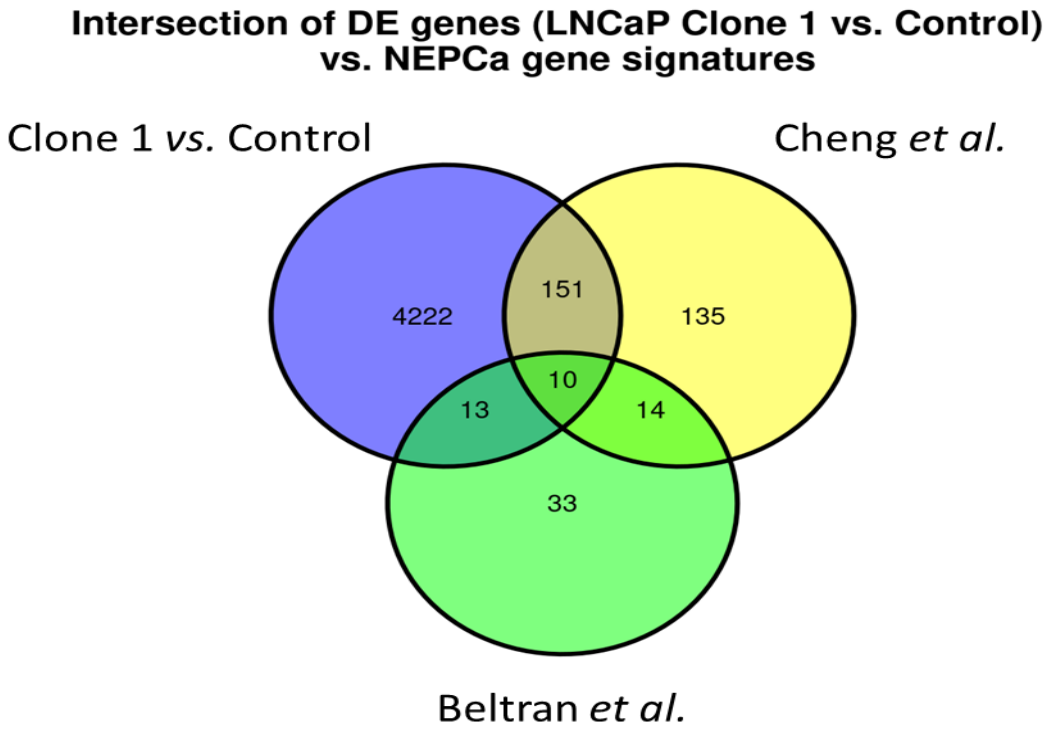

Figure 6.8. Venn diagram of NEPCa gene signature. The diagram showed DEGs in Clone 1 *vs.* Control data set overlapping with Cheng *et al.* and Beltran *et al.* NEPCa data set.

Image created by Barry Digby.

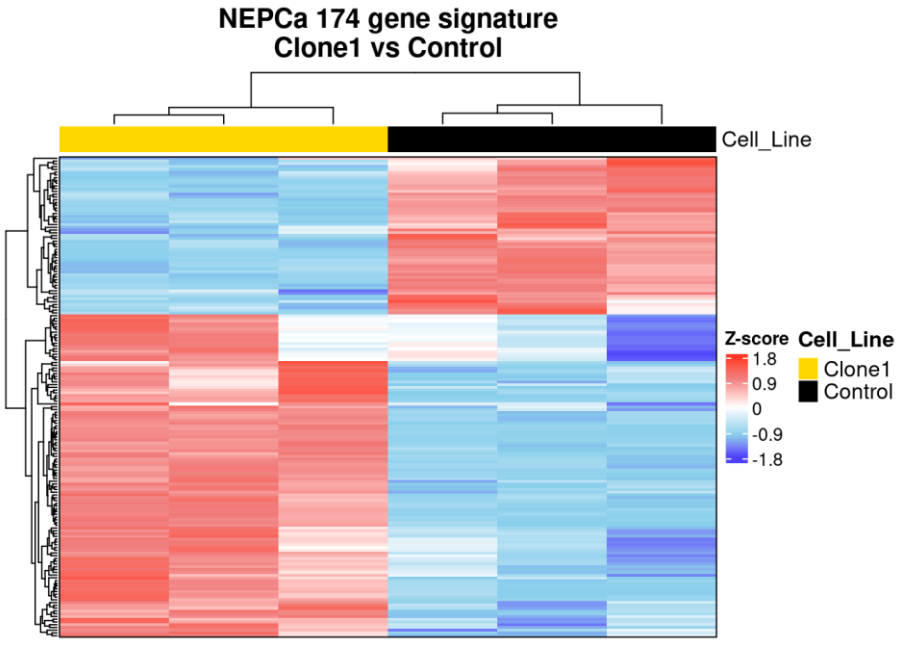

Figure 6.9. The heatmap of 174 NEPCa gene signature. The heatmap showed the 174 differentially expressed genes in Clone 1 *vs.* Control that overlapped with Cheng *et al.* and Beltran *et al.* NEPCa data set. Red indicated high expression, blue indicated low expression and white indicated no significant difference between Clone 1 *vs.* Control.

Image created by Barry Digby.

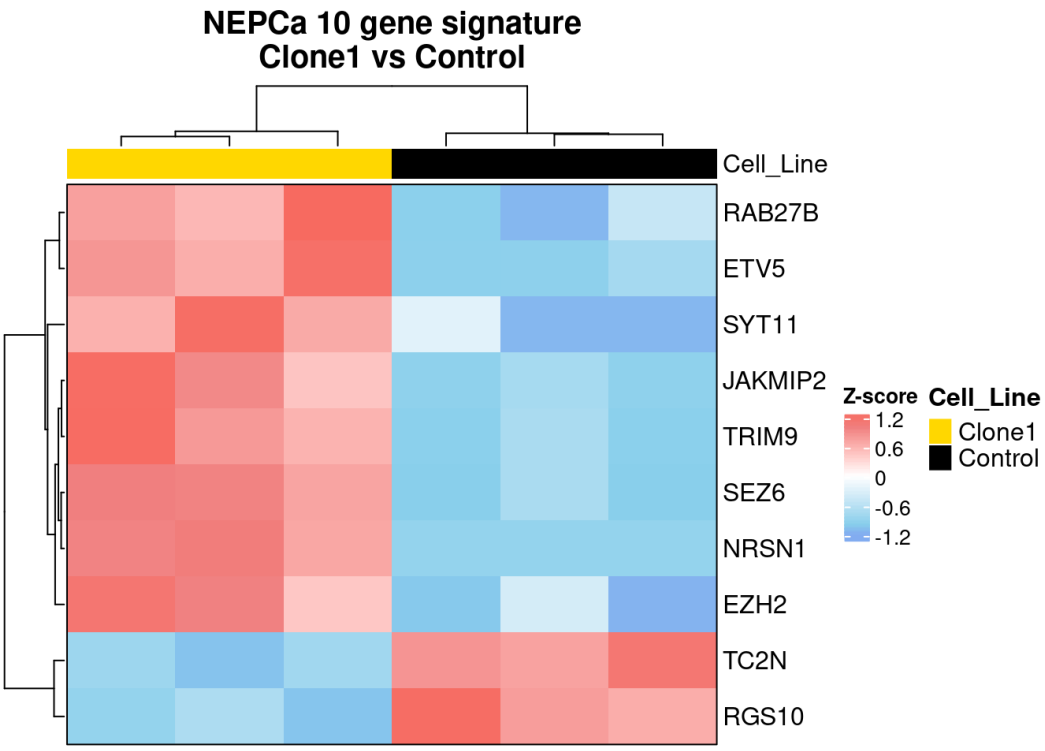

Figure 6.10. The heatmap of 10 NEPCa gene signature. The heatmap showed the 10 differentially expressed genes in Clone 1 *vs.* Control that overlapped with Cheng *et al.* and Beltran *et al.* NEPCa data set. Red indicated high expression, blue indicated low expression and white indicated no significant difference between Clone 1 *vs.* Control.

Image created by Barry Digby.

Table 6.6. The 10 NEPCa gene signature in Clone 1 *vs.* Control.

Gene	Description	Log2FC	P-value	Function
NRSN1	neurensin 1	7.64	2.17e-6	Important in neuronal organelle transport and conduction of nerve signals (483).
JAKMIP2	janus kinase and microtubule interacting protein 2	7.48	6.51e-10	Part of 4 genes panel that with overexpression predicts worse overall survival in PCa and important in vesicle related function which may aid metastasis (484).
SEZ6	seizure related 6 homolog	6.87	2.60e-5	Control synaptic plasticity and dendrite morphology with overexpression linked to increased cancer growth and poor prognosis in multiple malignancies (485).
TRIM9	tripartite motif containing 9	6.48	2.34e-7	Increased expression causes cell proliferation, and impedes cell apoptosis through NF-κB signalling pathway in uterine leiomyoma and part of the 4 novel biomarkers for NEPC identified (486).
ETV5	ETS variant transcription factor 5	3.56	1.95e-15	Increased aggressiveness, infiltrative pattern and migration of PCa cells (487).
SYT11	synaptotagmin 11	2.35	1.29e-2	Expression correlated with lymph node metastasis in colon cancer (488).
EZH2	enhancer of zeste 2 polycomb repressive complex 2 subunit	1.43	1.59e-15	Induced development of CRPC and facilitate transition of CRPC into a lineage infidelity state (489).
RAB27B	RAB27B, member RAS oncogene family	1.23	2.17e-8	Often repressed in advanced PCa and inversely correlated with PCa outcomes (490).
RGS10	regulator of G protein signalling 10	-2.13	1.93e-16	RGS proteins impede breast, lung, prostate, and ovarian cancer cell development through inhibition of G-protein coupled receptors signalling pathways (491).
TC2N	tandem C2 domains, nuclear	-1.59	1.78e-14	Inhibits PI3K-AKT signalling by preventing phosphorylation of p55γ and AKT in breast cancer (492).

6.3.2 RT-qPCR validation of NEPCa markers in enzalutamide resistance panel

Custom designed primers (Appendix - Table 1) were used for validation via RT-qPCR for four classical neuroendocrine markers (POU3F2 (BRN2), CHGA (Chromogranin A), ENO2 (NSE) and SOX2) (493). All three neuroendocrine markers, BRN2, CHGA and NSE were significantly

up-regulated in Clone 1 *vs.* Control (FC 21.1 ± SEM 5.94, p =0.0014; FC 113.2 ± SEM 54.77, p = 0.046; FC 10.25 ± SEM 2.29, p = 0.0061, respectively) (Figure 6.11A, 6.11B and 6.11C). While there was no difference in expression of SOX2 in Clone 1 *vs.* Control, the expression in Clone 9 *vs.* Control was up-regulated however it did not achieve statistical significance (Figure 6.11D).

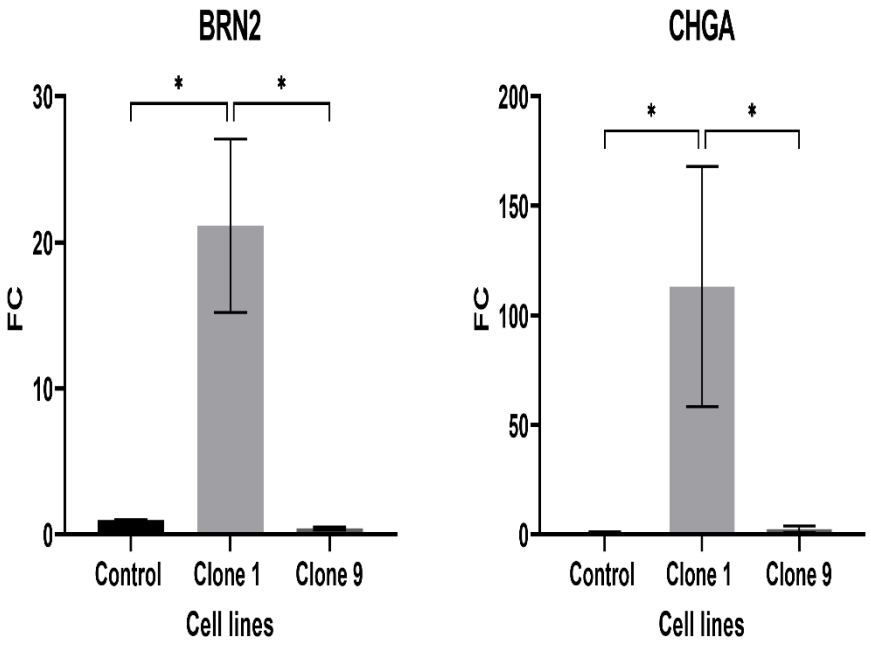

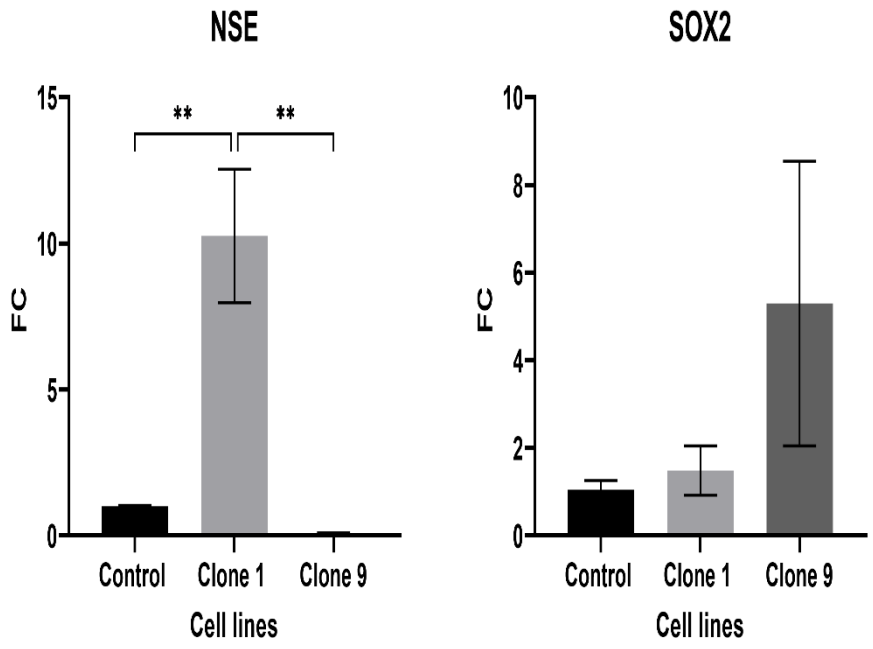

Figure 6.11. RT-qPCR expression level of neuroendocrine markers. (A) BRN2, (B) CHGA, (C) NSE, and (D) SOX2 in isogenic cell lines. Data graphed as mean ± SEM (n=3). Data analysed using an ordinary one-way ANOVA followed by Tukey's *post hoc* test (*p ≤ 0.05, **p ≤ 0.01).

6.4 Small molecular compound prediction on the enzalutamide resistance panel

The differentially expressed genes from the NGS data generated from the isogenic cell lines were used as input to query Connectivity Map (CMap) (494). This was done in order to elucidate the differences and similarities between drug-induced expression profiles and disease expression. This was performed as an effort to discover potential small molecular compounds, which may be used to prevent enzalutamide resistance.

As there were a large number of differentially expressed genes in the enzalutamide resistance panel returned by DESeq2, filtering strategies were devised for optimal number of genes selection along with an iterative process to assess the highest connectivity score returned by each iteration. The differentially expressed genes with a Log2 FC of ± 2 and $p < 0.05$ were selected. This was followed by calculation of their quartile range of mean expression value. The genes with mean expression values below Q2 were excluded from the analysis. The remaining selected genes were ranked according to their statistical

significance for input into the PharmacoGx platform (495). The match between these genes and small molecular compounds from CMap were assessed via connectivity score ranging between −1 to 1. A positive connectivity score signified agonist properties of the compound on the query gene signature, while a negative connectivity score indicated antagonistic properties of the compound on the query gene signature. Connectivity scores below 0.9 and -0.9 represented weak connections.

The analysis returned weak associations with perturbagens for gene signature in Clone 1 *vs.* Control (Table 6.7). The top five drugs with negative connectivity scores showed potential reversal effects of enzalutamide resistant gene expression were Isotretinoin, 5182598, Tretinoin, H-7 dihydrochloride and Lomustine (Table 6.7). Interestingly, Isotretinoin was previously investigated in a phase II trial in combination with complete androgen blockade in people with advanced hormone-naive PCa, which suggests early addition of Isotretinoin to first generation antiandrogen treatment enhanced PSA responses and sustained longer PSA free progression (496). The top 5 drugs with positive connectivity score, which were identified to mimic enzalutamide effects, were AH-6809, Cantharidin, Lycorine, Prestwick-864 and Emetine (Table 6.7).

Table 6.7. Potential small molecular compounds. Compounds acting as antagonist (negative connectivity score) or agonist (positive connectivity score) in enzalutamide resistance based on dysregulated gene signature in Clone 1 *vs.* Control.

Perturbagen	**Connectivity score**	**p value**	**Type of drug**	**Mode of action in general drug class**
Isotretinoin	-0.393115	0.00019855	Vitamin-A derivative	Induces apoptosis in PCa via FOXO regulation and inhibits Wnt pathway (497).
5182598	-0.383835	0.00207381	Benzylisoquinoline alkaloids	Repair the damaged metabolic pathways in metastatic PCa, and are good potential therapeutic drugs for the treatment of metastatic PCa (498).
Tretinoin	-0.380225	0.00024713	Retinoic acid (synthetic vitamin A)	Inhibit pathways responsible for EMT possibly through down-regulation of Wnt pathway (499) and inhibition of AR splice variant (500).

H-7 dihydrochloride	-0.37404	0.01008903	Protein kinase inhibitor	Induced a apoptosis in LNCaP via activation of caspase 3/7 (501).
Lomustine	-0.36775	0.02966594	Alkylating agent	Regained of hormonal sensitivity post Lomustine and Chlorambucil (502).
AH-6809	0.767275	0.01359326	Prostaglandin DP-receptor blocker	Non-selective EP receptor antagonist applied to explore the roles of PGE2/EP2 signalling (503).
Cantharidin	0.366015	0.01613633	Protein phosphatase 2 (PP2A) inhibition	Induce cell cycle arrest and apoptosis in the cancer cells (504).
Lycorine	0.343545	0.01133656	Toxic crystalline alkaloid	Reduce proliferation of PCa cell lines, induce apoptosis and cell death (505).
Prestwick-864	0.32994	0.00226873	Methylhydantoin-5-(D) (Imidazolines)	Unknown.
Emetine	0.329915	0.01739822	Block protein synthesis	Cytotoxicity in PCa cell lines (506).

6.5 Discussion

Recently, numerous studies undertaking comprehensive DNA and RNA sequencing of fresh frozen tissue samples have facilitated the characterisation of the genomic and transcriptomic landscape of primary PCa, CRPC, and NEPCa (94, 397, 399, 450). These studies revealed a heterogeneous set of somatic changes in CRPC and/or NEPCa compared to primary disease (94, 450). This included alterations such as *AR* in the form of adaptive amplification and mutations resulting in resistance of ADT therapies, *RB1* mutation and *TP53* deletion in the setting of NEPCa and the identification of alteration in DNA repair pathways genes, which could be targetable with PARPi, which is of particular relevance to the clinical setting (94, 399, 450). Besides these, the evolution of PCa to CRPC and subsequent evolvement of drug resistance may involve the cross talk of AR with other important signalling pathways such as EMT, given its role in metastatic cancer spread and implications in development of PCa resistance to ADT and chemotherapy in a number of recent *in-vitro* studies (211, 445-447).

The EMT pathway was evaluated further as it was significantly enriched in the Hallmark pathway of Clone 1 *vs.* Control. Bioinformatic analysis identified 177 up-regulated and 118 down-regulated EMT related genes in Clone 1 *vs.* Control. This suggested a possible association of EMT in the development of enzalutamide resistance. This may help to

identify a clinical signature to inform drug resistance during treatment as well as druggable targets to combat resistance. The functions of the top 10 up-regulated and down-regulated EMT related genes in relation to cancer were evaluated through a review of the literature. Interestingly all of the top 10 up-regulated genes were described as oncogenes in the literature, thus further suggesting that their overexpression could contribute to tumour growth, invasion and perhaps drug resistance. Indeed, these up-regulated EMT related genes have been described to induced EMT via signalling pathways such as Wnt, PIK3CA, TGF-β, cMET, and NOTCH signalling, which are known to play a vital role in tumourigenesis as well as drug resistance across tumour subtypes (403, 454, 456, 462, 507).

Recently, Wnt pathway activation has been reported as a frequent event in PCa that enhanced tumour progression and treatment resistance, hence targeting the pathway may be an effective treatment option (508). The interaction of the Wnt and AR pathways have been widely studied and shown to regulate AR signalling through numerous mechanisms either via canonical or non-canonical Wnt signalling (509-511). For instance, it has been shown that β-catenin and TCF4 interactions increased during androgen deprivation as well as the up-regulation of Wnt target genes such as *LEF1*, which promoted the androgen independent growth of PCa cells (509, 511). Indeed *TCF4* and *LEF1* were up-regulated in Clone 1 *vs.* Control in this study (Log2 FC 1.36, p = 0.000064; and Log2 FC 2.34, p = 2.225e-20, respectively), which further strengthens the association of EMT in promoting enzalutamide resistance.

The Wnt signalling pathway offers an attractive option for therapeutic intervention given that this oncogenic signalling is frequently observed in PCa (508). Currently, several therapeutic targets have been developed and investigated pre-clinically to treat PCa such as β-Catenin inhibitors (512, 513). The canonical Wnt signalling requires translocation of β-catenin from the cell cytoplasm into the nucleus and binds to TCF/LEF transcriptional factor family and transcription coactivator CBP to activate Wnt target gene transcription (512). Thus, β-Catenin inhibitors are good therapeutic candidates to inhibit downstream canonical Wnt signalling. A pre-clinical study investigating β-Catenin inhibitor (CWP232291) in androgen independent PCa cell lines has shown that the Wnt signalling was reduced by inhibiting β-catenin activity resulting in repression of Wnt target genes (512). When CWP232291 treatment was tested in androgen dependent cell lines, the AR and AR splice variant expression were significantly reduced and additionally, anti-tumour activity was

observed in primary cells derived from four CRPC patient samples including one with enzalutamide resistance (512). Many other signalling pathways related to EMT such as PIK3CA and NOTCH have also been shown to facilitate CRPC via interaction with the AR pathway (508). This highlights that the development of enzalutamide resistance encompasses a diverse molecular mechanism under the broad umbrella term of EMT.

Four of the top 10 down-regulated EMT related genes are described as tumour suppressors from studies in the literature. The other six EMT related genes were described as oncogenes in the literature but could be explained by the fact that numerous studies have reported the existence of paradoxical genes where they exhibit both oncogenic and tumour suppressor functions across different tumour subtypes (514-516). For instance, NOTCH signalling was reported to play an oncogenic role in acute lymphoblastic leukaemia while having a tumour suppressor role in squamous epithelial cells, thus suggesting that a gene may have dual functions in oncogenesis under diverse cellular settings (516, 517).

Changes in gene expression during EMT as a result of direct or indirect actions of EMT related transcription factors often play a fundamental role in driving EMT leading to the morphological and functional alteration observed in cancer cells (481). Most EMT processes are linked to the activation of one or several core EMT related transcription factors (481). To further evaluate the association of EMT with enzalutamide resistance, nine common EMT markers from studies in the literature were selected for RT-qPCR validation in the enzalutamide resistant panel. In Clone 1 *vs.* Control, ECAD (FC 0.56, $p < 0.05$) was significantly down-regulated while, NCAD (FC 126, $p < 0.05$), ZEB2 (FC 2.9, $p < 0.05$) and TWIST1 (FC 42, $p < 0.05$) was significantly increased. This was further confirmed using western blot, where ECAD protein was decreased but NCAD protein was significantly increased in Clone 1 *vs.* Control. Epithelial cells have highly polarised morphology, which are closely interconnected by cell-cell junctions. However, in EMT, the loss of these intercellular networks confers a critical step, which allows for the detachment of tumour cells from their primary site (481). The CDH1 gene encodes ECAD, which is a calcium-dependent cell adhesion molecule that helps with the formation and preservation of epithelial cell morphology (424). Thus, the loss of ECAD in Clone 1 was suggestive of a loss in epithelial junction proteins, which is one of the main characteristics of EMT. Over expression of mesenchymal markers, NCAD and both transcription factors, TWIST1 and ZEB2 in Clone 1 was consistent with reports in literature suggestive of EMT process. A study

in gliomas showed that ZEB2 and TWIST facilitated cutaneous metastasis (518) and another in oral squamous cell carcinoma showed that the co-expression of both EMT markers confers poor survival (519).

In Clone 9 *vs.* Control, ECAD was also significantly down-regulated (FC 0.49, $p < 0.05$) while the mesenchymal marker, VIM (FC 18, $p < 0.05$) and transcription factor ZEB1 (FC 498, $p < 0.05$) was significantly increased. This is suggestive of an EMT process, whereby the weakly enzalutamide resistant clone lost the epithelial markers and gained the mesenchymal marker. A study in hepatocellular cancer has shown that ZEB1 and VIM levels were higher in tumour tissues compared to adjacent normal tissues and confer poor prognosis (520). The silencing of *ZEB1* resulted in reduction of hepatocellular cancer cell proliferation, migration and invasion. Additionally, the group has shown that ZEB1 has a binding site in the VIM promoter and could regulate the transcriptional activity of VIM (520). Since both Clone 1 and Clone 9 overexpressed different EMT related transcription factors, this further indicated that different mechanisms were involved in the EMT process leading to different enzalutamide sensitivity within the cell lines.

It was interesting to note that the expression of these classic EMT markers from both strongly and weakly enzalutamide resistant clones were different which suggested the possibility of EMT expression reprogramming during progression of enzalutamide resistance. Perhaps during the early stage of enzalutamide resistance development, ZEB1 was up-regulated, which induced up-regulation of VIM and down-regulation of ECAD. Upon further increase of resistance, ZEB2 and TWIST were activated resulting in up-regulation of NCAD and down-regulation of ECAD, however, ZEB1/VIM as well as the SNAIL/SLUG pathway were somewhat “switched off”. This explanation was within the context of EMT transcription factors switch theory observed in the progression of malignant melanoma described by Caramel and colleagues (521). The group demonstrated mutual repression of *ZEB1* and *ZEB2* in melanoma with reciprocal regulations of ZEB proteins facilitating dynamic EMT transcription factors, which switches in the course of disease progression (521). EMT transcription factors play a role in the proliferative and invasive capabilities of carcinoma cells and are essential in other EMT-related processes such as cell state transition, cancer stem cell formation, therapy resistance, as well as tumour micro-environment reprogramming (522). ZEB-related EMT processes are regulated by similar micro-environmental signals, such as TGF-β, Wnt and Notch pathways (523).

Numerous studies have shown that terminally differentiated cells can gain pluripotent stem cell characteristics, by regulating related transcription factors towards transdifferentiation, EMT and mesenchymal–epithelial transition (MET) (524, 525). The cellular process of transdifferentiation is controlled by the close relationships between the neuroendocrine and EMT phenotype (526). Neuroendocrine phenotype characteristics in PCa have been increasingly recognised as a driver of disease progression (525, 527). Studies have reported that NEPCa tends to arise under the strong selective pressure of potent ADT, and may encompass up to 25% of drug-resistant CRPC (452). NEPCa is increasingly recognised as a variant of CRPC that is greatly resistant to androgen pathway inhibitors (528, 529). It is commonly differentiated from prostatic adenocarcinoma by reduced AR expression accompanied by distinctive small-cell morphology and positive staining for neuroendocrine markers (530). In this study, there were 174 differentially expressed genes in Clone 1 *vs.* Control that overlapped with either NEPCa gene lists provided by Beltran *et al.* or Cheng *et al.* and 10 were found to be consistently overlapped in both NEPCa data sets creating a signature gene set which may inform development of NEPCa leading to enzalutamide resistance. Validation via RT-qPCR of the common neuroendocrine markers BRN2, CHGA and NSE showed significant up-regulation in Clone 1 *vs.* Control suggesting that the strongly enzalutamide resistant cells acquired neuronal characteristic and transitioned towards a neuroendocrine state. Bishop *et al.* showed that the neural transcription factor, BRN2 served as the key driver of NEPCa differentiation and facilitated aggressive growth of enzalutamide CRPC *in vitro* as well as overexpressed in both people with NEPCa and people with mCRPC that expressed low PSA level (531). Additionally, CHGA and NSE expression was also shown to be overexpressed in neuroendocrine-like enzalutamide resistant cells and in human NEPCa by the same group (531).

In this study, the differentially expressed genes in Clone 1 *vs.* Control were queried using CMap to evaluate small molecular compounds, which may potentially be utilised to combat enzalutamide resistance. It is worth noting that Isotretinoin was found to be one of the top five small molecules, which had the potential to reverse enzalutamide resistance. Ferrari *et al.* demonstrated that by addition of Isotretinoin to androgen blockade in people with advanced hormone naive PCa enhanced PSA response (496). The group found that participants attained an undetectable PSA level faster and more attained undetectable PSA, which was sustained for a longer period compared to controls (496). Furthermore

Melnik *et al.* showed that Isotretinoin induces apoptosis in PCa via FOXO regulation and inhibits Wnt pathway (497). Thus, addition of Isotretinoin may be a good therapeutic candidate to prevent enzalutamide resistance. It is readily accessible as well as having minimal side effects in combination with first generation hormonal agents as reported in the previous phase II trial by Ferrari and colleagues (496). No study to date has evaluated the combination of Isotretinoin with second generation hormonal therapy in PCa.

In conclusion, this study has identified that both EMT and NEPCa pathways were altered in enzalutamide resistant cell lines. Additionally, data suggests that EMT expression reprogramming during the transition to enzalutamide resistance, may utilise different signalling pathways. Besides the EMT process, the enzalutamide resistant cell lines also gain features of NEPCa. In this study, a 10 NEPCa gene signature was identified, that may inform NEPCa transformation leading to enzalutamide resistance. Through CMap perturbagen evaluation, Isotretinoin was discovered to have the potential to reverse enzalutamide resistant associated gene expression. Thus, it may be utilised as a combination therapy with enzalutamide to delay resistance development. However, more research is warranted.

Chapter 7 - High throughput sequencing of blood and tissue samples in patients with mCRPC

7.0 Introduction

A number of sequencing efforts, such as the Stand Up to Cancer-PCF (SU2C-PCF) MCRPC project and the TCGA primary localised PCa study, have identified distinctive molecular subgroups of PCa and potentially targetable somatic or germline alterations (399, 532, 533). Though molecular profiling is not the clinical benchmark of care for in PCa currently, more evidence is emerging to support its use in paving the way for therapeutic selection. This treatment strategy may improve response to therapy and provide more therapeutic options such as the use of PARPi and platinum-based therapy in people with PCa who harbour genomic alterations in DNA damage repair (DDR) genes (534-536). A number of studies have demonstrated that targeted DNA and RNA profiling of clinically relevant somatic alterations may be an achievable strategy in advanced PCa (537, 538). Largely, these sequencing initiatives have assisted in outlining the practicality and efficacy of molecular profiling in people with CRPC, however, technical challenges persist in clinical settings.

This retrospective analysis of targeted NGS in people with PCa was performed to identify the actionable gene mutational landscape of an Irish cohort with mCRPC using both blood based and tissue based targeted NGS. Additionally, it was conducted to appraise the utility and barriers of targeted NGS in a clinical setting.

7.1 Experimental aims

The aim was to evaluate the use of targeted NGS to determine the presence of actionable gene mutations in tissue and blood from people with mCRPC.

7.2 Participants

A retrospective analysis of targeted NGS in participants with mCRPC from two different academic sites between July 2017 and October 2020 (Tallaght University Hospital and St Vincent's University Hospital) was undertaken. A comprehensive search was performed to collect baseline demographics and clinical characteristics. Data were collected in compliance with Good Clinical Practice guidelines and participants provided written informed consent before participation in the NGS screening study. The targeted NGS study was offered to those with mCRPC from the two academic sites as part of the screening for

enrolment into TRITON 2 (An international, open-label, phase II study evaluating rucaparib in people with mCRPC associated with DNA damage repair (DDR) deficiency) (536) or TRITON 3 (An international, randomised, open-label, phase III study of the rucaparib *vs.* physician's choice of therapy mCRPC associated with DDR deficiency) (539) if DDR deficiency were present.

Blood and tissue specimens from 164 participants with mCRPC who progressed on a second generation hormonal therapy (enzalutamide or abiraterone) were included (Figure 7.0). Seventy-one had blood based NGS only, 13 had tissue based NGS only and 80 had both. Participants were categorised into two groups; blood based NGS (n=151) and tissue based NGS (n=93) with 80 overlapping between both groups (Figure 7.0). Out of the 93 participants with tissue based NGS, 52.7% (n=49) of the participant's tissue sample was obtained in CSPC setting, 39.8% (n=37) of the participant's tissue sample was obtained in mCRPC setting and 7.5% (n=7) of the participant's tissue sample timing was indeterminate.

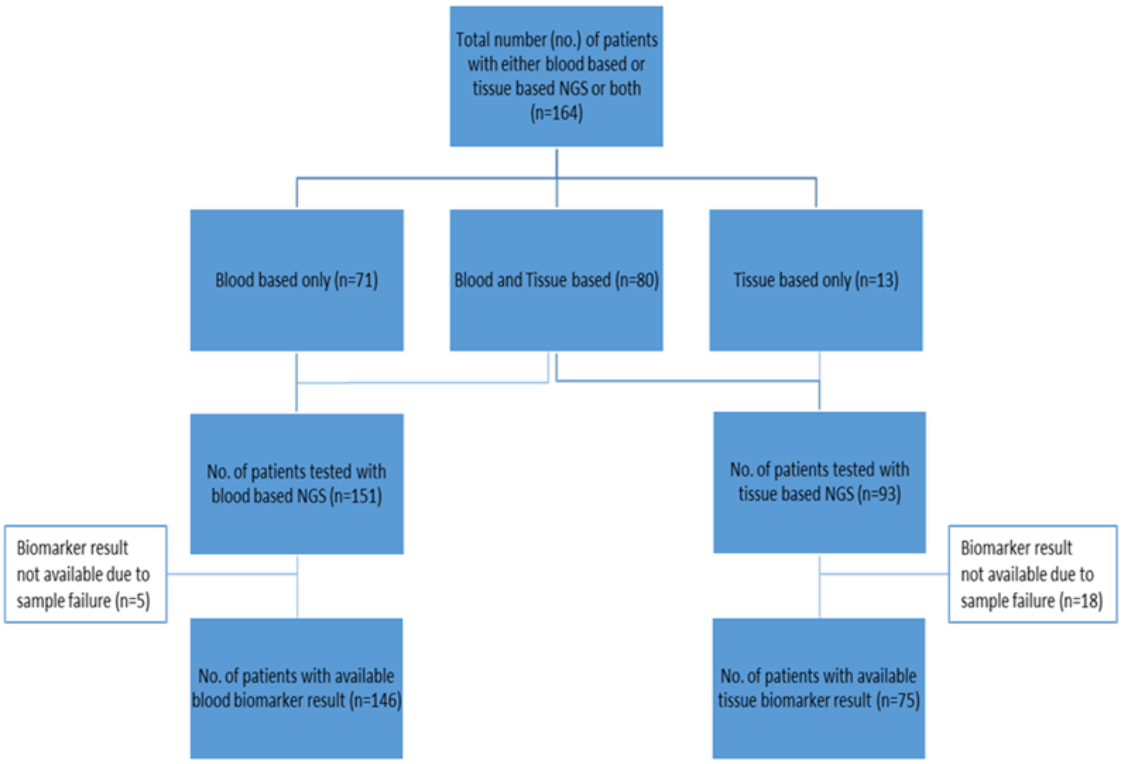

Figure 7.0. Participant flow chart.

A total of 121 tumour tissues and 167 blood samples were analysed by Foundation Medicine® (Cambridge, MA). A number of repeat samples per participant was also included. The targeted NGS FoundationOne® CDX assay uses DNA isolated from formalin-fixed, paraffin-embedded (FFPE) tumours to sequence exons from 324 genes and select gene rearrangements, as well as genomic signatures including microsatellite instability (MSI) (392). The FoundationOne® Liquid CDx assay uses circulating cell-free DNA (cfDNA) isolated from plasma derived from anti-coagulated peripheral whole blood to sequence exons from 311 genes, including rearrangements and copy number losses only in BRCA1 and BRCA2 (392, 540).

Actionable gene mutations were identified using OncoKB (Memorial Sloan Kettering Cancer Centre), where the clinical actionability to individual gene mutational events were assigned according to targeted treatment available that was classified by the levels of evidence system (ranging from standard of care to investigational or hypothetical treatments) (541). Actionable gene mutations were further categorised according to tumour subtypes based on OncoKB. Additionally, ClinVar (National Centre for Biotechnology Information) was used to complement the identification of variant gene mutation status in terms of its pathogenicity (542). Variants of gene mutations that were annotated as 'likely pathogenic' or 'pathogenic' were considered as actionable and variant gene mutations that were annotated as 'likely benign' or 'benign' were excluded. Sample failure was defined as an event where either blood or tissue submitted for sequencing yielded no biomarker status due to unsuccessful sequencing because of failed sample quality control (QC). Sample success was defined as an event when either blood or tissue submitted for sequencing successfully passed QC and was sequenced yielding a biomarker status. Objectives of this retrospective analysis encompassed clinical learnings in NGS testing in mCRPC and description of the presence of actionable gene mutations in this cohort.

7.3 Statistical Analysis

The cut-off date for analysis was October 2020. Descriptive statistics were used to present participant and treatment characteristics. Outcome data were analysed using Fisher's exact test, using GraphPad Prism 9 software.

7.4 Participant characteristics

A total of 164 participants with mCRPC, median age of 73 (43–90) and median PSA at time of initial NGS was 21.2 ng/mL (0.03–5000), were identified. Additional baseline clinical characteristics are provided in Table 7.0.

Table 7.0. Participant characteristics.

Age at time of NGS:	
median	73
(range)	(43-90 years)
Race:	
Caucasian, n (%)	157 (99%)
Black, n (%)	2 (1%)
PSA at time of NGS:	
median	21.2
(range)	0.03-5000
Chemotherapy status at time of NGS:	
Pre-Docetaxel, n (%)	107 (66%)
Post-Docetaxel, n (%)	55 (34%)

For tissue-based NGS, a total of 121 tumour tissue samples from 93 participants were submitted for sequencing. Tissue samples that failed in the first round were re-submitted for sequencing. Of the 121 tumour tissue samples, 84 (69%) passed QC and were successfully sequenced (Figure 7.1). QC failure included failure to meet minimum QC metrics for laboratory processing (n=12; 32%) and computational analysis (n=5; 14%), insufficient tumour nuclei content (n=11; 30%) and insufficient DNA extracted (n=9; 24%) (Figure 7.2). Laboratory processing failures were due to either sample failed in hybrid capture or in library construction. The majority of the 121 tissue samples were from the prostate gland (64%) followed by the lymph node (20%), bone (8%), liver (4%), adrenal (2%), bladder (1%), lung (1%), and soft tissue (1%) (Figure 7.3). Most samples were from archived tissue (> 3 years) (n=80; 66%) and the remaining were from newly collected tissue biopsy

(< 3 years) (n=41; 34%). The contemporaneous tissue had significantly lower sample failure rate compared to archived tissue (15% *vs*. 39%, respectively; p=0.0002, OR 0.28 (0.14 to 0.54)) (Figure 7.4). QC failure in the newly biopsied tissue was mainly due to insufficient tumour nuclei (n=5; 83%) followed by failure to meet minimum QC metrics for computational analysis (n=1; 17%). The median turnaround time for tissue-based NGS was 13 days (4-33).

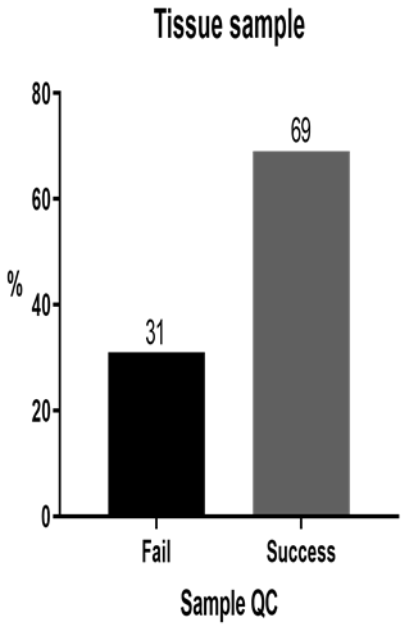

Figure 7.1. Tissue sample QC. Percentage of tissue samples which failed or passed QC. Failed sample (n=37) and passed sample (n=84).

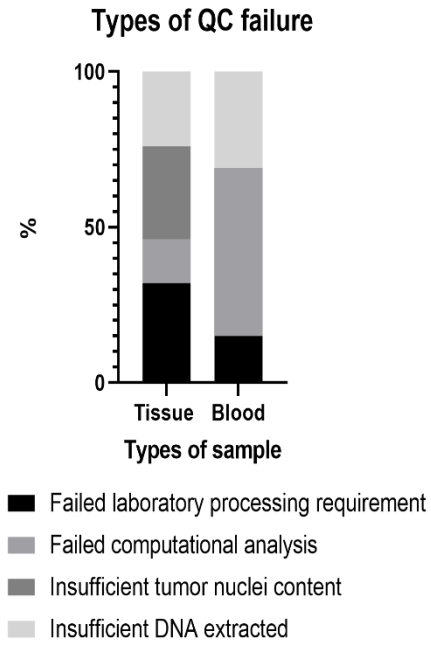

Figure 7.2. Types of QC failure. Distribution of reason for failing QC in tissue and blood samples. Tissue samples (n=121) and blood samples (n=167).

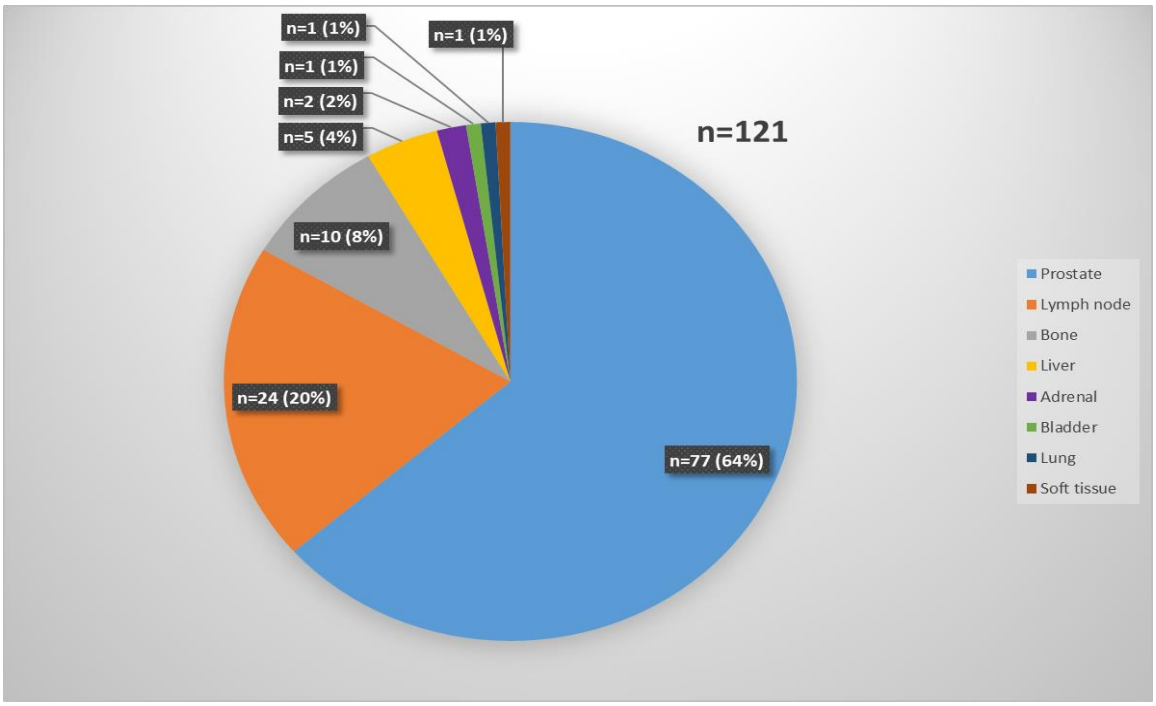

Figure 7.3. Distribution of tissue subtypes submitted for NGS. (n=121)

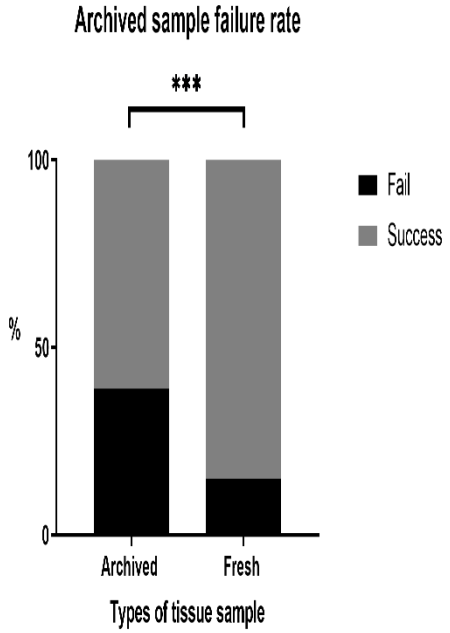

Figure 7.4. Comparison of archived tissue *vs.* contemporaneous (fresh) tissue sample QC failure or success rate. Archived tissue (n=80) and fresh tissue (n=41). Data analysed using Fisher's exact test followed by a Baptista-Pike method to compute confidence Interval (CI), (***p ≤ 0.001).

For blood-based NGS, 167 blood samples from 151 participants were submitted for sequencing. Of 167 blood samples, 154 (92%) passed QC and were successfully sequenced (Figure 7.5). The 13 (8%) samples that failed QC were due to failure to meet minimum QC metrics for computational analysis (n=7; 54%) or laboratory processing (n=2; 15%) or insufficient DNA extracted (n=4; 31%) (Figure 7.2). Blood samples had a significantly higher sample success rate compared with tissue samples (92% *vs.* 69%, respectively; p<0.0001, OR 5.17 (CI 2.20 to 11.18)) (Figure 7.6). The median turnaround time for blood-based NGS was 16 days (6-34).

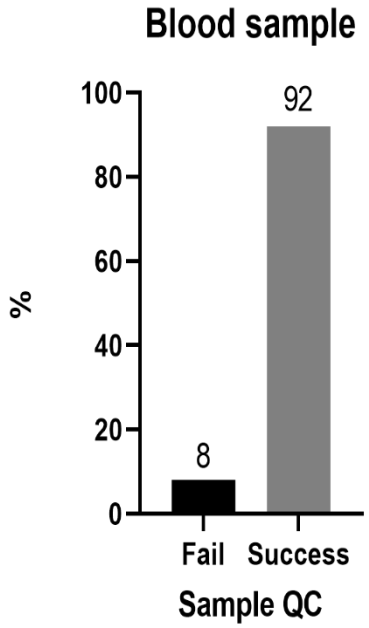

Figure 7.5. Percentage of blood samples failed or passed QC. Failed sample (n=13) and passed sample (n=154).

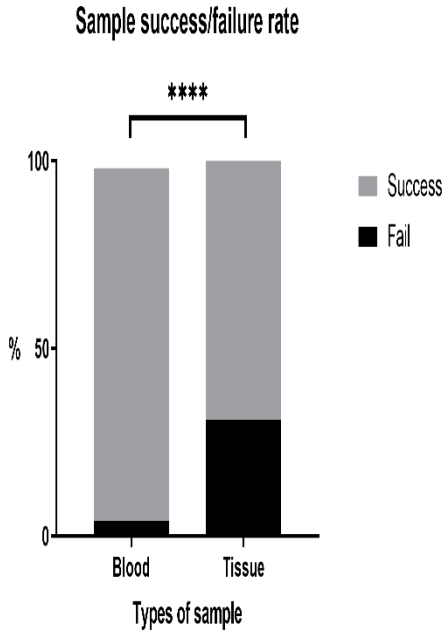

Figure 7.6. Sample success or failure rate. Comparison of blood *vs.* tissue sample QC failure or success rate. Blood sample (n=167) and tissue sample (n=121). Data analysed using Fisher's exact test followed by a Baptista-Pike method to compute confidence Interval (CI), (****$p \leq 0.0001$).

7.5 Genomic analysis of blood based NGS

The median number of cancer related gene mutations detected was two (range: 1–13). *TP53* (52%) was most commonly mutated followed by *AR* (27%), genes associated with DDR (25%), Wnt signalling (20%), PI3K-Akt signalling (10%), MAPK signalling (9%), *PTEN* (9%), TGF-Beta signalling (8%) and others (3%) (Figure 7.7). Microsatellite instability (MSI) status was evaluated, which revealed 2 out of 146 participants (1%) were MSI high and both also harboured DDR gene mutations (Figure 7.7).

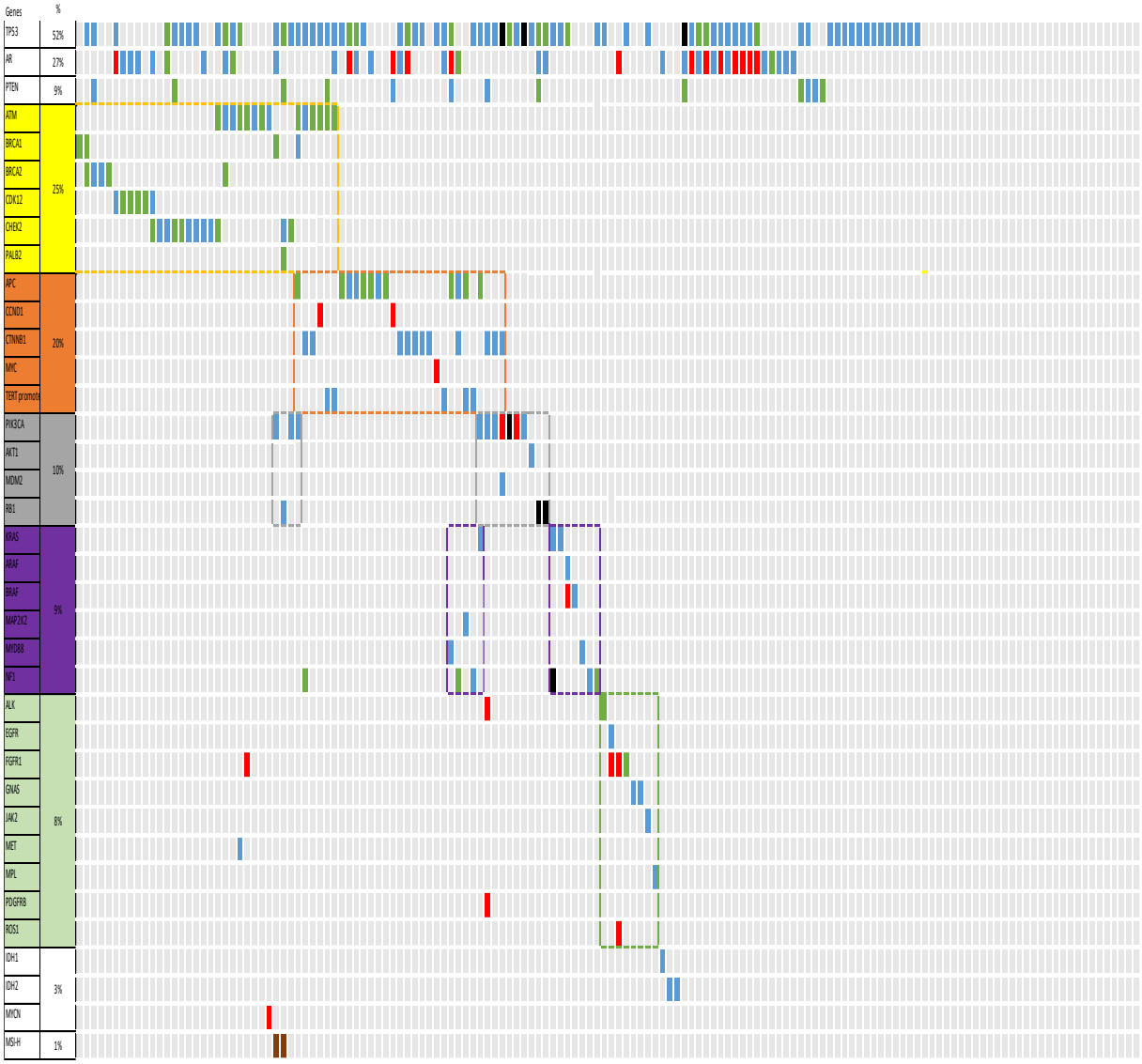

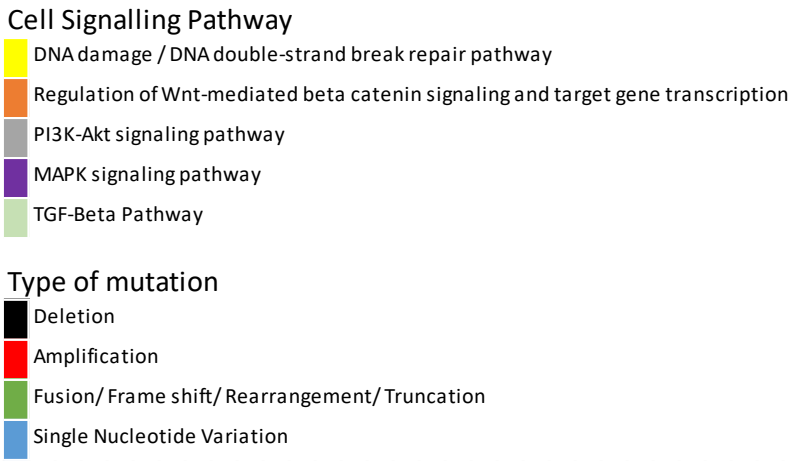

Figure 7.7. Blood based genomic alterations detected in the study cohort. Gene mutations were clustered to specific signaling pathways. Each column represents a cancer related gene mutation and each row represents an individual participant who had available blood biomarker results.

In the blood sample cohort, 47% (n=68/146) harboured at least one actionable gene mutation relevant to any tumour subtypes (Figure 7.8). However, when the actionable gene mutation was narrowed down to mutations clinically relevant to PCa, only 25% (n=36/146) of the cohort demonstrated these mutations (Figure 7.8). These consisted of 14 (*ATM*), 4 (*BRCA1*), 5 (*BRCA2*), 6 (*CDK12*), 12 (*CHEK2*), and 1 (*PALB2*) (Figure 7.9); with one actionable mutation relevant to PCa detected in 30 participants, and two concurrent actionable mutations relevant to PCa in 6 p (n=1; *BRCA1* and *BRCA2* mutation, n=1; *CHEK2* and *CDK12*, n=1; *ATM* and *CHEK2*, n=1; *ATM* and *BRCA2*, n=1; *CHEK2* and *PALB2*, n=1; *ATM* and *BRCA1*).

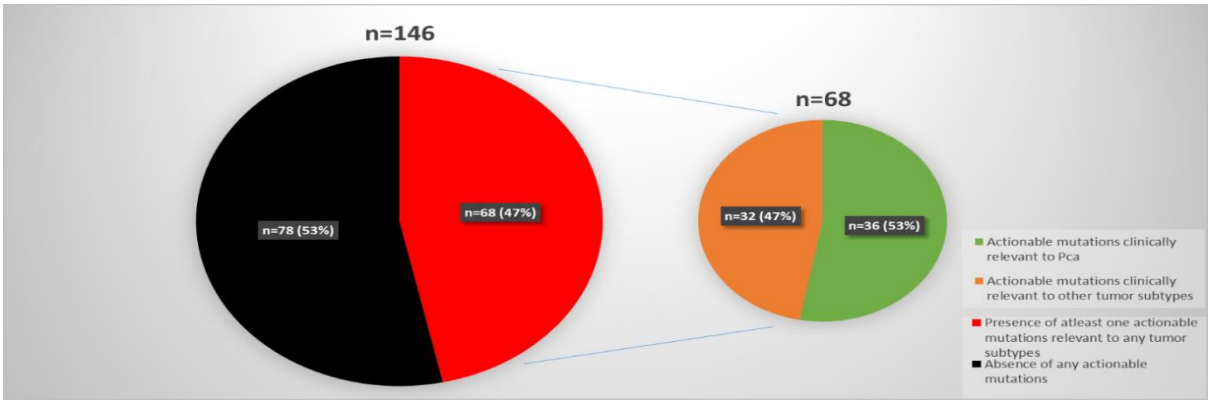

Figure 7.8. Distribution of participants with and without presence of any actionable mutations in blood based NGS. Those with actionable mutations are indicted by red and

those without are indicated by black. The right panel shows distribution actionable mutations clinically relevant to PCa (green segment) and other (orange segment) tumour subtypes.

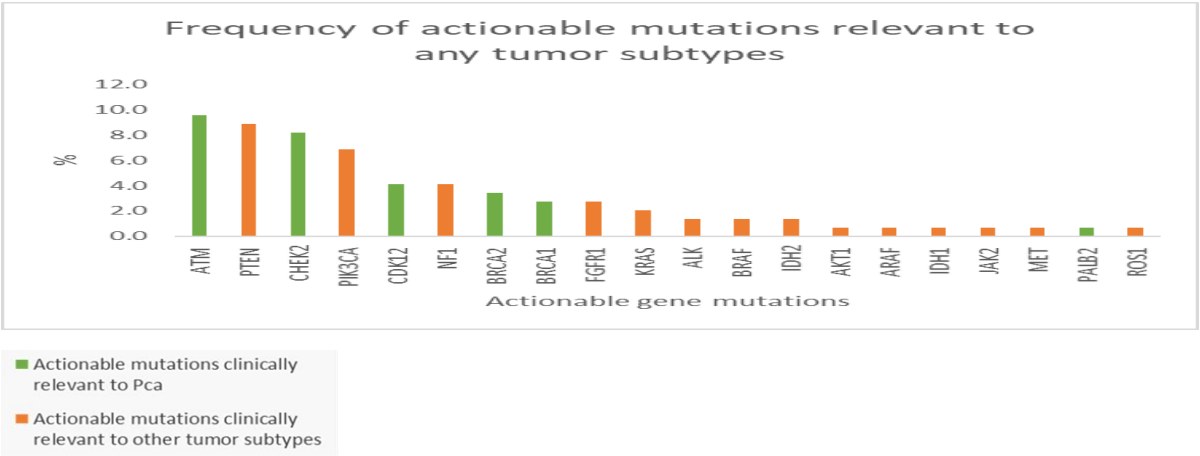

Figure 7.9. Frequency of actionable mutations relevant to PCa and other tumour subtypes in blood based NGS.

7.6 Genomic Analysis of tissue based NGS

The median number of cancer related gene mutations detected was three (range: 1–11). *TP53* (47%) was most commonly mutated followed by *PTEN* (37%), TMPRSS fusion (36%), genes associated with Wnt signalling (28%), PI3K-Akt signaling (24%), *AR* (19%), Cystic adenocarcinoma (19%), DDR (17%), TGF-Beta pathway (17%), Kit signalling (16%), Cell cycle (15%), Chromatin organisation (4%) and Others (25%) (Figure 7.10). One out of 75 (1%) had MSI high and harboured a DDR gene mutation (Figure 7.10).

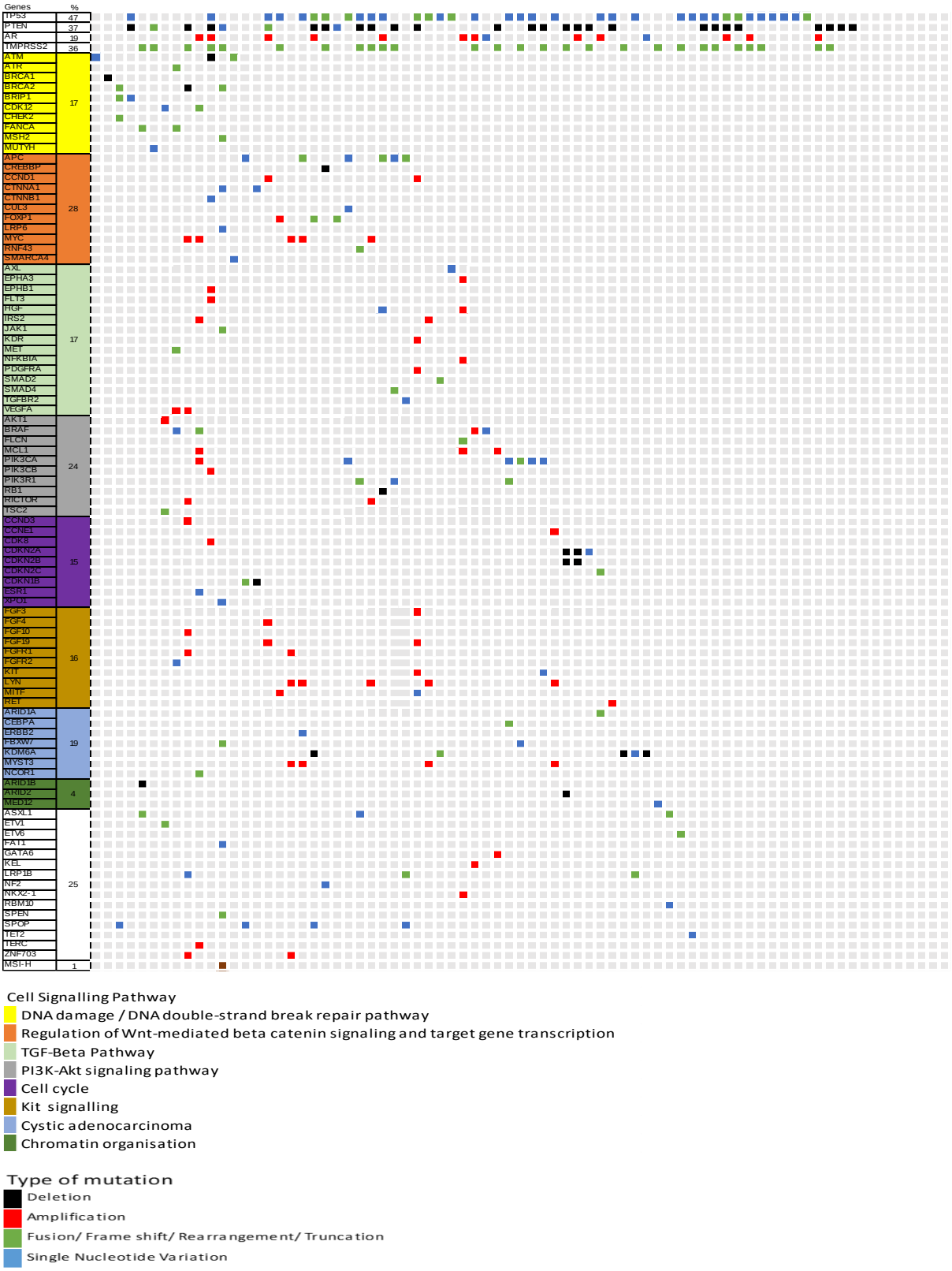

Figure 7.10. Tissue based genomic alterations detected in the study cohort. Gene mutations were clustered to specific signaling pathways. Each column represents an individual particpant who had available tissue biomarker results and each row represents a cancer related gene mutation.

In the tissue cohort, 60% (n=45/75) harboured at least one actionable gene mutation relevant to any tumour subtypes (Figure 7.11). However, when the actionable gene mutation was narrowed down to mutations clinically relevant to PCa, only 13% (n=10/75) of the cohort demonstrated these mutations (Figure 7.11). These included - 3 (*ATM*), 1 (*BRCA1*), 3 (*BRCA2*), 2 (*BRIP1*), 2 (*CDK12*) and 1 (*CHEK2*) (Figure 7.12); with one actionable mutation relevant to PCa detected in 9, and three concurrent actionable mutations relevant to PCa in 1 (*BRCA2, BRIP1 and CHEK2*).

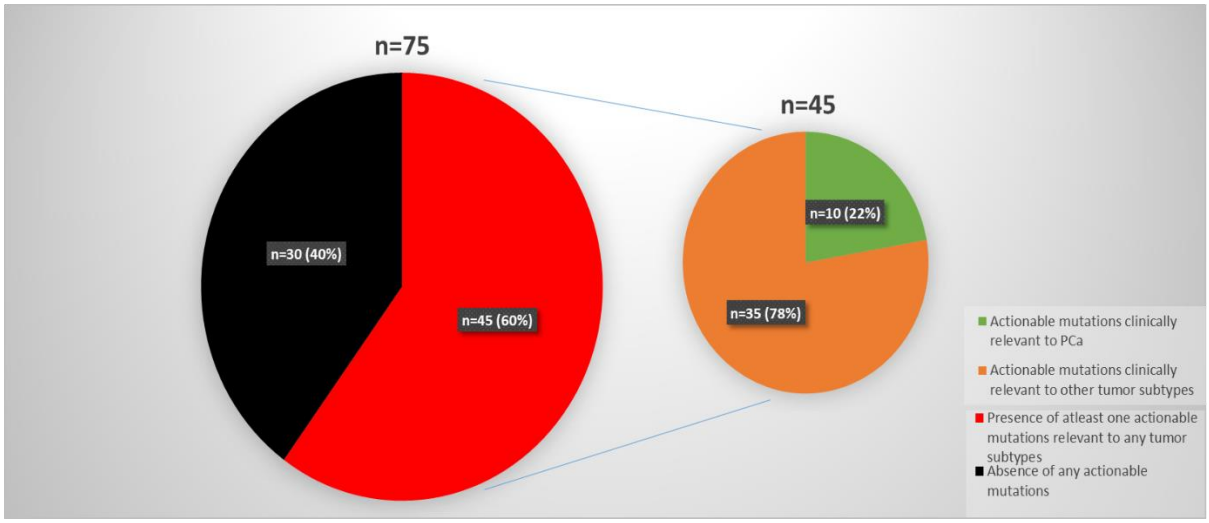

Figure 7.11. Distribution of participants with and without presence of any actionable mutations in tissue based NGS. Those with actionable mutations are indicted by red and those without are indicated by black.The right panel shows distribution of patients with actionable mutations clinically relevant to PCa (green segment) and other tumour subtypes (orange segment).

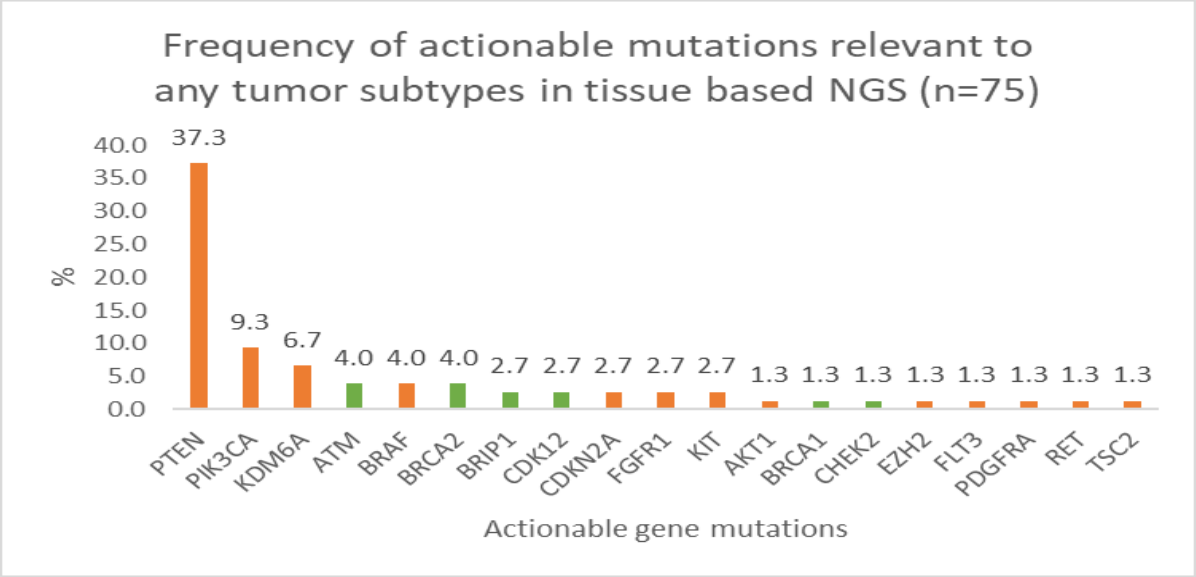

Figure 7.12. Frequency of actionable mutations clinically relevant to PCa and other tumour subtypes in tissue based NGS.

7.7 Discussion

Though AR directed treatments and chemotherapy have resulted in improvement in outcomes in mCRPC, eventually the majority will experience disease progression with limited treatment options (543). This underlines the necessity for additional effective treatments. PARPi have been shown to induce cytotoxicity through synthetic lethality in DDR deficient tumour cells (95, 544). Previous NGS studies have shown that approximately 25-30% of people with advanced PCa, including mCRPC harboured DNA repair defects (95, 398, 545). Largely, these sequencing initiatives have assisted in outlining the practicality and efficacy of molecular profiling in CRPC. However, technical challenges persist in the clinical setting. This study sought to determine whether routine targeted genomic profiling in clinical practice was practicable for people with mCRPC, as well as to describe the frequency of potential actionable mutations in this cohort of Irish men.

FFPE tissue samples are frequently used for many tumour sequencing studies, given that it is most convenient and readily available tissue resource for testing (537, 538). However, FFPE can be challenging due to low RNA or DNA yield (546, 547). In this study, most samples were from archived tissue (66%) and the remaining samples were collected contemporaneously (34%). Only 69% of total tumour tissue samples submitted passed QC and were successfully sequenced. QC failure included failure during hybrid capture, library

construction or computational analysis (46%), insufficient tumour nuclei content (30%) and insufficient DNA extracted (24%). The newly collected tissue samples had significantly lower sample failure rate compared to archived tissue (15% *vs.* 39%, respectively; p=0.0002). The median turnaround time for tissue-based NGS was 13 days (range: 4-33 days). Given that contemporaneous tissue had significantly less sample failure rates compared to archived tissue, routine re-biopsy to collect new tissue for molecular profiling upon disease progression should be considered. Furthermore, the median turnaround time for results was approximately two weeks but in some instance took up to a month. This would add an extra layer of clinical complexity if the anticipated results from sequencing delayed treatment decisions, as well as the possible loss of the period for therapeutic intervention. Thus, consideration to acquire a new tissue biopsy in such a setting can be discussed on an individual basis, with the understanding that technical benefit was observed with contemporaneous biopsies. Additionally, routine re-biopsy sampling of metastases in those with disease progression would help to improve the understanding of drug resistance and further propel the development of precision medicine approach in CRPC (548).

In this tissue-based molecular profiling study in mCRPC, *TP53* (47%) was found to be most commonly mutated followed by *PTEN* (37%), TMPRSS fusion (36%), genes associated with Wnt signalling (28%), PI3K-Akt signalling (24%), *AR* (19%), Cystic adenocarcinoma (19%), DDR (17%), TGF-Beta pathway (17%), Kit signalling (16%), Cell cycle (15%), Chromatin organisation (4%) and MSI high (1%). In this cohort, 60% (n=45/75) harboured at least one actionable gene mutation relevant to any tumour subtypes. However, when the actionable gene mutation was narrowed down to mutations clinically relevant to PCa, only 13% (n=10/75) of the cohort had the mutations.

Taking into account the early success in tissue-based targeted sequencing of CRPC, strategies for monitoring disease through re-biopsy of lesions with NGS profiling were proposed (549). However, this approach necessitates repeat invasive procedures and thus limits the practicality for widespread clinical implementation. For this reason, non-invasive NGS-based approaches to identify clinically relevant molecular alterations in CRPC has been widely studied (132, 133). These studies demonstrated that somatic point mutations, copy-number alterations and insertions/deletions could be detected across a broad spectrum of tumour-derived cell-free DNA (cfDNA) fractions using targeted sequencing of cfDNA. From

this study, 167 blood samples were submitted for sequencing with 92% passing QC and sequenced successfully. The 13 (8%) samples that failed QC were due to failure to meet minimum QC metrics for computational analysis (54%) or laboratory processing (15%) and insufficient DNA extracted (31%). Blood samples had a significantly higher sample success rate compared with tissue samples (92% *vs.* 69%, respectively; p<0.0001) and the median turnaround time for blood-based NGS was 16 days (range: 6-34). In this blood-based molecular profiling of people with mCRPC, *TP53* (52%) was the most commonly mutated followed by *AR* (27%), genes associated with DDR (25%), Wnt signalling (20%), PI3K-Akt signalling (10%), MAPK signalling (9%), *PTEN* (9%), TGF-Beta signalling (8%) and MSI high (1%). In this cohort, 47% (n=68/146) harboured at least one actionable gene mutation relevant to any tumour subtypes. However, when the actionable gene mutation was narrowed down to mutation clinically relevant to PCa, only 25% (n=36/146) of the cohort had the mutations, which was consistent with the mutational rate reported in literatures (545).

This study showed that people with mCRPC harboured a high rate of potential actionable gene mutations within their tumour (47% to 60%) as a whole, which may have therapeutic implications in due course. When narrowed down to current targeted therapy approved in PCa, 13% to 25% harboured somatic alterations in the DDR gene, which is targetable with PARPi (95) and 1% had high MSI, which is targetable with anti-PD-1 (550). These results have an important therapeutic bearing, given the recently reported effective response to PARPi (95) and immune checkpoint blockade in these tumours (550). These strategies offer additional therapeutic options for people with mCRPC who are already heavily pre-treated. The gene alterations detected in this study have involved in a number of important molecular pathways associated with resistance mechanisms that may have developed over the course of anti-androgen treatment (including both AR point mutations and amplifications).

Conceivably, this study has demonstrated that blood-based targeted NGS is clinically feasible, whereby most samples submitted passed QC and were successfully sequenced compared to FFPE tissue-based NGS. Furthermore, the molecular profile results of blood-based targeted NGS were comparable to tissue-based results. While tissue-based NGS is still considered gold-standard (551), this study demonstrated that blood-based targeted NGS could potentially be the benchmark for molecular profiling in PCa instead.

Tissue-based NGS can be used when either blood-based NGS are unsuccessful or results from blood-based NGS are contradictory. Additionally, due to the less invasive nature of blood-based NGS, serial blood-based NGS maybe a possibility in the future to evaluate the dynamic temporal alterations of tumour DNA fractions in cfDNA, which represent different tumour subclone expansion during the course of treatment in response to selective therapeutic pressure (552). For this reason, numerous non-invasive NGS-based approaches have been undertaken to recognise and monitor clinically relevant somatic alterations over time in CRPC (132, 133, 552). Overall, this retrospective study evaluated molecular profiling in the clinical setting and identified technical hurdles that must be overcome to enable widespread clinical use of NGS to monitor molecular alterations in Irish patients with mCRPC.

Chapter 8 – Discussion, future directions and conclusion

8.0 Overall discussion

PCa progression is principally driven by androgens acting through the AR, which enhances cellular proliferation and invasion (553, 554). Thus, AR directed therapies have remained the main treatment modality for people with PCa since 1941, where Huggins *et al.* showed the impressive benefit of ADT through surgical castration (554, 555). Modern advances in anti-androgen therapy have led to the introduction of novel potent AR inhibitors such as enzalutamide, apalutamide and darolutamide (111, 112, 115). These second generation anti-androgens have demonstrated superior efficacy compared to first generation anti-androgen therapy (111, 112, 115). Despite the success of these treatments, primary or acquired resistance remains a substantial clinical dilemma (556).

The mechanisms by which resistance occurs remains a dynamic area of investigation. AR splice variants are one of the best known mechanisms of resistance, however, this has yet to be translated to clinical practice (90, 149). Several other mechanisms of enzalutamide resistance have been identified such as AR mutation (138), loss of AR (557) and activation of AR-independent bypass mechanisms (557). However, the mechanism is not yet fully understood. There is a necessity to develop effective biomarkers that could assist in the improvement of the provision of precision medicine to people with PCa. Ongoing translational approaches have been used to further identify the molecular drivers in the disease as well as mechanisms driving intrinsic and acquired drug resistance.

This study initally investigated circRNAs across a panel of prostate cell lines. This allowed for the potential identification of circRNA signatures reflective of the continuum of prostate pathology, from normal to androgen dependent PCa and ultimately androgen independent PCa. Thus, helping to assess their value as disease biomarkers. Additionally, given the clinical relevance of enzalutamide resistance, circRNAs were also examined in terms of drug resistance.

Universally, the normal group had the highest number of up-regulated circRNAs and the malignant group having the least. Many studies have shown that circRNAs are generally reduced in highly proliferative cells across various cancer subtypes due to rapid cell division diluting the circRNA concentration (224, 379, 380). Five of the circRNAs that were consistently expressed between normal *vs.* malignant group and androgen dependent *vs.* androgen independent group were validated via RT-qPCR. Of particular interest, hsa_circ_0066631 demonstrated notable differential expression across the PCa disease spectrum. Using cell line models, the expression of hsa_circ_0066631 decreased early, where PCa cells were still AR dependent, but increased as the disease progressed to the AR independent stage. A recent study has shown that hsa_circ_0066631 was highly up-regulated in colorectal cancer spherical cells, which harbour features of cancer stem

cells, hence may be involved in the recurrence and metastasis of colorectal cancer (382). Additionally, in colorectal cancer, DCBLD2 overexpression has been linked with tumour progression and poor prognosis (361, 383). DCBLD2 was down-regulated in AR dependent PCa cell lines but up-regulated in AR independent PCa cell lines in parallel with the expression of hsa_circ_0066631. This suggests that the mechanism of malignant progression requires the synergistic effect of both the circRNA and its parental gene. Therefore it may hold potential as a therapeutic candidate in preventing the progression of PCa.

Next circRNAs were investigated in drug resistance, as there are a limited number of studies that have investigated their role in PCa drug resistance (335). The top 5 highly up-regulated circRNAs in Clone 1 *vs.* Control were validated via RT-qPCR. hsa_circ_0001275 overexpression increased resistance to enzalutamide ($p < 0.05$) based on proliferation assays. Further, previous studies in the literature have demonstrated the importance of circRNA in cancer initiation, development and progression (226, 335) through mechanisms such as acting as miRNA sponges (287). The top five most likely miRNA binding sites for hsa_circ_0001275 were validated via RT-qPCR. Three out of the five miRNA, were significantly up-regulated. The findings were in contrast to the early concept of miRNA sponging, whereby these miRNAs should be down-regulated when circRNA was up-regulated. However, more recent studies have shown that rather than acting as a sponge, circRNA may serve as a sanctuary for miRNA stabilisation. For instance, circRNA17 increased the expression of miR-181c-5p by maintaining its stability and in turn, the miRNA decreased the expression of AR-V7 in PCa cells (335). As circRNAs and miRNAs interact in the ceRNAs network, it is possible that despite the increased expression of miRNA witnessed in this study, these miRNAs might not be able to act on their target mRNA since they are bound to circRNAs. Thus, hsa_circ_0001275 may contribute to the development of enzalutamide resistance through these ceRNAs networks. However, further investigations are required to fully delineate the circRNA-miRNA-mRNA network.

circRNA has recently been the center of interest owing to their ability to be detected in human bodily fluids such as saliva, blood and gastric fluid (316, 327, 328). Following from *in vitro* experiments, hsa_circ_0001275 was investigated as a candidate biomarker to inform enzalutamide resistance in plasma samples. Additionally, a number of methodologies for detecting circRNA were assessed as studies in the literature have reported that RT-qPCR may overestimate the actual abundance of circRNA due to multiple PCR products of circRNA caused by rolling cDNA during reverse transcription (389). The level of circRNAs in plasma samples of 44 clinical trial participants (CTRIAL-IE 13-21, NCT02225704) (354) with PCa on enzalutamide treatment was examined. Both probe-based and EvaGreen RT-ddPCR results of hsa_circ_0001275 suggested a trend that

corresponded to the activity of the disease defined by PSA level, however, it did not reach statistical significance. This may be due to small participant numbers and/or copy numbers were close to the limit of detection for RT-ddPCR. Previous literature has described that circRNAs are tissue specific (325) and therefore this may explain the low abundance of hsa_circ_0001275 in plasma, particularly if it is not actively secreted by tumour tissue. In this study cohort, hsa_circ_0001275 was not expressed abundantly in plasma and this presently limits its potential use as a liquid-based predictive biomarker of enzalutamide resistance.

The transcriptomic landscape of enzalutamide resistant PCa was investigated *in vitro* to elucidate potential mechanisms associated with the development of enzalutamide resistance. Though studies in the literature have identified a number of mechanisms that may be involved in the development of enzalutamide resistance, the exact mechanisms are still poorly understood (423). RNA-Seq data generated from the enzalutamide resistant cell line panel demonstrated a large number of DEGs between Clone 1 *vs.* Control with a reduced number of DEGs between Clone 9 *vs.* Control. This highlighted that Clone 1, was phenotypically very different compared to the Control cell line. Thus, the dysregulated genes in Clone 1 *vs.* Control may be investigated further to identify a clinical signature that could be used as biomarker to inform drug resistance or as a potential for therapeutic targets. The Hallmarks GSEA of DEGs in Clone 1 *vs.* Control showed eight distinct pathways involved in *'terms'* of proliferation, cell cycle, wound healing, fibrosis, metastasis, cell signalling and DNA repair. EMT was one such hallmark pathway enriched along with other two pathways, which were reported to be closely related to EMT, known as TGF-β signalling and apical junctions. Correspondingly, KEGG GSEA of DEGs in Clone 1 *vs.* Control were enriched for *'terms'* broadly related to morphological changes further supporting the role of EMT in the development of enzalutamide resistance. Also, several signalling pathways were identified in KEGG enrichment such as TGF-β pathway and MAP Kinase pathway, which have been described to regulate and mediate EMT previously (440). Similarly, both GO biological and molecular process GSEA of DEGs for Clone 1 *vs.* Control supported roles of EMT in the development of enzalutamide resistance in PCa. Besides association with EMT, a number of enriched KEGG *'terms'* were broadly related to calcium homeostasis and signalling. A recent study in the literature demonstrated that increased in store-operated calcium entry through voltage gated calcium channels CaV1.3 promoted resistance to bicalutamide in PCa (441). Thus, calcium homeostasis and signalling may be involved in the development of enzalutamide resistant PCa. GO enrichment of DEGs in Clone 1 *vs.* Control also revealed the possible importance of membrane transporters in enzalutamide resistance. Overexpression of the ABC transporter superfamily has been well recognised as a reason for multi drug resistance in cancer cells (442). RNA-Seq data identified several pathways that may provide

more insight into the molecular mechanism of enzalutamide resistance in PCa. This serves as an essential first step in understanding the dynamic changes to the transcriptome in enzalutamide resistant PCa *in vitro*.

The prospect of EMT and NEPCa development contributing to enzalutamide resistance in PCa was further examined via RNA-Seq data generated from the enzalutamide resistance panel to identify a potential EMT and/or NEPCa signature. Also, DEGs from RNA-Seq were interogated to evaluate potential small molecular compounds, which may be used to prevent the development of enzalutamide resistance or indeed resensitise to the drug. The EMT pathway is of importance because it has been demonstrated to be a hallmark of metastatic cancer spread (211). Furthermore, recent *in vitro* studies have linked EMT to the development of PCa resistance to ADT and chemotherapy (446, 447). In addition to EMT, NEPCa differentiation is also an emerging mechanism of resistance to AR targeted therapy that involves epithelial plasticity (450). The EMT pathway was significantly enriched in the Hallmark pathway of Clone 1 *vs.* Control. There were 177 up-regulated and 118 down-regulated EMT related genes identified in Clone 1 *vs.* Control. Common EMT markers from studies in the literature were chosen for RT-qPCR validation. ECAD was significantly down-regulated while NCAD, ZEB2 and TWIST1 was significantly increased in Clone 1 *vs.* Control. Thus, suggesting that the strongly enzalutamide resistant clone expressed features of EMT. In Clone 9 *vs.* Control, ECAD was significantly down-regulated while VIM and ZEB1 were significantly increased, suggesting that the weakly enzalutamide resistant clone also expressed features of EMT. The expression of ECAD and NCAD was further confirmed using western blot. The loss of the intercellular networks in epithelial cells due to the alterations of EMT transcription factors represents a crucial step that permits tumour cells to detach from their primary location (481). Both Clone 1 *vs.* Control and Clone 9 *vs.* Control expressed different EMT-related transcription factors, suggesting that separate pathways were involved in the EMT process, possibly resulting in differing enzalutamide resistance status in the cell lines.

In terms of NEPCa, 10 DEGs in Clone 1 *vs.* Control were found to be consistently expressed in two NEPCa data sets. Thus, creating a signature gene set which may inform development of NEPCa. The common neuroendocrine markers BRN2, CHGA and NSE were significantly up-regulated in Clone 1 *vs.* Control. This suggested that strongly enzalutamide resistant clones acquired neural characteristics and transitioned towards a neuroendocrine state. A study have shown that BRN2 served as the key driver of NEPCa differentiation and facilitated aggressive growth of enzalutamide CRPC *in vitro*. Both CHGA and NSE expression were identified as overexpressed in neuroendocrine-like enzalutamide resistance cells previously (531). NEPCa is widely recognised as a CRPC subtype that is resistant to androgen pathway inhibitors (528, 529). DEGs in Clone 1 *vs.* Control were also

queried using CMap and Isotretinoin was one of the top five small molecules, which had the potential to reverse enzalutamide resistance. Research found that combining Isotretinoin with ADT improved PSA response in people with advanced hormone naive PCa with minimal side effects (496). To present, no study has investigated the use of Isotretinoin in combination with second-generation hormonal treatment in PCa.

The landscape of actionable gene mutations in 164 Irish men with mCRPC who progressed on a second generation hormonotherapy (enzalutamide or abiraterone) were evaluated with targeted NGS. Blood and tissue specimens were included. Although molecular profiling is not currently the clinical standard of care for PCa, more evidence is emerging to support its use in guiding therapeutic decisions (534-536). Several studies have shown that molecular profiling of clinically relevant somatic alterations is a feasible strategy in advanced PCa (537, 538). These sequencing initiatives have largely contributed to defining the feasibility and efficacy of molecular profiling in CRPC, but technical challenges persist in the clinical setting. Only 69% of all tumour tissue samples submitted passed QC and were sequenced successfully. Tumour tissue samples QC failures included failures during hybrid capture, library construction, or computational analysis (46%) as well as insufficient tumour nuclei content (30%) and insufficient DNA extracted (24%). This is not unexpected since previous studies have reported low RNA and DNA yield from archival FFPE tissue samples (546, 547). As high as 92% of blood samples submitted passed QC and were sequenced successfully. Blood sample QC failure included failure to meet minimum QC metrics for computational analysis (54%) or laboratory processing (15%) and insufficient DNA extracted (31%). In this study a high rate of potentially actionable gene mutations within their tumour (between 47% and 60%), which could have therapeutic implications in the future, were identified. Importantly, between 13% and 25% of cases had somatic alterations in the DDR gene, which is targetable with PARPi (95). Given the recently reported effective response to PARPi (95) and immune checkpoint blockade in these tumours (550), these findings have significant therapeutic implications in those with mCRPC who are already heavily pre-treated. Blood-based targeted NGS was clinically practicable, with the majority of samples submitted passing QC and being successfully sequenced when compared to FFPE tissue-based NGS. While tissue-based NGS remains the gold standard (551), this study demonstrated that blood-based targeted NGS could equally be useful for molecular profiling in PCa. Additionally, the frequency of DDR gene mutation in this Irish cohort with mCRPC was consistent with previous NGS studies which had shown approximately 25-30% of people with advanced PCa, including mCRPC, harboured DNA repair defects (95, 398, 545).

8.1 Future Work

This study is the first to show that the overexpression of certain circRNAs are invovled in enzalutamide resistance in PCa. It also established a solid approach from discovery to validation of circRNA that could be involved in cancer-related pathways. Though current research reveals that hsa_circ_0001275 has a role in enzalutamide resistance, the particular functional mechanisms underlying this remain unknown. The regulatory role of the circRNA-miRNA-mRNA network (such as hsa_circ_0001275/miR-361-5p/STAT6) was preliminarily investigated. According to the early theory of miRNA sponging (287), these miRNA would be expected to be down-regulated when circRNA is up-regulated but the results were contrary to this assumption. This is in keeping with more recent research, which suggests that circRNA can act as a refuge for miRNA stabilisation rather than just operating as a sponge (335). Further experiments such as a pull-down assay utilising biotinylated oligos to evaluate the interaction of circRNA with its target miRNA, circRNA silencing experiment to evaluate the stability of miRNA, miRNA mimics or antimiRs experiments to evaluate this network are all necessary to delineate the ceRNA network. The study used a single isogenic cell line model of enzalutamide resistance developed by Korpal *et al.* (138) and it would be valuable to explore the overexpression of hsa_circ_0001275 in additional enzalutamide sensitive PCa cell lines to further explore its association with drug resistance. Also, an *in vivo* investigation to evaluate the functional importance of hsa_circ_0001275 in modifying enzalutamide sensitivity is required. This may pave the way for more diagnostic, therapeutic, and functional studies into circRNAs and their role in enzalutamide resistant PCa.

Clinically, hsa_circ_0001275 was not expressed abundantly in plasma. Though the RT-ddPCR results for plasma derived hsa_circ_0001275 showed a trend that corresponded to the activity of the disease as defined by the PSA level of participants on enzalutamide treatment, it did not reach statistical significance. In the future, it may be necessary to first examine circRNA expression using an explant or organoid-based model to evaluate whether the circRNA of interest can be detected within conditioned medium, which will provide a basis for circRNA testing in plasma samples. Additionally, it would be ideal to investigate tissue circRNA expression by obtaining tissue biopsy upon disease progression. Also, the sample size of this study was relatively small and thus should be investigated in a larger cohort of people receiving enzalutamide alone.

RNA-Seq study of the enzalutamide resistant panel identified several pathways that may provide more insight into the molecular mechanisms of enzalutamide resistance in PCa. These key pathways included EMT, membrane transporter and calcium homeostasis. Going forward, the future work should validate the top dysregulated genes according to FC involved in each pathway respectively, followed by functional experiments *in vitro* and *in vivo*. This will allow for the

identification of potential therapeutic targets to combat the development of enzalutamide resistance in PCa. This work also discovered ten NEPCa gene signature marker in enzalutamide resistant cell lines, which suggests the possibility of NEPCa transformation contributing to enzalutamide resistance. Further validation via RT-qPCR is required followed by functional experiments *in vitro* as well as clinical validation of the gene signature in clinical samples.

From the interogation of small compounds via CMap, Isotretinoin may potentially be used in combination therapy with enzalutamide to stop or delay the development of enzalutamide resistance. More research is warranted in this space.

8.2 Conclusion

This study demonstrated that hsa_circ_0001275 was highly expressed in enzalutamide resistant cell lines and provided the first ever data to suggest that the overexpression of certain circRNAs provides a protective role against enzalutamide *in vitro*. Furthermore, data from this study suggests that circRNAs may serve as a sanctuary for miRNA stabilisation. These novel circRNAs are potential mechanisms of drug resistance. This work also provides a large database to examine circRNA-miRNA-mRNA network in PCa. The clinical data regarding hsa_circ_0001275 plasma expression mirrored disease activity according to PSA level, and suggests an association with enzalutamide resistance.

In the RNA-Seq study, a large number of DEGs were identified between Clone 1 compared to Control. This suggests that Clone 1, was phenotypically very different compared to the Control cell line. KEGG pathway analysis and Hallmark gene enrichment identified EMT as a major pathway. The expression of EMT markers from both strongly and weakly enzalutamide resistant clones were differentially expressed which suggested the possibility of EMT expression reprogramming during progression of enzalutamide resistance. This study also identified numerous other pathways via RNA-Seq data that may provide a greater insight into the molecular mechanisms of enzalutamide resistance in PCa. This serves as an essential first step in understanding the dynamic changes to the transcriptome in enzalutamide resistant PCa *in vitro*.

Additionally, the retrospective analysis of the targeted NGS investigation revealed that the incidence of DDR gene mutations in the Irish population with mCRPC was comparable to earlier NGS studies in the literature.

In conclusion, the findings in this study provides beneficial groundwork for further exploration of circRNAs potential as biomarkers and therapeutic targets for drug-resistant PCa, and this collection of work sets the foundation for identifying new biomarkers and targets for therapy in PCa, which could utimately improve outcomes for people impacted by this disease.

References

1. Lowsley OS. The development of the human prostate gland with reference to the development of other structures at the neck of the urinary bladder. American Journal of Anatomy. 1912;13(3):299-349.
2. McNeal JE. Anatomy of the prostate and morphogenesis of BPH. Prog Clin Biol Res. 1984;145:27-53.
3. McNeal JE. The zonal anatomy of the prostate. Prostate. 1981;2(1):35-49.
4. Leach DA, Need EF, Toivanen R, Trotta AP, Palethorpe HM, Tamblyn DJ, et al. Stromal androgen receptor regulates the composition of the microenvironment to influence prostate cancer outcome. Oncotarget. 2015;6(18):16135-50.
5. Lilja H, Abrahamsson PA. Three predominant proteins secreted by the human prostate gland. Prostate. 1988;12(1):29-38.
6. Eggener SE, Cifu AS, Nabhan C. Prostate Cancer Screening. Jama. 2015;314(8):825-6.
7. Putzi MJ, De Marzo AM. Morphologic transitions between proliferative inflammatory atrophy and high-grade prostatic intraepithelial neoplasia. Urology. 2000;56(5):828-32.
8. Packer JR, Maitland NJ. The molecular and cellular origin of human prostate cancer. Biochim Biophys Acta. 2016;1863(6 Pt A):1238-60.
9. Partin AW RR. The molecular biology, endocrinology, and physiology of the prostate and seminal vesicles. In: Walsh PC, Retik A, Vaughan E, et al. . 8th ed. Philadelphia Saunders 2002.
10. Berry SJ, Coffey DS, Walsh PC, Ewing LL. The development of human benign prostatic hyperplasia with age. J Urol. 1984;132(3):474-9.
11. Tan MH, Li J, Xu HE, Melcher K, Yong EL. Androgen receptor: structure, role in prostate cancer and drug discovery. Acta Pharmacol Sin. 2015;36(1):3-23.
12. Cooke PS, Young P, Cunha GR. Androgen receptor expression in developing male reproductive organs. Endocrinology. 1991;128(6):2867-73.
13. NCI. Combination Therapy Improves Survival for Some Men with Recurrent Prostate Cancer. 2017.
14. Saraon P, Jarvi K, Diamandis EP. Molecular alterations during progression of prostate cancer to androgen independence. Clin Chem. 2011;57(10):1366-75.

15. Lonergan PE, Tindall DJ. Androgen receptor signaling in prostate cancer development and progression. J Carcinog. 2011;10:20.

16. Umesono K, Evans RM. Determinants of target gene specificity for steroid/thyroid hormone receptors. Cell. 1989;57(7):1139-46.

17. Cutress ML, Whitaker HC, Mills IG, Stewart M, Neal DE. Structural basis for the nuclear import of the human androgen receptor. J Cell Sci. 2008;121(Pt 7):957-68.

18. Izumi K, Mizokami A, Lin WJ, Lai KP, Chang C. Androgen receptor roles in the development of benign prostate hyperplasia. Am J Pathol. 2013;182(6):1942-9.

19. Fang Y, Fliss AE, Robins DM, Caplan AJ. Hsp90 regulates androgen receptor hormone binding affinity in vivo. J Biol Chem. 1996;271(45):28697-702.

20. Picard D. The Role of Heat-Shock Proteins in the Regulation of Steroid Receptor Function. In: Freedman LP, editor. Molecular Biology of Steroid and Nuclear Hormone Receptors. Boston, MA: Birkhäuser Boston; 1998. p. 1-18.

21. Zoubeidi A, Zardan A, Beraldi E, Fazli L, Sowery R, Rennie P, et al. Cooperative interactions between androgen receptor (AR) and heat-shock protein 27 facilitate AR transcriptional activity. Cancer Res. 2007;67(21):10455-65.

22. Gao N, Zhang J, Rao MA, Case TC, Mirosevich J, Wang Y, et al. The role of hepatocyte nuclear factor-3 alpha (Forkhead Box A1) and androgen receptor in transcriptional regulation of prostatic genes. Mol Endocrinol. 2003;17(8):1484-507.

23. Grabowska MM, Kelly SM, Reese AL, Cates JM, Case TC, Zhang J, et al. Nfib Regulates Transcriptional Networks That Control the Development of Prostatic Hyperplasia. Endocrinology. 2016;157(3):1094-109.

24. Zhao Y, Tindall DJ, Huang H. Modulation of androgen receptor by FOXA1 and FOXO1 factors in prostate cancer. Int J Biol Sci. 2014;10(6):614-9.

25. Dehm SM, Tindall DJ. Molecular regulation of androgen action in prostate cancer. J Cell Biochem. 2006;99(2):333-44.

26. Bryce AH, Antonarakis ES. Androgen receptor splice variant 7 in castration-resistant prostate cancer: Clinical considerations. Int J Urol. 2016;23(8):646-53.

27. Dehm SM, Tindall DJ. Alternatively spliced androgen receptor variants. Endocr Relat Cancer. 2011;18(5):R183-96.

28. Lu J, Van der Steen T, Tindall DJ. Are androgen receptor variants a substitute for the full-length receptor? Nat Rev Urol. 2015;12(3):137-44.

29. Hu R, Dunn TA, Wei S, Isharwal S, Veltri RW, Humphreys E, et al. Ligand-independent androgen receptor variants derived from splicing of cryptic exons signify hormone-refractory prostate cancer. Cancer Res. 2009;69(1):16-22.

30. Renee E. Vickman OEF, Daniel C. Moline, Donald J. Vander Griend, Praveen Thumbikat, Simon W. Hayward,. The role of the androgen receptor in prostate development and benign prostatic hyperplasia: A review,. Asian Journal of Urology,. 2019,.

31. Bray F, Ferlay J, Soerjomataram I, Siegel RL, Torre LA, Jemal A. Global cancer statistics 2018: GLOBOCAN estimates of incidence and mortality worldwide for 36 cancers in 185 countries. CA Cancer J Clin. 2018;68(6):394-424.

32. Ferlay J, Colombet M, Soerjomataram I, Mathers C, Parkin DM, Pineros M, et al. Estimating the global cancer incidence and mortality in 2018: GLOBOCAN sources and methods. Int J Cancer. 2019;144(8):1941-53.

33. Quinn M, Babb P. Patterns and trends in prostate cancer incidence, survival, prevalence and mortality. Part I: international comparisons. BJU Int. 2002;90(2):162-73.

34. Foundation PC. Prostate Cancer Survival Rates [Internet]. 2018.

35. Ireland NCR. Cancer in Ireland 1994-2017 with estimates for 2017-2019: Annual report of the National Cancer Registry 2019.

36. De Angelis R, Sant M, Coleman MP, Francisci S, Baili P, Pierannunzio D, et al. Cancer survival in Europe 1999-2007 by country and age: results of EUROCARE--5-a population-based study. Lancet Oncol. 2014;15(1):23-34.

37. Delongchamps NB, Singh A, Haas GP. The role of prevalence in the diagnosis of prostate cancer. Cancer Control. 2006;13(3):158-68.

38. Sakr WA, Grignon DJ, Crissman JD, Heilbrun LK, Cassin BJ, Pontes JJ, et al. High grade prostatic intraepithelial neoplasia (HGPIN) and prostatic adenocarcinoma between the ages of 20-69: an autopsy study of 249 cases. In Vivo. 1994;8(3):439-43.

39. Baquet CR, Horm JW, Gibbs T, Greenwald P. Socioeconomic factors and cancer incidence among blacks and whites. J Natl Cancer Inst. 1991;83(8):551-7.

40. Parker PM, Rice KR, Sterbis JR, Chen Y, Cullen J, McLeod DG, et al. Prostate cancer in men less than the age of 50: a comparison of race and outcomes. Urology. 2011;78(1):110-5.

41. Tewari A, Horninger W, Pelzer AE, Demers R, Crawford ED, Gamito EJ, et al. Factors contributing to the racial differences in prostate cancer mortality. BJU Int. 2005;96(9):1247-52.

42. Agalliu I, Gern R, Leanza S, Burk RD. Associations of high-grade prostate cancer with BRCA1 and BRCA2 founder mutations. Clin Cancer Res. 2009;15(3):1112-20.

43. Chan JM, Gann PH, Giovannucci EL. Role of diet in prostate cancer development and progression. J Clin Oncol. 2005;23(32):8152-60.

44. Giovannucci EL, Liu Y, Leitzmann MF, Stampfer MJ, Willett WC. A prospective study of physical activity and incident and fatal prostate cancer. Arch Intern Med. 2005;165(9):1005-10.

45. MacInnis RJ, English DR. Body size and composition and prostate cancer risk: systematic review and meta-regression analysis. Cancer Causes Control. 2006;17(8):989-1003.

46. Carter BS, Bova GS, Beaty TH, Steinberg GD, Childs B, Isaacs WB, et al. Hereditary prostate cancer: epidemiologic and clinical features. J Urol. 1993;150(3):797-802.

47. Smith JR, Freije D, Carpten JD, Gronberg H, Xu J, Isaacs SD, et al. Major susceptibility locus for prostate cancer on chromosome 1 suggested by a genome-wide search. Science. 1996;274(5291):1371-4.

48. Schaid DJ. The complex genetic epidemiology of prostate cancer. Hum Mol Genet. 2004;13 Spec No 1:R103-21.

49. Giovannucci E, Ascherio A, Rimm EB, Colditz GA, Stampfer MJ, Willett WC. A prospective cohort study of vasectomy and prostate cancer in US men. Jama. 1993;269(7):873-7.

50. Checkoway H, DiFerdinando G, Hulka BS, Mickey DD. Medical, life-style, and occupational risk factors for prostate cancer. Prostate. 1987;10(1):79-88.

51. Matzkin H, Soloway MS. Cigarette smoking: a review of possible associations with benign prostatic hyperplasia and prostate cancer. Prostate. 1993;22(4):277-90.

52. Hamilton W, Sharp DJ, Peters TJ, Round AP. Clinical features of prostate cancer before diagnosis: a population-based, case-control study. Br J Gen Pract. 2006;56(531):756-62.

53. NCCN. NCCN Clinical Practice Guidelines in Prostate Cancer. 2020(Version 1.2020).

54. Buyyounouski MK CP, Kattan MW, et al. Prostate. In: AJCC Cancer Staging Manual,. Springer, . 2017(8th, Amin MB (Ed),):p.715. .

55. SEER Cancer Statistics Review 1975-2015 [Internet]. 2018. Available from: https://seer.cancer.gov/statfacts/html/prost.html.

56. Penson D.F. APC. The Natural History of Prostate Cancer. In: Ablin R.J., Mason M.D. (eds) Metastasis of Prostate Cancer. Cancer Metastasis – Biology and Treatment,. Springer, Dordrecht; 2008.

57. Stamey TA, Yang N, Hay AR, McNeal JE, Freiha FS, Redwine E. Prostate-specific antigen as a serum marker for adenocarcinoma of the prostate. N Engl J Med. 1987;317(15):909-16.

58. Allan GM, Chetner MP, Donnelly BJ, Hagen NA, Ross D, Ruether JD, et al. Furthering the prostate cancer screening debate (prostate cancer specific mortality and associated risks). Can Urol Assoc J. 2011;5(6):416-21.

59. Chou R, Dana T, Bougatsos C, Fu R, Blazina I, Gleitsmann K, et al. U.S. Preventive Services Task Force Evidence Syntheses, formerly Systematic Evidence Reviews. Treatments for Localized Prostate Cancer: Systematic Review to Update the 2002 US Preventive Services Task Force Recommendation. Rockville (MD): Agency for Healthcare Research and Quality (US); 2011.

60. Haythorn MR, Ablin RJ. Prostate-specific antigen testing across the spectrum of prostate cancer. Biomark Med. 2011;5(4):515-26.

61. Hugosson J, Carlsson S. Overdetection in screening for prostate cancer. Curr Opin Urol. 2014;24(3):256-63.

62. Sanda MG, Dunn RL, Michalski J, Sandler HM, Northouse L, Hembroff L, et al. Quality of life and satisfaction with outcome among prostate-cancer survivors. N Engl J Med. 2008;358(12):1250-61.

63. Klotz L. Prostate cancer overdiagnosis and overtreatment. Curr Opin Endocrinol Diabetes Obes. 2013;20(3):204-9.

64. Brawer MK, Aramburu EA, Chen GL, Preston SD, Ellis WJ. The inability of prostate specific antigen index to enhance the predictive the value of prostate specific antigen in the diagnosis of prostatic carcinoma. J Urol. 1993;150(2 Pt 1):369-73.

65. Hu JC, Williams SB, Carter SC, Eggener SE, Prasad S, Chamie K, et al. Population-based assessment of prostate-specific antigen testing for prostate cancer in the elderly. Urol Oncol. 2015;33(2):69.e29-34.

66. Nadler RB, Humphrey PA, Smith DS, Catalona WJ, Ratliff TL. Effect of inflammation and benign prostatic hyperplasia on elevated serum prostate specific antigen levels. J Urol. 1995;154(2 Pt 1):407-13.

67. Gaudreau PO, Stagg J, Soulieres D, Saad F. The Present and Future of Biomarkers in Prostate Cancer: Proteomics, Genomics, and Immunology Advancements. Biomark Cancer. 2016;8(Suppl 2):15-33.

68. Thompson IM, Pauler DK, Goodman PJ, Tangen CM, Lucia MS, Parnes HL, et al. Prevalence of prostate cancer among men with a prostate-specific antigen level < or =4.0 ng per milliliter. N Engl J Med. 2004;350(22):2239-46.

69. Parekh DJ, Ankerst DP, Troyer D, Srivastava S, Thompson IM. Biomarkers for prostate cancer detection. J Urol. 2007;178(6):2252-9.

70. Filella X, Foj L, Auge JM, Molina R, Alcover J. Clinical utility of %p2PSA and prostate health index in the detection of prostate cancer. Clin Chem Lab Med. 2014;52(9):1347-55.

71. Stephan C, Vincendeau S, Houlgatte A, Cammann H, Jung K, Semjonow A. Multicenter evaluation of [-2]proprostate-specific antigen and the prostate health index for detecting prostate cancer. Clin Chem. 2013;59(1):306-14.

72. Mottet N, Bellmunt J, Bolla M, Briers E, Cumberbatch MG, De Santis M, et al. EAU-ESTRO-SIOG Guidelines on Prostate Cancer. Part 1: Screening, Diagnosis, and Local Treatment with Curative Intent. Eur Urol. 2017;71(4):618-29.

73. Mehta S, Shelling A, Muthukaruppan A, Lasham A, Blenkiron C, Laking G, et al. Predictive and prognostic molecular markers for cancer medicine. Ther Adv Med Oncol. 2010;2(2):125-48.

74. D'Amico AV, Whittington R, Malkowicz SB, Cote K, Loffredo M, Schultz D, et al. Biochemical outcome after radical prostatectomy or external beam radiation therapy for patients with clinically localized prostate carcinoma in the prostate specific antigen era. Cancer. 2002;95(2):281-6.

75. Gittes RF. Carcinoma of the prostate. N Engl J Med. 1991;324(4):236-45.

76. Bostwick DG. Gleason grading of prostatic needle biopsies. Correlation with grade in 316 matched prostatectomies. Am J Surg Pathol. 1994;18(8):796-803.

77. Epstein JI, Zelefsky MJ, Sjoberg DD, Nelson JB, Egevad L, Magi-Galluzzi C, et al. A Contemporary Prostate Cancer Grading System: A Validated Alternative to the Gleason Score. Eur Urol. 2016;69(3):428-35.

78. Leapman MS, Cowan JE, Simko J, Roberge G, Stohr BA, Carroll PR, et al. Application of a Prognostic Gleason Grade Grouping System to Assess Distant Prostate Cancer Outcomes. Eur Urol. 2017;71(5):750-9.

79. Mathieu R, Moschini M, Beyer B, Gust KM, Seisen T, Briganti A, et al. Prognostic value of the new Grade Groups in Prostate Cancer: a multi-institutional European validation study. Prostate Cancer Prostatic Dis. 2017;20(2):197-202.

80. Borque A, Rubio-Briones J, Esteban LM, Sanz G, Dominguez-Escrig J, Ramirez-Backhaus M, et al. Implementing the use of nomograms by choosing threshold points in predictive models: 2012 updated Partin Tables vs a European predictive nomogram for organ-confined disease in prostate cancer. BJU Int. 2014;113(6):878-86.

81. Kattan MW, Eastham JA, Wheeler TM, Maru N, Scardino PT, Erbersdobler A, et al. Counseling men with prostate cancer: a nomogram for predicting the presence of small, moderately differentiated, confined tumors. J Urol. 2003;170(5):1792-7.

82. Makarov DV, Trock BJ, Humphreys EB, Mangold LA, Walsh PC, Epstein JI, et al. Updated nomogram to predict pathologic stage of prostate cancer given prostate-specific antigen level, clinical stage, and biopsy Gleason score (Partin tables) based on cases from 2000 to 2005. Urology. 2007;69(6):1095-101.

83. Kattan MW, Wheeler TM, Scardino PT. Postoperative nomogram for disease recurrence after radical prostatectomy for prostate cancer. J Clin Oncol. 1999;17(5):1499-507.

84. Ondracek RP, Kattan MW, Murekeyisoni C, Yu C, Kauffman EC, Marshall JR, et al. Validation of the Kattan Nomogram for Prostate Cancer Recurrence After Radical Prostatectomy. J Natl Compr Canc Netw. 2016;14(11):1395-401.

85. Voon PJ, Kong HL. Tumour genetics and genomics to personalise cancer treatment. Ann Acad Med Singapore. 2011;40(8):362-8.

86. Walther A, Johnstone E, Swanton C, Midgley R, Tomlinson I, Kerr D. Genetic prognostic and predictive markers in colorectal cancer. Nat Rev Cancer. 2009;9(7):489-99.

87. Fizazi K, Tran N, Fein L, Matsubara N, Rodriguez-Antolin A, Alekseev BY, et al. Abiraterone plus Prednisone in Metastatic, Castration-Sensitive Prostate Cancer. N Engl J Med. 2017;377(4):352-60.

88. Sweeney CJ, Chen YH, Carducci M, Liu G, Jarrard DF, Eisenberger M, et al. Chemohormonal Therapy in Metastatic Hormone-Sensitive Prostate Cancer. N Engl J Med. 2015;373(8):737-46.

89. Nelson WG, De Marzo AM, Isaacs WB. Prostate cancer. N Engl J Med. 2003;349(4):366-81.

90. Antonarakis ES, Lu C, Wang H, Luber B, Nakazawa M, Roeser JC, et al. AR-V7 and resistance to enzalutamide and abiraterone in prostate cancer. N Engl J Med. 2014;371(11):1028-38.

91. Antonarakis ES, Lu C, Luber B, Wang H, Chen Y, Nakazawa M, et al. Androgen Receptor Splice Variant 7 and Efficacy of Taxane Chemotherapy in Patients With Metastatic Castration-Resistant Prostate Cancer. JAMA Oncol. 2015;1(5):582-91.

92. Bernemann C, Schnoeller TJ, Luedeke M, Steinestel K, Boegemann M, Schrader AJ, et al. Expression of AR-V7 in Circulating Tumour Cells Does Not Preclude Response to Next Generation Androgen Deprivation Therapy in Patients with Castration Resistant Prostate Cancer. Eur Urol. 2017;71(1):1-3.

93. Mateo J, Boysen G, Barbieri CE, Bryant HE, Castro E, Nelson PS, et al. DNA Repair in Prostate Cancer: Biology and Clinical Implications. Eur Urol. 2017;71(3):417-25.

94. Robinson D, Van Allen EM, Wu YM, Schultz N, Lonigro RJ, Mosquera JM, et al. Integrative clinical genomics of advanced prostate cancer. Cell. 2015;161(5):1215-28.

95. Mateo J, Carreira S, Sandhu S, Miranda S, Mossop H, Perez-Lopez R, et al. DNA-Repair Defects and Olaparib in Metastatic Prostate Cancer. N Engl J Med. 2015;373(18):1697-708.

96. Cheng HH, Pritchard CC, Boyd T, Nelson PS, Montgomery B. Biallelic Inactivation of BRCA2 in Platinum-sensitive Metastatic Castration-resistant Prostate Cancer. Eur Urol. 2016;69(6):992-5.

97. Schulman CC, Altwein JE, Zlotta AR. Treatment options after failure of local curative treatments in prostate cancer: a controversial issue. BJU Int. 2000;86(9):1014-22.

98. Pound CR, Partin AW, Epstein JI, Walsh PC. Prostate-specific antigen after anatomic radical retropubic prostatectomy. Patterns of recurrence and cancer control. Urol Clin North Am. 1997;24(2):395-406.

99. Jemal A, Murray T, Ward E, Samuels A, Tiwari RC, Ghafoor A, et al. Cancer statistics, 2005. CA Cancer J Clin. 2005;55(1):10-30.

100. Moul JW. Prostate specific antigen only progression of prostate cancer. J Urol. 2000;163(6):1632-42.

101. Heidenreich A, Bastian PJ, Bellmunt J, Bolla M, Joniau S, van der Kwast T, et al. EAU guidelines on prostate cancer. Part II: Treatment of advanced, relapsing, and castration-resistant prostate cancer. Eur Urol. 2014;65(2):467-79.

102. Scher HI, Morris MJ, Stadler WM, Higano C, Basch E, Fizazi K, et al. Trial Design and Objectives for Castration-Resistant Prostate Cancer: Updated Recommendations From the Prostate Cancer Clinical Trials Working Group 3. J Clin Oncol. 2016;34(12):1402-18.

103. Eisenhauer EA, Therasse P, Bogaerts J, Schwartz LH, Sargent D, Ford R, et al. New response evaluation criteria in solid tumours: revised RECIST guideline (version 1.1). Eur J Cancer. 2009;45(2):228-47.

104. Trock BJ, Han M, Freedland SJ, Humphreys EB, DeWeese TL, Partin AW, et al. Prostate cancer-specific survival following salvage radiotherapy vs observation in men with biochemical recurrence after radical prostatectomy. Jama. 2008;299(23):2760-9.

105. Tannock IF, de Wit R, Berry WR, Horti J, Pluzanska A, Chi KN, et al. Docetaxel plus prednisone or mitoxantrone plus prednisone for advanced prostate cancer. N Engl J Med. 2004;351(15):1502-12.

106. Kantoff PW, Higano CS, Shore ND, Berger ER, Small EJ, Penson DF, et al. Sipuleucel-T immunotherapy for castration-resistant prostate cancer. N Engl J Med. 2010;363(5):411-22.

107. de Bono JS, Oudard S, Ozguroglu M, Hansen S, Machiels JP, Kocak I, et al. Prednisone plus cabazitaxel or mitoxantrone for metastatic castration-resistant prostate cancer progressing after docetaxel treatment: a randomised open-label trial. Lancet. 2010;376(9747):1147-54.

108. Scher HI, Fizazi K, Saad F, Taplin ME, Sternberg CN, Miller K, et al. Increased survival with enzalutamide in prostate cancer after chemotherapy. N Engl J Med. 2012;367(13):1187-97.

109. Fizazi K, Scher HI, Molina A, Logothetis CJ, Chi KN, Jones RJ, et al. Abiraterone acetate for treatment of metastatic castration-resistant prostate cancer: final overall survival analysis of the COU-AA-301 randomised, double-blind, placebo-controlled phase 3 study. Lancet Oncol. 2012;13(10):983-92.

110. Parker C, Nilsson S, Heinrich D, Helle SI, O'Sullivan JM, Fossa SD, et al. Alpha emitter radium-223 and survival in metastatic prostate cancer. N Engl J Med. 2013;369(3):213-23.

111. Smith MR, Saad F, Chowdhury S, Oudard S, Hadaschik BA, Graff JN, et al. Apalutamide Treatment and Metastasis-free Survival in Prostate Cancer. N Engl J Med. 2018;378(15):1408-18.

112. Fizazi K, Shore N, Tammela TL, Ulys A, Vjaters E, Polyakov S, et al. Darolutamide in Nonmetastatic, Castration-Resistant Prostate Cancer. New England Journal of Medicine. 2019;380(13):1235-46.

113. de Bono J, Mateo J, Fizazi K, Saad F, Shore N, Sandhu S, et al. Olaparib for Metastatic Castration-Resistant Prostate Cancer. New England Journal of Medicine. 2020;382(22):2091-102.

114. Sartor O, de Bono J, Chi KN, Fizazi K, Herrmann K, Rahbar K, et al. Lutetium-177–PSMA-617 for Metastatic Castration-Resistant Prostate Cancer. New England Journal of Medicine. 2021;385(12):1091-103.

115. Beer TM, Armstrong AJ, Rathkopf DE, Loriot Y, Sternberg CN, Higano CS, et al. Enzalutamide in metastatic prostate cancer before chemotherapy. N Engl J Med. 2014;371(5):424-33.

116. Visakorpi T, Hyytinen E, Koivisto P, Tanner M, Keinanen R, Palmberg C, et al. In vivo amplification of the androgen receptor gene and progression of human prostate cancer. Nat Genet. 1995;9(4):401-6.

117. Liu LL, Xie N, Sun S, Plymate S, Mostaghel E, Dong X. Mechanisms of the androgen receptor splicing in prostate cancer cells. Oncogene. 2014;33(24):3140-50.

118. Nakazawa M, Lu C, Chen Y, Paller CJ, Carducci MA, Eisenberger MA, et al. Serial blood-based analysis of AR-V7 in men with advanced prostate cancer. Ann Oncol. 2015;26(9):1859-65.

119. Onstenk W, Sieuwerts AM, Kraan J, Van M, Nieuweboer AJ, Mathijssen RH, et al. Efficacy of Cabazitaxel in Castration-resistant Prostate Cancer Is Independent of the Presence of AR-V7 in Circulating Tumor Cells. Eur Urol. 2015;68(6):939-45.

120. Lopez JP, Diallo A, Cruceanu C, Fiori LM, Laboissiere S, Guillet I, et al. Biomarker discovery: quantification of microRNAs and other small non-coding RNAs using next generation sequencing. BMC Med Genomics. 2015;8:35.

121. Nimse SB, Sonawane MD, Song KS, Kim T. Biomarker detection technologies and future directions. Analyst. 2016;141(3):740-55.

122. Xi X, Li T, Huang Y, Sun J, Zhu Y, Yang Y, et al. RNA Biomarkers: Frontier of Precision Medicine for Cancer. Noncoding RNA. 2017;3(1).

123. Tran C, Ouk S, Clegg NJ, Chen Y, Watson PA, Arora V, et al. Development of a second-generation antiandrogen for treatment of advanced prostate cancer. Science. 2009;324(5928):787-90.

124. Schaufele F, Carbonell X, Guerbadot M, Borngraeber S, Chapman MS, Ma AA, et al. The structural basis of androgen receptor activation: intramolecular and intermolecular amino-carboxy interactions. Proc Natl Acad Sci U S A. 2005;102(28):9802-7.

125. Yuan X, Cai C, Chen S, Chen S, Yu Z, Balk SP. Androgen receptor functions in castration-resistant prostate cancer and mechanisms of resistance to new agents targeting the androgen axis. Oncogene. 2014;33(22):2815-25.

126. Gibbons JA, Ouatas T, Krauwinkel W, Ohtsu Y, van der Walt JS, Beddo V, et al. Clinical Pharmacokinetic Studies of Enzalutamide. Clin Pharmacokinet. 2015;54(10):1043-55.

127. Edwards J, Krishna NS, Grigor KM, Bartlett JM. Androgen receptor gene amplification and protein expression in hormone refractory prostate cancer. Br J Cancer. 2003;89(3):552-6.

128. Chen CD, Welsbie DS, Tran C, Baek SH, Chen R, Vessella R, et al. Molecular determinants of resistance to antiandrogen therapy. Nat Med. 2004;10(1):33-9.

129. Yamamoto Y, Loriot Y, Beraldi E, Zhang F, Wyatt AW, Al Nakouzi N, et al. Generation 2.5 antisense oligonucleotides targeting the androgen receptor and its splice variants suppress enzalutamide-resistant prostate cancer cell growth. Clin Cancer Res. 2015;21(7):1675-87.

130. Romanel A, Gasi Tandefelt D, Conteduca V, Jayaram A, Casiraghi N, Wetterskog D, et al. Plasma AR and abiraterone-resistant prostate cancer. Sci Transl Med. 2015;7(312):312re10.

131. Conteduca V, Wetterskog D, Sharabiani MTA, Grande E, Fernandez-Perez MP, Jayaram A, et al. Androgen receptor gene status in plasma DNA associates with worse

outcome on enzalutamide or abiraterone for castration-resistant prostate cancer: a multi-institution correlative biomarker study. Ann Oncol. 2017;28(7):1508-16.

132. Wyatt AW, Azad AA, Volik SV, Annala M, Beja K, McConeghy B, et al. Genomic Alterations in Cell-Free DNA and Enzalutamide Resistance in Castration-Resistant Prostate Cancer. JAMA Oncol. 2016;2(12):1598-606.

133. Azad AA, Volik SV, Wyatt AW, Haegert A, Le Bihan S, Bell RH, et al. Androgen Receptor Gene Aberrations in Circulating Cell-Free DNA: Biomarkers of Therapeutic Resistance in Castration-Resistant Prostate Cancer. Clin Cancer Res. 2015;21(10):2315-24.

134. Waltering KK, Urbanucci A, Visakorpi T. Androgen receptor (AR) aberrations in castration-resistant prostate cancer. Mol Cell Endocrinol. 2012;360(1-2):38-43.

135. Suzuki H, Akakura K, Komiya A, Aida S, Akimoto S, Shimazaki J. Codon 877 mutation in the androgen receptor gene in advanced prostate cancer: relation to antiandrogen withdrawal syndrome. Prostate. 1996;29(3):153-8.

136. Yoshida T, Kinoshita H, Segawa T, Nakamura E, Inoue T, Shimizu Y, et al. Antiandrogen bicalutamide promotes tumor growth in a novel androgen-dependent prostate cancer xenograft model derived from a bicalutamide-treated patient. Cancer Res. 2005;65(21):9611-6.

137. Balbas MD, Evans MJ, Hosfield DJ, Wongvipat J, Arora VK, Watson PA, et al. Overcoming mutation-based resistance to antiandrogens with rational drug design. Elife. 2013;2:e00499.

138. Korpal M, Korn JM, Gao X, Rakiec DP, Ruddy DA, Doshi S, et al. An F876L mutation in androgen receptor confers genetic and phenotypic resistance to MDV3100 (enzalutamide). Cancer Discov. 2013;3(9):1030-43.

139. Clegg NJ, Wongvipat J, Joseph JD, Tran C, Ouk S, Dilhas A, et al. ARN-509: a novel antiandrogen for prostate cancer treatment. Cancer Res. 2012;72(6):1494-503.

140. Sartor AO, Tangen CM, Hussain MH, Eisenberger MA, Parab M, Fontana JA, et al. Antiandrogen withdrawal in castrate-refractory prostate cancer: a Southwest Oncology Group trial (SWOG 9426). Cancer. 2008;112(11):2393-400.

141. von Klot CA, Kramer MW, Boker A, Herrmann TR, Peters I, Kuczyk MA, et al. Is there an anti-androgen withdrawal syndrome for enzalutamide? World J Urol. 2014;32(5):1171-6.

142. Joseph JD, Lu N, Qian J, Sensintaffar J, Shao G, Brigham D, et al. A clinically relevant androgen receptor mutation confers resistance to second-generation antiandrogens enzalutamide and ARN-509. Cancer Discov. 2013;3(9):1020-9.

143. Guo Z, Yang X, Sun F, Jiang R, Linn DE, Chen H, et al. A novel androgen receptor splice variant is up-regulated during prostate cancer progression and promotes androgen depletion-resistant growth. Cancer Res. 2009;69(6):2305-13.

144. Ware KE, Garcia-Blanco MA, Armstrong AJ, Dehm SM. Biologic and clinical significance of androgen receptor variants in castration resistant prostate cancer. Endocr Relat Cancer. 2014;21(4):T87-t103.

145. Li Y, Chan SC, Brand LJ, Hwang TH, Silverstein KA, Dehm SM. Androgen receptor splice variants mediate enzalutamide resistance in castration-resistant prostate cancer cell lines. Cancer Res. 2013;73(2):483-9.

146. Hu R, Isaacs WB, Luo J. A snapshot of the expression signature of androgen receptor splicing variants and their distinctive transcriptional activities. Prostate. 2011;71(15):1656-67.

147. Hu R, Lu C, Mostaghel EA, Yegnasubramanian S, Gurel M, Tannahill C, et al. Distinct transcriptional programs mediated by the ligand-dependent full-length androgen receptor and its splice variants in castration-resistant prostate cancer. Cancer Res. 2012;72(14):3457-62.

148. Watson PA, Chen YF, Balbas MD, Wongvipat J, Socci ND, Viale A, et al. Constitutively active androgen receptor splice variants expressed in castration-resistant prostate cancer require full-length androgen receptor. Proc Natl Acad Sci U S A. 2010;107(39):16759-65.

149. Sun S, Sprenger CC, Vessella RL, Haugk K, Soriano K, Mostaghel EA, et al. Castration resistance in human prostate cancer is conferred by a frequently occurring androgen receptor splice variant. J Clin Invest. 2010;120(8):2715-30.

150. Hornberg E, Ylitalo EB, Crnalic S, Antti H, Stattin P, Widmark A, et al. Expression of androgen receptor splice variants in prostate cancer bone metastases is associated with castration-resistance and short survival. PLoS One. 2011;6(4):e19059.

151. Zhang X, Morrissey C, Sun S, Ketchandji M, Nelson PS, True LD, et al. Androgen receptor variants occur frequently in castration resistant prostate cancer metastases. PLoS One. 2011;6(11):e27970.

152. Todenhofer T, Azad A, Stewart C, Gao J, Eigl BJ, Gleave ME, et al. AR-V7 Transcripts in Whole Blood RNA of Patients with Metastatic Castration Resistant Prostate Cancer Correlate with Response to Abiraterone Acetate. J Urol. 2017;197(1):135-42.

153. Welti J, Rodrigues DN, Sharp A, Sun S, Lorente D, Riisnaes R, et al. Analytical Validation and Clinical Qualification of a New Immunohistochemical Assay for Androgen Receptor Splice Variant-7 Protein Expression in Metastatic Castration-resistant Prostate Cancer. Eur Urol. 2016;70(4):599-608.

154. Zhu Y, Sharp A, Anderson CM, Silberstein JL, Taylor M, Lu C, et al. Novel Junction-specific and Quantifiable In Situ Detection of AR-V7 and its Clinical Correlates in Metastatic Castration-resistant Prostate Cancer. Eur Urol. 2018;73(5):727-35.

155. Galon J, Franchimont D, Hiroi N, Frey G, Boettner A, Ehrhart-Bornstein M, et al. Gene profiling reveals unknown enhancing and suppressive actions of glucocorticoids on immune cells. Faseb j. 2002;16(1):61-71.

156. Lu NZ, Collins JB, Grissom SF, Cidlowski JA. Selective regulation of bone cell apoptosis by translational isoforms of the glucocorticoid receptor. Mol Cell Biol. 2007;27(20):7143-60.

157. Luisi BF, Xu WX, Otwinowski Z, Freedman LP, Yamamoto KR, Sigler PB. Crystallographic analysis of the interaction of the glucocorticoid receptor with DNA. Nature. 1991;352(6335):497-505.

158. Ren R, Oakley RH, Cruz-Topete D, Cidlowski JA. Dual role for glucocorticoids in cardiomyocyte hypertrophy and apoptosis. Endocrinology. 2012;153(11):5346-60.

159. Savory JG, Prefontaine GG, Lamprecht C, Liao M, Walther RF, Lefebvre YA, et al. Glucocorticoid receptor homodimers and glucocorticoid-mineralocorticoid receptor heterodimers form in the cytoplasm through alternative dimerization interfaces. Mol Cell Biol. 2001;21(3):781-93.

160. Arora VK, Schenkein E, Murali R, Subudhi SK, Wongvipat J, Balbas MD, et al. Glucocorticoid receptor confers resistance to antiandrogens by bypassing androgen receptor blockade. Cell. 2013;155(6):1309-22.

161. Yan TZ, Jin FS, Xie LP, Li LC. Relationship between glucocorticoid receptor signal pathway and androgen-independent prostate cancer. Urol Int. 2008;81(2):228-33.

162. Zhao XY, Malloy PJ, Krishnan AV, Swami S, Navone NM, Peehl DM, et al. Glucocorticoids can promote androgen-independent growth of prostate cancer cells through a mutated androgen receptor. Nat Med. 2000;6(6):703-6.

163. Borgmann H, Lallous N, Ozistanbullu D, Beraldi E, Paul N, Dalal K, et al. Moving Towards Precision Urologic Oncology: Targeting Enzalutamide-resistant Prostate Cancer and Mutated Forms of the Androgen Receptor Using the Novel Inhibitor Darolutamide (ODM-201). Eur Urol. 2018;73(1):4-8.

164. Izumi K, Chang C. Targeting inflammatory cytokines-androgen receptor (AR) signaling with ASC-J9((R)) to better battle prostate cancer progression. Oncoimmunology. 2013;2(12):e26853.

165. Lai KP, Huang CK, Chang YJ, Chung CY, Yamashita S, Li L, et al. New therapeutic approach to suppress castration-resistant prostate cancer using ASC-J9 via targeting androgen receptor in selective prostate cells. Am J Pathol. 2013;182(2):460-73.

166. Lin TH, Izumi K, Lee SO, Lin WJ, Yeh S, Chang C. Anti-androgen receptor ASC-J9 versus anti-androgens MDV3100 (Enzalutamide) or Casodex (Bicalutamide) leads to opposite effects on prostate cancer metastasis via differential modulation of macrophage infiltration and STAT3-CCL2 signaling. Cell Death Dis. 2013;4:e764.

167. Lin TH, Lee SO, Niu Y, Xu D, Liang L, Li L, et al. Differential androgen deprivation therapies with anti-androgens casodex/bicalutamide or MDV3100/Enzalutamide versus anti-androgen receptor ASC-J9(R) Lead to promotion versus suppression of prostate cancer metastasis. J Biol Chem. 2013;288(27):19359-69.

168. Wang R, Lin W, Lin C, Li L, Sun Y, Chang C. ASC-J9((R)) suppresses castration resistant prostate cancer progression via degrading the enzalutamide-induced androgen receptor mutant AR-F876L. Cancer Lett. 2016;379(1):154-60.

169. Wang R, Sun Y, Li L, Niu Y, Lin W, Lin C, et al. Preclinical Study using Malat1 Small Interfering RNA or Androgen Receptor Splicing Variant 7 Degradation Enhancer ASC-J9((R)) to Suppress Enzalutamide-resistant Prostate Cancer Progression. Eur Urol. 2017;72(5):835-44.

170. Wen S, Tian J, Niu Y, Li L, Yeh S, Chang C. ASC-J9((R)), and not Casodex or Enzalutamide, suppresses prostate cancer stem/progenitor cell invasion via altering the EZH2-STAT3 signals. Cancer Lett. 2016;376(2):377-86.

171. Yamashita S, Lai KP, Chuang KL, Xu D, Miyamoto H, Tochigi T, et al. ASC-J9 suppresses castration-resistant prostate cancer growth through degradation of full-length and splice variant androgen receptors. Neoplasia. 2012;14(1):74-83.

172. Yang Z, Chang YJ, Yu IC, Yeh S, Wu CC, Miyamoto H, et al. ASC-J9 ameliorates spinal and bulbar muscular atrophy phenotype via degradation of androgen receptor. Nat Med. 2007;13(3):348-53.

173. Asangani IA, Dommeti VL, Wang X, Malik R, Cieslik M, Yang R, et al. Therapeutic targeting of BET bromodomain proteins in castration-resistant prostate cancer. Nature. 2014;510(7504):278-82.

174. Chan SC, Selth LA, Li Y, Nyquist MD, Miao L, Bradner JE, et al. Targeting chromatin binding regulation of constitutively active AR variants to overcome prostate cancer resistance to endocrine-based therapies. Nucleic Acids Res. 2015;43(12):5880-97.

175. Pawar A, Gollavilli PN, Wang S, Asangani IA. Resistance to BET Inhibitor Leads to Alternative Therapeutic Vulnerabilities in Castration-Resistant Prostate Cancer. Cell Rep. 2018;22(9):2236-45.

176. Bitting RL, Schaeffer D, Somarelli JA, Garcia-Blanco MA, Armstrong AJ. The role of epithelial plasticity in prostate cancer dissemination and treatment resistance. Cancer Metastasis Rev. 2014;33(2-3):441-68.

177. Marin-Aguilera M, Codony-Servat J, Reig O, Lozano JJ, Fernandez PL, Pereira MV, et al. Epithelial-to-mesenchymal transition mediates docetaxel resistance and high risk of relapse in prostate cancer. Mol Cancer Ther. 2014;13(5):1270-84.

178. Grant CM, Kyprianou N. Epithelial mesenchymal transition (EMT) in prostate growth and tumor progression. Transl Androl Urol. 2013;2(3):202-11.

179. Wang L, Song G, Tan W, Qi M, Zhang L, Chan J, et al. MiR-573 inhibits prostate cancer metastasis by regulating epithelial-mesenchymal transition. Oncotarget. 2015;6(34):35978-90.

180. Chung LW, Baseman A, Assikis V, Zhau HE. Molecular insights into prostate cancer progression: the missing link of tumor microenvironment. J Urol. 2005;173(1):10-20.

181. Thiery JP, Acloque H, Huang RY, Nieto MA. Epithelial-mesenchymal transitions in development and disease. Cell. 2009;139(5):871-90.

182. Yilmaz M, Christofori G. EMT, the cytoskeleton, and cancer cell invasion. Cancer Metastasis Rev. 2009;28(1-2):15-33.

183. Liu Q, Tong D, Liu G, Xu J, Do K, Geary K, et al. Metformin reverses prostate cancer resistance to enzalutamide by targeting TGF-beta1/STAT3 axis-regulated EMT. Cell Death Dis. 2017;8(8):e3007.

184. Martin SK, Pu H, Penticuff JC, Cao Z, Horbinski C, Kyprianou N. Multinucleation and Mesenchymal-to-Epithelial Transition Alleviate Resistance to Combined Cabazitaxel and Antiandrogen Therapy in Advanced Prostate Cancer. Cancer Res. 2016;76(4):912-26.

185. Miao L, Yang L, Li R, Rodrigues DN, Crespo M, Hsieh JT, et al. Disrupting Androgen Receptor Signaling Induces Snail-Mediated Epithelial-Mesenchymal Plasticity in Prostate Cancer. Cancer Res. 2017;77(11):3101-12.

186. Ouyang G, Wang Z, Fang X, Liu J, Yang CJ. Molecular signaling of the epithelial to mesenchymal transition in generating and maintaining cancer stem cells. Cell Mol Life Sci. 2010;67(15):2605-18.

187. van der Pluijm G. Epithelial plasticity, cancer stem cells and bone metastasis formation. Bone. 2011;48(1):37-43.

188. Kalluri R, Weinberg RA. The basics of epithelial-mesenchymal transition. J Clin Invest. 2009;119(6):1420-8.

189. Thiery JP. Epithelial-mesenchymal transitions in tumour progression. Nat Rev Cancer. 2002;2(6):442-54.

190. Batlle E, Sancho E, Franci C, Dominguez D, Monfar M, Baulida J, et al. The transcription factor snail is a repressor of E-cadherin gene expression in epithelial tumour cells. Nat Cell Biol. 2000;2(2):84-9.

191. Cano A, Perez-Moreno MA, Rodrigo I, Locascio A, Blanco MJ, del Barrio MG, et al. The transcription factor snail controls epithelial-mesenchymal transitions by repressing E-cadherin expression. Nat Cell Biol. 2000;2(2):76-83.

192. Bergerheim US, Kunimi K, Collins VP, Ekman P. Deletion mapping of chromosomes 8, 10, and 16 in human prostatic carcinoma. Genes Chromosomes Cancer. 1991;3(3):215-20.

193. Guarino M, Rubino B, Ballabio G. The role of epithelial-mesenchymal transition in cancer pathology. Pathology. 2007;39(3):305-18.

194. Onder TT, Gupta PB, Mani SA, Yang J, Lander ES, Weinberg RA. Loss of E-cadherin promotes metastasis via multiple downstream transcriptional pathways. Cancer Res. 2008;68(10):3645-54.

195. Graff JR, Herman JG, Lapidus RG, Chopra H, Xu R, Jarrard DF, et al. E-cadherin expression is silenced by DNA hypermethylation in human breast and prostate carcinomas. Cancer Res. 1995;55(22):5195-9.

196. Davies G, Jiang WG, Mason MD. Matrilysin mediates extracellular cleavage of E-cadherin from prostate cancer cells: a key mechanism in hepatocyte growth factor/scatter factor-induced cell-cell dissociation and in vitro invasion. Clin Cancer Res. 2001;7(10):3289-97.

197. Umbas R, Isaacs WB, Bringuier PP, Schaafsma HE, Karthaus HF, Oosterhof GO, et al. Decreased E-cadherin expression is associated with poor prognosis in patients with prostate cancer. Cancer Res. 1994;54(14):3929-33.

198. Umbas R, Schalken JA, Aalders TW, Carter BS, Karthaus HF, Schaafsma HE, et al. Expression of the cellular adhesion molecule E-cadherin is reduced or absent in high-grade prostate cancer. Cancer Res. 1992;52(18):5104-9.

199. Chu K, Cheng CJ, Ye X, Lee YC, Zurita AJ, Chen DT, et al. Cadherin-11 promotes the metastasis of prostate cancer cells to bone. Mol Cancer Res. 2008;6(8):1259-67.

200. Yang J, Mani SA, Donaher JL, Ramaswamy S, Itzykson RA, Come C, et al. Twist, a master regulator of morphogenesis, plays an essential role in tumor metastasis. Cell. 2004;117(7):927-39.

201. Cho KH, Choi MJ, Jeong KJ, Kim JJ, Hwang MH, Shin SC, et al. A ROS/STAT3/HIF-1alpha signaling cascade mediates EGF-induced TWIST1 expression and prostate cancer cell invasion. Prostate. 2014;74(5):528-36.

202. Sun Y, Wang BE, Leong KG, Yue P, Li L, Jhunjhunwala S, et al. Androgen deprivation causes epithelial-mesenchymal transition in the prostate: implications for androgen-deprivation therapy. Cancer Res. 2012;72(2):527-36.

203. Jennbacken K, Tesan T, Wang W, Gustavsson H, Damber JE, Welen K. N-cadherin increases after androgen deprivation and is associated with metastasis in prostate cancer. Endocr Relat Cancer. 2010;17(2):469-79.

204. Nieman MT, Prudoff RS, Johnson KR, Wheelock MJ. N-cadherin promotes motility in human breast cancer cells regardless of their E-cadherin expression. J Cell Biol. 1999;147(3):631-44.

205. Tanaka H, Kono E, Tran CP, Miyazaki H, Yamashiro J, Shimomura T, et al. Monoclonal antibody targeting of N-cadherin inhibits prostate cancer growth, metastasis and castration resistance. Nat Med. 2010;16(12):1414-20.

206. Gravdal K, Halvorsen OJ, Haukaas SA, Akslen LA. A switch from E-cadherin to N-cadherin expression indicates epithelial to mesenchymal transition and is of strong and independent importance for the progress of prostate cancer. Clin Cancer Res. 2007;13(23):7003-11.

207. Kallakury BV, Sheehan CE, Winn-Deen E, Oliver J, Fisher HA, Kaufman RP, Jr., et al. Decreased expression of catenins (alpha and beta), p120 CTN, and E-cadherin cell adhesion proteins and E-cadherin gene promoter methylation in prostatic adenocarcinomas. Cancer. 2001;92(11):2786-95.

208. Satelli A, Li S. Vimentin in cancer and its potential as a molecular target for cancer therapy. Cell Mol Life Sci. 2011;68(18):3033-46.

209. Singh S, Sadacharan S, Su S, Belldegrun A, Persad S, Singh G. Overexpression of vimentin: role in the invasive phenotype in an androgen-independent model of prostate cancer. Cancer Res. 2003;63(9):2306-11.

210. Nieto M, Finn S, Loda M, Hahn WC. Prostate cancer: Re-focusing on androgen receptor signaling. Int J Biochem Cell Biol. 2007;39(9):1562-8.

211. Zhu ML, Kyprianou N. Role of androgens and the androgen receptor in epithelial-mesenchymal transition and invasion of prostate cancer cells. Faseb j. 2010;24(3):769-77.

212. Shiota M, Yokomizo A, Tada Y, Inokuchi J, Kashiwagi E, Masubuchi D, et al. Castration resistance of prostate cancer cells caused by castration-induced oxidative stress through Twist1 and androgen receptor overexpression. Oncogene. 2010;29(2):237-50.

213. Byrne NM, Nesbitt H, Ming L, McKeown SR, Worthington J, McKenna DJ. Androgen deprivation in LNCaP prostate tumour xenografts induces vascular changes and hypoxic stress, resulting in promotion of epithelial-to-mesenchymal transition. Br J Cancer. 2016;114(6):659-68.

214. Izumi K, Fang LY, Mizokami A, Namiki M, Li L, Lin WJ, et al. Targeting the androgen receptor with siRNA promotes prostate cancer metastasis through enhanced macrophage recruitment via CCL2/CCR2-induced STAT3 activation. EMBO Mol Med. 2013;5(9):1383-401.

215. Jacob S, Nayak S, Fernandes G, Barai RS, Menon S, Chaudhari UK, et al. Androgen receptor as a regulator of ZEB2 expression and its implications in epithelial-to-mesenchymal transition in prostate cancer. Endocr Relat Cancer. 2014;21(3):473-86.

216. Gregory PA, Bracken CP, Smith E, Bert AG, Wright JA, Roslan S, et al. An autocrine TGF-beta/ZEB/miR-200 signaling network regulates establishment and maintenance of epithelial-mesenchymal transition. Mol Biol Cell. 2011;22(10):1686-98.

217. Gregory PA, Bert AG, Paterson EL, Barry SC, Tsykin A, Farshid G, et al. The miR-200 family and miR-205 regulate epithelial to mesenchymal transition by targeting ZEB1 and SIP1. Nat Cell Biol. 2008;10(5):593-601.

218. Kung JT, Colognori D, Lee JT. Long noncoding RNAs: past, present, and future. Genetics. 2013;193(3):651-69.

219. Esteller M. Non-coding RNAs in human disease. Nat Rev Genet. 2011;12(12):861-74.

220. Jeck WR, Sorrentino JA, Wang K, Slevin MK, Burd CE, Liu J, et al. Circular RNAs are abundant, conserved, and associated with ALU repeats. Rna. 2013;19(2):141-57.

221. Warner JR. The economics of ribosome biosynthesis in yeast. Trends Biochem Sci. 1999;24(11):437-40.

222. Kamps R, Brandao RD, Bosch BJ, Paulussen AD, Xanthoulea S, Blok MJ, et al. Next-Generation Sequencing in Oncology: Genetic Diagnosis, Risk Prediction and Cancer Classification. Int J Mol Sci. 2017;18(2).

223. Bolton EM, Tuzova AV, Walsh AL, Lynch T, Perry AS. Noncoding RNAs in prostate cancer: the long and the short of it. Clin Cancer Res. 2014;20(1):35-43.

224. Bachmayr-Heyda A, Reiner AT, Auer K, Sukhbaatar N, Aust S, Bachleitner-Hofmann T, et al. Correlation of circular RNA abundance with proliferation--exemplified with colorectal and ovarian cancer, idiopathic lung fibrosis, and normal human tissues. Sci Rep. 2015;5:8057.

225. Gao D, Zhang X, Liu B, Meng D, Fang K, Guo Z, et al. Screening circular RNA related to chemotherapeutic resistance in breast cancer. Epigenomics. 2017;9(9):1175-88.

226. Hansen TB, Kjems J, Damgaard CK. Circular RNA and miR-7 in cancer. Cancer Res. 2013;73(18):5609-12.

227. Kong Z, Wan X, Zhang Y, Zhang P, Zhang Y, Zhang X, et al. Androgen-responsive circular RNA circSMARCA5 is up-regulated and promotes cell proliferation in prostate cancer. Biochem Biophys Res Commun. 2017;493(3):1217-23.

228. Lim MCJ, Baird AM, Aird J, Greene J, Kapoor D, Gray SG, et al. RNAs as Candidate Diagnostic and Prognostic Markers of Prostate Cancer-From Cell Line Models to Liquid Biopsies. Diagnostics (Basel). 2018;8(3).

229. Ambros V. The functions of animal microRNAs. Nature. 2004;431(7006):350-5.

230. Lee Y, Jeon K, Lee JT, Kim S, Kim VN. MicroRNA maturation: stepwise processing and subcellular localization. Embo j. 2002;21(17):4663-70.

231. Valinezhad Orang A, Safaralizadeh R, Kazemzadeh-Bavili M. Mechanisms of miRNA-Mediated Gene Regulation from Common Downregulation to mRNA-Specific Upregulation. Int J Genomics. 2014;2014:970607.

232. Vasudevan S, Tong Y, Steitz JA. Switching from repression to activation: microRNAs can up-regulate translation. Science. 2007;318(5858):1931-4.

233. Jansson MD, Lund AH. MicroRNA and cancer. Mol Oncol. 2012;6(6):590-610.

234. Esquela-Kerscher A, Slack FJ. Oncomirs - microRNAs with a role in cancer. Nat Rev Cancer. 2006;6(4):259-69.

235. Kim WT, Kim WJ. MicroRNAs in prostate cancer. Prostate Int. 2013;1(1):3-9.

236. Volinia S, Calin GA, Liu CG, Ambs S, Cimmino A, Petrocca F, et al. A microRNA expression signature of human solid tumors defines cancer gene targets. Proc Natl Acad Sci U S A. 2006;103(7):2257-61.

237. Ambs S, Prueitt RL, Yi M, Hudson RS, Howe TM, Petrocca F, et al. Genomic profiling of microRNA and messenger RNA reveals deregulated microRNA expression in prostate cancer. Cancer Res. 2008;68(15):6162-70.

238. Song C, Chen H, Wang T, Zhang W, Ru G, Lang J. Expression profile analysis of microRNAs in prostate cancer by next-generation sequencing. Prostate. 2015;75(5):500-16.

239. Ozen M, Creighton CJ, Ozdemir M, Ittmann M. Widespread deregulation of microRNA expression in human prostate cancer. Oncogene. 2008;27(12):1788-93.

240. Porkka KP, Pfeiffer MJ, Waltering KK, Vessella RL, Tammela TL, Visakorpi T. MicroRNA expression profiling in prostate cancer. Cancer Res. 2007;67(13):6130-5.

241. Martens-Uzunova ES, Jalava SE, Dits NF, van Leenders GJ, Moller S, Trapman J, et al. Diagnostic and prognostic signatures from the small non-coding RNA transcriptome in prostate cancer. Oncogene. 2012;31(8):978-91.

242. Larne O, Martens-Uzunova E, Hagman Z, Edsjo A, Lippolis G, den Berg MS, et al. miQ--a novel microRNA based diagnostic and prognostic tool for prostate cancer. Int J Cancer. 2013;132(12):2867-75.

243. Haflidadottir BS, Larne O, Martin M, Persson M, Edsjo A, Bjartell A, et al. Upregulation of miR-96 enhances cellular proliferation of prostate cancer cells through FOXO1. PLoS One. 2013;8(8):e72400.

244. Sarver AL, Li L, Subramanian S. MicroRNA miR-183 functions as an oncogene by targeting the transcription factor EGR1 and promoting tumor cell migration. Cancer Res. 2010;70(23):9570-80.

245. Zaman MS, Chen Y, Deng G, Shahryari V, Suh SO, Saini S, et al. The functional significance of microRNA-145 in prostate cancer. Br J Cancer. 2010;103(2):256-64.

246. Peng X, Guo W, Liu T, Wang X, Tu X, Xiong D, et al. Identification of miRs-143 and -145 that is associated with bone metastasis of prostate cancer and involved in the regulation of EMT. PLoS One. 2011;6(5):e20341.

247. Spahn M, Kneitz S, Scholz CJ, Stenger N, Rudiger T, Strobel P, et al. Expression of microRNA-221 is progressively reduced in aggressive prostate cancer and metastasis and predicts clinical recurrence. Int J Cancer. 2010;127(2):394-403.

248. Mainetti LE, Zhe X, Diedrich J, Saliganan AD, Cho WJ, Cher ML, et al. Bone-induced c-kit expression in prostate cancer: a driver of intraosseous tumor growth. Int J Cancer. 2015;136(1):11-20.

249. Wiesner C, Nabha SM, Dos Santos EB, Yamamoto H, Meng H, Melchior SW, et al. C-kit and its ligand stem cell factor: potential contribution to prostate cancer bone metastasis. Neoplasia. 2008;10(9):996-1003.

250. Zheng Q, Peskoe SB, Ribas J, Rafiqi F, Kudrolli T, Meeker AK, et al. Investigation of miR-21, miR-141, and miR-221 expression levels in prostate adenocarcinoma for associated risk of recurrence after radical prostatectomy. Prostate. 2014;74(16):1655-62.

251. Yaman Agaoglu F, Kovancilar M, Dizdar Y, Darendeliler E, Holdenrieder S, Dalay N, et al. Investigation of miR-21, miR-141, and miR-221 in blood circulation of patients with prostate cancer. Tumour Biol. 2011;32(3):583-8.

252. Sun T, Wang Q, Balk S, Brown M, Lee GS, Kantoff P. The role of microRNA-221 and microRNA-222 in androgen-independent prostate cancer cell lines. Cancer Res. 2009;69(8):3356-63.

253. Sun T, Yang M, Chen S, Balk S, Pomerantz M, Hsieh CL, et al. The altered expression of MiR-221/-222 and MiR-23b/-27b is associated with the development of human castration resistant prostate cancer. Prostate. 2012;72(10):1093-103.

254. Sun T, Wang X, He HH, Sweeney CJ, Liu SX, Brown M, et al. MiR-221 promotes the development of androgen independence in prostate cancer cells via downregulation of HECTD2 and RAB1A. Oncogene. 2014;33(21):2790-800.

255. Schaefer A, Jung M, Mollenkopf HJ, Wagner I, Stephan C, Jentzmik F, et al. Diagnostic and prognostic implications of microRNA profiling in prostate carcinoma. Int J Cancer. 2010;126(5):1166-76.

256. Brase JC, Johannes M, Schlomm T, Falth M, Haese A, Steuber T, et al. Circulating miRNAs are correlated with tumor progression in prostate cancer. Int J Cancer. 2011;128(3):608-16.

257. Shen J, Hruby GW, McKiernan JM, Gurvich I, Lipsky MJ, Benson MC, et al. Dysregulation of circulating microRNAs and prediction of aggressive prostate cancer. Prostate. 2012;72(13):1469-77.

258. Bryant RJ, Pawlowski T, Catto JW, Marsden G, Vessella RL, Rhees B, et al. Changes in circulating microRNA levels associated with prostate cancer. Br J Cancer. 2012;106(4):768-74.

259. Souza MF, Kuasne H, Barros-Filho MC, Ciliao HL, Marchi FA, Fuganti PE, et al. Circulating mRNAs and miRNAs as candidate markers for the diagnosis and prognosis of prostate cancer. PLoS One. 2017;12(9):e0184094.

260. Ma L, Li A, Zou D, Xu X, Xia L, Yu J, et al. LncRNAWiki: harnessing community knowledge in collaborative curation of human long non-coding RNAs. Nucleic Acids Res. 2015;43(Database issue):D187-92.

261. Lee JT. Epigenetic regulation by long noncoding RNAs. Science. 2012;338(6113):1435-9.

262. Rinn JL, Chang HY. Genome regulation by long noncoding RNAs. Annu Rev Biochem. 2012;81:145-66.

263. Gutschner T, Diederichs S. The hallmarks of cancer: a long non-coding RNA point of view. RNA Biol. 2012;9(6):703-19.

264. Mercer TR, Dinger ME, Sunkin SM, Mehler MF, Mattick JS. Specific expression of long noncoding RNAs in the mouse brain. Proc Natl Acad Sci U S A. 2008;105(2):716-21.

265. Leyten GH, Hessels D, Jannink SA, Smit FP, de Jong H, Cornel EB, et al. Prospective multicentre evaluation of PCA3 and TMPRSS2-ERG gene fusions as diagnostic and prognostic urinary biomarkers for prostate cancer. Eur Urol. 2014;65(3):534-42.

266. Ren S, Wang F, Shen J, Sun Y, Xu W, Lu J, et al. Long non-coding RNA metastasis associated in lung adenocarcinoma transcript 1 derived miniRNA as a novel plasma-based biomarker for diagnosing prostate cancer. Eur J Cancer. 2013;49(13):2949-59.

267. Bussemakers MJ, van Bokhoven A, Verhaegh GW, Smit FP, Karthaus HF, Schalken JA, et al. DD3: a new prostate-specific gene, highly overexpressed in prostate cancer. Cancer Res. 1999;59(23):5975-9.

268. Schalken JA, Hessels D, Verhaegh G. New targets for therapy in prostate cancer: differential display code 3 (DD3(PCA3)), a highly prostate cancer-specific gene. Urology. 2003;62(5 Suppl 1):34-43.

269. Lemos AE, Ferreira LB, Batoreu NM, de Freitas PP, Bonamino MH, Gimba ER. PCA3 long noncoding RNA modulates the expression of key cancer-related genes in LNCaP prostate cancer cells. Tumour Biol. 2016;37(8):11339-48.

270. He JH, Li BX, Han ZP, Zou MX, Wang L, Lv YB, et al. Snail-activated long non-coding RNA PCA3 up-regulates PRKD3 expression by miR-1261 sponging, thereby promotes invasion and migration of prostate cancer cells. Tumour Biol. 2016.

271. Ozgur E, Celik AI, Darendeliler E, Gezer U. PCA3 Silencing Sensitizes Prostate Cancer Cells to Enzalutamide-mediated Androgen Receptor Blockade. Anticancer Res. 2017;37(7):3631-7.

272. van Gils MP, Hessels D, van Hooij O, Jannink SA, Peelen WP, Hanssen SL, et al. The time-resolved fluorescence-based PCA3 test on urinary sediments after digital rectal examination; a Dutch multicenter validation of the diagnostic performance. Clin Cancer Res. 2007;13(3):939-43.

273. FDA approves PROGENSA® PCA3 assay 2012 [Available from: https://www.prnewswire.com/news-releases/fda-approves-progensa-pca3-assay-139349658.html.

274. Gittelman MC, Hertzman B, Bailen J, Williams T, Koziol I, Henderson RJ, et al. PCA3 molecular urine test as a predictor of repeat prostate biopsy outcome in men with previous negative biopsies: a prospective multicenter clinical study. J Urol. 2013;190(1):64-9.

275. Cui Y, Cao W, Li Q, Shen H, Liu C, Deng J, et al. Evaluation of prostate cancer antigen 3 for detecting prostate cancer: a systematic review and meta-analysis. Sci Rep. 2016;6:25776.

276. Ren S, Liu Y, Xu W, Sun Y, Lu J, Wang F, et al. Long noncoding RNA MALAT-1 is a new potential therapeutic target for castration resistant prostate cancer. J Urol. 2013;190(6):2278-87.

277. Xue D, Zhou CX, Shi YB, Lu H, He XZ. MD-miniRNA could be a more accurate biomarker for prostate cancer screening compared with serum prostate-specific antigen level. Tumour Biol. 2015;36(5):3541-7.

278. Sebastian A, Hum NR, Hudson BD, Loots GG. Cancer-Osteoblast Interaction Reduces Sost Expression in Osteoblasts and Up-Regulates lncRNA MALAT1 in Prostate Cancer. Microarrays (Basel). 2015;4(4):503-19.

279. Wang F, Ren S, Chen R, Lu J, Shi X, Zhu Y, et al. Development and prospective multicenter evaluation of the long noncoding RNA MALAT-1 as a diagnostic urinary biomarker for prostate cancer. Oncotarget. 2014;5(22):11091-102.

280. Cocquerelle C, Mascrez B, Hetuin D, Bailleul B. Mis-splicing yields circular RNA molecules. Faseb j. 1993;7(1):155-60.

281. Kos A, Dijkema R, Arnberg AC, van der Meide PH, Schellekens H. The hepatitis delta (delta) virus possesses a circular RNA. Nature. 1986;323(6088):558-60.

282. Nigro JM, Cho KR, Fearon ER, Kern SE, Ruppert JM, Oliner JD, et al. Scrambled exons. Cell. 1991;64(3):607-13.

283. Salzman J, Gawad C, Wang PL, Lacayo N, Brown PO. Circular RNAs are the predominant transcript isoform from hundreds of human genes in diverse cell types. PLoS One. 2012;7(2):e30733.

284. Memczak S, Jens M, Elefsinioti A, Torti F, Krueger J, Rybak A, et al. Circular RNAs are a large class of animal RNAs with regulatory potency. Nature. 2013;495(7441):333-8.

285. Jeck WR, Sharpless NE. Detecting and characterizing circular RNAs. Nat Biotechnol. 2014;32(5):453-61.

286. Lasda E, Parker R. Circular RNAs Co-Precipitate with Extracellular Vesicles: A Possible Mechanism for circRNA Clearance. PLoS One. 2016;11(2):e0148407.

287. Hansen TB, Jensen TI, Clausen BH, Bramsen JB, Finsen B, Damgaard CK, et al. Natural RNA circles function as efficient microRNA sponges. Nature. 2013;495(7441):384-8.

288. Salzman J, Chen RE, Olsen MN, Wang PL, Brown PO. Cell-type specific features of circular RNA expression. PLoS Genet. 2013;9(9):e1003777.

289. Chen LL, Yang L. Regulation of circRNA biogenesis. RNA Biol. 2015;12(4):381-8.

290. Vicens Q, Westhof E. Biogenesis of Circular RNAs. Cell. 2014;159(1):13-4.

291. Zhang XO, Wang HB, Zhang Y, Lu X, Chen LL, Yang L. Complementary sequence-mediated exon circularization. Cell. 2014;159(1):134-47.

292. Starke S, Jost I, Rossbach O, Schneider T, Schreiner S, Hung LH, et al. Exon circularization requires canonical splice signals. Cell Rep. 2015;10(1):103-11.

293. Panda AC, Grammatikakis I, Munk R, Gorospe M, Abdelmohsen K. Emerging roles and context of circular RNAs. Wiley Interdiscip Rev RNA. 2017;8(2).

294. Conn SJ, Pillman KA, Toubia J, Conn VM, Salmanidis M, Phillips CA, et al. The RNA binding protein quaking regulates formation of circRNAs. Cell. 2015;160(6):1125-34.

295. Ashwal-Fluss R, Meyer M, Pamudurti NR, Ivanov A, Bartok O, Hanan M, et al. circRNA biogenesis competes with pre-mRNA splicing. Mol Cell. 2014;56(1):55-66.

296. Meng X, Li X, Zhang P, Wang J, Zhou Y, Chen M. Circular RNA: an emerging key player in RNA world. Brief Bioinform. 2017;18(4):547-57.

297. Chenard CA, Richard S. New implications for the QUAKING RNA binding protein in human disease. J Neurosci Res. 2008;86(2):233-42.

298. Abe N, Matsumoto K, Nishihara M, Nakano Y, Shibata A, Maruyama H, et al. Rolling Circle Translation of Circular RNA in Living Human Cells. Sci Rep. 2015;5:16435.

299. Wang Y, Wang Z. Efficient backsplicing produces translatable circular mRNAs. Rna. 2015;21(2):172-9.

300. Zhang Y, Zhang XO, Chen T, Xiang JF, Yin QF, Xing YH, et al. Circular intronic long noncoding RNAs. Mol Cell. 2013;51(6):792-806.

301. Chen S, Huang V, Xu X, Livingstone J, Soares F, Jeon J, et al. Widespread and Functional RNA Circularization in Localized Prostate Cancer. Cell. 2019;176(4):831-43.e22.

302. Li Z, Huang C, Bao C, Chen L, Lin M, Wang X, et al. Exon-intron circular RNAs regulate transcription in the nucleus. Nat Struct Mol Biol. 2015;22(3):256-64.

303. Sun YM, Wang WT, Zeng ZC, Chen TQ, Han C, Pan Q, et al. circMYBL2, a circRNA from MYBL2, regulates FLT3 translation by recruiting PTBP1 to promote FLT3-ITD AML progression. Blood. 2019;134(18):1533-46.

304. Zeng Y, Du WW, Wu Y, Yang Z, Awan FM, Li X, et al. A Circular RNA Binds To and Activates AKT Phosphorylation and Nuclear Localization Reducing Apoptosis and Enhancing Cardiac Repair. Theranostics. 2017;7(16):3842-55.

305. Chen X, Mao R, Su W, Yang X, Geng Q, Guo C, et al. Circular RNA circHIPK3 modulates autophagy via MIR124-3p-STAT3-PRKAA/AMPKα signaling in STK11 mutant lung cancer. Autophagy. 2020;16(4):659-71.

306. Suzuki H, Zuo Y, Wang J, Zhang MQ, Malhotra A, Mayeda A. Characterization of RNase R-digested cellular RNA source that consists of lariat and circular RNAs from pre-mRNA splicing. Nucleic Acids Res. 2006;34(8):e63.

307. Vincent HA, Deutscher MP. Substrate recognition and catalysis by the exoribonuclease RNase R. J Biol Chem. 2006;281(40):29769-75.

308. Muhlrad D, Decker CJ, Parker R. Deadenylation of the unstable mRNA encoded by the yeast MFA2 gene leads to decapping followed by 5'-->3' digestion of the transcript. Genes Dev. 1994;8(7):855-66.

309. Capel B, Swain A, Nicolis S, Hacker A, Walter M, Koopman P, et al. Circular transcripts of the testis-determining gene Sry in adult mouse testis. Cell. 1993;73(5):1019-30.

310. Tabak HF, Van der Horst G, Smit J, Winter AJ, Mul Y, Groot Koerkamp MJ. Discrimination between RNA circles, interlocked RNA circles and lariats using two-dimensional polyacrylamide gel electrophoresis. Nucleic Acids Res. 1988;16(14a):6597-605.

311. Szabo L, Salzman J. Detecting circular RNAs: bioinformatic and experimental challenges. Nat Rev Genet. 2016;17(11):679-92.

312. Cocquet J, Chong A, Zhang G, Veitia RA. Reverse transcriptase template switching and false alternative transcripts. Genomics. 2006;88(1):127-31.

313. Luo GX, Taylor J. Template switching by reverse transcriptase during DNA synthesis. J Virol. 1990;64(9):4321-8.

314. Glazar P, Papavasileiou P, Rajewsky N. circBase: a database for circular RNAs. Rna. 2014;20(11):1666-70.

315. Burd CE, Jeck WR, Liu Y, Sanoff HK, Wang Z, Sharpless NE. Expression of linear and novel circular forms of an INK4/ARF-associated non-coding RNA correlates with atherosclerosis risk. PLoS Genet. 2010;6(12):e1001233.

316. Bahn JH, Zhang Q, Li F, Chan TM, Lin X, Kim Y, et al. The landscape of microRNA, Piwi-interacting RNA, and circular RNA in human saliva. Clin Chem. 2015;61(1):221-30.

317. Bassett AR, Azzam G, Wheatley L, Tibbit C, Rajakumar T, McGowan S, et al. Understanding functional miRNA-target interactions in vivo by site-specific genome engineering. Nat Commun. 2014;5:4640.

318. Danan M, Schwartz S, Edelheit S, Sorek R. Transcriptome-wide discovery of circular RNAs in Archaea. Nucleic Acids Res. 2012;40(7):3131-42.

319. Hoffmann S, Otto C, Doose G, Tanzer A, Langenberger D, Christ S, et al. A multi-split mapping algorithm for circular RNA, splicing, trans-splicing and fusion detection. Genome Biol. 2014;15(2):R34.

320. Wang K, Singh D, Zeng Z, Coleman SJ, Huang Y, Savich GL, et al. MapSplice: accurate mapping of RNA-seq reads for splice junction discovery. Nucleic Acids Res. 2010;38(18):e178.

321. Hansen TB, Veno MT, Damgaard CK, Kjems J. Comparison of circular RNA prediction tools. Nucleic Acids Res. 2016;44(6):e58.

322. Dudekula DB, Panda AC, Grammatikakis I, De S, Abdelmohsen K, Gorospe M. CircInteractome: A web tool for exploring circular RNAs and their interacting proteins and microRNAs. RNA Biol. 2016;13(1):34-42.

323. Ghosal S, Das S, Sen R, Basak P, Chakrabarti J. Circ2Traits: a comprehensive database for circular RNA potentially associated with disease and traits. Front Genet. 2013;4:283.

324. Suzuki H, Tsukahara T. A view of pre-mRNA splicing from RNase R resistant RNAs. Int J Mol Sci. 2014;15(6):9331-42.

325. Xia S, Feng J, Lei L, Hu J, Xia L, Wang J, et al. Comprehensive characterization of tissue-specific circular RNAs in the human and mouse genomes. Brief Bioinform. 2017;18(6):984-92.

326. Qu S, Yang X, Li X, Wang J, Gao Y, Shang R, et al. Circular RNA: A new star of noncoding RNAs. Cancer Lett. 2015;365(2):141-8.

327. Memczak S, Papavasileiou P, Peters O, Rajewsky N. Identification and Characterization of Circular RNAs As a New Class of Putative Biomarkers in Human Blood. PLoS One. 2015;10(10):e0141214.

328. Shao Y, Li J, Lu R, Li T, Yang Y, Xiao B, et al. Global circular RNA expression profile of human gastric cancer and its clinical significance. Cancer Med. 2017;6(6):1173-80.

329. Li Y, Zheng Q, Bao C, Li S, Guo W, Zhao J, et al. Circular RNA is enriched and stable in exosomes: a promising biomarker for cancer diagnosis. Cell Res. 2015;25(8):981-4.

330. Kristensen LS, Hansen TB, Veno MT, Kjems J. Circular RNAs in cancer: opportunities and challenges in the field. Oncogene. 2018;37(5):555-65.

331. Kohlhapp FJ, Mitra AK, Lengyel E, Peter ME. MicroRNAs as mediators and communicators between cancer cells and the tumor microenvironment. Oncogene. 2015;34(48):5857-68.

332. Du WW, Yang W, Liu E, Yang Z, Dhaliwal P, Yang BB. Foxo3 circular RNA retards cell cycle progression via forming ternary complexes with p21 and CDK2. Nucleic Acids Res. 2016;44(6):2846-58.

333. Dai Y, Li D, Chen X, Tan X, Gu J, Chen M, et al. Circular RNA Myosin Light Chain Kinase (MYLK) Promotes Prostate Cancer Progression through Modulating Mir-29a Expression. Med Sci Monit. 2018;24:3462-71.

334. Greene J, Baird A-M, Casey O, Brady L, Blackshields G, Lim M, et al. Circular RNAs are differentially expressed in prostate cancer and are potentially associated with resistance to enzalutamide. Scientific Reports. 2019;9(1):10739.

335. Wu G, Sun Y, Xiang Z, Wang K, Liu B, Xiao G, et al. Preclinical study using circular RNA 17 and micro RNA 181c-5p to suppress the enzalutamide-resistant prostate cancer progression. Cell Death Dis. 2019;10(2):37.

336. Xiang Z, Xu C, Wu G, Liu B, Wu D. CircRNA-UCK2 Increased TET1 Inhibits Proliferation and Invasion of Prostate Cancer Cells Via Sponge MiRNA-767-5p. Open Med (Wars). 2019;14:833-42.

337. Cao S, Ma T, Ungerleider N, Roberts C, Kobelski M, Jin L, et al. Circular RNAs add diversity to androgen receptor isoform repertoire in castration-resistant prostate cancer. Oncogene. 2019;38(45):7060-72.

338. Zhong Z, Lv M, Chen J. Screening differential circular RNA expression profiles reveals the regulatory role of circTCF25-miR-103a-3p/miR-107-CDK6 pathway in bladder carcinoma. Sci Rep. 2016;6:30919.

339. Yang C, Yuan W, Yang X, Li P, Wang J, Han J, et al. Circular RNA circ-ITCH inhibits bladder cancer progression by sponging miR-17/miR-224 and regulating p21, PTEN expression. Mol Cancer. 2018;17(1):19.

340. Li P, Yang X, Yuan W, Yang C, Zhang X, Han J, et al. CircRNA-Cdr1as Exerts Anti-Oncogenic Functions in Bladder Cancer by Sponging MicroRNA-135a. Cell Physiol Biochem. 2018;46(4):1606-16.

341. Liang HF, Zhang XZ, Liu BG, Jia GT, Li WL. Circular RNA circ-ABCB10 promotes breast cancer proliferation and progression through sponging miR-1271. Am J Cancer Res. 2017;7(7):1566-76.

342. Wang H, Xiao Y, Wu L, Ma D. Comprehensive circular RNA profiling reveals the regulatory role of the circRNA-000911/miR-449a pathway in breast carcinogenesis. Int J Oncol. 2018;52(3):743-54.

343. Xu XW, Zheng BA, Hu ZM, Qian ZY, Huang CJ, Liu XQ, et al. Circular RNA hsa_circ_000984 promotes colon cancer growth and metastasis by sponging miR-106b. Oncotarget. 2017;8(53):91674-83.

344. Xie H, Ren X, Xin S, Lan X, Lu G, Lin Y, et al. Emerging roles of circRNA_001569 targeting miR-145 in the proliferation and invasion of colorectal cancer. Oncotarget. 2016;7(18):26680-91.

345. Zeng K, Chen X, Xu M, Liu X, Hu X, Xu T, et al. CircHIPK3 promotes colorectal cancer growth and metastasis by sponging miR-7. Cell Death Dis. 2018;9(4):417.

346. Li F, Zhang L, Li W, Deng J, Zheng J, An M, et al. Circular RNA ITCH has inhibitory effect on ESCC by suppressing the Wnt/beta-catenin pathway. Oncotarget. 2015;6(8):6001-13.

347. Chen J, Li Y, Zheng Q, Bao C, He J, Chen B, et al. Circular RNA profile identifies circPVT1 as a proliferative factor and prognostic marker in gastric cancer. Cancer Lett. 2017;388:208-19.

348. Han D, Li J, Wang H, Su X, Hou J, Gu Y, et al. Circular RNA circMTO1 acts as the sponge of microRNA-9 to suppress hepatocellular carcinoma progression. Hepatology. 2017;66(4):1151-64.

349. Yu L, Gong X, Sun L, Zhou Q, Lu B, Zhu L. The Circular RNA Cdr1as Act as an Oncogene in Hepatocellular Carcinoma through Targeting miR-7 Expression. PLoS One. 2016;11(7):e0158347.

350. Zhu X, Wang X, Wei S, Chen Y, Chen Y, Fan X, et al. hsa_circ_0013958: a circular RNA and potential novel biomarker for lung adenocarcinoma. Febs j. 2017;284(14):2170-82.

351. Wan L, Zhang L, Fan K, Cheng ZX, Sun QC, Wang JJ. Circular RNA-ITCH Suppresses Lung Cancer Proliferation via Inhibiting the Wnt/beta-Catenin Pathway. Biomed Res Int. 2016;2016:1579490.

352. Zhang H, Wang G, Ding C, Liu P, Wang R, Ding W, et al. Increased circular RNA UBAP2 acts as a sponge of miR-143 to promote osteosarcoma progression. Oncotarget. 2017;8(37):61687-97.

353. Wang K, Sun Y, Tao W, Fei X, Chang C. Androgen receptor (AR) promotes clear cell renal cell carcinoma (ccRCC) migration and invasion via altering the circHIAT1/miR-195-5p/29a-3p/29c-3p/CDC42 signals. Cancer Lett. 2017;394:1-12.

354. McDermott RS, Greene J, McCaffrey J, Parker I, Helanova S, Baird AM, et al. Radium-223 in combination with enzalutamide in metastatic castration-resistant prostate cancer: a multi-centre, phase II open-label study. Ther Adv Med Oncol. 2021;13:17588359211042691.

355. Young L, Sung J, Stacey G, Masters JR. Detection of Mycoplasma in cell cultures. Nature protocols. 2010;5(5):929-34.

356. Romero-Cordoba SL, Salido-Guadarrama I, Rodriguez-Dorantes M, Hidalgo-Miranda A. miRNA biogenesis: biological impact in the development of cancer. Cancer biology & therapy. 2014;15(11):1444-55.

357. Sikand K, Slaibi JE, Singh R, Slane SD, Shukla GC. miR 488* inhibits androgen receptor expression in prostate carcinoma cells. International journal of cancer. 2011;129(4):810-9.

358. Lin PC, Chiu YL, Banerjee S, Park K, Mosquera JM, Giannopoulou E, et al. Epigenetic repression of miR-31 disrupts androgen receptor homeostasis and contributes to prostate cancer progression. Cancer research. 2013;73(3):1232-44.

359. Greene J, Baird A-M, Lim M, Flynn J, McNevin C, Brady L, et al. Differential CircRNA Expression Signatures May Serve as Potential Novel Biomarkers in Prostate Cancer. Frontiers in Cell and Developmental Biology. 2021;9(344).

360. V TRPfSC. Austria: The R Foundation.

361. Feng H, Lopez GY, Kim CK, Alvarez A, Duncan CG, Nishikawa R, et al. EGFR phosphorylation of DCBLD2 recruits TRAF6 and stimulates AKT-promoted tumorigenesis. J Clin Invest. 2014;124(9):3741-56.

362. Knight JF, Shepherd CJ, Rizzo S, Brewer D, Jhavar S, Dodson AR, et al. TEAD1 and c-Cbl are novel prostate basal cell markers that correlate with poor clinical outcome in prostate cancer. Br J Cancer. 2008;99(11):1849-58.

363. Wang Y, Qiu H, Hu W, Li S, Yu J. RPRD1B promotes tumor growth by accelerating the cell cycle in endometrial cancer. Oncol Rep. 2014;31(3):1389-95.

364. Lin SH, Nishino M, Luo W, Aumais JP, Galfione M, Kuang J, et al. Inhibition of prostate tumor growth by overexpression of NudC, a microtubule motor-associated protein. Oncogene. 2004;23(14):2499-506.

365. Xu D, Liu A, Wang X, Chen Y, Shen Y, Tan Z, et al. Repression of Septin9 and Septin2 suppresses tumor growth of human glioblastoma cells. Cell Death Dis. 2018;9(5):514.

366. Greene J, Baird AM, Casey O, Brady L, Blackshields G, Lim M, et al. Circular RNAs are differentially expressed in prostate cancer and are potentially associated with resistance to enzalutamide. Sci Rep. 2019;9(1):10739.

367. Rubicz R, Zhao S, Wright JL, Coleman I, Grasso C, Geybels MS, et al. Gene expression panel predicts metastatic-lethal prostate cancer outcomes in men diagnosed with clinically localized prostate cancer. Molecular oncology. 2017;11(2):140-50.

368. Soudy R, Etayash H, Bahadorani K, Lavasanifar A, Kaur K. Breast Cancer Targeting Peptide Binds Keratin 1: A New Molecular Marker for Targeted Drug Delivery to Breast Cancer. Molecular pharmaceutics. 2017;14(3):593-604.

369. Mahapatra S, Klee EW, Young CY, Sun Z, Jimenez RE, Klee GG, et al. Global methylation profiling for risk prediction of prostate cancer. Clinical cancer research : an official journal of the American Association for Cancer Research. 2012;18(10):2882-95.

370. Li XP, Jiao JU, Lu LI, Zou Q, Zhu S, Zhang Y. Overexpression of ribosomal L1 domain containing 1 is associated with an aggressive phenotype and a poor prognosis in patients with prostate cancer. Oncology letters. 2016;11(4):2839-44.

371. Umemoto T, Yamato M, Ishihara J, Shiratsuchi Y, Utsumi M, Morita Y, et al. Integrin-alphavbeta3 regulates thrombopoietin-mediated maintenance of hematopoietic stem cells. Blood. 2012;119(1):83-94.

372. Agarwal V, Bell GW, Nam JW, Bartel DP. Predicting effective microRNA target sites in mammalian mRNAs. Elife. 2015;4.

373. John B, Enright AJ, Aravin A, Tuschl T, Sander C, Marks DS. Human MicroRNA targets. PLoS biology. 2004;2(11):e363.

374. Liu D, Tao T, Xu B, Chen S, Liu C, Zhang L, et al. MiR-361-5p acts as a tumor suppressor in prostate cancer by targeting signal transducer and activator of transcription-6(STAT6). Biochem Biophys Res Commun. 2014;445(1):151-6.

375. He Z, Li Z, Zhang X, Yin K, Wang W, Xu Z, et al. MiR-422a regulates cellular metabolism and malignancy by targeting pyruvate dehydrogenase kinase 2 in gastric cancer. Cell death & disease. 2018;9(5):505.

376. Avgeris M, Stravodimos K, Scorilas A. Loss of miR-378 in prostate cancer, a common regulator of KLK2 and KLK4, correlates with aggressive disease phenotype and predicts the short-term relapse of the patients. Biological chemistry. 2014;395(9):1095-104.

377. Li J, Xu YH, Lu Y, Ma XP, Chen P, Luo SW, et al. Identifying differentially expressed genes and small molecule drugs for prostate cancer by a bioinformatics strategy. Asian Pacific journal of cancer prevention : APJCP. 2013;14(9):5281-6.

378. Wu Z, Sun H, Zeng W, He J, Mao X. Upregulation of MircoRNA-370 induces proliferation in human prostate cancer cells by downregulating the transcription factor FOXO1. PloS one. 2012;7(9):e45825.

379. Vo JN, Cieslik M, Zhang Y, Shukla S, Xiao L, Zhang Y, et al. The Landscape of Circular RNA in Cancer. Cell. 2019;176(4):869-81.e13.

380. Gruner H, Cortés-López M, Cooper DA, Bauer M, Miura P. CircRNA accumulation in the aging mouse brain. Sci Rep. 2016;6:38907.

381. Rong Z-H, Chang N-B, Yao Q-P, Li T, Zhu X-L, Cao Y, et al. Suppression of circDcbld1 Alleviates Intimal Hyperplasia in Rat Carotid Artery by Targeting miR-145-3p/Neuropilin-1. Molecular Therapy - Nucleic Acids. 2019;18:999-1008.

382. Rengganaten V, Huang CJ, Tsai PH, Wang ML, Yang YP, Lan YT, et al. Mapping a Circular RNA-microRNA-mRNA-Signaling Regulatory Axis That Modulates Stemness Properties of Cancer Stem Cell Populations in Colorectal Cancer Spheroid Cells. Int J Mol Sci. 2020;21(21).

383. He J, Huang H, Du Y, Peng D, Zhou Y, Li Y, et al. Association of DCBLD2 upregulation with tumor progression and poor survival in colorectal cancer. Cell Oncol (Dordr). 2020;43(3):409-20.

384. Amayo A, Obara W. Serum prostate specific antigen levels in men with benign prostatic hyperplasia and cancer of prostate. East Afr Med J. 2004;81(1):22-6.

385. Imawari Y, Mimoto R, Hirooka S, Morikawa T, Takeyama H, Yoshida K. Downregulation of dual-specificity tyrosine-regulated kinase 2 promotes tumor cell proliferation and invasion by enhancing cyclin-dependent kinase 14 expression in breast cancer. Cancer Sci. 2018;109(2):363-72.

386. Xu Y, Sun L, Hu J, Xu S. Knockdown of hsa_circ_0001275 reverses dexamethasone-induced osteoblast growth inhibition via mediation of miR-377/CDKN1B axis. PLoS One. 2021;16(5):e0252126.

387. Wu X, Xi X, Yan Q, Zhang Z, Cai B, Lu W, et al. MicroRNA-361-5p facilitates cervical cancer progression through mediation of epithelial-to-mesenchymal transition. Med Oncol. 2013;30(4):751.

388. Papatsirou M, Artemaki PI, Scorilas A, Kontos CK. The role of circular RNAs in therapy resistance of patients with solid tumors. Per Med. 2020;17(6):469-90.

389. Chen D-F, Zhang L-J, Tan K, Jing Q. Application of droplet digital PCR in quantitative detection of the cell-free circulating circRNAs. Biotechnology & Biotechnological Equipment. 2018;32(1):116-23.

390. Karousi P, Artemaki PI, Sotiropoulou CD, Christodoulou S, Scorilas A, Kontos CK. Identification of Two Novel Circular RNAs Deriving from BCL2L12 and Investigation of Their Potential Value as a Molecular Signature in Colorectal Cancer. Int J Mol Sci. 2020;21(22).

391. Halabi S, Vogelzang NJ, Ou SS, Owzar K, Archer L, Small EJ. Progression-free survival as a predictor of overall survival in men with castrate-resistant prostate cancer. J Clin Oncol. 2009;27(17):2766-71.

392. Frampton GM, Fichtenholtz A, Otto GA, Wang K, Downing SR, He J, et al. Development and validation of a clinical cancer genomic profiling test based on massively parallel DNA sequencing. Nat Biotechnol. 2013;31(11):1023-31.

393. Roychowdhury S, Iyer MK, Robinson DR, Lonigro RJ, Wu YM, Cao X, et al. Personalized oncology through integrative high-throughput sequencing: a pilot study. Sci Transl Med. 2011;3(111):111ra21.

394. Haimovich AD. Methods, challenges, and promise of next-generation sequencing in cancer biology. Yale J Biol Med. 2011;84(4):439-46.

395. Singleton AB. Exome sequencing: a transformative technology. Lancet Neurol. 2011;10(10):942-6.

396. Siegel RL, Miller KD, Jemal A. Cancer statistics, 2020. CA Cancer J Clin. 2020;70(1):7-30.

397. Abeshouse A, Ahn J, Akbani R, Ally A, Amin S, Andry Christopher D, et al. The Molecular Taxonomy of Primary Prostate Cancer. Cell. 2015;163(4):1011-25.

398. Robinson D, Van Allen Eliezer M, Wu Y-M, Schultz N, Lonigro Robert J, Mosquera J-M, et al. Integrative Clinical Genomics of Advanced Prostate Cancer. Cell. 2015;161(5):1215-28.

399. Grasso CS, Wu YM, Robinson DR, Cao X, Dhanasekaran SM, Khan AP, et al. The mutational landscape of lethal castration-resistant prostate cancer. Nature. 2012;487(7406):239-43.

400. Rajan P, Stockley J, Sudbery IM, Fleming JT, Hedley A, Kalna G, et al. Identification of a candidate prognostic gene signature by transcriptome analysis of matched pre- and post-treatment prostatic biopsies from patients with advanced prostate cancer. BMC Cancer. 2014;14(1):977.

401. Prensner JR, Zhao S, Erho N, Schipper M, Iyer MK, Dhanasekaran SM, et al. RNA biomarkers associated with metastatic progression in prostate cancer: a multi-institutional high-throughput analysis of SChLAP1. Lancet Oncol. 2014;15(13):1469-80.

402. Love MI, Huber W, Anders S. Moderated estimation of fold change and dispersion for RNA-seq data with DESeq2. Genome Biol. 2014;15(12):550.

403. Yan J, Ojo D, Kapoor A, Lin X, Pinthus JH, Aziz T, et al. Neural Cell Adhesion Protein CNTN1 Promotes the Metastatic Progression of Prostate Cancer. Cancer Research. 2016;76(6):1603-14.

404. Deng Q-K, Lei Y-G, Lin Y-L, Ma J-G, Li W-P. Prognostic Value of Protocadherin10 (PCDH10) Methylation in Serum of Prostate Cancer Patients. Med Sci Monit. 2016;22:516-21.

405. Weber H, Ruoff R, Garabedian MJ. MED19 alters AR occupancy and gene expression in prostate cancer cells, driving MAOA expression and growth under low androgen. PLoS Genet. 2021;17(1):e1008540-e.

406. Grolez GP, Gkika D. TRPM8 Puts the Chill on Prostate Cancer. Pharmaceuticals (Basel). 2016;9(3).

407. Wang B, Yang X, Zhao T, Du H, Wang T, Zhong S, et al. Upregulation of contactin-1 expression promotes prostate cancer progression. Oncol Lett. 2020;19(2):1611-8.

408. Wang L, Zhang Y, Chen YB, Skala SL, Al-Ahmadie HA, Wang X, et al. VSTM2A Overexpression Is a Sensitive and Specific Biomarker for Mucinous Tubular and Spindle Cell Carcinoma (MTSCC) of the Kidney. Am J Surg Pathol. 2018;42(12):1571-84.

409. Narayan G, Freddy AJ, Xie D, Liyanage H, Clark L, Kisselev S, et al. Promoter methylation-mediated inactivation of PCDH10 in acute lymphoblastic leukemia contributes to chemotherapy resistance. Genes Chromosomes Cancer. 2011;50(12):1043-53.

410. Sasahira T, Kirita T, Nishiguchi Y, Kurihara M, Nakashima C, Bosserhoff AK, et al. A comprehensive expression analysis of the MIA gene family in malignancies: MIA gene family members are novel, useful markers of esophageal, lung, and cervical squamous cell carcinoma. Oncotarget. 2016;7(21):31137-52.

411. Yuan Y, Chen J, Wang J, Xu M, Zhang Y, Sun P, et al. Development and Clinical Validation of a Novel 4-Gene Prognostic Signature Predicting Survival in Colorectal Cancer. Frontiers in Oncology. 2020;10(595).

412. Zhang T, Guan G, Chen T, Jin J, Zhang L, Yao M, et al. Methylation of PCDH19 predicts poor prognosis of hepatocellular carcinoma. Asia Pac J Clin Oncol. 2018;14(5):e352-e8.

413. Chengwei Zhou WZ, Yonggang Zhu, Xiaodong Zhao. DNASE2B silencing suppresses proliferation and induces cell cycle arrest in non-small cell lung cancer cells. Int J Clin Exp Med 2018;11(11):11846-11854.

414. Bell JC, Strobel HW. Regulation of cytochrome P450 4F11 by nuclear transcription factor-κB. Drug Metab Dispos. 2012;40(1):205-11.

415. Sun WY, Wu JJ, Peng WT, Sun JC, Wei W. The role of G protein-coupled receptor kinases in the pathology of malignant tumors. Acta Pharmacol Sin. 2018;39(11):1699-705.

416. Li J, Wang H, Li Z, Zhang C, Zhang C, Li C, et al. A 5-Gene Signature Is Closely Related to Tumor Immune Microenvironment and Predicts the Prognosis of Patients with Non-Small Cell Lung Cancer. BioMed Research International. 2020;2020:2147397.

417. Zhang X, Sun Y, Wang P, Yang C, Li S. Exploration of the molecular mechanism of prostate cancer based on mRNA and miRNA expression profiles. Onco Targets Ther. 2017;10:3225-32.

418. Mo F, Wyatt AW, Sun Y, Brahmbhatt S, McConeghy BJ, Wu C, et al. Systematic identification and characterization of RNA editing in prostate tumors. PLoS One. 2014;9(7):e101431.

419. Okai I, Wang L, Gong L, Arko-Boham B, Hao L, Zhou X, et al. Overexpression of JAKMIP1 associates with Wnt/β-catenin pathway activation and promotes cancer cell proliferation in vitro. Biomed Pharmacother. 2013;67(3):228-34.

420. Subramanian A, Tamayo P, Mootha VK, Mukherjee S, Ebert BL, Gillette MA, et al. Gene set enrichment analysis: A knowledge-based approach for interpreting genome-wide expression profiles. Proceedings of the National Academy of Sciences. 2005;102(43):15545-50.

421. Liberzon A, Birger C, Thorvaldsdóttir H, Ghandi M, Mesirov Jill P, Tamayo P. The Molecular Signatures Database Hallmark Gene Set Collection. Cell Systems. 2015;1(6):417-25.

422. Kanehisa M, Goto S. KEGG: kyoto encyclopedia of genes and genomes. Nucleic Acids Res. 2000;28(1):27-30.

423. Yuan F, Hankey W, Wu D, Wang H, Somarelli J, Armstrong AJ, et al. Molecular determinants for enzalutamide-induced transcription in prostate cancer. Nucleic Acids Research. 2019;47(19):10104-14.

424. Cavallaro U, Christofori G. Cell adhesion and signalling by cadherins and Ig-CAMs in cancer. Nature Reviews Cancer. 2004;4(2):118-32.

425. Wei CH, Ryu SE. Homophilic interaction of the L1 family of cell adhesion molecules. Experimental & Molecular Medicine. 2012;44(7):413-23.

426. Bizzoca A, Virgintino D, Lorusso L, Buttiglione M, Yoshida L, Polizzi A, et al. Transgenic mice expressing F3/contactin from the TAG-1 promoter exhibit developmentally regulated changes in the differentiation of cerebellar neurons. Development. 2003;130(1):29-43.

427. Bizzoca A, Corsi P, Polizzi A, Pinto MF, Xenaki D, Furley AJW, et al. F3/Contactin acts as a modulator of neurogenesis during cerebral cortex development. Developmental Biology. 2012;365(1):133-51.

428. Falk J, Bonnon C, Girault J-A, Faivre-Sarrailh C. F3/contactin, a neuronal cell adhesion molecule implicated in axogenesis and myelination. Biology of the Cell. 2002;94(6):327-34.

429. Compton AG, Albrecht DE, Seto JT, Cooper ST, Ilkovski B, Jones KJ, et al. Mutations in Contactin-1, a Neural Adhesion and Neuromuscular Junction Protein, Cause a Familial Form of Lethal Congenital Myopathy. The American Journal of Human Genetics. 2008;83(6):714-24.

430. Rauluseviciute I, Drabløs F, Rye MB. DNA hypermethylation associated with upregulated gene expression in prostate cancer demonstrates the diversity of epigenetic regulation. BMC Medical Genomics. 2020;13(1):6.

431. Witte T, Plass C, Gerhauser C. Pan-cancer patterns of DNA methylation. Genome Med. 2014;6(8):66.

432. Thebault S, Flourakis M, Vanoverberghe K, Vandermoere F, Roudbaraki M, Lehen'kyi V, et al. Differential role of transient receptor potential channels in Ca2+ entry and proliferation of prostate cancer epithelial cells. Cancer Res. 2006;66(4):2038-47.

433. Flourakis M, Prevarskaya N. Insights into Ca2+ homeostasis of advanced prostate cancer cells. Biochim Biophys Acta. 2009;1793(6):1105-9.

434. Prevarskaya N, Zhang L, Barritt G. TRP channels in cancer. Biochim Biophys Acta. 2007;1772(8):937-46.

435. Bernardini M, Fiorio Pla A, Prevarskaya N, Gkika D. Human transient receptor potential (TRP) channel expression profiling in carcinogenesis. Int J Dev Biol. 2015;59(7-9):399-406.

436. Gkika D, Prevarskaya N. Molecular mechanisms of TRP regulation in tumor growth and metastasis. Biochim Biophys Acta. 2009;1793(6):953-8.

437. Gkika D, Lolignier S, Grolez GP, Bavencoffe A, Shapovalov G, Gordienko D, et al. Testosterone-androgen receptor: The steroid link inhibiting TRPM8-mediated cold sensitivity. Faseb j. 2020;34(6):7483-99.

438. Wang Y, Chen J, Wu Z, Ding W, Gao S, Gao Y, et al. Mechanisms of enzalutamide resistance in castration-resistant prostate cancer and therapeutic strategies to overcome it. British Journal of Pharmacology. 2021;178(2):239-61.

439. Vasaikar SV, Deshmukh AP, den Hollander P, Addanki S, Kuburich NA, Kudaravalli S, et al. EMTome: a resource for pan-cancer analysis of epithelial-mesenchymal transition genes and signatures. British Journal of Cancer. 2021;124(1):259-69.

440. Ouyang G, Wang Z, Fang X, Liu J, Yang CJ. Molecular signaling of the epithelial to mesenchymal transition in generating and maintaining cancer stem cells. Cellular and Molecular Life Sciences. 2010;67(15):2605-18.

441. O'Reilly D, Downing T, Kouba S, Potier-Cartereau M, McKenna DJ, Vandier C, et al. CaV1.3 enhanced store operated calcium promotes resistance to androgen deprivation in prostate cancer. Cell Calcium. 2022;103:102554.

442. Begicevic R-R, Falasca M. ABC Transporters in Cancer Stem Cells: Beyond Chemoresistance. International Journal of Molecular Sciences. 2017;18(11):2362.

443. Copsel S, Garcia C, Diez F, Vermeulem M, Baldi A, Bianciotti LG, et al. Multidrug resistance protein 4 (MRP4/ABCC4) regulates cAMP cellular levels and controls human leukemia cell proliferation and differentiation. J Biol Chem. 2011;286(9):6979-88.

444. Henderson MJ, Haber M, Porro A, Munoz MA, Iraci N, Xue C, et al. ABCC multidrug transporters in childhood neuroblastoma: clinical and biological effects independent of cytotoxic drug efflux. J Natl Cancer Inst. 2011;103(16):1236-51.

445. Zhu ML, Kyprianou N. Androgen receptor and growth factor signaling cross-talk in prostate cancer cells. Endocr Relat Cancer. 2008;15(4):841-9.

446. Duran GE, Wang YC, Francisco EB, Rose JC, Martinez FJ, Coller J, et al. Mechanisms of resistance to cabazitaxel. Mol Cancer Ther. 2015;14(1):193-201.

447. Shiota M, Yokomizo A, Takeuchi A, Imada K, Kashiwagi E, Song Y, et al. Inhibition of protein kinase C/Twist1 signaling augments anticancer effects of androgen deprivation and enzalutamide in prostate cancer. Clin Cancer Res. 2014;20(4):951-61.

448. Puhr M, Hoefer J, Schafer G, Erb HH, Oh SJ, Klocker H, et al. Epithelial-to-mesenchymal transition leads to docetaxel resistance in prostate cancer and is mediated by reduced expression of miR-200c and miR-205. Am J Pathol. 2012;181(6):2188-201.

449. Shang BQ, Li ML, Quan HY, Hou PF, Li ZW, Chu SF, et al. Functional roles of circular RNAs during epithelial-to-mesenchymal transition. Mol Cancer. 2019;18(1):138.

450. Beltran H, Prandi D, Mosquera JM, Benelli M, Puca L, Cyrta J, et al. Divergent clonal evolution of castration-resistant neuroendocrine prostate cancer. Nat Med. 2016;22(3):298-305.

451. Wang W, Epstein JI. Small cell carcinoma of the prostate. A morphologic and immunohistochemical study of 95 cases. Am J Surg Pathol. 2008;32(1):65-71.

452. Aparicio A, Logothetis CJ, Maity SN. Understanding the lethal variant of prostate cancer: power of examining extremes. Cancer Discov. 2011;1(6):466-8.

453. Zhao M, Kong L, Liu Y, Qu H. dbEMT: an epithelial-mesenchymal transition associated gene resource. Sci Rep. 2015;5:11459.

454. Varkaris A, Corn PG, Gaur S, Dayyani F, Logothetis CJ, Gallick GE. The role of HGF/c-Met signaling in prostate cancer progression and c-Met inhibitors in clinical trials. Expert Opin Investig Drugs. 2011;20(12):1677-84.

455. Zhang G, Huang P, Chen A, He W, Li Z, Liu G, et al. How BMP-2 induces EMT and breast cancer stemness through Rb and CD44? Cell Death & Disease. 2018;9(2):20.

456. Yang L, Tang H, Kong Y, Xie X, Chen J, Song C, et al. LGR5 Promotes Breast Cancer Progression and Maintains Stem-Like Cells Through Activation of Wnt/β-Catenin Signaling. Stem Cells. 2015;33(10):2913-24.

457. Lecarpentier Y, Schussler O, Hébert J-L, Vallée A. Multiple Targets of the Canonical WNT/β-Catenin Signaling in Cancers. Frontiers in Oncology. 2019;9.

458. Niu H, Qu A, Guan C. Suppression of MGAT3 expression and the epithelial–mesenchymal transition of lung cancer cells by miR-188-5p. Biomedical Journal. 2021;44(6):678-85.

459. Zhang M, Sui C, Dai B, Shen W, Lu J, Yang J. PEG10 is imperative for TGF-β1-induced epithelial-mesenchymal transition in hepatocellular carcinoma. Oncol Rep. 2017;37(1):510-8.

460. Hu J, Tian J, Zhu S, Sun L, Yu J, Tian H, et al. Sox5 contributes to prostate cancer metastasis and is a master regulator of TGF-β-induced epithelial mesenchymal transition through controlling Twist1 expression. Br J Cancer. 2018;118(1):88-97.

461. Prickett TD, Zerlanko BJ, Hill VK, Gartner JJ, Qutob N, Jiang J, et al. Somatic mutation of GRIN2A in malignant melanoma results in loss of tumor suppressor activity via aberrant NMDAR complex formation. J Invest Dermatol. 2014;134(9):2390-8.

462. Chen JH, Kuo KT, Bamodu OA, Lin YC, Yang RB, Yeh CT, et al. Upregulated SCUBE2 expression in breast cancer stem cells enhances triple negative breast cancer aggression through modulation of notch signaling and epithelial-to-mesenchymal transition. Exp Cell Res. 2018;370(2):444-53.

463. Lehtinen L, Vainio P, Wikman H, Reemts J, Hilvo M, Issa R, et al. 15-Hydroxyprostaglandin dehydrogenase associates with poor prognosis in breast cancer,

induces epithelial-mesenchymal transition, and promotes cell migration in cultured breast cancer cells. J Pathol. 2012;226(4):674-86.

464. Zhu G, Wang X, Yang Z, Cao H, Meng Z, Wang Y, et al. Effects of TRPM8 on the proliferation and angiogenesis of prostate cancer PC-3 cells in vivo. Oncol Lett. 2011;2(6):1213-7.

465. Gkika D, Flourakis M, Lemonnier L, Prevarskaya N. PSA reduces prostate cancer cell motility by stimulating TRPM8 activity and plasma membrane expression. Oncogene. 2010;29(32):4611-6.

466. Gorjala P, Kittles RA, Goodman OB, Jr., Mitra R. Role of CYP3A5 in Modulating Androgen Receptor Signaling and Its Relevance to African American Men with Prostate Cancer. Cancers (Basel). 2020;12(4).

467. Tung MC, Hsieh SC, Yang SF, Cheng CW, Tsai RT, Wang SC, et al. Knockdown of lipocalin-2 suppresses the growth and invasion of prostate cancer cells. Prostate. 2013;73(12):1281-90.

468. Feng S, Wang F, Matsubara A, Kan M, McKeehan WL. Fibroblast Growth Factor Receptor 2 Limits and Receptor 1 Accelerates Tumorigenicity of Prostate Epithelial Cells1. Cancer Research. 1997;57(23):5369-78.

469. Lee JE, Shin S-H, Shin H-W, Chun Y-S, Park J-W. Nuclear FGFR2 negatively regulates hypoxia-induced cell invasion in prostate cancer by interacting with HIF-1 and HIF-2. Scientific Reports. 2019;9(1):3480.

470. Sarraf P, Mueller E, Jones D, King FJ, DeAngelo DJ, Partridge JB, et al. Differentiation and reversal of malignant changes in colon cancer through PPARgamma. Nat Med. 1998;4(9):1046-52.

471. Tsubouchi Y, Sano H, Kawahito Y, Mukai S, Yamada R, Kohno M, et al. Inhibition of human lung cancer cell growth by the peroxisome proliferator-activated receptor-gamma agonists through induction of apoptosis. Biochem Biophys Res Commun. 2000;270(2):400-5.

472. Kubota T, Koshizuka K, Williamson EA, Asou H, Said JW, Holden S, et al. Ligand for peroxisome proliferator-activated receptor gamma (troglitazone) has potent antitumor effect against human prostate cancer both in vitro and in vivo. Cancer Res. 1998;58(15):3344-52.

473. Kulke MH, Demetri GD, Sharpless NE, Ryan DP, Shivdasani R, Clark JS, et al. A phase II study of troglitazone, an activator of the PPARgamma receptor, in patients with chemotherapy-resistant metastatic colorectal cancer. Cancer J. 2002;8(5):395-9.

474. Santagata S, Demichelis F, Riva A, Varambally S, Hofer MD, Kutok JL, et al. JAGGED1 expression is associated with prostate cancer metastasis and recurrence. Cancer Res. 2004;64(19):6854-7.

475. Leong KG, Niessen K, Kulic I, Raouf A, Eaves C, Pollet I, et al. Jagged1-mediated Notch activation induces epithelial-to-mesenchymal transition through Slug-induced repression of E-cadherin. J Exp Med. 2007;204(12):2935-48.

476. Bergamaschi A, Kim YH, Kwei KA, La Choi Y, Bocanegra M, Langerød A, et al. CAMK1D amplification implicated in epithelial-mesenchymal transition in basal-like breast cancer. Mol Oncol. 2008;2(4):327-39.

477. Cmero M, Kurganovs NJ, Stuchbery R, McCoy P, Grima C, Ngyuen A, et al. Loss of SNAI2 in Prostate Cancer Correlates With Clinical Response to Androgen Deprivation Therapy. JCO Precision Oncology. 2021(5):1048-59.

478. Emadi Baygi M, Soheili Z-S, Essmann F, Deezagi A, Engers R, Goering W, et al. Slug/SNAI2 regulates cell proliferation and invasiveness of metastatic prostate cancer cell lines. Tumor Biology. 2010;31(4):297-307.

479. Keyimu R, Tuerdi M, Zhao Z. MSX2 represses tumor stem cell phenotypes within oral squamous cell carcinomas via SOX2 degradation. Exp Biol Med (Maywood). 2021;246(24):2660-70.

480. Zhang J, Zhu L, Fang J, Ge Z, Li X. LRG1 modulates epithelial-mesenchymal transition and angiogenesis in colorectal cancer via HIF-1α activation. Journal of Experimental & Clinical Cancer Research. 2016;35(1):29.

481. Yang J, Antin P, Berx G, Blanpain C, Brabletz T, Bronner M, et al. Guidelines and definitions for research on epithelial–mesenchymal transition. Nature Reviews Molecular Cell Biology. 2020;21(6):341-52.

482. Cheng S, Yu X. Bioinformatics analyses of publicly available NEPCa datasets. Am J Clin Exp Urol. 2019;7(5):327-40.

483. Araki M, Nagata K, Satoh Y, Kadota Y, Hisha H, Adachi Y, et al. Developmentally regulated expression of Neuro-p24 and its possible function in neurite extension. Neurosci Res. 2002;44(4):379-89.

484. Olivan M, Garcia M, Suárez L, Guiu M, Gros L, Méndez O, et al. Loss of microRNA-135b Enhances Bone Metastasis in Prostate Cancer and Predicts Aggressiveness in Human Prostate Samples. Cancers. 2021;13(24):6202.

485. Qiu WQ, Luo S, Ma SA, Saminathan P, Li H, Gunnersen JM, et al. The Sez6 Family Inhibits Complement by Facilitating Factor I Cleavage of C3b and Accelerating the Decay of C3 Convertases. Frontiers in Immunology. 2021;12.

486. Zhang C, Qian J, Wu Y, Zhu Z, Yu W, Gong Y, et al. Identification of Novel Diagnosis Biomarkers for Therapy-Related Neuroendocrine Prostate Cancer. Pathology and Oncology Research. 2021;27.

487. Hollenhorst PC, Ferris MW, Hull MA, Chae H, Kim S, Graves BJ. Oncogenic ETS proteins mimic activated RAS/MAPK signaling in prostate cells. Genes Dev. 2011;25(20):2147-57.

488. Wang X, Duanmu J, Fu X, Li T, Jiang Q. Analyzing and validating the prognostic value and mechanism of colon cancer immune microenvironment. Journal of Translational Medicine. 2020;18(1):324.

489. Xin L. EZH2 accompanies prostate cancer progression. Nature Cell Biology. 2021;23(9):934-6.

490. Worst TS, Meyer Y, Gottschalt M, Weis CA, von Hardenberg J, Frank C, et al. RAB27A, RAB27B and VPS36 are downregulated in advanced prostate cancer and show functional relevance in prostate cancer cells. Int J Oncol. 2017;50(3):920-32.

491. Cacan E, Ali MW, Boyd NH, Hooks SB, Greer SF. Inhibition of HDAC1 and DNMT1 Modulate RGS10 Expression and Decrease Ovarian Cancer Chemoresistance. PLOS ONE. 2014;9(1):e87455.

492. Hao X-l, Gao L-y, Deng X-j, Han F, Chen H-q, Jiang X, et al. Identification of TC2N as a novel promising suppressor of PI3K-AKT signaling in breast cancer. Cell Death & Disease. 2019;10(6):424.

493. Puca L, Vlachostergios PJ, Beltran H. Neuroendocrine Differentiation in Prostate Cancer: Emerging Biology, Models, and Therapies. Cold Spring Harb Perspect Med. 2019;9(2):a030593.

494. Lamb J, Crawford ED, Peck D, Modell JW, Blat IC, Wrobel MJ, et al. The Connectivity Map: using gene-expression signatures to connect small molecules, genes, and disease. Science. 2006;313(5795):1929-35.

495. Smirnov P, Safikhani Z, El-Hachem N, Wang D, She A, Olsen C, et al. PharmacoGx: an R package for analysis of large pharmacogenomic datasets. Bioinformatics. 2016;32(8):1244-6.

496. Ferrari AC, Stone N, Stock R, Bednar M, Esseesse I, Singh H, et al. 13-cis retinoic acid and complete androgen blockade in advanced hormone-naive prostate cancer patients: report of a phase II randomized study. J Clin Oncol. 2002;20(2):538-44.

497. Melnik BC. Isotretinoin and FoxO1: A scientific hypothesis. Dermatoendocrinol. 2011;3(3):141-65.

498. Xu A, Sun S. Genomic profiling screens small molecules of metastatic prostate carcinoma. Oncol Lett. 2015;10(3):1402-8.

499. Hałubiec P, Łazarczyk A, Szafrański O, Bohn T, Dulińska-Litewka J. Synthetic Retinoids as Potential Therapeutics in Prostate Cancer-An Update of the Last Decade of Research: A Review. Int J Mol Sci. 2021;22(19).

500. Ramamurthy VP, Ramalingam S, Gediya LK, Njar VCO. The retinamide VNLG-152 inhibits f-AR/AR-V7 and MNK–eIF4E signaling pathways to suppress EMT and castration-resistant prostate cancer xenograft growth. The FEBS Journal. 2018;285(6):1051-63.

501. Jäntti MH, Talman V, Räsänen K, Tarvainen I, Koistinen H, Tuominen RK. Anticancer activity of the protein kinase C modulator HMI-1a3 in 2D and 3D cell culture models of androgen-responsive and androgen-unresponsive prostate cancer. FEBS Open Bio. 2018;8(5):817-28.

502. Shamash J, Dancey G, Barlow C, Wilson P, Ansell W, Oliver RT. Chlorambucil and lomustine (CL56) in absolute hormone refractory prostate cancer: re-induction of endocrine sensitivity an unexpected finding. Br J Cancer. 2005;92(1):36-40.

503. Sun X, Li Q. Prostaglandin EP2 receptor: Novel therapeutic target for human cancers (Review). Int J Mol Med. 2018;42(3):1203-14.

504. Chen YN, Chen JC, Yin SC, Wang GS, Tsauer W, Hsu SF, et al. Effector mechanisms of norcantharidin-induced mitotic arrest and apoptosis in human hepatoma cells. Int J Cancer. 2002;100(2):158-65.

505. Hu M, Peng S, He Y, Qin M, Cong X, Xing Y, et al. Lycorine is a novel inhibitor of the growth and metastasis of hormone-refractory prostate cancer. Oncotarget. 2015;6(17):15348-61.

506. Akinboye ES, Bamji ZD, Kwabi-Addo B, Ejeh D, Copeland RL, Denmeade SR, et al. Design, synthesis and cytotoxicity studies of dithiocarbamate ester derivatives of emetine in prostate cancer cell lines. Bioorg Med Chem. 2015;23(17):5839-45.

507. Kumar V, Vashishta M, Kong L, Wu X, Lu JJ, Guha C, et al. The Role of Notch, Hedgehog, and Wnt Signaling Pathways in the Resistance of Tumors to Anticancer Therapies. Frontiers in Cell and Developmental Biology. 2021;9.

508. Koushyar S, Meniel VS, Phesse TJ, Pearson HB. Exploring the Wnt Pathway as a Therapeutic Target for Prostate Cancer. Biomolecules. 2022;12(2).

509. Luo J, Wang D, Wan X, Xu Y, Lu Y, Kong Z, et al. Crosstalk Between AR and Wnt Signaling Promotes Castration-Resistant Prostate Cancer Growth. Onco Targets Ther. 2020;13:9257-67.

510. Pakula H, Xiang D, Li Z. A Tale of Two Signals: AR and WNT in Development and Tumorigenesis of Prostate and Mammary Gland. Cancers (Basel). 2017;9(2).

511. Lee E, Ha S, Logan SK. Divergent Androgen Receptor and Beta-Catenin Signaling in Prostate Cancer Cells. PLoS One. 2015;10(10):e0141589.

512. Pak S, Park S, Kim Y, Park J-H, Park C-H, Lee K-J, et al. The small molecule WNT/β-catenin inhibitor CWP232291 blocks the growth of castration-resistant prostate cancer by activating the endoplasmic reticulum stress pathway. Journal of Experimental & Clinical Cancer Research. 2019;38(1):342.

513. Zhang Z, Cheng L, Li J, Farah E, Atallah NM, Pascuzzi PE, et al. Inhibition of the Wnt/β-Catenin Pathway Overcomes Resistance to Enzalutamide in Castration-Resistant Prostate Cancer. Cancer Research. 2018;78(12):3147-62.

514. Soussi T, Wiman KG. TP53: an oncogene in disguise. Cell Death Differ. 2015;22(8):1239-49.

515. Yang L, Han Y, Suarez Saiz F, Minden MD. A tumor suppressor and oncogene: the WT1 story. Leukemia. 2007;21(5):868-76.

516. Aster JC, Pear WS, Blacklow SC. The Varied Roles of Notch in Cancer. Annu Rev Pathol. 2017;12:245-75.

517. Grabher C, von Boehmer H, Look AT. Notch 1 activation in the molecular pathogenesis of T-cell acute lymphoblastic leukaemia. Nat Rev Cancer. 2006;6(5):347-59.

518. Nagaishi M, Fujii Y, Sugiura Y, Takano I, Takigawa T, Yokoo H, et al. Increased Twist and ZEB2 expression in a cutaneous metastasis of high-grade glioma. Neuropathology. 2020;40(2):196-201.

519. Kong YH, Syed Zanaruddin SN, Lau SH, Ramanathan A, Kallarakkal TG, Vincent-Chong VK, et al. Co-Expression of TWIST1 and ZEB2 in Oral Squamous Cell Carcinoma Is Associated with Poor Survival. PLOS ONE. 2015;10(7):e0134045.

520. Qin Y, Yu J, Zhang M, Qin F, Lan X. ZEB1 promotes tumorigenesis and metastasis in hepatocellular carcinoma by regulating the expression of vimentin. Mol Med Rep. 2019;19(3):2297-306.

521. Caramel J, Papadogeorgakis E, Hill L, Browne Gareth J, Richard G, Wierinckx A, et al. A Switch in the Expression of Embryonic EMT-Inducers Drives the Development of Malignant Melanoma. Cancer Cell. 2013;24(4):466-80.

522. Goossens S, Vandamme N, Van Vlierberghe P, Berx G. EMT transcription factors in cancer development re-evaluated: Beyond EMT and MET. Biochimica et Biophysica Acta (BBA) - Reviews on Cancer. 2017;1868(2):584-91.

523. Vandewalle C, Van Roy F, Berx G. The role of the ZEB family of transcription factors in development and disease. Cellular and Molecular Life Sciences. 2009;66(5):773-87.

524. Nouri M, Ratther E, Stylianou N, Nelson CC, Hollier BG, Williams ED. Androgen-targeted therapy-induced epithelial mesenchymal plasticity and neuroendocrine transdifferentiation in prostate cancer: an opportunity for intervention. Front Oncol. 2014;4:370.

525. Parimi V, Goyal R, Poropatich K, Yang XJ. Neuroendocrine differentiation of prostate cancer: a review. Am J Clin Exp Urol. 2014;2(4):273-85.

526. Vlachostergios PJ, Papandreou CN. Targeting neuroendocrine prostate cancer: molecular and clinical perspectives. Front Oncol. 2015;5:6.

527. Beltran H, Jendrisak A, Landers M, Mosquera JM, Kossai M, Louw J, et al. The Initial Detection and Partial Characterization of Circulating Tumor Cells in Neuroendocrine Prostate Cancer. Clin Cancer Res. 2016;22(6):1510-9.

528. Beltran H, Tomlins S, Aparicio A, Arora V, Rickman D, Ayala G, et al. Aggressive Variants of Castration-Resistant Prostate Cancer. Clinical Cancer Research. 2014;20(11):2846-50.

529. Small EJ, Huang J, Youngren J, Sokolov A, Aggarwal RR, Thomas G, et al. Characterization of neuroendocrine prostate cancer (NEPC) in patients with metastatic castration resistant prostate cancer (mCRPC) resistant to abiraterone (Abi) or enzalutamide (Enz): Preliminary results from the SU2C/PCF/AACR West Coast Prostate Cancer Dream Team (WCDT). Journal of Clinical Oncology. 2015;33(15_suppl):5003-.

530. Epstein JI, Amin MB, Beltran H, Lotan TL, Mosquera J-M, Reuter VE, et al. Proposed Morphologic Classification of Prostate Cancer With Neuroendocrine Differentiation. The American Journal of Surgical Pathology. 2014;38(6):756-67.

531. Bishop JL, Thaper D, Vahid S, Davies A, Ketola K, Kuruma H, et al. The Master Neural Transcription Factor BRN2 Is an Androgen Receptor–Suppressed Driver of Neuroendocrine Differentiation in Prostate Cancer. Cancer Discovery. 2017;7(1):54-71.

532. Aggarwal R, Beer TM, Gleave M, Stuart JM, Rettig M, Evans CP, et al. Targeting Adaptive Pathways in Metastatic Treatment-Resistant Prostate Cancer: Update on the Stand Up 2 Cancer/Prostate Cancer Foundation-Supported West Coast Prostate Cancer Dream Team. Eur Urol Focus. 2016;2(5):469-71.

533. The Molecular Taxonomy of Primary Prostate Cancer. Cell. 2015;163(4):1011-25.

534. Cheng HH, Pritchard CC, Boyd T, Nelson PS, Montgomery B. Biallelic Inactivation of BRCA2 in Platinum-sensitive Metastatic Castration-resistant Prostate Cancer. European Urology. 2016;69(6):992-5.

535. Mateo J, Carreira S, Sandhu S, Miranda S, Mossop H, Perez-Lopez R, et al. DNA-Repair Defects and Olaparib in Metastatic Prostate Cancer. New England Journal of Medicine. 2015;373(18):1697-708.

536. Abida W, Patnaik A, Campbell D, Shapiro J, Bryce AH, McDermott R, et al. Rucaparib in Men With Metastatic Castration-Resistant Prostate Cancer Harboring a BRCA1 or BRCA2 Gene Alteration. Journal of Clinical Oncology. 2020;38(32):3763-72.

537. Beltran H, Yelensky R, Frampton GM, Park K, Downing SR, MacDonald TY, et al. Targeted next-generation sequencing of advanced prostate cancer identifies potential therapeutic targets and disease heterogeneity. Eur Urol. 2013;63(5):920-6.

538. Cheng HH, Klemfuss N, Montgomery B, Higano CS, Schweizer MT, Mostaghel EA, et al. A Pilot Study of Clinical Targeted Next Generation Sequencing for Prostate Cancer: Consequences for Treatment and Genetic Counseling. Prostate. 2016;76(14):1303-11.

539. Ryan CJ, Abida W, Bryce AH, Balar AV, Dumbadze I, Given RW, et al. TRITON3: An international, randomized, open-label, phase III study of the PARP inhibitor rucaparib vs. physician's choice of therapy for patients with metastatic castration-resistant prostate cancer (mCRPC) associated with homologous recombination deficiency (HRD). Journal of Clinical Oncology. 2018;36(6_suppl):TPS389-TPS.

540. Clark TA, Chung JH, Kennedy M, Hughes JD, Chennagiri N, Lieber DS, et al. Analytical Validation of a Hybrid Capture-Based Next-Generation Sequencing Clinical Assay for Genomic Profiling of Cell-Free Circulating Tumor DNA. J Mol Diagn. 2018;20(5):686-702.

541. Chakravarty D, Gao J, Phillips SM, Kundra R, Zhang H, Wang J, et al. OncoKB: A Precision Oncology Knowledge Base. JCO Precis Oncol. 2017;2017.

542. Landrum MJ, Lee JM, Benson M, Brown GR, Chao C, Chitipiralla S, et al. ClinVar: improving access to variant interpretations and supporting evidence. Nucleic Acids Res. 2018;46(D1):D1062-d7.

543. Gillessen S, Attard G, Beer TM, Beltran H, Bjartell A, Bossi A, et al. Management of Patients with Advanced Prostate Cancer: Report of the Advanced Prostate Cancer Consensus Conference 2019. Eur Urol. 2020;77(4):508-47.

544. Nguyen M, Simmons AD, Harding TC. Abstract 2476: Preclinical assessment of the PARP inhibitor rucaparib in homologous recombination deficient prostate cancer models. Cancer Research. 2017;77(13_Supplement):2476-.

545. Abida W, Armenia J, Gopalan A, Brennan R, Walsh M, Barron D, et al. Prospective Genomic Profiling of Prostate Cancer Across Disease States Reveals Germline and Somatic Alterations That May Affect Clinical Decision Making. JCO precision oncology. 2017;2017:PO.17.00029.

546. Cieslik M, Chugh R, Wu Y-M, Wu M, Brennan C, Lonigro R, et al. The use of exome capture RNA-seq for highly degraded RNA with application to clinical cancer sequencing. Genome research. 2015;25(9):1372-81.

547. Bonin S, Hlubek F, Benhattar J, Denkert C, Dietel M, Fernandez PL, et al. Multicentre validation study of nucleic acids extraction from FFPE tissues. Virchows Arch. 2010;457(3):309-17.

548. Beltran H, Rubin MA. New strategies in prostate cancer: translating genomics into the clinic. Clin Cancer Res. 2013;19(3):517-23.

549. Rajan P, Stockley J, Sudbery IM, Fleming JT, Hedley A, Kalna G, et al. Identification of a candidate prognostic gene signature by transcriptome analysis of matched pre- and post-treatment prostatic biopsies from patients with advanced prostate cancer. BMC Cancer. 2014;14:977.

550. Le DT, Uram JN, Wang H, Bartlett BR, Kemberling H, Eyring AD, et al. PD-1 Blockade in Tumors with Mismatch-Repair Deficiency. N Engl J Med. 2015;372(26):2509-20.

551. Hines A, Hakim N, Wang K, Shah P, Lee C-S, Seetharamu N. A retrospective analysis examining the use of tissue-based and blood-based NGS in patients (pts) with advanced non-small cell lung cancer (NSCLC). Journal of Clinical Oncology. 2021;39(15_suppl):e21195-e.

552. Lallous N, Volik SV, Awrey S, Leblanc E, Tse R, Murillo J, et al. Functional analysis of androgen receptor mutations that confer anti-androgen resistance identified in circulating cell-free DNA from prostate cancer patients. Genome Biol. 2016;17:10.

553. Dai C, Heemers H, Sharifi N. Androgen Signaling in Prostate Cancer. Cold Spring Harb Perspect Med. 2017;7(9).

554. Huggins C, Hodges CV. Studies on prostatic cancer. I. The effect of castration, of estrogen and of androgen injection on serum phosphatases in metastatic carcinoma of the prostate. Cancer research. 1941;1(4):293-7.

555. Mills IG. Maintaining and reprogramming genomic androgen receptor activity in prostate cancer. Nat Rev Cancer. 2014;14(3):187-98.

556. Watson PA, Arora VK, Sawyers CL. Emerging mechanisms of resistance to androgen receptor inhibitors in prostate cancer. Nat Rev Cancer. 2015;15(12):701-11.

557. Bluemn EG, Coleman IM, Lucas JM, Coleman RT, Hernandez-Lopez S, Tharakan R, et al. Androgen Receptor Pathway-Independent Prostate Cancer Is Sustained through FGF Signaling. Cancer Cell. 2017;32(4):474-89.e6.

Appendices

Table 1. Custom designed Primer sequence for mRNA.

Gene	Custom Designed Primers
Mycoplasma	F: 5’-GGGAGCAAACAGGATTAGATACCCT -3’ R: 5’-TGCACCATCTGTCACTCTGTTAACCTC -3’
GAPDH	F: 5'- CGACCTGACCTGCCGTCTAGAA -3' R: 5'- GGTGTCGCTGGTGAAGTCCAGAG -3'
ZEB1	F: 5'- TGACTCTGATTCTACACCGCC -3' R: 5'- CAGATTCCACACTCATGAGGTC -3'
ZEB2	F: 5'- GCAGTTCCCTTCTGCGACATA -3' R: 5'- ACACTGATAGGGCTTCTCGCC -3'
ECAD	F: 5'- CCAATCCCGATGAAATTGGA -3' R: 5'- TCGGAACCGCTTCCTTCATA -3'
NCAD	F: 5'- CCCTGGAGACATTGGGGACT -3' R: 5'- CTCAAGGACCCAGCAGTGGA -3'
FN1	F: 5'- GGAGATTCATGGGAGAAGTATGTG -3' R: 5'- AAATACTTCGACAGGACCACTTGAG -3'
TWIST	F: 5'- GCCTTCTCGGTCTGGAGGAT -3' R: 5'- CTGTCCATTTTCTCCTTCTCTGGA -3'
SNAI1	F: 5'- GCTGCTACAAGGCCATGTCC -3' R: 5'- ACTCTTGGTGCTTGTGGAGCA -3'
SLUG	F: 5'- TCGGACCCACACATTACCTTGT -3' R: 5'- CTGCAAATGCTCTGTTGCAGTG -3'
VIM	F: 5'- AACCTGGCCGAGGACATCAT -3' R: 5'- GTGCCAGAGACGCATTGTCA -3'
EPCAM	F: 5'- CAACTGGATCTGGATCCTGGTC -3' R: 5'- TGAGTTCCCTATGCATCTCACCC -3'
SMAD2	F: 5'- TCAGGGTTTTGAAGCCGTCT -3' R: 5'- CACTGAAGGGGATCCCATCT -3'
PDK3	F: 5'- TGCCAATTTCCCGTCTGTATG -3' R: 5'- TCAGGCGTGGTCTTGTAATGG -3'
KLK4	F: 5'- TATGACCCGCTGTACCACCC -3' R: 5'- CCTGGACGGTTTTCTCTATCCAC -3'
KLK2	F: 5'- GACCAGATGAAGACTCCAGCCA -3' R: 5'- CTGAGGCGTAGCAGGTGGTC -3'
STAT6	F: 5'- GCCTCTCCCCAGAAGAATCAG -3' R: 5'- GACACAGCATGCTCCTGAGG -3'
PDK2	F: 5'- CCAGAGCCTCCTGGACATCA -3' R: 5'- TCCTTGTACTCAAGCACGCCTT -3'
PDK1	F: 5'- TCCCTAGAGGGTTACGGGACAG -3' R: 5'- CCAGTCATCAGCCTCGTGGT -3'
TGFB2	F: 5'- CGTTTGCAGAACCCAAAAGC -3' R: 5'- CGCCTTCTGCTCTTGTTTTCA -3'
TGFB1	F: 5'- CCCTGGACACCAACTATTGCTTC -3' R: 5'- CCAGGCTCCAAATGTAGGGG -3'
SMAD4	F: 5'- AGGTGCCTTAGTGACCACGC -3' R: 5'- CTGCTGCTGCATCTGTCGAT -3'

Table 2. STR Profile of Cell lines.

Loci	**Cell Lines**									
	Control	Clone 1	Clone 9	LNCaP	22RV 1	PC-3	DU145	BPH-1	RWPE-1	PWR-1E
AMEL	X, Y	X, Y	X, Y	X, X	X, Y	X, X	X, Y	X, Y	X, X	X, X
D5S818	10, 11, 12	11, 12, 13	11, 12	10, 11	11, 13	13, 13	10, 13	11, 12	12, 15	13, 13
D13S317	10, 12	9, 10, 12	10, 12	12, 12	9, 12	11, 11	12, 14	11, 12	8, 14	12, 12
D7S820	9.1, 10.3	9.1, 10, 10.3	9.1, 10.3	NA, NA	9, 10	8, 11	7, 10	10, 11	10, 11	9, 11
D16S539	11, 11	11, 12	11, 11	11, 11	12, 12	11, 11	11, 13	9, 9	9, 11	12, 13
vWA	16, 17, 18, 19	15, 16, 17, 18, 19, 20, 21	16, 17, 18	16, 18	15, 21	17, 17	17, 18	17, 17	14, 18	14, 16
TH01	9, 9	6, 9, 9.3	9, 9	9, 9	6, 9.3	6, 7	7, 7	7, 7	8, 9.3	8, 9.3
TPOX	8, 9	8, 9	8, 9	NA, NA	8, 8	8, 9	11, 11	8, 12	8, 11	8, 11
CSF1PO	10, 11	10, 11	10, 11	NA, NA	10, 11	11, 11	10, 11	10, 12	13, 13	10, 10

Table 3. Custom designed primer sequence for circRNAs and its associated parental gene.

circRNA	Custom Designed Divergent Primers	Parental Gene	Custom Designed Convergent Primers
hsa_circ_0001275	F: 5'-CCATCCCAGTCCAGTTCCTA-3' R: 5'-AAGGGCCCTAGCTCAAGAAG-3'	PLCL2	F: 5'-GCACCAAGGAAGGTTTGAAGG-3' R: 5'-TCAGTCCACATGAAACAGCAGC-3'
hsa_circ_0026462	F: 5'-CCCATTTCCTTGTTTTGCTG-3' R: 5'-TCCAGAGCCACCTCTGTAGC-3'	KRT1	F: 5'-CCTGGATCTGGAGATTGCCA-3' R: 5'-TGCCACCTCCACTGATGGT-3'
hsa_circ_0033144	F: 5'-GACGAAGATGACCACCTGCT-3' R: 5'-AGGCCACTTGGCTCCTCTAT-3'	BCL11B	F: 5'-TGATCACTTCACCTCTGCGT-3' R: 5'-CAAATGTAGCTGGAAGGCTCA-3'
hsa_circ_0000673	F: 5'-TCCAGTATCTGTAAACCTTCTGTCC-3' R: 5'-GGAGCTTGGCTTCATAGGATT-3'	RSL1D1	F: 5'-CGAAATCCCACAGCTGGTACC-3' R: 5'-GGGTCTCAGATGCTGGCAAA-3'
hsa_circ_0000129	F: 5'-AGAGGGAAATCCCAGCAGAG-3' R: 5'-GCATGAGGAGTCAATGCAGA-3'	VPS72	F: 5'-TTCTGGGCTTTTGGAGGCAG-3' R: 5'-GGCCTTGGTGACTACTCGGC-3'
hsa_circ_0001721	F: 5’-TCCTCCACTGGCAAAGAGTC-3’ R: 5’-CAGGAATTGTGTCCAGGGGTT-3’	CDK14	F: 5'-CTGGCCTCCAAGCTCCTACA-3' R: 5'-CCAGCTTCTGGTTGCAATCTC-3'
hsa_circ_0007058	F: 5’-GGAGGCCCTGGCTATCTATC-3’ R: 5’-TTCCACTTGAATGTGCAATGA-3’	TEAD1	F: 5'-GAACTGTTTGGAAAGGGCCC-3' R: 5'-CACCATAAAAAGCCCCAGCA-3'
hsa_circ_0005320	F: 5’-CCTGTGGCTGAGGCTACAC-3’ R: 5’-ACAGTGGCTCGGAGTAGGG-3’	SEPT9	F: 5'-CACCCTGGAGGAGAGGGTCC-3' R: 5'-CCGGTCCTCCGAGTCCTCAT-3'
hsa_circ_0005087	F: 5’-TTGATGGGGAGCTCTACAATG-3’ R: 5’-TGGGCTTCAGTTTTCCTTTG-3’	NUDC	F: 5'-TGAAGGTGGAGGAGAGCTCG-3' R: 5'-GATCTCAGGGTCACTGGACACC-3'
hsa_circ_0007365	F: 5’-GCTCGGATGTTGGTGGAGTA-3’ R: 5’-CCTCCTCCTGAATTTGCTGA-3’	RPRD1B	F: 5'-CGGATGTTGGTGGAGTATACCC-3' R: 5'-CTTGCGGACCTGGGTTACTC-3'
hsa_circ_0066631	F: 5’-CGGATTTTTGGCCTCATACT-3’ R: 5’-TCCCATTCACAAACAGTGCT-3’	DCBLD2	F: 5'-GAGGAAACCCCAGTTCGCTA-3' R: 5'-CCTCCTACCAGTGGCTGAGC-3'
hsa_circ_0074595	F: 5’-ACATCTGGCCACTTCAGGAG-3’ R: 5’-CGGCCAAAGTGAGACTTGA-3’	ANXA6	F: 5'-TGTCAGGGATGCATTTGTGG-3' R: 5'-GGGATACCATGATCCTGGTCAG-3'
hsa_circ_0077109	F: 5’-TCCCAGATAGCCATGTCACC-3’ R: 5’-GTGGGCTGATGACAACAGAG-3’	IRAK1BP1	F: 5'-CGTTTGTCGCCGTCTAGATT-3' R: 5'-GGGCTGATGACAACAGAGCT-3'
hsa_circ_0044226	F: 5’-TGGACAAAGCATTAGCTTGTTT-3’ R: 5’-TTGGTTGTGGAGCTGTCACT-3’	CDC27	F: 5'-CTTGCAGAAATGCATTTCCAA-3' R: 5'-GGGTATCCAAAGCCTTCTCTGA-3'
hsa_circ_0003738	F: 5’-TGAGGTGCTGGCTCACATAG-3’ R: 5’-GACGCCATGAATCTCCAAGT-3’	CARMIL1	F: 5'-CTGGCAGAGATGAAAGCCAA-3' R: 5'-CCTCCATCCGACCGTTCTAC-3'

Table 4. TaqMan® Advanced miRNA assays.

miRNAs	Assay ID
hsa-miR-1228-3p	478643_mir
hsa-miR-361-5p	478056_mir
hsa-miR-422a	478481_mir
hsa-miR-378a-3p	478349_mir
hsa-miR-370-3p	478326_mir
hsa-miR-506-3p	478958_mir
hsa-miR-149-3p	478720_mir
hsa-miR-301a-5p	478796_mir
hsa-miR-371a-3p	478070_mir
hsa-miR-29b-1-5p	478794_mir
hsa-miR-221-5p	478778_mir
hsa-miR-372-3p	478071_mir
hsa-miR-122-3p	477874_mir

Table 5. Custom design gBlock as positive control for hsa_circ_0001275 and hsa_circ_000721.

circRNA	Custom Designed gBlock
hsa_circ_0001275 and hsa_circ_000721	5'-GAGTCCTCCACTGGCAAAGAGTCACCTAAAGTTAGGCGGCACTCCAGCCCCAGCTCGATATGTGTCACAAAGATGTCTACACGGAACTGCCAGGGAATGGACTCAGTGATCAAACCCCTGGACACAATTCCTGCCAGAGGAGGAGCAGCTTTACACTGATGAAGTGTTAGACATCGAGATCAATGAACCTTTAGATGAATTTACAAATCAGTCGGATTTGTCAGATGAAGAGCTAAATGATGATCTTTTGCAGAGTGATAATGAAGATGAAGAAAATTTCAGTTCTCAGGGTGTTACAACCATCCCAGTCCAGTTCCTACTAAAACTCCCTTAATCTGCCTAGTCTAAGGAGGTGTGTGAATTTCTCTTCTTCTCCACTCCTGAATGGCTCTGATACCTGTCTTCTTGAGCTAGGGCCCTTACGC-3'

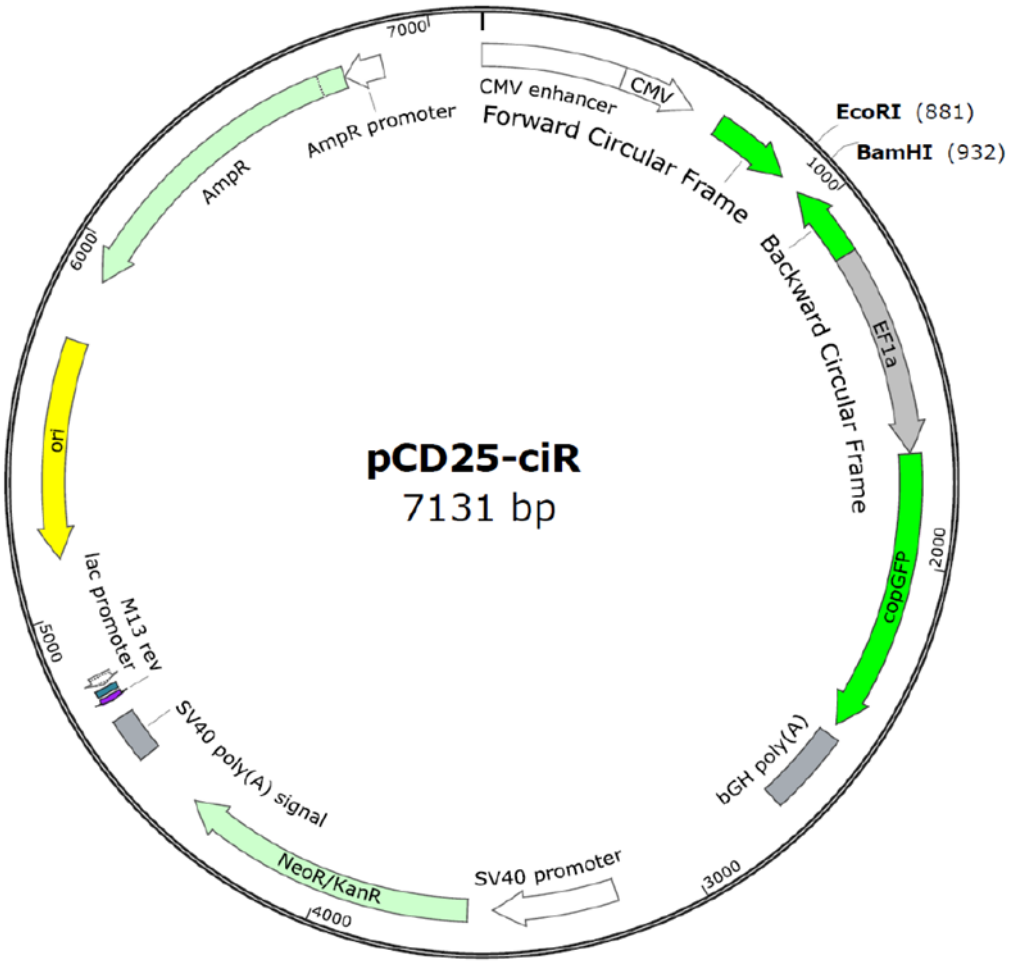

Figure 1. circRNA expressing vector pCD25-ciR (Cat no. GS0106). The sequences of the primers are as below:

Primer-F: 5'-CGGAATTCTAATACTTTCAG + Original primer sequence-3',

Primer-R: 5'-CGGGATCCAGTTGTTCTTAC + Original primer sequence-3'.

The sequence of the PCR product of linear circRNA is as follow:

GAATTC TAATACTTTC AG Linear sequence of circRNA GT AAGAACAACT GGATCC
CTTAAG ATTATGAAAG TC CA TTCTTGTTGA CCTAGG

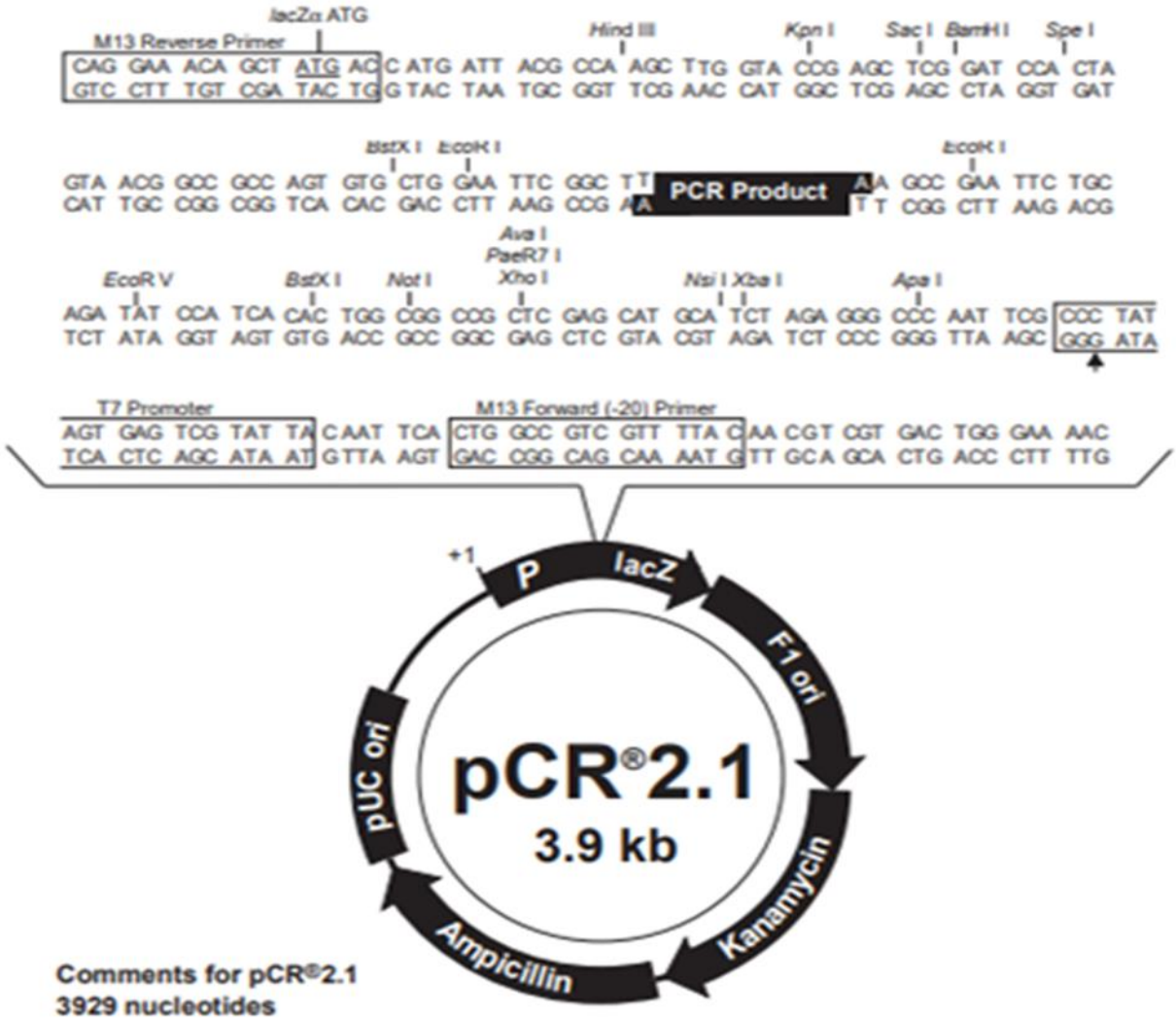

Figure 2. pCR™2.1-TOPO® vector (Cat no. K203001). The sequences of the primers are as above.

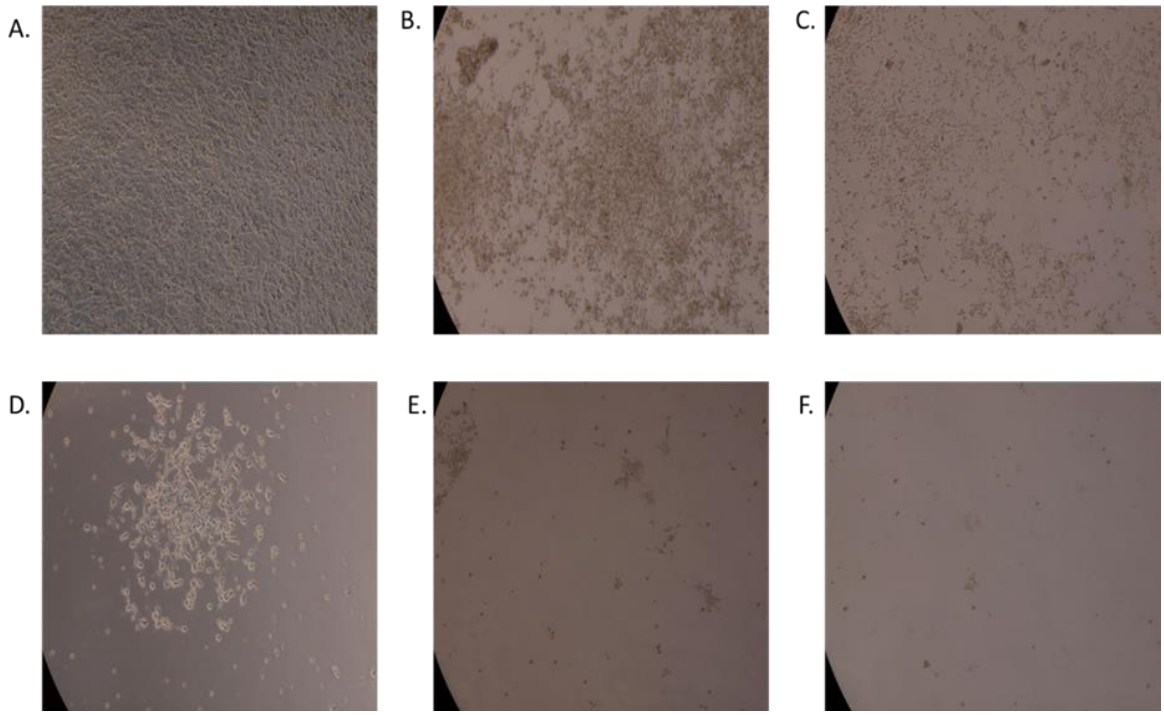

Figure 3. Representative images of LNCaP cells treated with a range of G418 concentration at the end of 7 days using bright field microscopy. G418 concentration: A=untreated, B=300 µg/ mL, C=400 µg/ mL, D=500 µg/ mL, E=600 µg/ mL, F=700 µg/ mL. All images are X10 magnification.

Table 6. Preparation of BSA standards.

Vial	**Volume of H_2O (µL)**	**Volume and source of BSA (µL)**	**Final BSA concentration (µg/mL)**
A	0	300 of stock solution	2000
B	125	375 of stock solution	1500
C	325	325 of stock solution	1000
D	175	175 from vial B	750
E	325	325 from vial C	500
F	325	325 from vial E	250
G	325	325 from vial F	125
H	400	100 from vial G	25
I	400	0	0

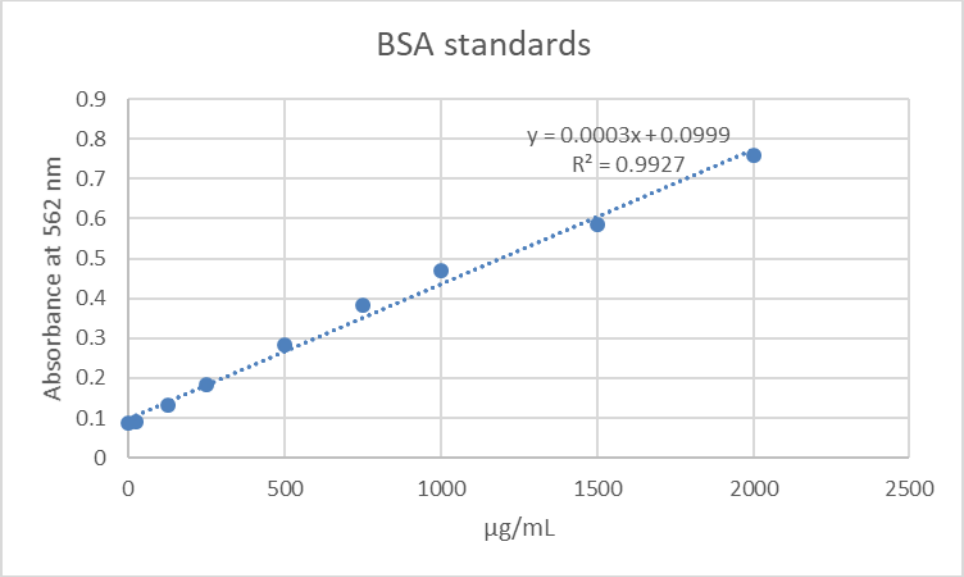

Figure 4. Standard curve of known concentrations of BSA ranging from 0 to 2000 µg/mL.

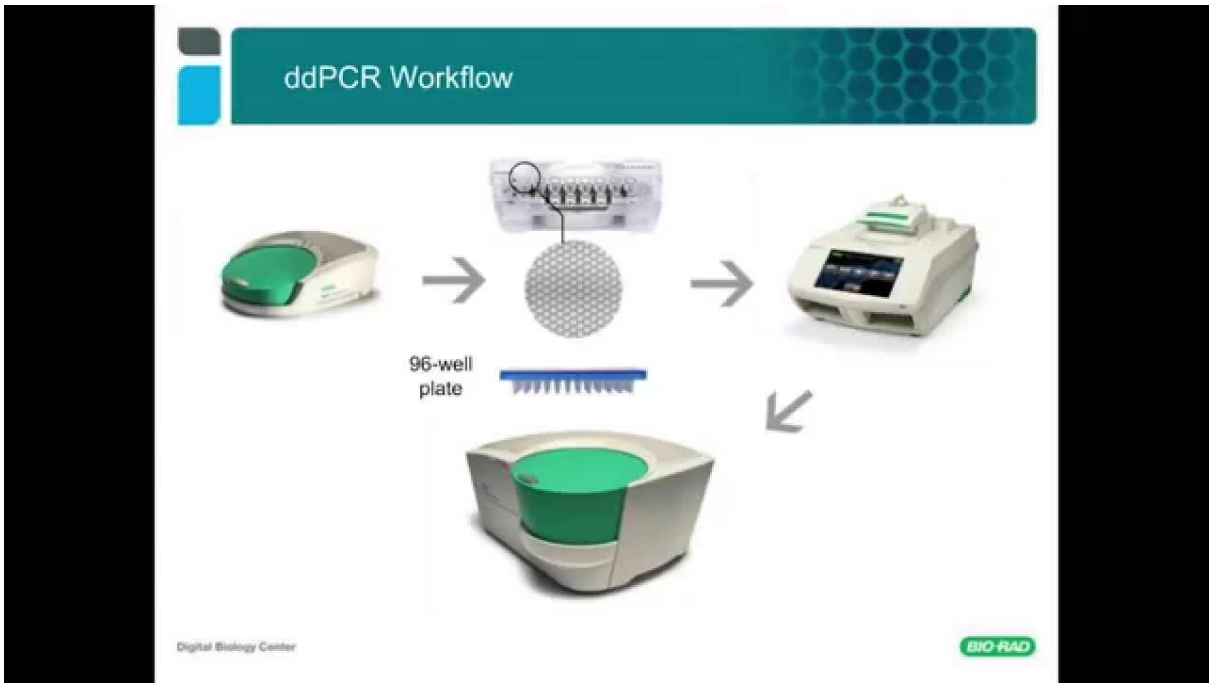

Figure 5. Image of QX200™ Droplet Digital PCR System and work flow.

Figure 6. Image of Agilent 2100 Bioanalyzer.